043
MAJ
15357

NUCLEAR LEVEL DENSITIES AND OTHER STATISTICAL QUANTITIES WITH INTERACTIONS IN SPECTRAL AVERAGING THEORY: SYSTEMATIC STUDIES AND APPLICATIONS

BY

DEBASISH MAJUMDAR

PHYSICAL RESEARCH LABORATORY
AHMEDABAD 380 009, INDIA

A THESIS

submitted to

The Maharaja Sayajirao University of Baroda
Baroda 390 002, India

For the degree of

Doctor of Philosophy in Physics

DECEMBER 1994

043
B15357

तस्मादसक्तः सततं कार्यं कर्म समाचर ।
असक्तो ह्याचरन्कर्म परमाप्नोति पूरुषः ।।

कर्मयोग, श्रीमद् भगवद्गीता

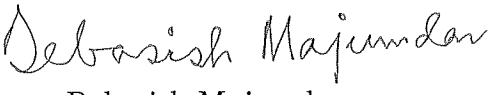
"Therefore, without attachment, perform always the work that has to be done, for man attains to the highest by doing work without attachment."

Karmayoga, Shrimad Bhagavat Gita

Translated by Dr. Sarvepalli Radhakrishnan

CERTIFICATE

I hereby declare that the work presented in this thesis is original and has not formed the basis for the award of any degree or diploma by any University or Institution.



Debasish Majumdar

(Author)

Certified by :



Dr. V. Krishna Brahmam Kota

(Guide)

Physical Research Laboratotry,

Ahmedabad 380 009, India.

Prof. Vijay N. Potbhare

(Co-Guide)

The M.S. University of Baroda,

Baroda 390 002, India.

Acknowledgements

I am greatly indebted to Dr. V.K.B. Kota for his relentless effort and meticulous guidance during the period of my research work. Without his keen interest and tenacity the thesis wouldn't have taken the present shape. I profusely thank and acknowledge him for extending me this favour.

I am grateful to Prof. V.N. Potbhare for guidance, encouragement and for many discussions, from time to time.

I am thankful to Dr. R.U. Haq for permitting me to use freely the package LVLDEN_INT which has been used for calculations throughout the thesis and for valuable inputs I received through Dr. V.K.B. Kota, Dr. K. Jain for collaboration during the initial stages of the work reported in Chapter 4 and Prof. K. Kar and Dr. S. Sarkar for supplying some of their results prior to publication.

During the course of my work I benefitted a lot from the discussions Dr. V.K.B. Kota had with Prof. J.B. French. They are helpful in many ways and most of the studies presented in the thesis have grown out of these discussions. I am also grateful to Prof. J.B. French for his keen interest in the work carried out in this thesis. I thank Profs. J.C. Parikh and S.B. Khadkikar for some valuable suggestions and comments for betterment of the thesis.

I express my gratitude to Prof. R.K. Varma, Director, Physical Research Laboratory for a grant towards computational work at Institute for Plasma Research (IPR) and Prof. Abhijit Sen for facilities at IPR. I thank Ganesh, Sudip and other students of IPR for being extremely cooperative during my visits to IPR. Thankfully I acknowledge the help I have received from Drs. D.R.

Kulkarni, B.R. Sitaram and Sai Iyer towards computational work. Thanks are due to Dr. Y.D. Devi for many useful suggestions and comments from time to time during the course of my thesis work.

This acknowledgement would never be complete if I do not mention various other facilities that I have availed and the people associated with them. To mention a few, this includes Mr. Ghanashyam Dholakia and all other staff members of PRL Computer Centre, Mrs. Urmila Ghiya, Mrs. Rohini Patil and other staff members of PRL library, Mr. D.R. Ranpura of the photography section and Mr. S.C. Bhavsar of drafting section. I remember them with deep gratitude for the support and service I have obtained from them during my thesis work.

It is impossible to name all of my friends and colleagues at PRL hostel and PDF quarters in this limited space whose constant moral support and lively company have been a source of joy, pleasure and refreshment in many ups and downs during my stay at Ahmedabad. Himadri Chakrabarty and his family, S. Ramachandran, M.S. Santhanam, Devashis Banerjee, G. Srinivasan, V. Sivakumaran, Sam Ragland, Tarun Pant, D. Pallam Raju, V. Prahlad, W. Watson, P. Poulose and Biju Thomas to name a few. Thanks are due to Mr. T.P. Muralidharan for some secretarial help. My experiences, stretching beyond the curricular boundaries at PRL, still remain green in my memory. Every time, I derive more and more pleasure and feel rejuvenated as I reveal those with a new dose of vision and imagination. I always try to enshrine them from not being scattered through the winds of time.

Words are perhaps inadequate to express my overwhelming gratitude to my parents back home in Calcutta. They have extended their full moral support

during this long period of my thesis work. I am grateful to my other family members and relatives for providing me constant inspiration through their letters or otherwise.

I conclude by extending my thanks to the innumerable tax payers of my country for supporting me indirectly.

Abstract

The subject of statistical nuclear spectroscopy, that started with Bethe's statistical mechanical level density formula , Wigner's treatment of spectral fluctuations using matrix ensembles and French's embedded ensembles and Gaussian densities, continues to be an important field of research as it has large variety of applications in nuclear structure and nuclear astrophysics. Statistical spectroscopy divides into two parts; one is spectral averages which give smoothed (with respect to energy) forms of observables and the other being spectral fluctuations around these smoothed forms; the later are ignored for most purposes. The smoothed forms of spectroscopic observables follow from the action of Central Limit Theorems (CLT) in nuclear shell model spaces. Recent progress in statistical spectroscopy is in deriving and applying the smoothed forms in indefinitely large spaces with *interactions* by using unitary group decompositions (of hamiltonians and the spectroscopic spaces), CLT's locally, and convolutions - the resulting theory is the Spectral Averaging Theory in Large Shell Model Spaces (SAT-LSS). The aim of the present thesis is to study (and test) some aspects of SAT-LSS for state, expectation value and strength densities in large spaces and apply them to calculate nuclear level densities and β-decay rates. The problems solved to this end are described below along with corresponding results.

In SAT-LSS, (i) using a significant unitary group decomposition under which a one plus two-body nuclear hamiltonian decomposes into orthogonal effective one-body part $\mathbf{h}$ and irreducible two-body part $\mathbf{V}$ ($H \rightarrow \mathbf{h} + \mathbf{V}$); (ii) applying the CLT's locally and (iii) decomposing the shell model space

into distant non-interacting S - subspaces (for light nuclei S denotes $\hbar\omega$ excitation), the state densities take a convolution form, $I^H = \sum_S I^{\mathrm{h},S} \otimes \rho_{\mathcal{G}}^{\mathrm{V},S}[E]$ where I^{h} is renormalized non-interacting particle (NIP) state density and $\rho_{\mathcal{G}}$ is a normalized spreading Gaussian. Similar convolution forms are derived for spin-cutoff and occupancy densities. Firstly, systematic studies of two important aspects of the level density theory are carried out in the thesis and they are: (a) a part of the interaction that produces non-NIP like shifts of the single particle energies, that is neglected in the theory, is conclusively demonstrated (using norms of operators and considering large number of effective interactions) to be indeed small all across the periodic table; (b) moment methods for constructing locally smoothed forms for NIP state, spin-cutoff and occupancy densities which are one of the convolution factors in the IP theory, are comprehensively tested for the three densities and also for their S - decompositions in an example of 12 protons and 12 neutrons in a large shell model space consisting of 16 orbits (s, p, ds, fp, sdg, $1h_{11/2}$) with $0 - 4$ $\hbar\omega$ excitations; moment methods give an excellent representation of exact results.

For a first systematic analysis of experimental data using the convolution forms for state and spin-cutoff densities, in a given region of the periodic table, fp-shell nuclei are chosen as the example. Nuclei in this region of the periodic table have acquired new significance recently as some of them play an important role in nuclear astrophysics problems, double β - decay, problem of quenching of GT sum rule strengths etc. The calculations, using surface delta interaction with strength G, are carried out in large spaces by including configurations upto $2\hbar\omega$ excitations and by employing eight spherical orbits (ds, fp, $1g_{9/2}$) for the five nuclei ^{55}Mn, ^{56}Fe, ^{59}Co, ^{60}Co and ^{60}Ni and by extending for obvious reasons, to ten spherical orbits (ds, fp, $1g_{9/2}$, $2d_{5/2}$,

$1g_{7/2}$) for the three $A > 60$ nuclei ^{62}Ni, ^{63}Cu and ^{65}Cu. In general the convolution form for the densities is seen to provide an excellent representation of the observed total level densities and spin-cutoff factors. The calculations determine a magnitude parameter of the interaction - the strength G which is found to be $\sim 20/A\ MeV$ for all the nuclei, is compatible with the values deduced from low-energy spectroscopy.

In SAT-LSS the bivariate strength density $\mathbf{I}^H_{\mathcal{O}}(E_i, E_f)$ for a transition operator $\mathcal{O}$ takes a convolution form, $\mathbf{I}^H_{\mathcal{O}}(E_i, E_f) = \mathbf{I}^{\mathbf{h}}_{\mathcal{O}} \otimes \rho^{\mathbf{V}}_{BIV-g;\mathcal{O}}[E_i, E_f]$. Leaving aside the spreading bivariate Gaussian $\rho^{\mathbf{V}}_{BIV-g;\mathcal{O}}$, one needs good methods for constructing the NIP density $\mathbf{I}^{\mathbf{h}}_{\mathcal{O}}$ in large spaces. For one-body transition operators, a complete formalism for constructing the exact NIP strength densities using spherical orbits is worked out. For rapid construction of the bivariate NIP densities and also to carry out S-decomposition, trace propagation formulas for bivariate moments M_{rs} with $r + s \leq 2$ are derived for unitary orbit partial densities which determine the bivariate Gaussian representation for the partial densities. This formalism is tested in a large space numerical example with $GT(\beta^-)$ transition operator. Trace propagation formulas for M_{rs} with $r + s \leq 4$ are also derived in m-particle scalar spaces, which are useful for many purposes.

A method to calculate β-decay rates at finite temperature is developed by writing the expression for the rates explicitly in terms of bivariate GT strength densities ($\mathbf{I}^H_{\mathcal{O}(GT)}$) and state densities of parent nucleus besides having the usual phase space factors. For constructing $\mathbf{I}^H_{\mathcal{O}(GT)}$, the method developed in this thesis for constructing NIP strength densities is applied together with a plausible

procedure for generating the GT bivariate spreading Gaussians due to interactions. Recently there is considerable interest in evaluating β-decay rates for $A > 60$ neutron excess fp-shell nuclei as these rates play a very important role in determining the structure of the core of massive supernova stars and hence on their subsequent evolution towards gravitational collapse and supernova explosion phases. Therefore as an example, using our method, β-decay rates for $^{61,62}Fe$ and $^{62-64}Co$ isotopes are calculated at presupernova matter densities $\rho = 10^7 - 10^8$ gm/cc, temperatures $T = (3-5) \times 10^9\ ^oK$ and for various values of the electron fraction Y_e. As a biproduct, the calculations produced a value (via observed β-decay half lifes) for the bivariate correlation coefficient $\bar{\zeta}$ between the hamiltonian and the GT operator to be $\bar{\zeta} \sim 0.67$, and thus new information about the nuclear hamiltonians is deduced. In addition an expression for the GT non-energy weighted summed strengths is also deduced.

To summarize, SAT-LSS is explored by carrying out first systematic analysis of fp-shell level density data using the convolution forms for the state and spin-cutoff densities, developed further by deriving an essentially complete theory for constructing NIP strength densities produced by one-body transition operators, and applied to neutron excess fp-shell nuclei relevant for presupernova evolution calculations in nuclear astrophysics by developing a method to calculate β-decay rates at finite temperature in terms of state and bivariate strength densities. The results of the present thesis together with the earlier investigations, show that the convolution forms for state, expectation value and strength densities in large spaces as given by SAT-LSS can be used profitably to study a variety of nuclear physics and nuclear astrophysics problems.

Contents

Abstract vii

Chapters

1 Introduction 1

2 Some Mathematical Aspects of Spectral Averaging Theory 22

2.1 Preview 22

2.2 Statistical distributions 23

2.2.1 Univariate distributions 23

2.2.2 Bivariate distributions 26

2.3 State, expectation value and strength densities: CLT results . 31

2.3.1 State densities 31

2.3.2 Expectation values and expectation value densities . . 32

2.3.3 Strength densities 34

2.4 Partitioning : spherical and unitary configurations 36

2.5 Unitary decomposition of operators 40

2.5.1 $U(N)$ group 40

2.5.2 Spherical configuration group $U(N_\alpha) \oplus U(N_\beta) \oplus$ 43

2.5.3 Unitary configuration group $U(N_{\boldsymbol{\alpha}}) \oplus U(N_{\boldsymbol{\beta}}) \oplus$ 44

2.6 Trace propagation 46

2.6.1 $U(N)$ group averages 46

2.6.2 Spherical configuration averages 51

2.6.3 Unitary configuration averages 52

2.7 Summary 55

3 Tests of Some Aspects of Spectral Averaging Theory in Large Shell Model Spaces for State, Spin-Cutoff and Occupancy Densities **56**

3.1 Introduction 56

3.1.1 S - decomposition 57

3.1.2 Convolution form for state densities 61

3.1.3 Convolution forms for spin-cutoff and occupancy densities 67

3.1.4 Moment methods and convolution forms for NIP state, spin-cutoff and occupancy densities 68

3.1.5 Summary of convolution results and conventions for pn systems 71

3.2 Test of the smallness of $V^{[0][2]}$ part of various interactions . . . 73

3.3 Tests of moment methods for NIP state, spin-cutoff and occupancy densities 91

3.4 Summary 103

4 Analysis of Level Density Data for fp-Shell Nuclei: Systematic Calculations Using SAT-LSS **105**

4.1 Preview 105

4.2 Selection of nuclei, choice of orbits and the hamiltonian and the procedure for calculations 107

4.2.1 Choice of fp-shell nuclei 107

4.2.2 Reference energy 108

4.2.3 Choice of the single particle orbits and the two-body interaction 110

4.2.4 Unitary orbits for spreading variances and NIP calculations 112

4.2.5 Ratio of J^2-density variance and state density variance 116

4.2.6 Procedure for calculations 118

4.3 8-orbit results for ^{55}Mn, ^{56}Fe, ^{59}Co, ^{60}Co, ^{60}Ni and ^{63}Cu . . . 121

4.3.1 Nucleus ^{55}Mn 121

4.3.2 Nucleus ^{56}Fe 128

4.3.3 Nucleus ^{59}Co 131

Chapter 1

Introduction

Atomic nuclei are endowed with a large variety of structures and a major classification of these is in terms of single particle, collective (representing co-operative motion among the nucleons) and statistical (representing a type of random or chaotic motion) features. These three structures are distinctly seen in some selective nuclei in selective energy domains; for example the low energy spectrum of (^{40}K, ^{42}Ca), levels upto about 2.5 MeV excitation in ^{168}Er and resonances at neutron separation energy in ^{238}U respectively, clearly show the above three features. These three structures led to the development of the nuclear shell model by Mayer and Jensen [Ma-65], geometric models by Bohr and Mottelson [Bo-69, Bo-75] and statistical mechanical methods / random matrix models by Bethe and Wigner [Be-36, Wi-55].

Recognizing that the statistical features extend throughout the spectrum of a complex nucleus [Br-81], the scope of statistical approach to nuclear structure was enlarged by French [Fr-67, Fr-69a, Ch-71, Fr-72, Mo-75, Dr-77a, Dr-77b, Fr-79], by combining shell model ideas with Bethe and Wigner's treatment of statistical properties of nuclei, by introducing and developing the subject of

statistical nuclear spectroscopy. Before proceeding further it should be stressed that statistical spectroscopy provides a path for understanding the deeper connections between symmetries, statistical behavior and quantum chaos on one hand and information propagation on the other in complex nuclei (in general in complex many body systems); see Fig. 1.1. Statistical spectroscopy divides into two parts, spectral average being one part and fluctuation (around the averages) being the other with little communication between the two. The origin and nature of the separation is understood analytically by using ensemble of hamiltonian matrices [Mo-75] and two good numerical examples are also available [Br-81, La-90]. The separation gives a permit to deal with averages and fluctuations separately and by using different methods. The model for energy level and strength fluctuations is the so called GOE (Gaussian orthogonal ensemble of random matrices) model. It is well known that GOE describes fluctuations in slow neutron resonance domain to a very high degree of precision [Ha-82a] and also GOE is closely connected with 'quantum chaos' [Bo-84, Bo-88]. The Dyson Mehta [Dy-63] spectral rigidity ensures that spectral fluctuations are small and they essentially carry no information except for symmetries (Ref. [Fr-88a, Fr-88b] gives a good example where a bound on the size of time reversal non-invariant (TRNI) part of nucleon-nucleon interaction is derived from slow neutron resonance data). Hence fluctuations can be ignored for most purposes and spectral averages carry most of the significant physical information about observables [1]. The theory that allows one to derive

[1] All spectroscopic observables, broadly speaking, belong to one (or products) of the three basic quantities: (1) state density $I(E)$ which counts the number of states in the interval E and $E + \Delta E$, or its normalized version $\rho(E)$, (2) expectation values $\langle K \rangle^E$ – diagonal matrix elements of an operator K in the hamiltonian (H) diagonal basis or expectation value densities $I_K(E) = \langle K \rangle^E I(E)$, and (3) strengths $|\langle E'|\mathcal{O}|E\rangle|^2$ – squares of matrix elements connecting two H-eigenstates or strength densities $\mathbf{I}_\mathcal{O}(E, E') = I(E')|\langle E'|\mathcal{O}|E\rangle|^2 I(E)$. Energies are also observables and they are tacitly included in (1) above.

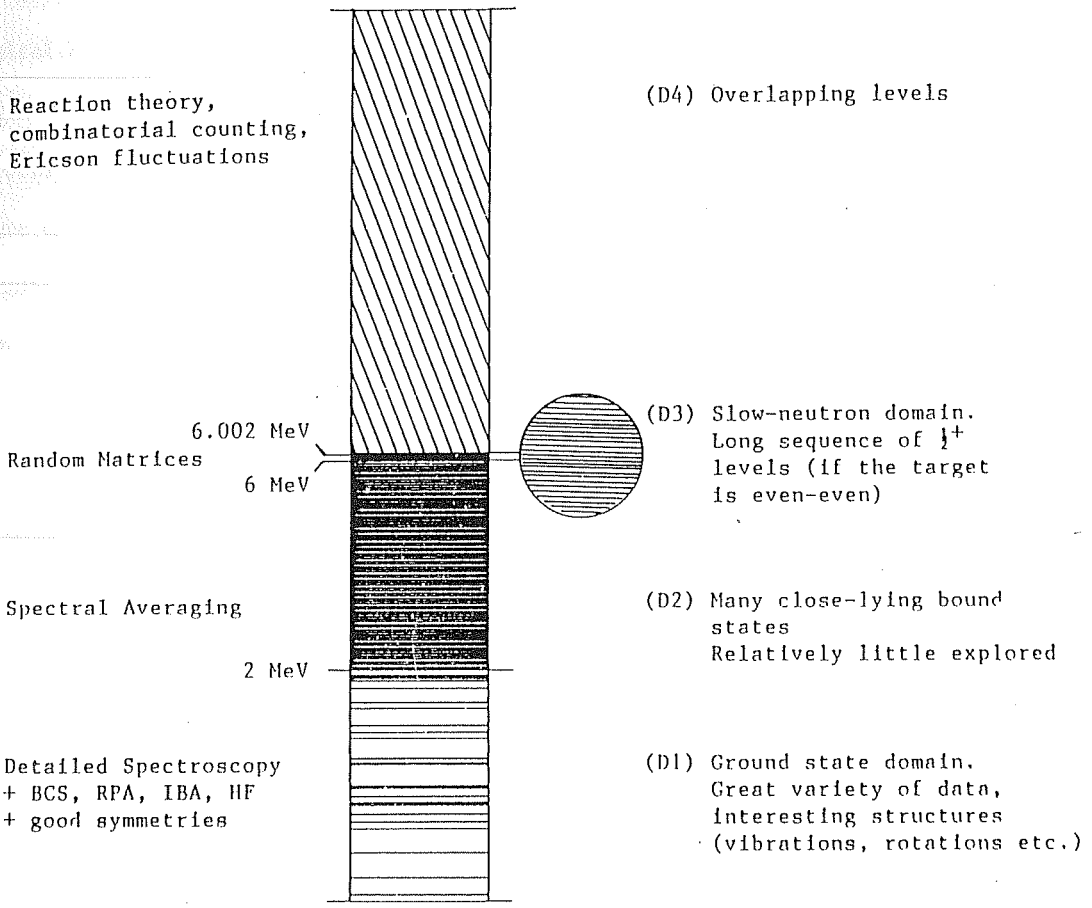
Figure 1.1

Typical spectrum of a heavy nucleus. Figure is taken from [Fr-89c]. As French and Kota state [Fr-89c]: "If we start at the ground state and go up in the spectrum of such a nucleus we can identify in order the following domains: (D1) the shell model domain (0-2 MeV); (D2) no man's land (2-6 MeV); (D3) the fluctuation window (6 - 6.002 MeV); (D4) the true continuum (> 6.002 MeV), where typical values are given for the domain boundary energies which of course vary somewhat from nucleus to nucleus. The two domains D1, D3 where spectra can be studied in exquisite detail, contain no more than a few hundred states at best and are separated by D2 which contains many millions of states about which because of experimental limitation, almost nothing is known. ..... Up to now there have been for example no serious attempts to cross the no-man's land and calculate from the D1 spectrum and the general features of the interaction, the absolute state or level density in the resonance region D3, (the only part of the complete spectrum where unambiguously-defined smoothed densities have been measured with some precision)..... We justify our description of D1 as the "shell-model domain" by the argument that the shell model supplies the foundation for most microscopic models. D1 is of course extraordinarily rich in experimental data, and in theoretical concepts and models which involve, among other things, a wide range of symmetries with their more-or-less-well conserved quantum numbers. Some of the D1 data, yrast states and giant resonances for example, do extend to higher domains, but since these extensions involve only a small fraction of the states in the upper domains, this does not negate our classification. In D2 a transition occurs from a spectrum (of D1) which is profitably studied in detail, level by level, to one (of D3) in which the only sensible treatment would appear to be statistical one. (..... one must distinguish between the use of *statistical methods* (as in our use of central limit theorems for the state density generated by a given Hamiltonian) and *statistical assumptions* (as with fluctuations where we assume *a priori*, and justfy by the results that averaging over a Hamiltonian

ensemble is an appropriate procedure)). One might take for granted that we proceed to such a treatment of D3 because the D3 complexities make it impossible to do better. After all only a part of the spectrum is available (often only the $1/2^+$ levels; see below), the shell model spaces are enormous (dimensionality $\sim 10^{15} - 10^{30}$; the present diagonalization limit is $\sim 10^4$), and not enough could be known about the Hamiltonian, or deduced from the data, to support such a study. These practical reasons however are essentially irrelevant. The real point is that, just as the introduction of temperature and entropy concepts into mechanics give us a completely new view of things, so also with D3 spectrum which gives an extraordinary "window" through which we can study important aspects of a quantum-chaotic system; indeed it gives by far the best experimental data on quantum chaos available now for any real system. ..... The latter effect weakens, and the resonances broaden, as the neutron energy increases and the resultant overlapping of levels marks the beginning of the true continuum D4. In the lower part of D4 the effects due to underlying resonances can still be observed as Ericson cross-section fluctuations. ..... our study of the D1 - D3 relationship splits into two parts. The first, the 1-point problem, is the extension of the *detailed* D1 spectrum into the *smoothed* level density of D3 and then to other domains both above and below D3. The second part is the study, and comparison with data of the spectral fluctuations ....."

THEORY

GENERAL FEATURES



Typical Spectrum of a Heavy Nucleus

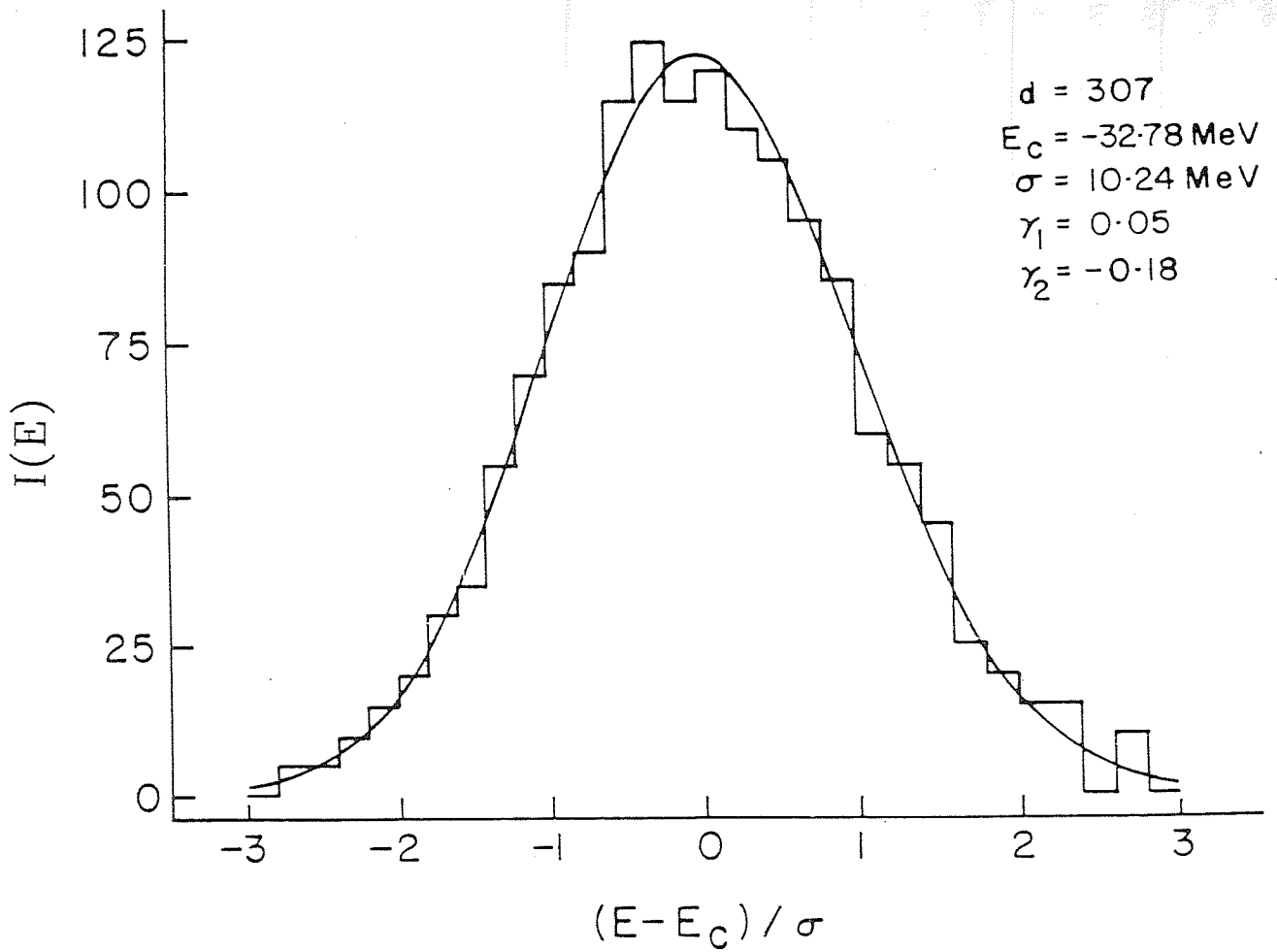
and apply the smoothed (with respect to energy) forms of spectroscopic observables is called spectral averaging theory (SAT) and the resulting method for nuclear spectroscopy studies is often called spectral distribution methods (SDM). The subject matter of this thesis is SAT/SDM.

The fundamental result based on which SAT is developed is that there are central limit theorems (CLT's) operating in nuclear shell model spaces. We begin with state densities. For a non-interacting particle (NIP) system (i.e. ignoring interaction) energies are additive and then the m - particle eigenvalue density (state density $I(E)$) is an m - fold convolution of one-particle density which in general tends to a Gaussian ($\mathcal{G}$), due to CLT, very rapidly as m increases. The remarkable result is that even with interactions, though the energies are no longer additive, state densities take Gaussian form. This feature is demonstrated in an example in Fig. 1.2. The origin of CLT for interacting particle (IP) systems lies in an ensemble representation of the IP hamiltonian (H). As studied by Mon and French [Mo-75], the appropriate ensemble is the so called embedded Gaussian orthogonal ensemble generated (in m - particle spaces) by k - body interactions or EGOE(k) [2]; for nuclear case $k = 2$. With EGOE(k), in the dilute limit ($m \rightarrow \infty$, $N \rightarrow \infty$, $k << m$, $m/N \rightarrow 0$) one sees immediately that the lower order cumulants tend to zero; for example the excess parameter $\gamma_2 \sim -k^2/m \rightarrow 0$ as $m \rightarrow \infty$ and $k << m$. Thus in the CLT limit state densities take a Gaussian form and in practice one can add the skewness and excess corrections (Edgeworth corrections described in Chapter 2) to the Gaussian. Inverting the distribution function

[2] In general in nuclear shell model, EGOE(k) for m ($m > k$) particle systems is generated by defining the H to be GOE in k - particle spaces and then propagating it to m - particle spaces by using the geometry of the shell model spaces.

Figure 1.2

Density of states $I(E)$ (in MeV^{-1}) vs energy E. The histogram is for the shell model results where the calculations are made in $(ds)^{6,J=2\,T=0}$ space with (KUO+^{17}O) interaction [Ku-67]. The smooth curve is the Gaussian approximation. The dimensionality (d) of the space, centroid E_c, variance σ, skewness γ_1 and excess γ_2 are also shown in the figure. Figure is taken from [Ko-89].

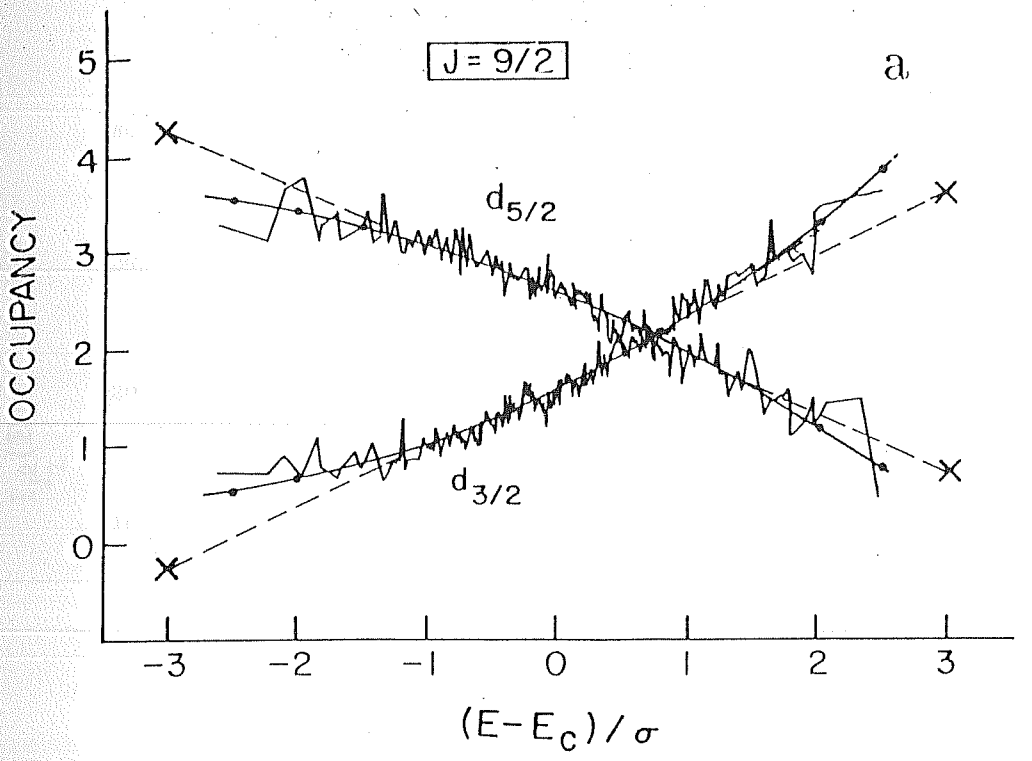

125
100
75
50
25
0
I(E)
-3
-2
-1
0
1
2
3
(E-E_c) / σ
d = 307
E_c = -32·78 MeV
σ = 10·24 MeV
γ_1 = 0·05
γ_2 = -0·18

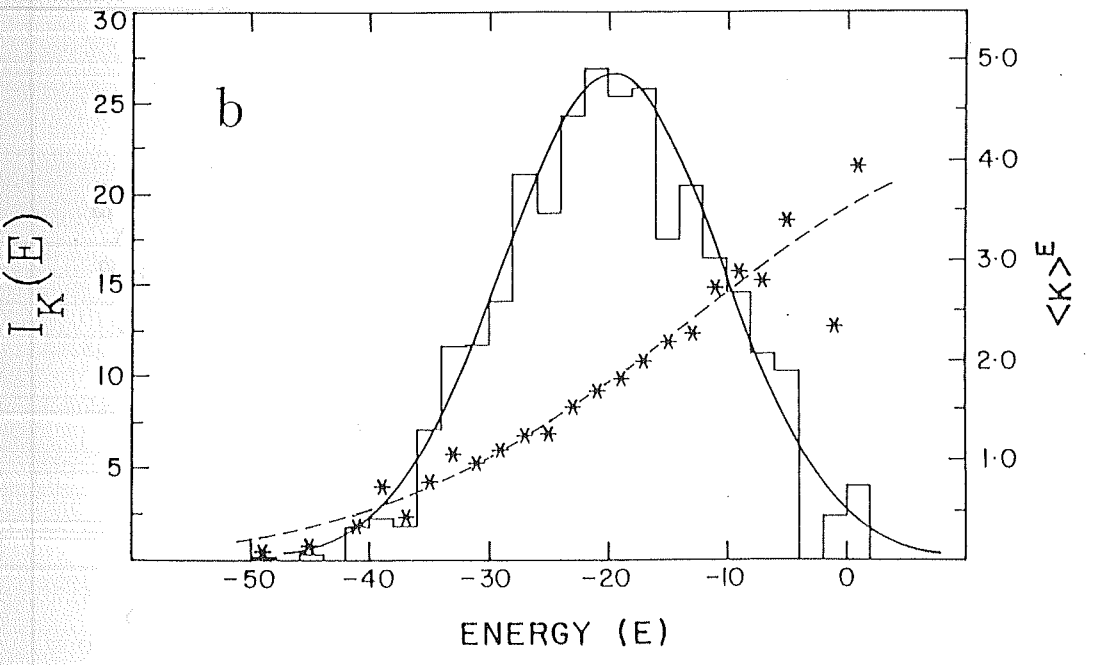
$F(E)$ ($F(E) = \int_{-\infty}^{E} I(E)dE$) gives the smoothed spectrum [Ra-71] with deviations from the corresponding exact ones by $\sim 2\ MeV$ for ds-shell nuclei and even less for heavy nuclei. Using the polynomials defined by the state density or otherwise, lead to CLT forms for expectation values of operators and the corresponding expectation value densities. For operators K for which $H + \alpha K$ (α is a small parameter) has a Gaussian density, then by CLT one has the remarkable result that expectation values ($\langle K \rangle^E$) are linear in energy with the slope given by the correlation coefficient [3] between the operators K and H. An expression for $\langle K \rangle^E$ in terms of orthogonal polynomials defined by the state densities gives this result when truncated at the first two terms, with the remaining terms giving corrections to the CLT result [Dr-77a]. A good example for the linear behavior of expectation values comes from occupancies as shown in Fig. 1.3a. In general for positive definite operators (K is $\mathcal{O}^\dagger\mathcal{O}$ type; $\mathcal{O}$ is a transition operator) the expectation value density ($I_K(E)$) in the CLT limit takes a Gaussian form [Fr-89b, Ko-89] and thus the expectation values can be written as a ratio of two Gaussians; Figs 1.3b, 1.3c give examples for these CLT results. There are in general many other forms or expansions one can derive for expectation values and they will be interrelated as they all are derivable from the traces $\langle H^p \rangle$ and $\langle KH^p \rangle$. In addition to state and expectation value densities, transition strength densities ($\mathbf{I}_\mathcal{O}(E, E')$) also take CLT forms. In general, strength densities take bivariate Gaussian ($BIV - \mathcal{G}$) form

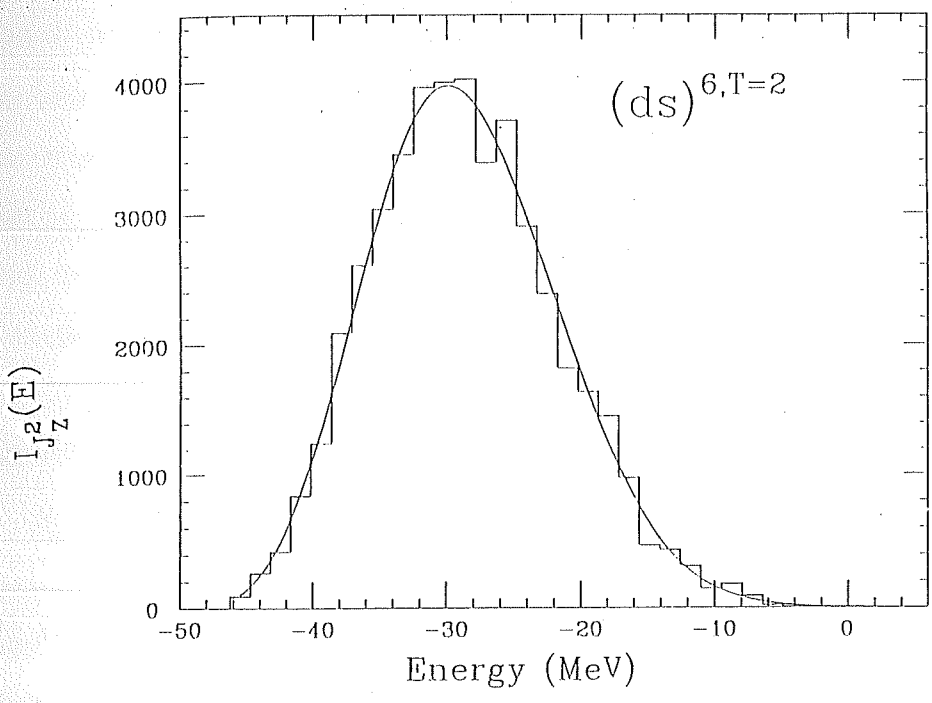
[3] The CLT defines a geometry [Fr-72] with norm $|K|_m$ of an operator K in m - particle spaces defined by $|K|_m = \{\langle (K - \langle K \rangle^m)^\dagger (K - \langle K \rangle^m) \rangle^m\}^{1/2}$ where the m - particle average $\langle X \rangle^m$ of an operator X is $\langle X \rangle^m = \sum_{\alpha \in m} \langle m\alpha | X | m\alpha \rangle / d(m)$; $d(m)$ is the dimensionality of m - particle space and the m - particle trace $\langle\langle X \rangle\rangle^m = d(m)\langle X \rangle^m$. The norm defined here has all the properties of an Euclidean norm. With this geometry, correlation coefficient $\zeta_{K_1 - K_2}$ between two operators K_1 and K_2 is $\zeta_{K_1-K_2}(m) = \langle (K_1 - \langle K_1 \rangle^m)^\dagger (K_2 - \langle K_2 \rangle^m) \rangle^m / (|K_1|_m |K_2|_m)$.

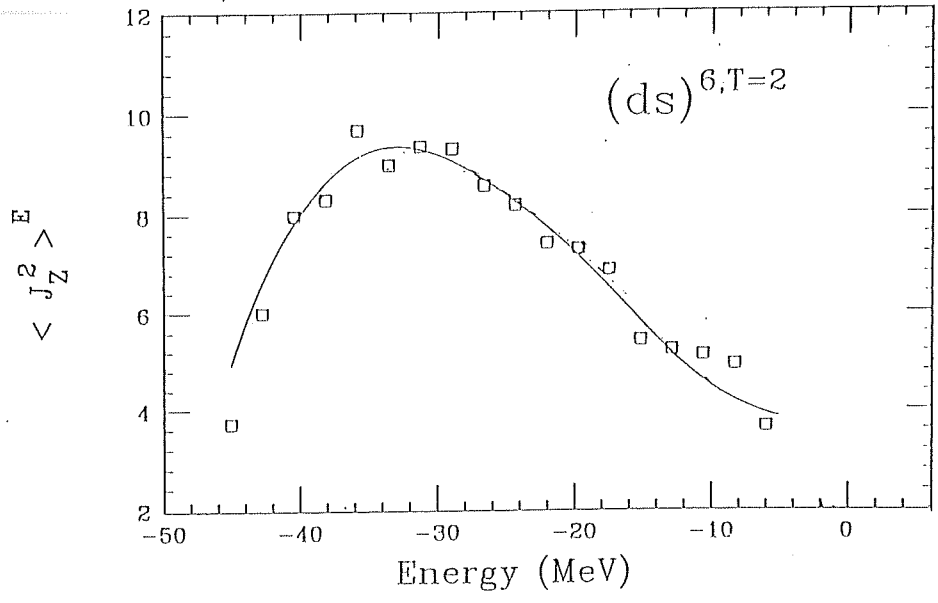
Figure 1.3

Comparison of shell model results with the CLT results (with or without corrections) for expectation values and expectation value densities. (a) $d_{5/2}$ and $d_{3/2}$ orbit occupancies vs energy. The calculations are in $(ds)^{5,T=1/2}$ space and the plots are for $J = 9/2$. The wavy line represents the shell model results, - - - - line is for the CLT result (linear form derived from the polynomial expansion) and • — • — •— is by including the higher order terms in the polynomial expansion. Although the CLT (with and without corrections) results shown in the figure are obtained using the polynomial expansion, essentially similar results are also obtained by using the CLT results (Gaussian or Gaussian with Edgeworth correction) for the occupancy densities. Figure is taken from [Ko-85]. (b) $I_K(E)$ vs E and $\langle K \rangle^E$ vs E for Gamow - Teller sum-rule operator K. The energy E is in MeV. The spectroscopic space used is $(ds)^5$ and the results are for the transition (J,T) = (3/2, 1/2) to (5/2, 3/2). The dimensionality (d) of the (3/2, 1/2) space is 188. The shell model $I_K(E)$ density is shown in bins of width 2 MeV and the continuous curve is its Gaussian (CLT) representation. Similarly $\star$'s are shell model results for $\langle K \rangle^E$ and the dashed curve is its CLT approximation (ratio of the expectation value and state density Gaussians). Figure is taken from [Ko-89]. (c) Spin-cutoff density $I_{J_Z^2}(E)$ and spin-cutoff factor $\langle J_Z^2 \rangle^E$ vs E. The histogram and the boxes are shell model results and the continuous curves are the CLT results including Edgeworth corrections to the densities (the state and spin-cutoff densities are Gaussians in the CLT limit). The histogram (exact shell model) for the spin-cutoff density is constructed by averaging over a bin size of $0.2\sigma \sim 1.5\ MeV$, σ is the spectrum width. Similarly the boxes for the spin-cutoff factors are constructed by averaging over a bin size of $0.3\sigma \sim 2.3\ MeV$. All the calculations are carried out using KUO + ^{17}O interaction [Ku-67]. One sees from the figures that the CLT results (with corrections) are in excellent confirmity with the shell model results. Figure is taken from [Fr-89b].


J = 9/2
a
OCCUPANCY
$d_{5/2}$
$d_{3/2}$
$(E-E_c)/\sigma$


b
$I_K(E)$
$\langle K \rangle_E$
ENERGY (E)


$(ds)^{6,T=2}$
$I_{J_Z^2}(E)$
4000
3000
2000
1000
0
−50
−40
−30
−20
−10
0
Energy (MeV)


$(ds)^{6,T=2}$
$< J_Z^2 >^E$
12
10
8
6
4
2
−50
−40
−30
−20
−10
0
Energy (MeV)

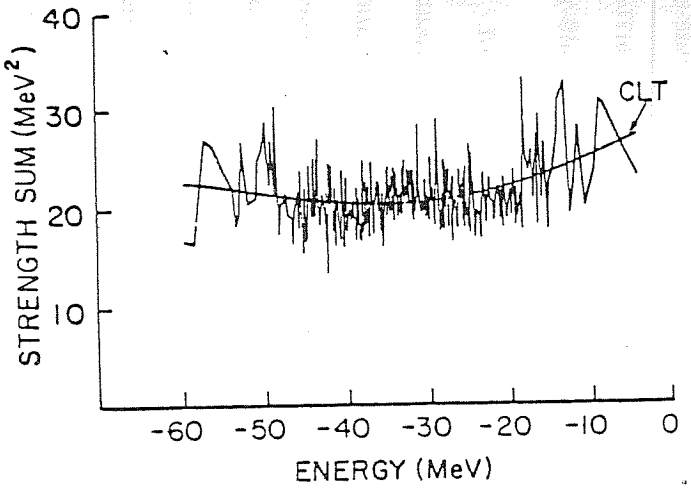
c

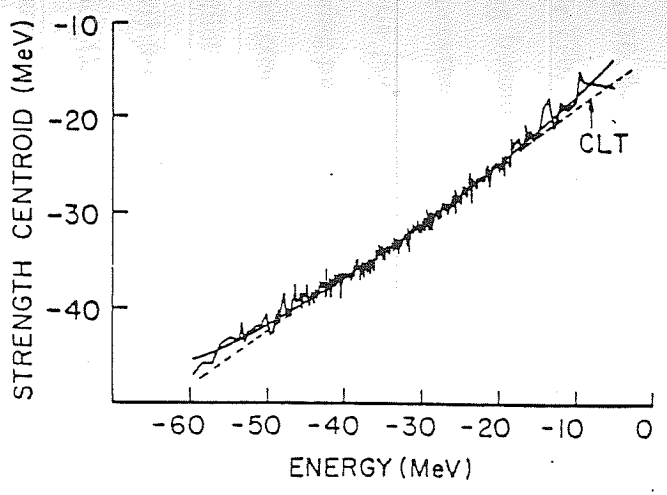
and its origin can be understood by using ensemble (EGOE) representation for both the hamiltonian and the transition operators [Fr-88b]. This leads to the important results that the strength sum (originating from an energy E) will be a ratio of two Gaussians, the strength centroids will be linear in energy with slope given by the bivariate correlation coefficient and the strength width a constant. Fig. 1.4 gives a shell model example for these results. In addition, the CLT result for strength densities provides an understanding of the CLT result for $I_K(E)$.

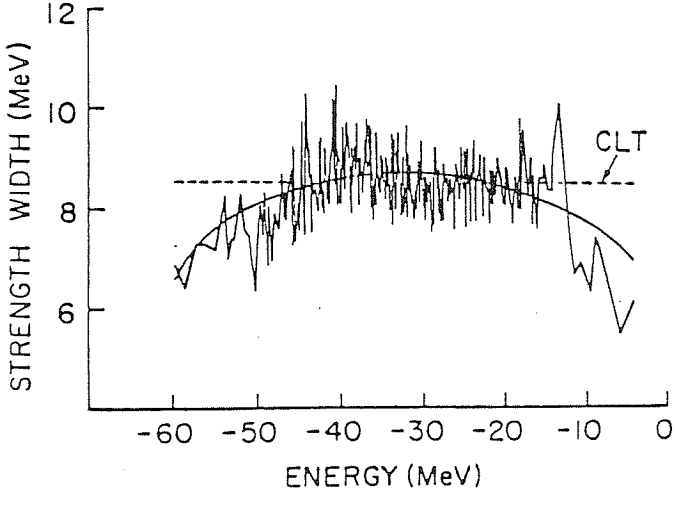
The CLT results described above are in general valid only in strongly interacting shell model subspaces, i.e. essentially in $0\hbar\omega$ spaces (for example: $(ds)^8$ for ^{24}Mg and $(fp)^{16}$ for ^{56}Fe). It should be stressed that the CLT forms involve traces of products of lower order powers of operators (e.g. $I_{\mathcal{G}}(E)$ is defined in terms of $\langle H\rangle$, $\langle H^2\rangle$; $I_{K;\mathcal{G}}(E)$ by $\langle KH\rangle$, $\langle KH^2\rangle$; $\mathbf{I}_{\mathcal{O};BIV-\mathcal{G}}(E,E')$ by $\langle \mathcal{O}^\dagger H^P \mathcal{O} H^Q\rangle$ with $P+Q \leq 2$ etc.). The shell model $(0\hbar\omega)$ spaces can be partitioned into subspaces and then the state and expectation value densities decompose similarly, though there are some complications with strength densities, and the CLT results extend to the partitioned subspaces. The partitioning, on one hand takes into account the departures from CLT (smooth) forms and on the other hand brings in more information and fine structures. Much of this works in practice as the trace information propagates i.e. many particle traces can be expressed in terms of the few particle input traces, when the partitioning is done using group symmetries that can be realized in shell model spaces; for example using spherical configuration group which is a direct sum group of unitary groups, Wigner supermultiplet $SU(4)$ group etc. With this, SAT provides a formalism for addressing wide variety of nuclear structures problems. Some of the studies that are carried out in literature

Figure 1.4

Strength sum, strength centroid and strength width vs energy. The dashed curves correspond to the bivariate Gaussian (CLT) approximation for the strength density, the solid curve by including the bivariate Edgeworth corrections (given by (2.21) in Chapter 2 ahead) and the wavy curve corresponds to exact shell model results. The hamiltonian is KUO + ^{17}O interaction [Ku-67], the transition operator is the unitary two-body part ($\nu = 2$ part defined ahead in Chapter 2) of H and the space is the 307 dimensional $(ds)^{6,J=2\,T=0}$. Figure is taken from [Fr-88b].


STRENGTH SUM (MeV²)
40
30
20
10
CLT
-60 -50 -40 -30 -20 -10 0
ENERGY (MeV)


STRENGTH CENTROID (MeV)
-10
-20
-30
-40
CLT
-60 -50 -40 -30 -20 -10 0
ENERGY (MeV)


STRENGTH WIDTH (MeV)
12
10
8
6
CLT
-60 -50 -40 -30 -20 -10 0
ENERGY (MeV)

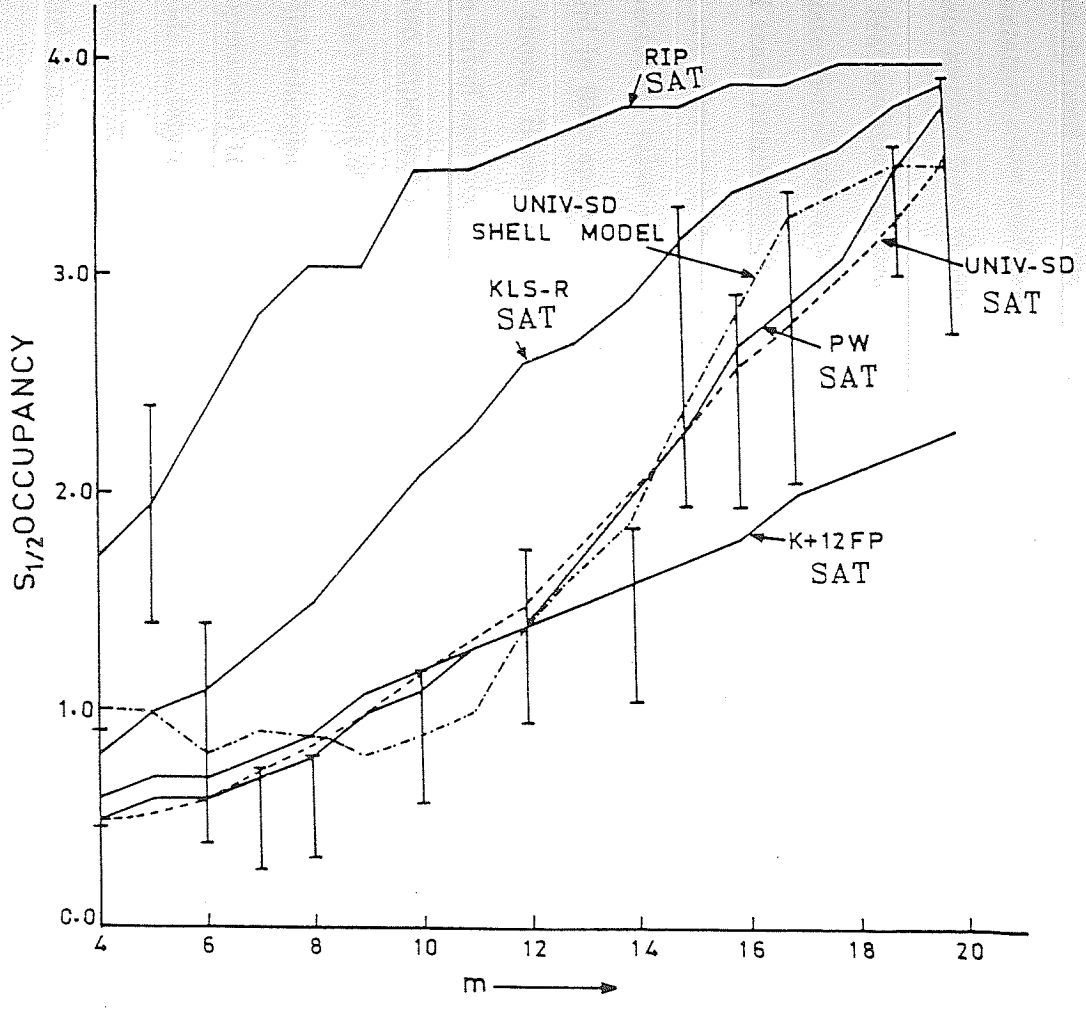
include: (i) binding energies of ds and fp-shell nuclei [Ch-71, Pa-78, Wo-86, Sa-87a]; (ii) spherical orbit occupancies for ds and fp-shell nuclei [Ch-71, Po-76, Ko-79a, Ko-82, Sa-87b]; (iii) Electromagnetic (EM) sumrules [Dr-75, Dr-77b, Ha-79, Ha-82a, Ha-82b] which include the Kurath sum rule, deriving bounds on EM summed strengths etc.; (iv) comparison and analysis of operators using the geometry (norms and correlation coefficients) defined by CLT [Ch-71, Po-77, Ko-79b, Ch-80]; (v) investigating goodness of symmetries using partial densities and their moments defined over subspaces generated by the group symmetries, good examples are the studies involving Wigner $SU(4)$, Elliot $SU(3)$ and pairing $Sp(N)$ groups [Fr-71b, Qu-74, Qu-75, Pa-78, Ch-80]; (vi) β-decay sum rule strengths and strength distributions [Ka-81, Sa-88; see also Chapter 6 ahead]; (vii) predicting collectivities [Dr-77a, Dr-77b]. As an example of the application of SAT, the analysis of $s_{1/2}$ orbit occupancies of ds-shell nuclei is shown in Fig. 1.5. The large number of studies that are carried out in $0\hbar\omega$ spaces, essentially upto 1980, are well documented [Fr-67, Fr-69a, Fr-72, Pa-78, Fr-79, Da-80, Fr-82, Fr-83a, Wo-86, Ko-89].

Recent progress in statistical spectroscopy is in deriving and applying the smoothed forms in indefinitely large shell model spaces with *interactions* by using unitary group decompositions (of hamiltonians and the spectroscopic spaces), CLT's locally, and convolutions [4] [Fr-83b, Fr-88b, Fr-89a, Fr-89b, Fr-94]. In the resulting spectral averaging theory in large shell model spaces (SAT-LSS), it is seen that the essential role of interactions is to produce local spreadings of the non-interacting particle (NIP) densities and the spreadings

[4] Convolution of two functions A and B is denoted as $A \otimes B[x] = \int_{-\infty}^{+\infty} A(y)B(x-y)dy$.

Figure 1.5

$s_{1/2}$ - ground state occupancies in SAT calculated using UNIV-SD [Wi-84], PW [Pr-72], RIP [Ha-71], KLS-R [Ka-69] and K+12FP [Ha-71] interactions compared with experimental values. The results for PW, RIP, K+12FP and KLS-R interactions and the compilation of experimental data are from [Po-76]. The results of UNIV-SD interaction are from [Sa-87b]. The analysis shown in the figure clearly demonstrates that one should exclude RIP, KLS and K+12FP interactions and favor PW and UNIV-SD interactions. The shell model results for UNIV-SD interaction show that the spectral method reproduces very well the shell model results which in turn are very close to data. All the spectral averaging calculations are done using spherical orbit configuration partitioning. Figure is taken from [Sa-87b].


RIP
/SAT
UNIV-SD
SHELL MODEL
KLS-R
SAT
UNIV-SD
SAT
PW
SAT
K+12FP
SAT
$S_{1/2}$OCCUPANCY
4.0
3.0
2.0
1.0
0.0
4
6
8
10
12
14
16
18
20
m

are in general Gaussian in nature. With SAT-LSS one can calculate level densities, orbit occupancies, spin-cutoff factors [5] and other statistical observables where one needs to go beyond $0\hbar\omega$ spaces. *The aim of the present thesis is to study (and test) some aspects of this extended theory (SAT-LSS) for state, expectation value and strength densities in large spaces and apply them to calculate nuclear level densities and β-decay rates.* We will now give a preview.

Mathematical preliminaries regarding the properties of univariate and bivariate distributions, unitary group decompositions of operators, partitioning and trace propagation formulas (for cases that are of relevance for the thesis) are given in Chapter 2 along with the mathematical definitions of state, expectation value and strength densities and the corresponding CLT results (valid in $0\hbar\omega$ spaces). The results given in Chapter 2 are used throughout the thesis. Besides giving a brief overview of the convolution form for state, spin-cutoff and occupancy densities in SAT-LSS, results of systematic studies of two important aspects of SAT-LSS are given in Chapter 3 – these studies are: (a) a part of the interaction that produces non-NIP like shifts of the single particle energies, that is neglected in the theory, is demonstrated (using norms of operators) to be indeed small all across the periodic table by considering a wide variety of effective interactions; (b) moment methods for constructing locally smoothed forms for NIP state, spin-cutoff and occupancy densities are tested in a large space example including 16 spherical orbits and considering

[5] Level densities $I_\ell(E)$ count the number of levels per MeV at the given energy E; this definition can be extended for fixed angular momentum (J) and/or parity level densities (see Chapter 4 and Appendix C ahead). Spin-cutoff factors $\sigma_J^2(E)$ are nothing but the expectation values of J_Z^2 (Z - component of angular momentum J operator) operator; $\sigma_J^2(E) = \langle J_Z^2 \rangle^E$ and this definition can be extended for fixed parity spin-cutoff factors (see Appendix C ahead). Spin-cutoff factors decompose state densities into observable level densities. Finally orbit occupancies are defined by the expectation values $\langle n_\alpha \rangle^E$ where n_α is the number operator for the orbit α.

a realistic proton - neutron system. Using the convolution forms for state and spin-cutoff densities, first systematic analysis of level densities is carried out for eight fp-shell nuclei (meaningful data exist only for the eight nuclei considered) and a magnitude parameter of the effective nucleon-nucleon interaction is deduced for ^{55}Mn, ^{56}Fe, ^{59}Co, ^{60}Co and ^{60}Ni isotopes by carrying out calculations in a 8-orbit shell model space and for ^{62}Ni, ^{63}Cu and ^{65}Cu isotopes in a 10-orbit shell model space. The calculations include upto $2\hbar\omega$ excitations. The results of the fp-shell analysis are given in Chapter 4. The experimental data for all the eight fp-shell nuclei are compiled in Appendix C. Going beyond state and expectation value densities, in SAT-LSS the bivariate strength densities take a convolution form with the non-interacting particle (NIP) strength density being convoluted with a spreading bivariate Gaussian due to interactions. In order to apply this result in practice, leaving aside the question of determining the parameters of the spreading bivariate Gaussian, one needs good methods for constructing the NIP bivariate strength densities ($\mathbf{I}_O^h$) in large shell model spaces. In Chapter 5 a formalism for constructing $\mathbf{I}_O^h$ is developed for one-body transition operators by using spherical orbits and spherical configurations. For rapid construction and also for applying the statistical theory in large shell model spaces, $\mathbf{I}_O^h$ is decomposed into partial densities defined by unitary orbit configurations (unitary orbit is a set of spherical orbits). Trace propagation formulas for the bivariate moments M_{rs} with $r + s \leq 2$ of the partial NIP strength densities, which will determine the Gaussian representation, are derived and the goodness of the Gaussian representation is tested in a large space numerical example using Gamow - Teller (GT) β^- transition operator. Trace propagation formulas for M_{rs} with $r + s \leq 4$ are also derived in m-particle scalar spaces which are useful for

many purposes. Construction of level densities and β-decay strength densities (in some cases even occupancy densities) have very important applications in nuclear astrophysics problems [Wo-80a]. As a first application of SAT-LSS in this important area, in Chapter 6 a method to calculate temperature dependent β-decay rates is developed by writing the expression for the rates explicitly in terms of bivariate GT strength densities for a given hamiltonian and state densities of the parent nucleus besides having the usual phase space factors. Constructing NIP GT - strength densities using the theory developed in Chapter 5, together with a simple prescription for generating the spreading bivariate Gaussians, the bivariate GT densities are constructed. Applying this theory, β-decay rates of some neutron excess fp-shell nuclei, relevant for massive presupernova stars, are calculated at presupernova matter densities, temperatures and electron fractions. In addition, the convolution form for GT densities led to a simple expression for calculating GT non-energy weighted summed strengths. Finally Chapter 7 gives concluding remarks and future outlook [6].

[6]The cut-off date for the references given in the thesis is July 1^{st}, 1994; the synopsis of this thesis was defended on July 1^{st} at the Physical Research Laboratory, Ahmedabad.

Chapter 2

Some Mathematical Aspects of Spectral Averaging Theory

2.1 Preview

In spectral averaging theory, as briefly described in Chapter 1, one derives and applies smoothed forms for state, expectation value and strength densities. In Sect. 2.2 some important properties of univariate (that characterize for example state and expectation value densities) and bivariate (that characterize for example strength densities) distributions, well known to statisticians [Ke-69], are given. The definitions, in terms of a given hamiltonian H and m-particle spectroscopic spaces, of state, expectation value and strength densities, their moments and the corresponding CLT results are given in Sect. 2.3. Spherical and unitary configurations partitioning of m-particle scalar spaces and the corresponding decompositions of various densities into partial densities, which play a special role in SAT-LSS are introduced in Sect. 2.4. An important ingredient of spectral theory which plays a vital role in the result presented in Chapters 3 - 6 and also which is essential for deriving trace propagation

formulas that enable one to calculate moments is the unitary group (tensorial) decomposition of operators and this is briefly described with examples in Sect. 2.5. Finally the basic elements of trace propagation and some important trace propagation formulas are given in Sect. 2.6. The results given in Sects. 2.3 - 2.6 are limited to those that are essential for following Chapters 3 - 6 and it should be mentioned that all the results in this chapter are borrowed from available literature.

2.2 Statistical distributions

2.2.1 Univariate distributions

Given a univariate probability density function (or simply density) $\rho(x)$, at the outset it is assumed that, it is positive definite and normalized to unity,

$$\int_{-\infty}^{+\infty} \rho(x)dx = 1 \ ,$$
$$\rho(x) > 0 \, ; \ -\infty \leq x \leq +\infty \tag{2.1}$$

The characteristic function $\phi(t)$ which is the Fourier transform of $\rho(x)$, define the moments M_r of $\rho(x)$,

$$\begin{aligned} \phi(t) &= \int_{-\infty}^{+\infty} exp(itx)\rho(x)dx = \sum_r \frac{(it)^r}{r!} M_r \\ M_r &= \int_{-\infty}^{+\infty} \rho(x)x^r dx. \end{aligned} \tag{2.2}$$

The centroid ϵ that defines the location is given by $\epsilon = M_1$. Then the central moments $\mathcal{M}_r$ are given by

$$\begin{aligned} \mathcal{M}_r &= \int_{-\infty}^{+\infty} (x-\epsilon)^r \rho(x)dx \\ &= \sum_{p=0}^{r} \binom{r}{p} (-1)^{r-p} M_p \, \epsilon^{r-p} \end{aligned} \tag{2.3}$$

The second equality in the above equation gives the relationship between central and non-central moments. The width σ, of $\rho(x)$, that defines the scale is given by $\sigma = \mathcal{M}_2^{1/2}$ and the variance $\sigma^2 = \mathcal{M}_2$. Just as M_r's derive from $\phi(t)$, the cumulants K_r derive from $\ell n\, \phi(t)$ and they are related to the central moments $\mathcal{M}_r$; $\ell n\, \phi(t) = \sum_{r>0} \frac{(it)^r}{r!} K_r$. Similarly, the reduced central moments $\mu_r = \frac{\mathcal{M}_r}{\sigma^r}$,

$$\mu_r = \int_{-\infty}^{+\infty} \left(\frac{x-\epsilon}{\sigma}\right)^r \rho(x)dx \tag{2.4}$$

define the reduced cumulants $k_r = K_r/\sigma^r$. It is useful to point out that the cumulants K_r add under convolution. Before giving the relationship between K_r's and $\mathcal{M}_r$'s and other details, let us define the Gaussian density $\rho_{\mathcal{G}}(x)$ and the standard Gaussian $\eta_{\mathcal{G}}(\widehat{x})$ which involves standardized variable $\widehat{x}$,

$$\begin{aligned}
\rho_{\mathcal{G}}(x) &= \frac{1}{\sqrt{2\pi}\sigma} exp\left\{-\frac{(x-\epsilon)^2}{2\sigma^2}\right\}; \\
\eta_{\mathcal{G}}(\widehat{x}) &= \frac{1}{\sqrt{2\pi}} exp\left\{-\frac{\widehat{x}^2}{2}\right\} \\
\widehat{x} &= (x - M_1)/(M_2 - M_1^2)^{1/2} = (x-\epsilon)/\sigma\,, \\
\rho_{\mathcal{G}}(x)dx &= \eta_{\mathcal{G}}(\widehat{x})d\widehat{x}.
\end{aligned} \tag{2.5}$$

One very important property is that all the cumulants K_r $(r > 2)$ are zero for a Gaussian. This follows from the results that $\mu_r = 0$ for r odd and $\mu_r = (r-1)!!$ for r even for a Gaussian density. Therefore $K_r (r > 2)$ are called shape parameters and in particular, $k_3 = \gamma_1$ is called skewness and $k_4 = \gamma_2$ is the excess. The relationships between the cumulants $(K_r,\, k_r)$ and the reduced central moments μ_r are (for $r \leq 6$),

$$\begin{aligned}
&K_1 = \epsilon, \quad K_2 = \sigma^2, \quad k_3 = \mu_3, \quad k_4 = \mu_4 - 3 \\
k_5 &= \mu_5 - 10\mu_3, \quad k_6 = \mu_6 - 15\mu_4 - 10\mu_3^2 + 30
\end{aligned} \tag{2.6}$$

In general, one can seek an expansion of a given distribution ρ in terms of the cumulants k_r, by starting with the Gaussian density $\rho_{\mathcal{G}}$,

$$\begin{aligned} \rho(x)dx &= \eta(\hat{x})d\hat{x}, \\ \eta(\hat{x}) &= exp\left\{\sum_{r\geq 3}\frac{(-1)^r}{r!}k_r D_{\hat{x}}^r\right\}\eta_{\mathcal{G}}(\hat{x}) \end{aligned} \tag{2.7}$$

The Edgeworth (Ed) expansion which is asymptotically convergent assumes that the cumulants $k_r \propto 1/p^{r-2}$ for $r \geq 3$ where p is a parameter of the system under consideration. Collecting terms upto order $1/p$ in (2.7) (thus incorporating γ_1, γ_2 corrections) gives the Edgeworth corrected Gaussian which is denoted by η_{Ed},

$$\eta_{Ed}(\hat{x}) = \eta_{\mathcal{G}}(\hat{x})\left\{1 + \left[\frac{\gamma_1}{6}He_3(\hat{x})\right] + \left[\frac{\gamma_2}{24}He_4(\hat{x}) + \frac{\gamma_1^2}{72}He_6(\hat{x})\right]\right\} ,$$

$$He_0(\hat{x}) = 1,\ He_1(\hat{x}) = \hat{x},\ He_2(\hat{x}) = \hat{x}^2 - 1,$$

$$He_3(\hat{x}) = \hat{x}^3 - 3\hat{x},\ He_4(\hat{x}) = \hat{x}^4 - 6\hat{x}^2 + 3,$$

$$He_5(\hat{x}) = \hat{x}^5 - 10\hat{x}^3 + 15\hat{x},$$

$$He_6(\hat{x}) = \hat{x}^6 - 15\hat{x}^4 + 45\hat{x}^2 - 15 \tag{2.8}$$

In (2.8) $He_r(\hat{x})$ are Hermite polynomials. In applying (2.7) and (2.8) it should be kept in mind that the centroid and the width of $\rho(x)$ and $\rho_{\mathcal{G}}(x)$ should be kept identical. Finally, it is useful to mention that corresponding to a given $\rho(x)$, one can define a set of orthonormal polynomials $P_\mu(x)$ such that $\int_{-\infty}^{+\infty} P_\mu(x)P_\nu(x)\rho(x)dx = \delta_{\mu\nu}$. Explicit form of the polynomials $P_\mu(x)$ in terms of the moments of $\rho(x)$ is

$$P_\mu(x) = [D_\mu D_{\mu-1}]^{-1/2}\begin{vmatrix} 1 & M_1 & - & - & - & M_\mu \\ M_1 & M_2 & - & - & - & M_{\mu+1} \\ - & - & - & - & - & - \\ - & - & - & - & - & - \\ M_{\mu-1} & M_\mu & - & - & - & M_{2\mu-1} \\ 1 & x & x^2 & - & - & x^\mu \end{vmatrix} ;$$

$$D_\mu = \begin{vmatrix} 1 & M_1 & - & - & - & M_\mu \\ M_1 & M_2 & - & - & - & M_{\mu+1} \\ - & - & - & - & - & - \\ - & - & - & - & - & - \\ M_\mu & M_{\mu+1} & - & - & - & M_{2\mu} \end{vmatrix} \tag{2.9}$$

For example $P_1(x)$ and $P_2(x)$ for a given density $\rho(x)$ are $P_1(x) = \hat{x}$, $P_2(x) = (\hat{x}^2 - \gamma_1\hat{x} - 1)/(\gamma_2 + 2 - \gamma_1^2)^{1/2}$. The Hermite polynomials $He_\mu(\hat{x}) = (-1)^\mu \eta_G^{-1}(\hat{x})$ $\frac{\partial^\mu}{\partial \hat{x}^\mu}\eta_G(\hat{x})$ are in fact orthogonal polynomials with respect to the standard Gaussian $\eta_G(\hat{x})$.

2.2.2 Bivariate distributions

Many of the properties of bivariate distributions are similar to that of univariate distributions and therefore much of the discussion in this subsection is in the same lines as in the previous subsection. Given a bivariate joint probability density (or simply a bivariate density) $\rho(x_1, x_2)$, at the outset it is assumed that it is positive definite and normalized to unity,

$$\int_{-\infty}^{+\infty}\int \rho(x_1, x_2)dx_1dx_2 = 1,$$

$$\rho(x_1, x_2) \geq 0\,;\ -\infty \leq x_1 \leq +\infty,\ -\infty \leq x_2 \leq +\infty\,. \tag{2.10}$$

The Fourier transform of $\rho(x_1, x_2)$ gives the bivariate characteristic function $\phi(t_1, t_2)$ whose expansion in powers of t_1 and t_2 defines the bivariate moments M_{rs} and a simple expression for M_{rs} is,

$$M_{rs} = \int_{-\infty}^{+\infty}\int x_1^r x_2^s \rho(x_1, x_2)dx_1dx_2. \tag{2.11}$$

The eigenvalue density $\rho_1(x_1)$ of x_1 is $\rho_1(x_1) = \int_{-\infty}^{+\infty} \rho(x_1, x_2) dx_2$ and in connection with $\rho(x_1, x_2)$, it is referred to as the marginal density (similarly $\rho_2(x_2)$ is defined). The centroids $\epsilon_1(\epsilon_2)$ of the marginal densities $\rho_1(\rho_2)$ are related to the moments M_{rs} by the relations $\epsilon_1 = M_{10}$ and $\epsilon_2 = M_{01}$. The bivariate central moments $\mathcal{M}_{rs}$ are given by,

$$\mathcal{M}_{rs} = \int_{-\infty}^{+\infty} \int (x_1 - M_{10})^r (x_2 - M_{01})^s \rho(x_1, x_2) dx_1 dx_2 \qquad (2.12)$$

and it is easy to write $\mathcal{M}_{rs}$ in terms of the non-central moments M_{rs}. The $\sigma_1 = \mathcal{M}_{20}^{1/2}$ and $\sigma_2 = \mathcal{M}_{02}^{1/2}$ are the widths of the marginal densities $\rho_1(x_1)$ and $\rho_2(x_2)$ respectively. The central moments $\mathcal{M}_{rs}$ define the bivariate cumulants K_{rs}; K_{rs} derive from $\ell n\, \phi(t_1, t_2)$ just as M_{rs} derive from $\phi(t_1, t_2)$. Similarly the bivariate reduced central moments $\mu_{rs} = \mathcal{M}_{rs}/\sigma_1^r \sigma_2^s$,

$$\mu_{rs} = \int_{-\infty}^{+\infty} \int \left(\frac{x_1 - M_{10}}{\sigma_1}\right)^r \left(\frac{x_2 - M_{01}}{\sigma_2}\right)^s \rho(x_1, x_2) dx_1 dx_2 \,, \qquad (2.13)$$

define the reduced cumulants $k_{rs} = K_{rs}/\sigma_1^r \sigma_2^s$. The k_{11} cumulant defines the bivariate correlation coefficient ζ,

$$\zeta = k_{11} = \mu_{11} = \int_{-\infty}^{+\infty} \int \left(\frac{x_1 - \epsilon_1}{\sigma_1}\right) \left(\frac{x_2 - \epsilon_2}{\sigma_2}\right) \rho(x_1, x_2) dx_1 dx_2 \,. \qquad (2.14)$$

Before going further let us first introduce the bivariate Gaussian density $\rho_{BIV-\mathcal{G}}$ which is defined in terms of the five variables (ϵ_1, ϵ_2, σ_1, σ_2, ζ),

$$\rho_{BIV-\mathcal{G}}(x_1, x_2) = \frac{1}{2\pi\sigma_1\sigma_2\sqrt{1-\zeta^2}} \times$$

$$exp\left\{ - \frac{\left[\left(\frac{x_1 - \epsilon_1}{\sigma_1}\right)^2 - 2\zeta\left(\frac{x_1 - \epsilon_1}{\sigma_1}\right)\left(\frac{x_2 - \epsilon_2}{\sigma_2}\right) + \left(\frac{x_2 - \epsilon_2}{\sigma_2}\right)^2\right]}{2(1-\zeta^2)} \right\} \qquad (2.15)$$

One very important property is that k_{rs} for $r+s \geq 3$ are all zero for a bivariate Gaussian. In Chapters 3 - 6 the suffix BIV is dropped whenever there is no confusion. The standard bivariate Gaussian $\eta_{\mathcal{G}}(\hat{x}_1, \hat{x}_2)$ and the relationship between $\eta_{\mathcal{G}}$ and $\rho_{\mathcal{G}}$, involving the standardized variables $(\hat{x}_1, \hat{x}_2)$; $\hat{x}_1 = (x_1 - \epsilon_1)/\sigma_1$, $\hat{x}_2 = (x_2 - \epsilon_2)/\sigma_2$, are

$$\begin{aligned} \rho_{\mathcal{G}}(x_1, x_2)dx_1dx_2 &= \eta_{\mathcal{G}}(\hat{x}_1, \hat{x}_2)d\hat{x}_1d\hat{x}_2\,, \\ \eta_{\mathcal{G}}(\hat{x}_1, \hat{x}_2) &= \frac{1}{2\pi\sqrt{(1-\zeta^2)}} exp\left\{-\frac{\hat{x}_1^2 - 2\zeta\hat{x}_1\hat{x}_2 + \hat{x}_2^2}{2(1-\zeta^2)}\right\} \end{aligned} \tag{2.16}$$

Following (2.16), $\rho(x_1, x_2)$ is expressible in terms of $\eta(\hat{x}_1, \hat{x}_2)$ where,

$$\eta(\hat{x}_1, \hat{x}_2)d\hat{x}_1d\hat{x}_2 = \rho(x_1, x_2)dx_1dx_2 \tag{2.17}$$

For a general bivariate density $\rho(x_1, x_2)$ the higher order cumulants (shape parameters) k_{rs} for $r+s \geq 3$ are non-zero and it is easy to write down k_{rs} in terms of μ_{rs} (or $\mathcal{M}_{rs}$). The relationships for $r+s \leq 4$ are (see [Ke-69] for more details),

$$\begin{gathered} K_{10} = M_{10} = \epsilon_1, \quad K_{01} = M_{01} = \epsilon_2, \\ K_{20} = \mathcal{M}_{20} = \sigma_1 \quad K_{02} = \mathcal{M}_{02} = \sigma_2 \\ k_{11} = \mu_{11} = \zeta \\ k_{30} = \mu_{30}, \quad k_{21} = \mu_{21}, \quad k_{12} = \mu_{12}, \quad k_{03} = \mu_{03} \\ k_{40} = \mu_{40} - 3, \quad k_{31} = \mu_{31} - 3\zeta, \quad k_{22} = \mu_{22} - 1 - 2\zeta^2 \\ k_{13} = \mu_{13} - 3\zeta, \quad k_{04} = \mu_{04} - 3 \end{gathered} \tag{2.18}$$

Once again it should be pointed out that the bivariate cumulants K_{rs} add under bivariate convolution. Starting from a bivariate Gaussian density $\rho_{\mathcal{G}}$, one can seek an expansion of a general distribution ρ in terms of the cumulants k_{rs} using (2.18) and

$$\eta(\hat{x}_1, \hat{x}_2) = exp\left\{\sum_{r+s\geq 3} \frac{(-1)^{r+s}}{r!s!} k_{rs} D^r_{\hat{x}_1} D^s_{\hat{x}_2}\right\} \eta_{\mathcal{G}}(\hat{x}_1, \hat{x}_2) \tag{2.19}$$

The bivariate Ed expansion, which is asymptotically convergent, starts with the assumption that the cumulants $k_{rs} \propto 1/p^{r+s-2}$ for $r+s \geq 3$ where p is a parameter of the system described by $\rho(x_1, x_2)$, i.e. the existence of p is assumed. Expanding the exponential in (2.19) and collecting terms to orders $p^{-1/2}$, p^{-1}, $p^{-3/2}$, p^{-2} etc. give the Ed expansion in powers of $p^{-1/2}$. Using the bivariate Hermite polynomials $He_{m_1 m_2}(\hat{x}_1, \hat{x}_2)$,

$$He_{m_1 m_2}(\hat{x}_1, \hat{x}_2)\eta_{\mathcal{G}}(\hat{x}_1, \hat{x}_2) = (-1)^{m_1+m_2} \frac{\partial}{\partial \hat{x}_1^{m_1}} \frac{\partial}{\partial \hat{x}_2^{m_2}} \eta_{\mathcal{G}}(\hat{x}_1, \hat{x}_2), \tag{2.20}$$

the Ed expansion to order $1/p$ (here one needs k_{rs} with $r+s \leq 4$) is explicitly given by (hereafter denoted as η_{BIV-Ed} or ρ_{BIV-Ed}),

$$\begin{aligned}
\eta_{BIV-Ed}(\hat{x}_1, \hat{x}_2) &= \left\{1 + \left(\frac{k_{30}}{6} He_{30}(\hat{x}_1, \hat{x}_2) + \frac{k_{21}}{2} He_{21}(\hat{x}_1, \hat{x}_2)\right.\right. \\
&+ \left.\frac{k_{12}}{2} He_{12}(\hat{x}_1, \hat{x}_2) + \frac{k_{03}}{6} He_{03}(\hat{x}_1, \hat{x}_2)\right) \\
&+ \left(\left\{\frac{k_{40}}{24} He_{40}(\hat{x}_1, \hat{x}_2) + \frac{k_{31}}{6} He_{31}(\hat{x}_1, \hat{x}_2)\right.\right. \\
&+ \left.\left.\frac{k_{22}}{4} He_{22}(\hat{x}_1, \hat{x}_2) + \frac{k_{13}}{6} He_{13}(\hat{x}_1, \hat{x}_2) + \frac{k_{04}}{24} He_{04}(\hat{x}_1, \hat{x}_2)\right\}\right. \\
&+ \left\{\frac{k_{30}^2}{72} He_{60}(\hat{x}_1, \hat{x}_2) + \frac{k_{30}k_{21}}{12} He_{51}(\hat{x}_1, \hat{x}_2)\right. \\
&+ \left[\frac{k_{21}^2}{8} + \frac{k_{30}k_{12}}{12}\right] He_{42}(\hat{x}_1, \hat{x}_2) \\
&+ \left[\frac{k_{30}k_{03}}{36} + \frac{k_{12}k_{21}}{4}\right] He_{33}(\hat{x}_1, \hat{x}_2) \\
&+ \left[\frac{k_{12}^2}{8} + \frac{k_{21}k_{03}}{12}\right] He_{24}(\hat{x}_1, \hat{x}_2) + \frac{k_{12}k_{03}}{12} He_{15}(\hat{x}_1, \hat{x}_2) \\
&+ \left.\left.\left.\frac{k_{03}^2}{72} He_{06}(\hat{x}_1, \hat{x}_2)\right\}\right)\right\} \eta_{\mathcal{G}}(\hat{x}_1, \hat{x}_2)
\end{aligned} \tag{2.21}$$

The expression (2.21) together with (2.16, 2.17) is referred to in the text as Edgeworth corrected bivatiate Gaussian η_{BIV-Ed} or ρ_{BIV-Ed}. Finally the

Hermite polynomials $He_{m_1,m_2}(\widehat{x}_1,\widehat{x}_2)$ are calculated easily using the following relations,

$$(1-\zeta^2)He_{m_1+1,m_2}(\widehat{x}_1,\widehat{x}_2) = (\widehat{x}_1-\zeta\widehat{x}_2)He_{m_1,m_2}(\widehat{x}_1,\widehat{x}_2)$$
$$-m_1He_{m_1-1,m_2}(\widehat{x}_1,\widehat{x}_2)+m_2\zeta He_{m_1,m_2-1}(\widehat{x}_1,\widehat{x}_2);$$

$$\begin{aligned}
He_{00}(\widehat{x}_1,\widehat{x}_2) &= 1\\
He_{10}(\widehat{x}_1,\widehat{x}_2) &= \frac{\widehat{x}_1-\zeta\widehat{x}_2}{1-\zeta^2}\\
He_{01}(\widehat{x}_1,\widehat{x}_2) &= \frac{\widehat{x}_2-\zeta\widehat{x}_1}{1-\zeta^2}\\
He_{11}(\widehat{x}_1,\widehat{x}_2) &= \frac{(\widehat{x}_1-\zeta\widehat{x}_2)(\widehat{x}_2-\zeta\widehat{x}_1)}{(1-\zeta^2)^2}+\frac{\zeta}{1-\zeta^2}
\end{aligned} \tag{2.22}$$

The probability densities $\rho_{12}(x_1|x_2)$ and $\rho_{21}(x_2|x_1)$ that are referred to as the conditional densities are given by,

$$\begin{aligned}
\rho_{12}(x_1|x_2) &= \rho(x_1,x_2)/\rho_2(x_2)\\
\rho_{21}(x_2|x_1) &= \rho(x_1,x_2)/\rho_1(x_1).
\end{aligned} \tag{2.23}$$

The conditional moments $M_p(x_2)$ of ρ_{12} (and similarly $M_p(x_1)$ of ρ_{21}) are

$$\begin{aligned}
M_p(x_2) &= \int_{-\infty}^{+\infty} x_1^p\rho_{12}(x_1|x_2)dx_1\\
&= \int_{-\infty}^{+\infty} x_1^p\rho(x_1,x_2)dx_1 \Big/ \int_{-\infty}^{+\infty}\rho(x_1,x_2)dx_1.
\end{aligned} \tag{2.24}$$

It is important to note that given $\eta_{BIV-\mathcal{G}}$, the corresponding conditional densities will be Gaussians,

$$\eta_{12;\mathcal{G}}(\widehat{x}_1|\widehat{x}_2) = \frac{1}{\sqrt{2\pi(1-\zeta^2)}}exp\left\{-\frac{(\widehat{x}_1-\zeta\widehat{x}_2)^2}{2(1-\zeta^2)}\right\}. \tag{2.25}$$

Therefore, for a bivariate Gaussian, conditional centroids are linear in the fixed variable with the slope given by correlation coefficient. Similarly the conditional width is a constant and it is a simple function of the bivariate correlation coefficient.

2.3 State, expectation value and strength densities: CLT results

2.3.1 State densities

Given a hamiltonian H acting in a m-particle space, the state density $I^m(E)$ and the corresponding normalized density $\rho^m(E)$ are defined by

$$\begin{aligned} I^m(E) &= \sum_r g_r \delta(E - E_r) = \langle\langle \delta(H - E) \rangle\rangle^m \\ &= \sum_{\alpha \in m} \langle m\alpha | \delta(H - E) | m\alpha \rangle = d(m) \langle \delta(H - E) \rangle^m \\ &= d(m) \rho^m(E) \end{aligned} \tag{2.26}$$

In the above equation g_r is the degeneracy of r^{th} eigenvalue E_r, $d(m)$ is m-particle space dimensionality, $\langle\langle\ \rangle\rangle^m$ denotes m-particle trace and $\langle\ \rangle^m$ is m-particle average. Using the definition of $\rho^m(E)$ in (2.26), the moments M_r (2.2) and the corresponding central moments $\mathcal{M}_r$ (2.3) for $\rho^m(E)$ are

$$M_r(m) = \langle H^r \rangle^m; \quad \mathcal{M}_r(m) = \langle (H - \langle H \rangle^m)^r \rangle^m \tag{2.27}$$

As stated in Chapter 1, due to CLT action in strongly interacting m-particle spaces, $\rho^m(E)$ takes a Gaussian form defined by the centroid $\epsilon_H(m) = \epsilon(m) = \langle H \rangle^m$ and variance $\sigma_H^2(m) = \sigma^2(m) = \langle (H - \epsilon(m))^2 \rangle^m$,

$$\rho^m(E) \overset{CLT}{\longrightarrow} \rho_G^m(E) = \frac{1}{\sqrt{2\pi}\sigma} exp\left\{ -\frac{(E - \epsilon(m))^2}{2\sigma^2(m)} \right\} \tag{2.28}$$

By using Edgeworth corrected Gaussian given by (2.8), the departures from CLT result as represented by non-zero skewness γ_1 and excess γ_2 values can be taken into account. From now onwards the suffix m appearing in (2.26 - 2.28) is dropped when there is no confusion.

2.3.2 Expectation values and expectation value densities

Formally the expectation value $\langle K\rangle^E$ of an operator K is defined by

$$\langle K\rangle^E = \left[\sum_{\alpha\in E}\langle E\alpha|K|E\alpha\rangle\right] \Big/ I(E) = I_K(E)/I(E) \tag{2.29}$$

where the expectation value denstity $I_K(E)$ is,

$$I_K(E) = \langle K\rangle^E I(E) = \langle\langle K\delta(H-E)\rangle\rangle^m. \tag{2.30}$$

Definition of $\langle K\rangle^E$ as given by (2.29) takes into account properly the degeneracies in the spectrum and because of this one is led to consider expectation value densities. Observables like spherical-orbit occupancies, spin-cutoff factors, static moments etc. are expressible as expectation values. Using the property $\delta(H-E) = \rho(E)\sum_\mu P_\mu(H)P_\mu(E)$, of the orthogonal polynomials $P_\mu(E)$ defined by (2.9) with respect to $\rho(E)$, an expansion of $\langle K\rangle^E$ in terms of traces can be written down

$$\langle K\rangle^E = \sum_{\mu=0}^{\infty}\langle KP_\mu(H)\rangle^m P_\mu(E) \underset{\mu=0,1}{\overset{CLT}{\longrightarrow}} \epsilon_K(m) + \langle\hat{K}\hat{H}\rangle^m\sigma_K(m)\hat{E} \tag{2.31}$$

In (2.31) $\hat{K}$ and $\hat{H}$ are standard operators and following (2.5), $\hat{K} = (K - \epsilon_K(m))/\sigma_K(m)$ and $\hat{H} = (H-\epsilon_H(m))/\sigma_H(m)$. Similarly $\hat{E} = (E-\epsilon_H(m))/\sigma_H(m)$. Note that $\langle\hat{K}\hat{H}\rangle$ is nothing but the correlation coefficient ζ_{K-H}. The CLT result which shows linear behavior of $\langle K\rangle^E$ with respect to E (see Fig. 1.3a

By using Edgeworth corrected Gaussian given by (2.8), the departures from CLT result as represented by non-zero skewness γ_1 and excess γ_2 values can be taken into account. From now onwards the suffix m appearing in (2.26 - 2.28) is dropped when there is no confusion.

2.3.2 Expectation values and expectation value densities

Formally the expectation value $\langle K\rangle^E$ of an operator K is defined by

$$\langle K\rangle^E = \left[\sum_{\alpha\in E}\langle E\alpha|K|E\alpha\rangle\right] \Big/ I(E) = I_K(E)/I(E) \tag{2.29}$$

where the expectation value denstity $I_K(E)$ is,

$$I_K(E) = \langle K\rangle^E I(E) = \langle\langle K\delta(H-E)\rangle\rangle^m. \tag{2.30}$$

Definition of $\langle K\rangle^E$ as given by (2.29) takes into account properly the degeneracies in the spectrum and because of this one is led to consider expectation value densities. Observables like spherical-orbit occupancies, spin-cutoff factors, static moments etc. are expressible as expectation values. Using the property $\delta(H-E) = \rho(E)\sum_\mu P_\mu(H)P_\mu(E)$, of the orthogonal polynomials $P_\mu(E)$ defined by (2.9) with respect to $\rho(E)$, an expansion of $\langle K\rangle^E$ in terms of traces can be written down

$$\langle K\rangle^E = \sum_{\mu=0}^{\infty}\langle KP_\mu(H)\rangle^m P_\mu(E) \underset{\mu=0,1}{\overset{CLT}{\longrightarrow}} \epsilon_K(m) + \langle\hat{K}\hat{H}\rangle^m\sigma_K(m)\hat{E} \tag{2.31}$$

In (2.31) $\hat{K}$ and $\hat{H}$ are standard operators and following (2.5), $\hat{K} = (K - \epsilon_K(m))/\sigma_K(m)$ and $\hat{H} = (H-\epsilon_H(m))/\sigma_H(m)$. Similarly $\hat{E} = (E-\epsilon_H(m))/\sigma_H(m)$. Note that $\langle\hat{K}\hat{H}\rangle$ is nothing but the correlation coefficient ζ_{K-H}. The CLT result which shows linear behavior of $\langle K\rangle^E$ with respect to E (see Fig. 1.3a

for an example) follows immediately by considering the deformation $H \rightarrow H + \alpha K \Longrightarrow \rho \rightarrow \rho_\alpha$ and assuming that CLT applies for ρ as well as ρ_α densities. An alternative to the polynomial expansion method (2.31) which is more appropriate for the operators of the form $\mathcal{O}^\dagger\mathcal{O}$ is to directly construct the expectation value densities $I_K(E)$ defined in (2.30) in terms of its moments. With $K = \mathcal{O}^\dagger\mathcal{O}$ being positive definite operator, $I_K(E)$ can be treated as a probability distribution function and this gives the following important result,

$$\langle K \rangle^E = I_K(E)/I(E) \overset{CLT}{\longrightarrow} I_{K:\mathcal{G}}(E)/I_{\mathcal{G}}(E) \tag{2.32}$$

The origin of the CLT result given in (2.32) lies in the bivariate Gaussian form for strength densities given by (2.39) ahead. The normalized density $\rho_K(E)$ and the corresponding moments $M_r(K)$ are defined by

$$\begin{aligned} \rho_K(E) &= I_K(E)/\langle\langle K \rangle\rangle \\ \widetilde{M}_r(K) &= \langle K H^r \rangle \\ M_r(K) &= \widetilde{M}_r(K)/\widetilde{M}_0(K) = \langle K H^r \rangle / \langle K \rangle \end{aligned} \tag{2.33}$$

The moments $\widetilde{M}_r(K)$, defined in (2.33), of $I_K(E)$ can be derived by parametric differentiation of the moments $M_r(\alpha)$ of ρ_α produced by $H_\alpha = H + \alpha K$,

$$\widetilde{M}_r(K) = (r+1)^{-1} \lim_{\alpha \rightarrow 0} \frac{\partial}{\partial \alpha} [M_{r+1}(\alpha)] \tag{2.34}$$

For an operator of the type $K = T^2$ with the commutator $[T, H] = 0$, one can write $\langle K H^r \rangle = \langle T^2 H^r \rangle$ traces, by double parametric differentiation, in terms of the moments of ρ_α produced by $H \rightarrow H + \alpha T$,

$$\langle T^2 H^r \rangle = [(r+1)(r+2)]^{-1} \lim_{\alpha \rightarrow 0} \frac{\partial^2}{\partial \alpha^2} [\langle H + \alpha T \rangle^{r+2}] \tag{2.35}$$

Results given by (2.26) - (2.35) are used in Chapter 3.

2.3.3 Strength densities

The strength $R_{\mathcal{O}}(E,E')$ for a transition operator $\mathcal{O}$, is the square of the matrix element connecting the eigenstates with energies E and E' (assuming no degeneracies for the eigenvalues E and E')

$$R_{\mathcal{O}}(E,E') = |\langle E'm'|\mathcal{O}|Em\rangle|^2 \tag{2.36}$$

The corresponding strength density $\mathbf{I}_{\mathcal{O}}(E,E')$, which properly takes care of degeneracies, is defined by,

$$\begin{aligned}
\mathbf{I}_{\mathcal{O}}^{H;m,m'}(E,E') &= I^{m'}(E')\,|\langle E'm'|\mathcal{O}|Em\rangle|^2\, I^{m}(E) \\
&= \langle\langle \mathcal{O}^\dagger \delta(H-E')\mathcal{O}\delta(H-E)\rangle\rangle^m \ ; \\
\rho_{\mathcal{O};BIV}^{H;m,m'} &= \langle \mathcal{O}^\dagger \delta(H-E')\mathcal{O}\delta(H-E)\rangle^m / \langle \mathcal{O}^\dagger\mathcal{O}\rangle^m
\end{aligned} \tag{2.37}$$

In (2.37) ρ is normalized bivariate strength density (for non-zero $\langle\mathcal{O}^\dagger\mathcal{O}\rangle$). As $\mathbf{I}_{\mathcal{O}}(E,E')$ is positive definite, it can be represented by a bivariate probability distribution function and therefore the results of Sect. 2.2.2 will apply. The trace expressions for the centroids and variances of the marginal densities $I_1(E)$ and $I_2(E')$, the bivariate correlation coefficient ζ and for the reduced central moments μ_{pq} are given below:

$$\begin{aligned}
\epsilon_1 &= \langle \mathcal{O}^\dagger \mathcal{O} H\rangle^m / \langle \mathcal{O}^\dagger\mathcal{O}\rangle^m \\
\epsilon_2 &= \langle \mathcal{O}^\dagger H \mathcal{O}\rangle^m / \langle \mathcal{O}^\dagger\mathcal{O}\rangle^m \\
\sigma_1^2 &= \langle \mathcal{O}^\dagger \mathcal{O} H^2\rangle^m / \langle \mathcal{O}^\dagger\mathcal{O}\rangle^m - \epsilon_1^2 \\
\sigma_2^2 &= \langle \mathcal{O}^\dagger H^2 \mathcal{O}\rangle^m / \langle \mathcal{O}^\dagger\mathcal{O}\rangle^m - \epsilon_2^2 \\
\zeta &= \left\langle \mathcal{O}^\dagger \left(\frac{H-\epsilon_2}{\sigma_2}\right) \mathcal{O} \left(\frac{H-\epsilon_1}{\sigma_1}\right)\right\rangle^m \Big/ \langle \mathcal{O}^\dagger\mathcal{O}\rangle^m \\
\mu_{pq} &= \left\langle \mathcal{O}^\dagger \left(\frac{H-\epsilon_2}{\sigma_2}\right)^q \mathcal{O} \left(\frac{H-\epsilon_1}{\sigma_1}\right)^p\right\rangle^m \Big/ \langle \mathcal{O}^\dagger\mathcal{O}\rangle^m
\end{aligned} \tag{2.38}$$

15357

The CLT result (smoothed form) for $\mathbf{I}_{\mathcal{O}}(E, E')$ under some plausible arguments is that $\rho(E, E')$ takes a bivariate Gaussian form

$$\rho(E, E') \overset{CLT}{\longrightarrow} \rho_{BIV-\mathcal{G}}(E, E') \tag{2.39}$$

Explicit form of $\rho_{BIV-\mathcal{G}}(E, E')$ is given by (2.15). It has very important consequences for non-energy weighted sum rule or sum strength (NEWSR), for the strength centroid, strength width etc. The strength moments $M_P(E)$ originating from energy E are defined by (assuming that the states $|E\rangle$ and $|E'\rangle$ are non- degenerate)

$$M_P(E) = \sum_{E'} (E')^P |\langle E'|\mathcal{O}|E\rangle|^2 \tag{2.40}$$

In continuous version (2.40) becomes

$$\begin{aligned} M_P(E) &= [I(E)]^{-1} \int \mathbf{I}_{\mathcal{O}}(E, E')(E')^P dE' \\ &= \frac{I_{1;\mathcal{O}}(E)}{I(E)} \int \rho_{21;\mathcal{O}}(E'|E)(E')^P dE' \end{aligned} \tag{2.41}$$

In (2.41), $I(E)$ is state density, $I_{1;\mathcal{O}}(E) = \langle\langle \mathcal{O}^\dagger \mathcal{O} \delta(H - E)\rangle\rangle = \langle\langle \mathcal{O}^\dagger \mathcal{O}\rangle\rangle \rho_{1;\mathcal{O}}(E)$ is one of the marginal densities (similarly $I_{2;\mathcal{O}}(E')$ is defined) corresponding to $\mathbf{I}_{\mathcal{O}}(E, E')$ and $\rho_{21;\mathcal{O}}(E'|E)$ is one of the conditional densities corresponding to $\rho_{\mathcal{O};BIV}(E, E')$; Sect. 2.2.2 gives definitions and properties for marginal and conditional densities. With $(\epsilon_c\ ,\ \sigma_c)$, $(\epsilon_1\ ,\ \sigma_1)$ and $(\epsilon_2\ ,\ \sigma_2)$, the centroid and width of $I(E)$, $I_{1;\mathcal{O}}(E)$ and $I_{2;\mathcal{O}}(E')$ the bivariate Gaussian form of $\mathbf{I}_{\mathcal{O}}(E, E')$ and the Gaussian form of $I(E)$ give simple expressions for NEWSR which equals to $M_0(E)$, the strength centroid $\epsilon(E) = M_1(E)/M_0(E)$ and strength width $\sigma(E) = \{M_2(E)/M_0(E) - [M_1(E)/M_0(E)]^2\}^{1/2}$ (follow easily from (2.15, 2.25, 2.5)),

$$
\begin{aligned}
M_0(E) &\overset{CLT}{\longrightarrow} \langle \mathcal{O}^\dagger \mathcal{O} \rangle \frac{\sigma_c}{\sigma_1} exp\left\{ -\frac{1}{2}\left[\left(\frac{E-\epsilon_1}{\sigma_1} \right)^2 - \left(\frac{E-\epsilon_c}{\sigma_c} \right)^2 \right] \right\}, \\
\epsilon(E) &\overset{CLT}{\longrightarrow} \epsilon_2 + \zeta \frac{\sigma_2}{\sigma_1}(E-\epsilon_1) \\
\sigma(E) &\overset{CLT}{\longrightarrow} \sigma_2(1-\zeta^2)^{1/2}. \qquad (2.42)
\end{aligned}
$$

Results given by (2.42) are well verified in Fig. 1.4 and they are used in Chapter 6.

2.4 Partitioning : spherical and unitary configurations

As stated in Chapter 1, in order to extend the applicability of CLT results given in Sect. 2.3 to large spaces, to improve the accuracy of the predictions based on CLT results (including Edgeworth corrections) and to bring in more information it is essential to partition the m-particle spaces to subspaces. Simple partitioning of m-particle spaces is according to spherical and unitary configurations and in order to define them, we begin with m-particles distributed over spherical shell model j-orbits (single particle s.p. orbits) denoted by α, β etc. (j_α being the angular momentum and $N_\alpha = 2j_\alpha + 1$ is the degeneracy of the orbit α). The m-particle spectroscopic space can be decomposed into spherical configurations $\mathbf{m} = (m_\alpha, m_\beta ...)$ where m_α is the number of particles in the orbit α and $m = \sum_\alpha m_\alpha ; m = \sum \mathbf{m}$. Note that the dimensionality $d(\mathbf{m})$ of the configuration $\mathbf{m}$ is $d(\mathbf{m}) = \prod_\alpha \begin{pmatrix} N_\alpha \\ m_\alpha \end{pmatrix}$. For example, for identical particles, denoting $1d_{5/2}$, $2s_{1/2}$ and $1d_{3/2}$ orbits as #1, #2 and #3 orbits,

$(ds)^4$ spherical configurations are $\mathbf{m} = (m_1, m_2, m_3) = (4,0,0) \oplus (3,1,0) \oplus (3,0,1) \oplus (2,2,0) \oplus (2,1,1) \oplus (2,0,2) \oplus (1,2,1) \oplus (1,1,2) \oplus (1,0,3) \oplus (0,2,2) \oplus (0,1,3) \oplus (0,0,4)$. A unitary orbit $\boldsymbol{\alpha}$ is defined as a set of spherical orbits. With this, decomposition of m-particle space into unitary configurations $[\mathbf{m}]$ is possible; $m \rightarrow \sum[\mathbf{m}]$. As above, a unitary configuration $[\mathbf{m}] = (m_{\boldsymbol{\alpha}}, m_{\boldsymbol{\beta}}, ...)$; $m = \sum m_{\boldsymbol{\alpha}}$. Using the convention that the spherical orbits α belong to unitary orbit $\boldsymbol{\alpha}$ and similarly the orbits β belong to $\boldsymbol{\beta}$ etc., the number of s.p. states in a unitary orbit $\boldsymbol{\alpha}$ is $N_{\boldsymbol{\alpha}} = \sum_{\alpha \in \boldsymbol{\alpha}} N_\alpha$. The dimensionality of the configuration $[\mathbf{m}]$ is $d([\mathbf{m}]) = \prod_{\boldsymbol{\alpha}} \begin{pmatrix} N_{\boldsymbol{\alpha}} \\ m_{\boldsymbol{\alpha}} \end{pmatrix}$. For example in the above ds-shell case one can choose $(1d_{5/2}, 2s_{1/2})$ and $(1d_{3/2})$ to be two unitary orbits (#1, #2 orbits) and then $(ds)^4 \rightarrow [\mathbf{m}] = (m_1, m_2) = (4,0) \oplus (3,1) \oplus (2,2) \oplus (1,3) \oplus (0,4)$. It is important to recognize that $[\mathbf{m}] \rightarrow \sum \mathbf{m}$ and the set of spherical configurations $\mathbf{m}$ that belong to a given unitary configuration is easy to enumerate. For example in the above case, $(4,0) \rightarrow (4,0,0) \oplus (3,1,0) \oplus (2,2,0)$; $(3,1) \rightarrow (3,0,1) \oplus (2,1,1) \oplus (1,2,1)$ etc. With spherical or unitary configurations, the decomposition of m-particle space is,

$$m \rightarrow \sum[\mathbf{m}]\,; \; [\mathbf{m}] \rightarrow \sum \mathbf{m}. \tag{2.43}$$

It is worth remarking that the decomposition given by (2.43) automatically produces fixed-parity subspaces by choosing the unitary orbits $\boldsymbol{\alpha}$ to be set of spherical orbits with all of them having same parity. One remarkable result is that under the above partitioning of the shell model space the state density $I^m(E)$ decomposes exactly into sum of partial $I^{\mathbf{m}}(E)$ and $I^{[\mathbf{m}]}(E)$ densities,

$$\begin{aligned} I^{H,m}(E) = \sum_{[\mathbf{m}]} I^{H,[\mathbf{m}]}(E) = \sum_{[\mathbf{m}]} \left\{ \sum_{\mathbf{m} \in [\mathbf{m}]} I^{H,\mathbf{m}}(E) \right\}\,; \\ I^{H,[\mathbf{m}]}(E) = \langle\langle \delta(H-E) \rangle\rangle^{[\mathbf{m}]}\,, \\ I^{H,\mathbf{m}}(E) = \langle\langle \delta(H-E) \rangle\rangle^{\mathbf{m}} \end{aligned} \tag{2.44}$$

It is important to recognize that corresponding to m, $\mathbf{m}$ and $[\mathbf{m}]$ there are group structures associated with them as given in Sect. 2.5 ahead. The moments $M_p(\mathbf{m})$ of $I^{H,\mathbf{m}}(E)$ and $M_p([\mathbf{m}])$ of $I^{H,[\mathbf{m}]}(E)$ are easily defined as traces of H^p over the corresponding subspaces,

$$\begin{aligned} M_p(\mathbf{m}) &= \langle H^p \rangle^{\mathbf{m}} \\ M_p([\mathbf{m}]) &= \langle H^p \rangle^{[\mathbf{m}]} = [d([\mathbf{m}])]^{-1} \sum_{\mathbf{m} \in [\mathbf{m}]} \langle\langle H^p \rangle\rangle^{\mathbf{m}} \\ &= \sum_{\mathbf{m} \in [\mathbf{m}]} \frac{d(\mathbf{m})}{d([\mathbf{m}])} M_p(\mathbf{m}) \end{aligned} \tag{2.45}$$

It should be recognized that unlike the scalar moments, $M_r(m)$ defined in (2.27), the fixed-$\mathbf{m}$ (similarly $[\mathbf{m}]$) moments involve intermediate configurations as the hamiltonian does not preserve these symmetries. For example the second moment $M_2(\mathbf{m})$ decomposes into partial moments $M_2(\mathbf{m} \to \mathbf{m}')$,

$$\begin{aligned} M_2(\mathbf{m}) &= [d(\mathbf{m})]^{-1} \langle\langle H^2 \rangle\rangle^{\mathbf{m}} \\ &= [d(\mathbf{m})]^{-1} \sum_{\mathbf{m}'} \sum_{\substack{\alpha \in \mathbf{m} \\ \beta \in \mathbf{m}'}} |\langle \mathbf{m}\alpha | H | \mathbf{m}'\beta \rangle|^2 \\ &= \sum_{\mathbf{m}'} M_2(\mathbf{m} \to \mathbf{m}') \,; \\ M_2(\mathbf{m} \to \mathbf{m}') &= [d(\mathbf{m})]^{-1} \sum_{\substack{\alpha \in \mathbf{m} \\ \beta \in \mathbf{m}'}} |\langle \mathbf{m}\alpha | H | \mathbf{m}'\beta \rangle|^2 \end{aligned} \tag{2.46}$$

With the centroids denoted by $\epsilon(\mathbf{m})$ and the variances denoted by $\sigma^2(\mathbf{m})$, the decomposition of $\sigma^2(\mathbf{m})$ into partial variances $\sigma^2(\mathbf{m} \to \mathbf{m}')$ ($\sigma^2(\mathbf{m} \to \mathbf{m})$ is called internal variance and $\sigma^2(\mathbf{m} \to \mathbf{m}')$; $\mathbf{m} \neq \mathbf{m}'$ is called external variance) is given by,

$$
\begin{aligned}
\sigma^2(\mathrm{m}) &= \sum_{\mathrm{m}'} \sigma^2(\mathrm{m} \to \mathrm{m}') \ , \\
\sigma^2(\mathrm{m} \to \mathrm{m}) &= M_2(\mathrm{m} \to \mathrm{m}) - (\epsilon(\mathrm{m}))^2 \ , \\
\sigma^2(\mathrm{m} \to \mathrm{m}') &= M_2(\mathrm{m} \to \mathrm{m}') \qquad (2.47)
\end{aligned}
$$

Just as the state densities decompose into partial densities, the expectation value densities also decompose into partial densities exactly in the same way. On the other hand decomposition of strength densities into partial densities still remains an unsolved problem. However there are ways to circumvent this problem; see Chapter 6.

Partitioning of the shell model space can be carried out in many different ways and the partitioning defined by irreducible representations (irreps) of groups that can be realized in shell model spaces (for example Wigner $SU(4)$, Elliot $SU(3)$, pairing $Sp(n)$ etc.) are in fact the most significant ones. The significance derives from the fact (as will be seen in Sects. 2.5 - 2.6) that the moments defined over the irreps in fact propagate from the few particle spaces to the many particle spaces and this is elaborated in Sect. 2.6. As mentioned earlier there are group structures associated with spherical and unitary configurations and before turning to this, it is useful to introduce the following symbols.

With m particles in N s.p. states, the number of holes $m^{\times} = N - m$. Similarly for m_α particles in N_α states, $m_\alpha^{\times} = N_\alpha - m_\alpha$ (note that $n_\alpha^{\times} = N_\alpha - n_\alpha$) and for $m_{\boldsymbol{\alpha}}$ particles in $N_{\boldsymbol{\alpha}}$ states, $m_{\boldsymbol{\alpha}}^{\times} = N_{\boldsymbol{\alpha}} - m_{\boldsymbol{\alpha}}$ (note that $n_{\boldsymbol{\alpha}}^{\times} = N_{\boldsymbol{\alpha}} - n_{\boldsymbol{\alpha}}$); spherical orbits and unitary orbits, spherical configurations and unitary configurations are already defined. Finally, the symbols $[X]_r$,

$X_{\alpha\beta....}$, $X_{\boldsymbol{\alpha\beta}.....}$, $\check{X}_{\alpha\beta}$ and $\check{X}_{\boldsymbol{\alpha\beta}}$ are defined as

$$
\begin{aligned}
[X]_r &= X(X-1)(X-2).....(X-r+1)\,; \\
X_{\alpha\beta\gamma...} &= X_\alpha(X_\beta-\delta_{\beta\alpha})(X_\gamma-\delta_{\gamma\alpha}-\delta_{\gamma\beta}).....; \\
X_{\boldsymbol{\alpha\beta\gamma}...} &= X_{\boldsymbol{\alpha}}(X_{\boldsymbol{\beta}}-\delta_{\boldsymbol{\beta\alpha}})(X_{\boldsymbol{\gamma}}-\delta_{\boldsymbol{\gamma\alpha}}-\delta_{\boldsymbol{\gamma\beta}}).....; \\
\check{X}_{\alpha\beta} &= X_\alpha(X_\beta-\delta_{\alpha\beta})/(1+\delta_{\alpha\beta}) \\
\check{X}_{\boldsymbol{\alpha\beta}} &= X_{\boldsymbol{\alpha}}(X_{\boldsymbol{\beta}}-\delta_{\boldsymbol{\alpha\beta}})/(1+\delta_{\boldsymbol{\alpha\beta}}) \\
& X = m,\, N,\, m^{\times},\, n,\, n^{\times}
\end{aligned}
\tag{2.48}
$$

2.5 Unitary decomposition of operators

2.5.1 $U(N)$ group

With m identical fermions distributed over N single particle states, one can recognize the appearence of $U(N)$ group which is generated by the N^2 operators $a^{\dagger}_{j_\alpha m_\alpha} a_{j_\beta m_\beta}$; $\alpha,\, \beta = 1, 2, ..., N$. Then the $\begin{pmatrix} N \\ m \end{pmatrix}$ antisymmetric states form an irrep of the group $U(N)$, usually denoted by Young shape $\{1^m\}$. With this the single particle creation operators $a^{\dagger}_{j_\alpha m_\alpha}$ belong to $\{1\}$ and the destruction operators $a_{j_\beta m_\beta}$ belong to $\left\{1^{N-1}\right\}$. The only scalar operator in m-particle space is number operator n as it remains invariant under the transformation produced by the generators of $U(N)$ group. One can in general seek a decomposition of a given operator into tensor operators (belonging to a definite irrep of $U(N)$) with respect to $U(N)$ group similar to what one does with respect to $O(3)$ in angular momentum algebra. The tensor decomposition is illustrated below with examples that are relevant for the results given in Chapters 3 - 6.

Let us begin with a NIP hamiltonian $h = \sum \epsilon_\alpha n_\alpha$; ϵ_α are single particle

energies (SPE) and as stated before n_α is number operator for the spherical α. From the above discussions it should be clear that the scalar part h^0 of h with respect to $U(N)$ should be a first order polynomial in number operator n. Then one-body nature of h gives $h^0 = a_0 + a_1 n$. Now taking trace on both sides over 0 and 1-particle spaces immediately gives the result that $h^0 = \langle h \rangle^1 n$. The remaining piece $h^1 = h - h^0$ is the unitary one-body part of h and it has a definite group theoretical meaning in trems of the $U(N)$ group. Thus the unitary decompositon of h is,

$$\begin{aligned} h &= \sum_\alpha \epsilon_\alpha n_\alpha = h^0 + h^1 \\ h^0 &= \sum_\alpha \bar{\epsilon}\, n_\alpha = \bar{\epsilon}\, n \;;\; \bar{\epsilon} = N^{-1} \sum_\alpha \epsilon_\alpha N_\alpha \;,\; n = \sum n_\alpha \\ h^1 &= h - h^0 = \sum_\alpha \epsilon^1_\alpha n_\alpha = \sum \tilde{\epsilon}_\alpha n_\alpha \;;\; \epsilon^1_\alpha = \tilde{\epsilon}_\alpha = \epsilon_\alpha - \bar{\epsilon} \end{aligned} \tag{2.49}$$

Note that in the remainder of the thesis $\tilde{\epsilon}_\alpha$ and ϵ^1_α are used interchangeably when there is no confusion; some time $\epsilon^1_\alpha(1)$ is used to emphasize that the SPE are derived from a one-body hamiltonian. Unitary decomposition of a two-body interaction V defined by the two-body matrix elements (TBME) $V^J_{\alpha\beta\gamma\delta}$ is easy to work out in terms of the average two-particle matrix elements $V_{\alpha\beta}$,

$$V_{\alpha\beta} = \left\{\check{N}_{\alpha\beta}\right\}^{-1} \left\{\sum_J [J] V^J_{\alpha\beta\alpha\beta}\right\} = \{N_{\alpha\beta}\}^{-1} \left\{\sum_J [J] V^J_{\alpha\beta\alpha\beta}(1+\delta_{\alpha\beta})\right\} . \tag{2.50}$$

In (2.50), $[J] = (2J+1)$. Recognizing that the scalar part V^0 of V with respect to $U(N)$ group should be a second order polynomial in n gives the result $V^0 = a_0 + a_1 n + a_2 n^2$. Once again taking the traces over 0, 1 and 2-particle spaces on both sides of the above equation leads to the following simple formula for V^0,

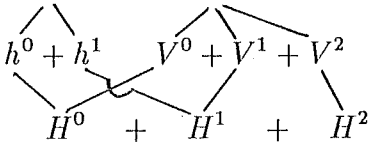
$$\begin{aligned} V^0 &= \binom{n}{2} \langle V \rangle^2 = \binom{n}{2} \bar{V} = [n]_2 [N]_2^{-1} \left[\sum_{\alpha \geq \beta} \check{N}_{\alpha\beta} V_{\alpha\beta}\right] \\ &= [n]_2 [N]_2^{-1} \left[\frac{1}{2} \sum_{\alpha,\beta} N_{\alpha\beta} V_{\alpha\beta}\right] \end{aligned} \tag{2.51}$$

Just as h has h^1 part, V should have a one-body part with respect to $U(N)$ group. This part which is denoted as V^1, should vanish in 0 and 1-particle spaces. Therefore the form of V^1 is $V^1 = (n-1)F^1 = (n-1)\sum \epsilon^1_\alpha(2) n_\alpha$. Then, $V - V^0 = V^1 + V^2$; it should be obvious that the V^2 part cannot be reduced to a piece that behaves as neither V^0 nor V^1. The explicit forms of F^1 and V^2 are derived by using the particle-hole (p-h) symmetries of these operators, $F^1 \overset{p-h}{\longrightarrow} -F^1$ and $V^2 \overset{p-h}{\longrightarrow} V^2$. This gives the results

$$
\begin{aligned}
V^1 &= (n-1)\sum \epsilon^1_\alpha(2) n_\alpha \overset{\substack{For\ m \\ particles}}{\longrightarrow} \sum_\alpha \zeta^1_\alpha(m) n_\alpha \ , \\
V^2 &= V - V^0 - V^1 \ ; \\
\zeta^1_\alpha(m) &= (m-1)\epsilon^1_\alpha(2) \\
\epsilon^1_\alpha(2) &= (N-2)^{-1} \sum_\gamma (N_\gamma - \delta_{\alpha\gamma})(V_{\alpha\gamma} - \langle V \rangle^2)
\end{aligned}
\tag{2.52}
$$

Eqs. (2.49) - (2.52) give the unitary decomposition of $V = \sum_{\nu=0,1,2} V^\nu$ of V with respect to $U(N)$ group. It is obvious that V^0 is scalar with respect to $U(N)$ (hence denoted as $\nu = 0$ part) , V^1 is effective one-body operator with respect to $U(N)$ as n behaves as a constant when acted on a $U(N)$ irrep $\{1^m\}$ (hence denoted as $\nu = 1$ part) and the remaining piece must be an irreducible two-body part (hence denoted as $\nu = 2$ part); for details regarding Young columnar shapes associated with each ν, see [Ch-71]. Combining the decompositions given by (2.49) - (2.52) one has the following pictorial representation for $U(N)$ decomposition of a one plus two-body hamiltonian $H = h(1) + V(2)$,

$$H = h(1) + V(2)$$



(2.53)

In m-particle space, $H^0 = m\bar{\epsilon} + \begin{pmatrix} m \\ 2 \end{pmatrix} \bar{V}$ while H^1 is defined by m - dependent s.p. energies $\xi^1_\alpha(m)$,

$$\begin{aligned} H^1 &= \sum \{\epsilon^1_\alpha(1) + \zeta^1_\alpha(m)\} n_\alpha = \sum_\alpha \xi^1_\alpha(m) n_\alpha \,; \\ \xi^1_\alpha(m) &= \epsilon^1_\alpha(1) + (m-1)\epsilon^1_\alpha(2) \end{aligned} \tag{2.54}$$

In (2.54), $\epsilon^1_\alpha(2)$ are the (defined by (2.52)) induced (by V) s.p. energies and $\xi^1_\alpha(m)$ are the renormalized (by V) s.p. energies.

2.5.2 Spherical configuration group $U(N_\alpha) \oplus U(N_\beta) \oplus .....$

The unitary group $U(N_\alpha)$ acting in each spherical orbit α generates m_α of spherical configurations $\mathbf{m}$; i.e. $\mathbf{m}$ behaves as $\{1^{m_\alpha}\} \otimes \{1^{m_\beta}\} \otimes .....$ with respect to the direct sum group $U(N_\alpha) \oplus U(N_\beta) \oplus .....$ Thus in the spherical configurations space, the scalar operators are n_α's. Therefore it should be obvious that the NIP hamiltonian h is a scalar with respect to the spherical configuration group,

$$h = \sum \epsilon_\alpha n_\alpha = h^{[0]}. \tag{2.55}$$

In (2.55) $h^{[0]} = h^{[0,0,...]}$ denotes that it is a scalar with respect to each spherical orbit. In order to extract out $V^{[0]}$ the scalar part of V with respect to spherical configurations, it should be recognized that $V^{[0]}$ must be a second order

polynomial in n_α's. Therefore $V^{[0]} = a_0 + \sum_\alpha b_\alpha n_\alpha + \sum_{\alpha \geq \beta} C_{\alpha\beta} \check{n}_{\alpha\beta}$ and then taking traces on both sides in 0, 1 and 2-particle spaces, one has the result

$$V^{[0]} = \sum_{\alpha \geq \beta} V_{\alpha\beta} \check{n}_{\alpha\beta} = \frac{1}{2} \sum_{\alpha,\beta} V_{\alpha\beta} n_{\alpha\beta} \tag{2.56}$$

As a one-body hamiltonian will be a scalar with respect to spherical configuration group (see [Ch-71] for exceptions), there cannot be an effective one-body part of V with respect to spherical configuration group. Thus $\mathbf{V} = V - V^{[0]}$ should be like the $\nu = 2$ part $V^{\nu=2}$ introduced in the $U(N)$ case. Just as $V^{[0]}$ is scalar with respect to each of the $U(N_\alpha)$ groups (therefore the notation $[0] = [0, 0, ...]$), $\mathbf{V}$ behaves as $[2] = (\nu_\alpha, \nu_\beta, ...)$; $\sum \nu_\alpha = 2$. The exact definitions of ν_α's and the methods for enumerating and constructing the various $V^{(\nu_\alpha, \nu_\beta, ...)}$; $\sum \nu_\alpha = 2$, are given by Chang et al [Ch-71]. It suffices for the results presented in Chapters 3 - 6 to mention that $\mathbf{V}$ behaves as [2];

$$\mathbf{V} = V^{[2]} = V - V^{[0]} \tag{2.57}$$

It is important to point out that the tensorial nature of $\mathbf{V}$ with respect to $U(N)$ is exactly $\nu = 2$, i.e. $\mathbf{V} \rightarrow \mathbf{V}^{\nu=2}$ and $\mathbf{V}^{\nu=0} = 0$ and $\mathbf{V}^{\nu=1} = 0$.

2.5.3 Unitary configuration group $U(N_\alpha) \oplus U(N_\beta) \oplus .....$

The unitary group $U(N_{\boldsymbol{\alpha}})$ acting in each unitary orbit $\boldsymbol{\alpha}$ generates $m_{\boldsymbol{\alpha}}$ of a unitary configuration [m]; i.e. [m] behaves as $\{1^m \boldsymbol{\alpha}\} \otimes \left\{1^m \boldsymbol{\beta}\right\} \otimes .....$ with respect to the direct sum group $U(N_{\boldsymbol{\alpha}}) \oplus U(N_{\boldsymbol{\beta}}) \oplus .....$ Thus in the unitary configurations space, the scalar operators are $m_{\boldsymbol{\alpha}}$'s. One can carry out decomposition of $H = h(1) + V(2)$ with respect to the group $U(N_{\boldsymbol{\alpha}}) \oplus U(N_{\boldsymbol{\beta}}) \oplus ....$ However the only decomposition is of relevance for present thesis is the decomposition of $h^{[0]} + V^{[0]}$. They will have $[\mathbf{0}] \oplus [\mathbf{1}] \oplus [\mathbf{2}]$ tensor parts with respect

to the above direct sum group and these various tensor parts are obtained as follows.

Given a general one plus two-body operator $A = B(1) + C(2)$ [1] defined by the SPE $\mathcal{E}_\alpha$ and TBME $C^J_{\alpha\beta\gamma\delta}$, $B = \sum \mathcal{E}_\alpha n_\alpha$ and the two-body operator C relevant for the present discussion is described by the average two-particle matrix elements $C_{\alpha\beta}$, $C \Leftrightarrow C_{\alpha\beta} = \check{N}^{-1}_{\alpha\beta}\left[\sum_J [J] C^J_{\alpha\beta\alpha\beta}\right]$. It should be noted that $B = B^{[0]} + B^{[1]}$, $C = C^{[0]} + C^{[1]} + C^{[2]}$ and $A = A^{[0]} + A^{[1]} + A^{[2]}$; $A^{[0]} = B^{[0]} + C^{[0]}$, $A^{[1]} = B^{[1]} + C^{[1]}$ and $A^{[2]} = C^{[2]}$. The explicit expressions for $B^{[\boldsymbol{\nu}]}$, $C^{[\boldsymbol{\nu}]}$ and $A^{[\boldsymbol{\nu}]}$ are derived using the results [Fr-89a]: (i) $\boldsymbol{\nu} = [\nu_{\boldsymbol{\alpha}}, \nu_{\boldsymbol{\beta}}, ...]$, $\sum \nu_{\boldsymbol{\alpha}} = \boldsymbol{\nu}$ and $\nu_{\boldsymbol{\alpha}}$ are integers; (ii) the part that behaves as, $[\mathbf{0}] = [0, 0, ...]$ should be a polynomial in $m_{\boldsymbol{\alpha}}$ (first order for $B^{[\mathbf{0}]}$ and second order for $C^{[\mathbf{0}]}$); (iii) subtraction of $B^{[\mathbf{0}]}$ from B gives $B^{[\mathbf{1}]}$; (iv) the $C^{[\mathbf{1}]}$ part of $C_{\alpha\beta}$ term with α and β belonging to the same $\boldsymbol{\alpha}$, follows directly from (2.52) and in the case where α and β belong to different unitary orbits, one has to change the $(m-1)$ factor in (2.52) to $m_{\boldsymbol{\alpha}}$ and $m_{\boldsymbol{\beta}}$ appropriately. The final results are,

$$B^{[\mathbf{0}]} = \sum_{\boldsymbol{\alpha}} [\mathcal{E}_{\boldsymbol{\alpha}}(A)] n_{\boldsymbol{\alpha}} \quad ; \quad \mathcal{E}_{\boldsymbol{\alpha}}(A) = \left(\sum_{\alpha \in \boldsymbol{\alpha}} \mathcal{E}_\alpha N_\alpha\right) N^{-1}_{\boldsymbol{\alpha}}$$

$$B^{[\mathbf{1}]} = \sum [\mathcal{E}^{[\mathbf{1}]}_\alpha(A)] n_\alpha \quad ; \quad \mathcal{E}^{[\mathbf{1}]}_\alpha(A) = \mathcal{E}_\alpha - [\mathcal{E}_{\boldsymbol{\alpha}}(A)]$$

$$C^{[\mathbf{0}]} \Leftrightarrow C_{\boldsymbol{\alpha\beta}}(A) = \left[\sum_{\alpha \in \boldsymbol{\alpha}, \beta \in \boldsymbol{\beta}} N_{\alpha\beta} C_{\alpha\beta}\right] \left[N_{\boldsymbol{\alpha\beta}}\right]^{-1}$$

[1] General notations are used here for one plus two-body operator. This is because, the unitary decomposition results of this section are used in Chapter 5 ahead where the one plus two-body operator does not come from a hamiltonian but it derives for example from a transition operator. Unitary decomposition being a group decomposition, it applies for any one plus two-body operator. In terms of these general notations different parts of the hamiltonian H are $H \equiv A$, $h(1) \equiv B(1)$ and $V(2) \equiv C(2)$.

$$C^{[1]} \Leftrightarrow \mathcal{E}_{\alpha}^{[1];\boldsymbol{\beta}}(A)$$

$$= \left\{ \left[\sum_{\beta \in \boldsymbol{\beta}} (N_{\beta} - \delta_{\alpha\beta}) C_{\alpha\beta} \right] - (N_{\boldsymbol{\beta}} - \delta_{\boldsymbol{\alpha\beta}}) C_{\boldsymbol{\alpha\beta}} \right\} \times \{N_{\boldsymbol{\beta}} - 2\delta_{\boldsymbol{\alpha\beta}}\}^{-1}$$

$$C^{[2]} \Leftrightarrow C_{\alpha\beta}^{[2]}(A) = C_{\alpha\beta} - [C_{\boldsymbol{\alpha\beta}}(A)] - \left\{ \left[\mathcal{E}_{\alpha}^{[1];\boldsymbol{\beta}}(A) \right] + \left[\mathcal{E}_{\beta}^{[1];\boldsymbol{\alpha}}(A) \right] \right\}$$

$$\begin{aligned}
A^{[0]} &= \sum_{\boldsymbol{\alpha}} [\mathcal{E}_{\boldsymbol{\alpha}}(A)]\, n_{\boldsymbol{\alpha}} + \sum_{\boldsymbol{\alpha} \geq \boldsymbol{\beta}} [C_{\boldsymbol{\alpha\beta}}(A)] \check{n}_{\boldsymbol{\alpha\beta}} \\
A^{[1]} &= \sum_{\alpha} \left\{ \left[\mathcal{E}_{\alpha}^{[1]}(A) \right] + \sum_{\boldsymbol{\beta}} (n_{\boldsymbol{\beta}} - \delta_{\boldsymbol{\alpha\beta}}) \left[\mathcal{E}_{\alpha}^{[1];\boldsymbol{\beta}}(A) \right] \right\} n_{\alpha} \\
&\xrightarrow{\text{for a } [\mathrm{m}]} \sum_{\alpha} \xi_{\alpha}^{1}([\mathrm{m}] : A) n_{\alpha} \; ; \\
\xi_{\alpha}^{1}([\mathrm{m}] : A) &= \mathcal{E}_{\alpha}^{[1]}(A) + \zeta_{\alpha}^{[1]}([\mathrm{m}] : A) \; , \\
\zeta_{\alpha}^{[1]}([\mathrm{m}] : A) &= \sum_{\boldsymbol{\beta}} (m_{\boldsymbol{\beta}} - \delta_{\boldsymbol{\alpha\beta}}) \mathcal{E}_{\alpha}^{[1];\boldsymbol{\beta}}(A) \\
A^{[2]} &\Leftrightarrow C_{\alpha\beta}^{[2]}(A)
\end{aligned} \tag{2.58}$$

Just as the case with (2.54), $\zeta_{\alpha}^{1}([\mathrm{m}])$ are the induced SPE and $\xi_{\alpha}^{[1]}([\mathrm{m}])$ are the renormalized SPE (for a fixed unitary configuration $[\mathrm{m}]$). In the case of $H^{[0]} = h^{[0]} + V^{[0]}$ decomposition $A = H^{[0]}$, $B = h^{[0]}$ and $C = V^{[0]}$ in (2.58). It is useful to point out that $\mathbf{V}$ given in (2.57) is $V^{[2]}$ type with respect to the unitary configurations, i.e. $\mathbf{V}^{[0]} = 0$, $\mathbf{V}^{[1]} = 0$ and it should be recognized that the $\nu_{\boldsymbol{\alpha}}$ of $[2]$ in $\mathbf{V}^{[2]}$ need not be integers (they can be half integers) [Ch-71].

2.6 Trace propagation

2.6.1 $U(N)$ group averages

Given a m-particle space generated by distributing the particles in N s.p. states the $U(N)$ (or scalar) trace ($\sum_{\alpha \in m} \langle m\alpha | \mathcal{O} | m\alpha \rangle$) of an operator $\mathcal{O}$ over the

entire m-particle space propagates from the corresponding traces in few particle spaces, i.e. the trace will be a polynomial in particle number m with the expansion coefficients determined by the basic few particle (or input) traces. The general principles of $U(N)$ or scalar trace (the word trace and average are used synonymously) propagation are described below with examples that are relevant for the thesis.

i) The trace $\langle F(K)\rangle^m$ of a K-body operator $F(K)$ over the m-particle space is nothing but the trace over the space defined by $\{1^m\}$ of $U(N)$. As traces are invariant under unitary transformations, the trace equivalent operator in the $U(N)$ case of interest should be a function of the invariant operators of $U(N)$. In the scalar case the only invariant operator is the number operator n and therefore one has the elementary result

$$\langle F(K)\rangle^m = \begin{pmatrix} m \\ K \end{pmatrix} \langle F(K)\rangle^K \tag{2.59}$$

which shows that the m-particle average propagates from the defining K-particle average via the binomial $\begin{pmatrix} m \\ K \end{pmatrix}$. A simple application of (2.59) is writing down the m-particle average of h defined by the SPE ϵ_α's and V defined by the TBME $V^J_{\alpha\beta\gamma\delta}$,

$$\begin{aligned} \langle h\rangle^m &= m\langle h\rangle^1 = \frac{m}{N}\sum_\alpha \epsilon_\alpha N_\alpha = m\bar{\epsilon} \\ \langle V\rangle^m &= \begin{pmatrix} m \\ 2 \end{pmatrix} \langle V\rangle^2 = \begin{pmatrix} m \\ 2 \end{pmatrix} \bar{V} \\ &= [m]_2[N]_2^{-1} \sum_{J,\alpha\geq\beta} [J] V^J_{\alpha\beta\alpha\beta} \end{aligned} \tag{2.60}$$

The $\bar{\epsilon}$ and $\bar{V}$ in (2.60) are defined by (2.49 - 2.51).

ii) Extending (2.59), it is very easy to recognize that the scalar average of a $0+1+2+...+K$-body operator $F(0-K)$ is a K^{th} degree polynomial

in m,

$$\langle F(0-K)\rangle^m = \sum_{r=0}^{K} a_r m_r. \tag{2.61}$$

The $(K+1)$ - inputs a_r's can be written in terms of the averages of $F(0-K)$ for any $(K+1)$ values of m. For example let us consider $\langle \widetilde{H}^2\rangle^m = \langle (H - \langle H\rangle^m)^2\rangle^m = \langle (h - \langle h\rangle^m + V - \langle V\rangle^m)^2\rangle^m$. Now $r = 4$ in (2.61). Solving for a_r's in terms of $\langle \widetilde{H}^2\rangle^m$ with $m = 0, 1, 2, N-1, N$ and recognizing that the averages for $m = 0$, N are zero, gives the result,

$$\langle \widetilde{H}^2\rangle^m = [m]_2[N-m]_2[N-2]_2^{-1} \times$$

$$\left[\tfrac{1}{2}\langle \widetilde{H}^2\rangle^2 - \frac{(N-3)(m-2)}{(N-1)(m-1)}\langle \widetilde{H}^2\rangle^1 + \frac{(m-2)}{(N-1)(N-m-1)}\langle \widetilde{H}^2\rangle^{N-1}\right] \tag{2.62}$$

Alternatively $\langle \widetilde{H}^2\rangle^m$ can be written in terms of averages over $m = 0$, 1, 2, 3, 4 which then would have involved calculation of the input traces over 3 and 4-particle spaces. However as (2.62) shows, by exploiting the properties of the operator under question it is possible to reduce the input traces to a minimal set of easily calculable traces.

iii) There are further simplifications in the choice of the input traces if operators with definite unitary rank are used (unitary decomposition of operators with respect to $U(N)$ is already discussed in Sect. 2.5.1); the simplicity arises from the p-h symmetries of these operators. For example using the unitary decomposition of $h = h^0 + h^1$ as given by (2.49), it is easy to see that the trace of h is completely given by h^0 and for calculating the trace of $(h^1)^2$ a good choice of inputs is the points at $m = 0$ and 1. These immediately give the following propagation equations,

$$\langle h\rangle^m = \langle h^0\rangle^m = m\bar{\epsilon}$$

$$\langle (h^1)^2 \rangle^m = \frac{mm^\times}{[N]_2} \langle (h^1)^2 \rangle^1 \; ; \langle (h^1)^2 \rangle^1 = \frac{\sum (\epsilon^1_\alpha)^2 N_\alpha}{N} \tag{2.63}$$

Using the p-h symmetry $\langle (h^1)^3 \rangle^m = -\langle (h^1)^3 \rangle^{N-m}$ and choosing the inputs to be the values of $\langle (h^1)^3 \rangle^m$ for $m = 0,\ N,\ 1,\ N-1$, yield the following propagation equation for $\langle (h^1)^3 \rangle^m$,

$$\begin{aligned} \langle (h^1)^3 \rangle^m &= \frac{mm^\times (m^\times - m)}{[N]_3} \langle (h^1)^3 \rangle^1 ; \\ \langle (h^1)^3 \rangle^1 &= \frac{\sum (\epsilon^1_\alpha)^3 N_\alpha}{N} \end{aligned} \tag{2.64}$$

Similarly the propagation equation for $\langle (V^{\nu=2})^2 \rangle^m$ is derived by using the p-h symmetry $\langle (V^{\nu=2})^2 \rangle^m = \langle (V^{\nu=2})^2 \rangle^{N-m}$. Choosing the input points for $m = 0, 1, 2, N, N-1$ and the property $\langle (V^{\nu=2})^2 \rangle^m = 0$ for $m = 0,\ 1,\ N,\ N-1$, the final result in terms of the TBME $V^J_{\alpha\beta\gamma\delta}(\nu = 2)$ of $V^{\nu=2}$ is

$$\langle (V^{\nu=2})^2 \rangle^m = \frac{[m]_2 [m^\times]_2}{[N]_4} \times \sum_{\alpha \geq \beta, \gamma \geq \delta, J} [J] (V^J_{\alpha\beta\gamma\delta}(\nu = 2))^2. \tag{2.65}$$

Using the unitary decomposition of h and V as given by (2.49) - (2.52) and using the propagation equations of $(h^1)^2$ and $(V^{\nu=2})^2$ given by (2.63) and (2.65), an explicit expression (unlike what is given by (2.65)) for $\langle \widetilde{H}^2 \rangle^m$ is,

$$\begin{aligned} \langle \widetilde{H}^2 \rangle^m &= \frac{mm^\times}{[N]_2} \left[\sum_\alpha (\epsilon^1_\alpha + (m-1)\epsilon^1_\alpha(2))^2 N_\alpha \right] \\ &+ \frac{[m]_2 [m^\times]_2}{[N]_4} \sum_{\alpha \geq \beta, \gamma \geq \delta, J} [J] (V^J_{\alpha\beta\gamma\delta}(\nu = 2))^2. \end{aligned} \tag{2.66}$$

(iv) In general it is possible to combine the principles involved in (i) - (iii) to derive simple propagation equations in some complicated examples. For example, in evaluating $\langle (h^1)^P \rangle^m$ for $P = 4$ and 5 one needs to extract

only the one and two-body parts of $(h^1)^P$ denoted as $X_P(i)$, $i = 1, 2$. The unitary tensor nature of h^1 and p-h symmetry will allow us to write $\langle (h^1)^P \rangle^m$ as $p_1(m)X_P(1) + p_2(m)X_P(2)$ and the polynomials p_1 and p_2 are easily determined using (i) and (ii). Then the propagation equation for $\langle (h^1)^4 \rangle^m$ is

$$\langle (h^1)^4 \rangle^m = \frac{mm^{\times}N}{[N]_4} \left\{ \left[N(N+1) - 6mm^{\times} \right] \left[N^{-1} \sum_{\alpha} (\epsilon^1_{\alpha})^4 N_{\alpha} \right] \right.$$
$$\left. +3(m-1)(m^{\times}-1)N \left[N^{-1} \sum_{\alpha} (\epsilon^1_{\alpha})^2 N_{\alpha} \right]^2 \right\} \qquad (2.67)$$

Similarly for $\langle (h^1)^6 \rangle^m$ one needs to extract out $X_6(i)$, $i = 1, 2, 3$. An equally simple case is the propagation equation for $\langle h^1 (V^{\nu=2})^2 \rangle^m$ and one needs here the input trace over 2-particle space and the final result is

$$\langle h^1 (V^{\nu=2})^2 \rangle^m = \frac{[m]_2 [m^{\times}]_2 (m^{\times} - m)}{[N]_5} \times$$
$$\frac{1}{2} \sum_{rtuv} [J] \epsilon^1_r (V^J_{rtuv}(\nu = 2))^2 (1 + \delta_{rt})(1 + \delta_{uv}). \qquad (2.68)$$

(v) The elementary traces of basic one to three-body operators in $1 - 3$ - particle spaces are: $\langle\langle a^{\dagger}_A a_B \rangle\rangle^1 = \delta_{AB}$; $\langle\langle a^{\dagger}_A a^{\dagger}_B a_C a_D \rangle\rangle^2 = \delta_{BC}\delta_{AD} - \delta_{AC}\delta_{BD}$; $\langle\langle a^{\dagger}_A a^{\dagger}_B a^{\dagger}_C a_D a_E a_F \rangle\rangle^3 = \delta_{FA}\delta_{DC}\delta_{EB} - \delta_{FA}\delta_{DB}\delta_{EC} - \delta_{EA}\delta_{DC}\delta_{FB} + \delta_{EA}\delta_{DB}\delta_{FC} + \delta_{DA}\delta_{EC}\delta_{FB} - \delta_{DA}\delta_{EB}\delta_{FC}$, where A, B, C etc. are single particle state indices. Extracting out the definite body rank parts of an operator which is a product of several (say $\nu = 2$) operators is tedious but straight forward. To do this, one has to put the operator in normal order form which follows by applying the anticommutation properties of single fermion state operators; $[a^{\dagger}_A a^{\dagger}_B]_+ = 0$, $[a_A a_B]_+ = 0$, $[a_A a^{\dagger}_B]_+ = \delta_{AB}$. Applying this together with (i), (ii), (iii) for the $\langle \mathbf{UVW} \rangle^m$ trace ($\mathbf{U}$, $\mathbf{V}$ and $\mathbf{W}$ are three different two-body interactions; note that as stated

below (2.57) **U**, **V** and **W** are automatically $\nu = 2$ with repect to $U(N)$) gives (we carried out this exercise although the final result is available in [Ay-74a, Wo-86]) the formula,

$$\langle \mathbf{UVW} \rangle^m = \left[\frac{[m]_3 [m^\times]_3}{[N]_6} \right] \mathbf{A} + \left[\frac{[m]_4 [m^\times]_2}{[N]_6} + \frac{[m]_2 [m^\times]_4}{[N]_6} \right] \mathbf{B}$$

$$\mathbf{A} = \sum_{\substack{\Delta \\ rstuxy}} (-1)^{r-t-\Delta} [\Delta]^{-1/2} \beta^{\Delta}_{rtsu}(\mathbf{U}) \beta^{\Delta}_{xysu}(\mathbf{V}) \beta^{\Delta}_{xytr}(\mathbf{W})$$

$$\mathbf{B} = \frac{1}{8} \sum_{\substack{J \\ \alpha\beta\gamma\delta\phi\psi}} [J] \widetilde{\mathbf{U}}^J_{\alpha\beta\gamma\delta} \widetilde{\mathbf{V}}^J_{\gamma\delta\phi\psi} \widetilde{\mathbf{W}}^J_{\phi\psi\alpha\beta} \; ;$$

$$\beta^{\Delta}_{rtsu}(\mathbf{X}) = \sum_J (-1)^{s+t+J+\Delta} [\Delta]^{1/2} [J] \left\{ \begin{matrix} r & s & J \\ u & t & \Delta \end{matrix} \right\} \widetilde{\mathbf{X}}^J_{rstu}$$

$$\widetilde{\mathbf{X}}^J_{rstu} = \sqrt{(1+\delta_{rs})(1+\delta_{tu})} \mathbf{X}^J_{rstu} \; ; \; \mathbf{X} = \mathbf{U}, \mathbf{V} or \mathbf{W} \qquad (2.69)$$

2.6.2 Spherical configuration averages

The principles used in deriving scalar trace propagation equations apply equally well for configuration traces $\langle F \rangle^{[\mathrm{m}]}$ of an operator F. This was done in detail in [Fr-71a, Ch-71, Ay-74a, He-75, Po-75, Pa-78, Wo-86]. However there is a simple method to produce fixed configuration traces [Fr-89a, Fr-89b, Fr-94] of operator products with the operators having fixed unitary rank with respect to the spherical configuration group. To derive the propagation equation for the trace $\langle A^{[\nu_1]} B^{[\nu_2]} .... \rangle^{\mathrm{m}}$ one has to start with the scalar trace propagation formula for $\langle A^{\nu_1} B^{\nu_2} ... \rangle^m$. Then one has to attach appropriate spherical orbit indices to particle number m and degeneracy N in the corresponding scalar propagation formulas and carry out the summation over all the spherical orbit indices after multiplying the propagator with the input with spherical orbit

indices. The input matrix elements of A^{ν_1}, B^{ν_2},... etc. are to be replaced by the matrix elements of $A^{[\nu_1]}$, $B^{[\nu_2]}$,... respectively. The right correspondence between the indices of inputs and those of propagators is to be decided and this can easily be done with a computer program. Simple examples are $\langle h\rangle^{\mathrm{m}} = \sum \epsilon_\alpha m_\alpha$ and $\langle V\rangle^{\mathrm{m}} = \sum_{\alpha\leq\beta} V_{\alpha\beta}\check{m}_{\alpha\beta}$ and they follow from (2.60) as $\langle h\rangle^{\mathrm{m}} = \langle h^{[0]}\rangle^{\mathrm{m}}$ and $\langle V\rangle^{\mathrm{m}} = \langle V^{[0]}\rangle^{\mathrm{m}}$. Propagation equation for $\langle \mathbf{V}^2\rangle^{\mathrm{m}}$ is easily obtained by starting with (2.65), changing $[m]_2 = m(m-1)$ by $m_{\alpha\beta}$ and $[m^{\times}]_2$ by $m^{\times}_{\alpha\beta}$ and noting that $\mathbf{V} = \mathbf{V}^{[2]}$. Thus for the traces $\langle \mathbf{UV}\rangle^{\mathrm{m}}$ or $\langle \mathbf{V}^2\rangle^{\mathrm{m}}$, ($\mathbf{U}$, $\mathbf{V}$ are of $\nu = [2]$ type with respect to spherical configuration group) it is easy to recognize the right combination of the indices in the propagators and the inputs,

$$\langle \mathbf{UV}\rangle^{\mathrm{m}} = \sum_{\substack{\alpha,\beta\\ \gamma,\delta}} m_{\alpha\beta} m^{\times}_{\gamma\delta} \left[N_{\alpha\beta\gamma\delta}\right]^{-1} \left\{ \frac{1}{4} \sum_J [J] \mathbf{U}^J_{\alpha\beta\gamma\delta} \mathbf{V}^J_{\alpha\beta\gamma\delta} (1+\delta_{\alpha\beta})(1+\delta_{\gamma\delta}) \right\} \tag{2.70}$$

The trace $\langle h^{[1]}\mathbf{V}^2\rangle^{\mathrm{m}}$ is zero because $h^{[1]}$ is zero. Using the method described above, it is possible to write down the formula for $\langle \mathbf{UVW}\rangle^{\mathrm{m}}$ using (2.69). The explicit formula is given in [Wo-86].

2.6.3 Unitary configuration averages

For unitary configuration traces $\langle F\rangle^{[\mathrm{m}]}$ the same procedure as above can be adopted (after carrying out tensorial decomposition of the operators involved with respect to the unitary configuration group). In this case unitary orbit indices are to be attached with m, N etc. of the propagators of the corresponding scalar trace propagation formulas and the summation is now over all unitary orbit indices. For the inputs, the indices are spherical orbit indices that belong

to particular unitary orbits and then the summation over those spherical orbit indices are to be carried out. Like in the spherical configurations case, the right combination of indices in the propagators and the inputs can be found out using a computer program. The formulas for $\langle \mathbf{UV} \rangle^{[\mathbf{m}]}$, $\langle h^{[1]}(\mathbf{V})^2 \rangle^{[\mathbf{m}]}$ and $\langle \mathbf{UVW} \rangle^{[\mathbf{m}]}$ are given below.

The derivation of trace propagation formula for $\langle \mathbf{UV} \rangle^{[\mathbf{m}]}$ is straight forward as $\mathbf{U}$ and $\mathbf{V}$ both have unitary rank [**2**] as stated below (2.58). Using the scalar result (2.65) (and also (2.70)) the formula for $\langle \mathbf{UV} \rangle^{[\mathbf{m}]}$ can be written down,

$$\begin{aligned} \langle \mathbf{UV} \rangle^{[\mathbf{m}]} \;=\; & \sum_{\mathbf{r,s,t,u}} \left[m_{\mathbf{rs}} m^{\times}_{\mathbf{tu}} \right] (N_{\mathbf{rstu}})^{-1} \times \\ & \frac{1}{4} \sum_{J} \quad [J] \mathbf{U}^{J}_{rstu} \mathbf{V}^{J}_{rstu} (1+\delta_{rs})(1+\delta_{tu}) \\ & \quad r \in \mathbf{r},\, s \in \mathbf{s} \\ & \quad t \in \mathbf{t},\, u \in \mathbf{u} \end{aligned} \tag{2.71}$$

The formula for $\langle (h^{\mathbf{1}})\mathbf{V}^2 \rangle^{[\mathbf{m}]}$ (required to calculate spin-cutoff density variance) is derived using the scalar result (2.68) and then looking for the correct combination of indices with the help of a computer program [Ha-92, Fr-94],

$$\begin{aligned} \langle (h)^{[1]}(\mathbf{V})^2 \rangle^{[\mathbf{m}]} \;=\; & \sum_{\mathbf{r,t,u,v}} \left[N^{-1}_{\mathbf{rtuvr}} m_{\mathbf{rt}} m^{\times}_{\mathbf{uvr}} - N^{-1}_{\mathbf{uvrrt}} m_{\mathbf{uvr}} m^{\times}_{\mathbf{tr}} \right] \times \\ & \frac{1}{2} \sum_{J} \quad [J] \epsilon^{[1]}_{r} \mathbf{V}^{J}_{rtuv} \mathbf{V}^{J}_{uvrt} (1+\delta_{rt})(1+\delta_{uv}) \\ & \quad r \in \mathbf{r}, t \in \mathbf{t} \\ & \quad u \in \mathbf{u}, v \in \mathbf{v} \end{aligned} \tag{2.72}$$

The trace propagation formula for $\langle \mathbf{UVW} \rangle^{[\mathbf{m}]}$ where all $\mathbf{U}$, $\mathbf{V}$, $\mathbf{W}$ are of tensorial rank [**2**] with respect to unitary configuration group, follows from (2.69) and the expression for $\langle \mathbf{UVW} \rangle^{\mathbf{m}}$ given in [Wo-86]. The final result is

[Ha-92, Fr-94],

$$\langle \mathbf{UVW} \rangle^{[\mathbf{m}]} = \sum_{\substack{\mathbf{r,s,t,u} \\ \mathbf{x,y}}} \left[\left\{ m_{\mathbf{rsy}} m^{\times}_{\mathbf{tux}} N^{-1}_{\mathbf{rsytux}} \right\} \mathbf{A}_{\mathbf{r,s,t,u,x,y}} \right] + \left[\left\{ [m_{\mathbf{rs}} m^{\times}_{\mathbf{tuxy}} N^{-1}_{\mathbf{rstuxy}} + m_{\mathbf{xytu}} m^{\times}_{\mathbf{rs}} \times N^{-1}_{\mathbf{xyturs}} \right\} \mathbf{B}_{\mathbf{r,s,t,u,x,y}} \right]$$

$$\mathbf{A}_{\mathbf{r,s,t,u,x,y}} = \sum_{\substack{\Delta \\ r \in \mathbf{r}, s \in \mathbf{s} \\ t \in \mathbf{t}, u \in \mathbf{u} \\ x \in \mathbf{x}, y \in \mathbf{y}}} (-1)^{r-t-\Delta} [\Delta]^{-1/2} \beta^{\Delta}_{rtsu}(\mathbf{U}) \, \beta^{\Delta}_{xysu}(\mathbf{V}) \beta^{\Delta}_{xytr}(\mathbf{W})$$

$$\mathbf{B}_{\mathbf{r,s,t,u,x,y}} = \frac{1}{8} \sum_{\substack{J \\ r \in \mathbf{r}, s \in \mathbf{s} \\ t \in \mathbf{t}, u \in \mathbf{u} \\ x \in \mathbf{x}, y \in \mathbf{y}}} [J] \mathbf{U}^{J}_{rstu} \mathbf{V}^{J}_{tuxy} \mathbf{W}^{J}_{xyrs} (1+\delta_{rs})(1+\delta_{tu})(1+\delta_{xy}) \tag{2.73}$$

The definition of the multipole coefficient β^{Δ}_{rstu} appearing in (2.73) is given in (2.69) and it follows from [Fr-66]. The formulas given in (2.71) - (2.73) are used in Chapters 3, 4 and 6. For example the variance $\langle \mathbf{V}^2 \rangle^{[\mathbf{m}]}$ of the density $\rho^{\mathbf{V},[\mathbf{m}]}_{\mathcal{G}}(x) = \langle \delta(\mathbf{V}-x) \rangle^{[\mathbf{m}]}$ follows from (2.71). Similarly the centroids and variances of the spin-cutoff density $\rho^{\mathbf{V},[\mathbf{m}]}_{J^2_Z} = \langle J^2_Z \delta(\mathbf{V}-x) \rangle^{[\mathbf{m}]} / \langle J^2_Z \rangle^{[\mathbf{m}]}$ follow from (2.71 - 2.73). The centroid of the J^2_Z - density derives from the trace $\langle J^2_Z \mathbf{V} \rangle^{[\mathbf{m}]} = \langle (J^2_Z)^{[2]} \mathbf{V} \rangle^{[\mathbf{m}]}$ (since $\langle \mathbf{V} \rangle^{[\mathbf{m}]} = 0$ and $\langle (J^2_Z)^{[1]} \mathbf{V} \rangle^{[\mathbf{m}]} = 0$) and $\langle (J^2_Z)^{[2]} \mathbf{V} \rangle^{[\mathbf{m}]}$ follows from Eq. (2.71). The spin-cutoff density variance derives from the trace $\langle J^2_Z \mathbf{V}^2 \rangle^{[\mathbf{m}]} = \langle (J^2_Z)^{[0]} \mathbf{V}^2 \rangle^{[\mathbf{m}]} + \langle (J^2_Z)^{[1]} \mathbf{V}^2 \rangle^{[\mathbf{m}]} + \langle (J^2_Z)^{[2]} \mathbf{V}^2 \rangle^{[\mathbf{m}]}$ and the three averages on R.H.S. follow from (2.71), (2.72) and (2.73) respectively.

2.7 Summary

Extension and application of the CLT results given in Sect. 2.3 to indefinitely large shell model spaces is the aim of SAT-LSS. This is achieved by using the unitary decompositions of operators described in Sect. 2.5 together with the S - decomposition, introduced ahead in Chapter 3, via spherical and unitary configuration partitioning (Sect. 2.4) and it is made practical by the trace propagation formulas given in Sect. 2.6. It is useful to mention that programs are available [Ko-84b, Ha-92] for carrying out unitary decompositions given in Sect. 2.5 and for the trace propagation formulas given in Sect. 2.6. In the next chapter the basic convolution result for state densities in SAT-LSS is described briefly before turning to a study (and tests) of two important aspects of SAT-LSS. The trace propagation methods described in Sect. 2.6 are used extensively in Chapter 5 to derive large number of trace propagation formulas relevant for the construction of non-interacting particle strength densities.

Chapter 3

Tests of Some Aspects of Spectral Averaging Theory in Large Shell Model Spaces for State, Spin-Cutoff and Occupancy Densities

3.1 Introduction

Extensions of the CLT results given in Chapter 2 to indefinitely large shell model spaces, enlarge the scope of spectral averaging theory as this will enable one to address problems in statistical nuclear physics, i.e. calculation of level densities and spin-cutoff factors, construction of strength functions of various kinds etc. However in doing so one faces two serious problems – as French and Kota [Fr-83b] state: "A problem of form, however, arises, with spectral averaging, from the initial restriction of the s.p. spectrum to a finite set of s.p. states. This leads to the level density as a superposition of configuration densities valid only for a restricted part of the spectrum. The consequence is that one loses contact with

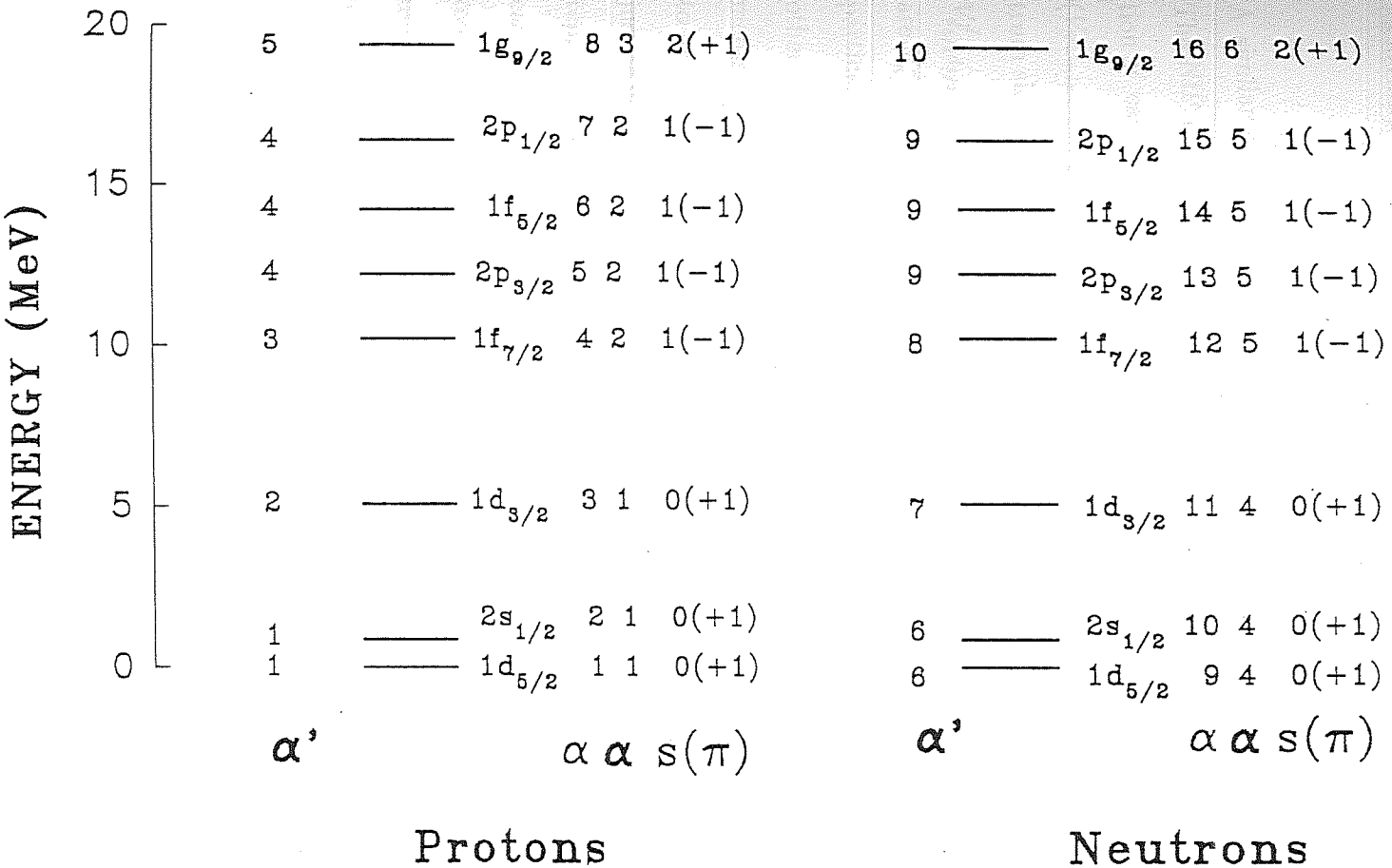
the essentially combinatorial NIP form. Moreover, as we extend the s.p. spectrum in order to proceed to higher energies we encounter a problem of substance, namely that the variances of all the configuration distributions increase indefinitely; this, on the face of it, generates ever larger orbital admixings and spreadings, destroying the shell model stability. We shall dispose of both of these problems." The problem of form is cured by employing unitary group decompositions of the hamiltonian (and other operators) from the beginning together with the use of a moment method for constructing NIP densities. The problem of substance is cured by introducing the so called s - quantum number to catalog configurations so that distant configurations can be identified and the admixing among them are then treated separately or ignored. With this one has the subject of SAT-LSS and as stated in Chapter 1, the present thesis undertakes to study some aspects of SAT-LSS and apply the theory to problems of interest in nuclear physics and nuclear astrophysics.

3.1.1 S - decomposition

Starting with the decomposition of m-particle spaces into unitary and spherical configurations given by (2.43), a further decomposition is possible by attaching a s_α label to each spherical orbit α where s_α for lighter nuclei denotes $s\hbar\omega$ excitation value; for heavy nuclei the definition of s has to be somewhat modified. The purpose of the s quantum number is to catalog distant configurations. Fig. 3.1 gives an example. Given s^π values for the spherical orbits α, one can define the unitary orbits $\boldsymbol{\alpha}$ such that all the spherical orbits with the same s^π values belong to $\boldsymbol{\alpha}$ (in Fig. 3.1, the unitary orbits $\boldsymbol{\alpha}'$ do not satisfy this criterion). Then the corresponding unitary configurations [m] define uniquely the S-subspaces of the m-particle space. With this, the m-particle space can

Figure 3.1

Classification of $(ds, fp, g_{9/2})$ spherical orbits in pn case in terms of unitary orbits and the corresponding s labels. The parity and all other quantum numbers for the orbits are shown. For example $1d_{5/2}$ implies $n = 0$, $\ell = 2$, $j = 5/2$ and the major oscillator number $N = 2n + \ell = 2$ and similarly $2p_{1/2}$ correspond to $n = 1$, $\ell = 1$, $j = 1/2$, $N = 3$ etc. Given the s^π quantum numbers for the spherical orbits, the largest possible unitary orbits correspond to $\boldsymbol{\alpha}$ in the figure. The unitary orbits $\boldsymbol{\alpha}'$ are finer than $\boldsymbol{\alpha}$. For the pn case shown in the figure, the conventions defined in Sect. 3.1.4 are followed.


ENERGY (MeV)
20
15
10
5
0
5 — 1g9/2 8 3 2(+1)
4 — 2p1/2 7 2 1(−1)
4 — 1f5/2 6 2 1(−1)
4 — 2p3/2 5 2 1(−1)
3 — 1f7/2 4 2 1(−1)
2 — 1d3/2 3 1 0(+1)
1 — 2s1/2 2 1 0(+1)
1 — 1d5/2 1 1 0(+1)
α' α α s(π)
Protons
10 — 1g9/2 16 6 2(+1)
9 — 2p1/2 15 5 1(−1)
9 — 1f5/2 14 5 1(−1)
9 — 2p3/2 13 5 1(−1)
8 — 1f7/2 12 5 1(−1)
7 — 1d3/2 11 4 0(+1)
6 — 2s1/2 10 4 0(+1)
6 — 1d5/2 9 4 0(+1)
α' α α s(π)
Neutrons

be decomposed into S-subspaces as follows:

$$m \rightarrow \sum S^{\pi} \; ; \; S^{\pi} \rightarrow \sum [\mathbf{m}]; \; [\mathbf{m}] \rightarrow \sum \mathbf{m} \; ; \; S = \sum m_{\alpha} s_{\alpha} \tag{3.1}$$

A similar decomposition of the hamiltonian $H = h(1) + V(2)$ is possible. The NIP hamiltonian $h = \epsilon_{\alpha} n_{\alpha}$, by definition is S - preserving. The interaction V can be decomposed into a part (V_{S-pres}) that preserves S and a part (V_{S-mix}) that mixes different S-subspaces. For example with the s.p. spectrum shown in Fig. 3.1, the $V^J_{\alpha\beta\gamma\delta}$ matrix elements that belong to V_{S-pres} are $V^J_{d_{5/2}d_{3/2}d_{5/2}s_{1/2}}$, $V^J_{d_{5/2}f_{7/2}d_{3/2}f_{5/2}}$, $V^J_{f_{5/2}p_{3/2}f_{7/2}p_{1/2}}$ etc. and those belong to V_{S-mix} are $V^J_{d_{5/2}d_{3/2}f_{7/2}f_{5/2}}$, $V^J_{d_{5/2}d_{3/2}f_{7/2}p_{3/2}}$ etc. With the S - decomposition of the m-particle space, there is a similar decomposition for the state densities (also for other densities as mentioned in Sect. 2.4); $I^m(E) = \sum_S I^{m,S}(E)$ and the moments $M_p(S)$ of $I^S(E)$ are $[\sum_{[\mathbf{m}]\in S} d([\mathbf{m}])]^{-1} \sum_{[\mathbf{m}]\in S} \langle\langle H^p \rangle\rangle^{[\mathbf{m}]}$. It is important to recognize that the fixed-S variance $\sigma^2(S) = \sigma^2(S \rightarrow S) + \sum_{S \neq S'} \sigma^2(S \rightarrow S')$ just as in (2.46, 2.47). The partial variance $\sigma^2(S \rightarrow S')$, which is due to V_{S-mix}, represents admixing between distant configurations (at least $2\hbar\omega$ away from each other) and this leads to multimodal forms for densities unlike the unimodal forms given by the CLT results in Sect. 2.3. A schematic model to understand the origin of the multimodal forms was introduced in [Fr-83b, Fr-84] and tests of some of the results of this model are given in Appendix A. Therefore in large shell model spaces either one should derive a method for incorporating the $\sigma^2(S \rightarrow S')$ partial variance corrections (i.e. V_{S-mix} effects) to the CLT results given in Sect. 2.3 or to the extent they are not harmful, just ignore them. The later is what is done in the remainder of the thesis and we will return to the former in Chapter 7. Thus by ignoring the V_{S-mix} part of the interaction $H \rightarrow h(1) + V_{S-pres} = h + V$ and in the thesis, from now onwards V stands for V_{S-pres} unless otherwise specified. Thus H is S preserving

and $I(E)$ decomposes into non-interacting partial $I^{m,S}(E)$ densities,

$$I^{H,m} = \sum_S I^{H,S}(E) = \sum_S \sum_{[\mathbf{m}]\in S} I^{H,[\mathbf{m}]}(E)$$

$$I^{H,S} \Leftrightarrow M_p(S) = \left[\sum_{[\mathbf{m}]\in S} d([\mathbf{m}])\right]^{-1} \sum_{[\mathbf{m}]\in S} d([\mathbf{m}]) M_p([\mathbf{m}]) \qquad (3.2)$$

Before going further, three points are worth mentioning and they are: (i) unlike the case with unitary configurations [m] which are defined by a group as described in Sect. 2.5, the s quantum number is not defined by a group and hence direct trace propagation for calculating $M_p(S)$ is not possible. However, as described in Sect. 2.6 $M_p([\mathbf{m}])$ given in (3.2) can be calculated using trace propagation equations; (ii) the V_{S-pres} in general admixes different unitary configurations [m] belonging to a given S and this admixing must be included while constructing the $I^{H,[\mathbf{m}]}$ densities appearing in (3.2); (iii) Eq. (3.2) extends directly to the case of expectation value densities. With the S - decomposition of the densities, we are in a position to describe the convolution results for state, spin-cutoff and occupancy densities in large shell model spaces. In the following section the state density results are described in some detail and only the final results for the last two densities are given.

3.1.2 Convolution form for state densities

In the absence of interactions, $H = h$ will produce spikes corresponding to each spherical configuration $\mathbf{m}$ at energies $\sum \epsilon_\alpha m_\alpha$ with degeneracy $\prod_\alpha \begin{pmatrix} N_\alpha \\ m_\alpha \end{pmatrix}$. Now, under spherical configuration group decomposition, $V(= V_{S-pres})$ splits into two parts, $V = V^{[0]} + \mathbf{V}$ as given in Sect. 2.5.2; $h \rightarrow h^{[0]}$ under spherical configurations. When the interction V is turned on, the spikes will shift (due to $V^{[0]}$) and spread and admix (due to $\mathbf{V}$). Leaving aside $\mathbf{V}$, the $V^{[0]}$ part only

moves the NIP spikes without spreading or admixing. The nature of the motion due to $V^{[0]}$ is understood by decomposing $V^{[0]}$ with respect to the unitary configuration group that defines the S quantum number. Then $V^{[0]}$ decomposes into three parts as given by (2.58): (i) a scalar $V^{[0][0]}$; (ii) an effective one-body part $V^{[0][1]}$ and (iii) an irreducible two-body part $V^{[0][2]}$. Similarly $h^{[0]}$ decomposes into $h^{[0][0]}$ and $h^{[0][1]}$. The $V^{[0][0]} + V^{[0][1]}$ part of $V^{[0]}$ just renormalizes the s.p. spectrum produced by $h = h^{[0]}$ and the renormalization is a simple function, as given explicitly by (2.58), of the unitary configuration one is dealing with. However the $V^{[0][2]}$ part will produce motion of NIP spikes that are not NIP type. Thus, to the extent that one can ignore the $V^{[0][2]}$ part of $V^{[0]}$ one has $H = \mathbf{h} + \mathbf{V}$ with $\mathbf{h}$ $(= h^{[0][0]} + h^{[0][1]} + V^{[0][0]} + V^{[0][1]})$ and $\mathbf{V}$ being orthogonal to each other ((3.13) ahead gives an example). Now the normalized density $\rho(E)$ for fixed-S can be written as

$$\rho^m(E) = \langle \delta(H-E)\rangle^m \Rightarrow \langle \delta(\mathbf{h}+\mathbf{V}-E)\rangle^{\mathbf{m}}$$

$$= [d(m)]^{-1} \sum_{\mathbf{m}} d(\mathbf{m}) \langle \delta(\mathbf{h}+\mathbf{V}-E)\rangle^{\mathbf{m}}$$

$$\xrightarrow[\substack{\text{each } \mathbf{m} \\ \text{subspace}}]{\substack{\text{CLT for} \\ }} [d(m)]^{-1} \sum d(\mathbf{m}) \langle \epsilon(\mathbf{m}) + \mathbf{V} - E\rangle^{\mathbf{m}}$$

$$= [d(m)]^{-1} \sum d(\mathbf{m}) \int \langle \mathbf{h}-x\rangle^{\mathbf{m}} \langle \mathbf{V}+x-E\rangle^{\mathbf{m}} dx$$

$$= [d(m)]^{-1} \sum I^{\mathbf{h},\mathbf{m}} \otimes \rho_{\mathcal{G}}^{\mathbf{v},\mathbf{m}}[E]$$

$$\begin{array}{l} \text{spreading variances} \\ \longrightarrow \\ \text{produced by } \mathbf{V} \text{ are} \\ \text{independent of } \mathbf{m} \end{array} \quad d^{-1}(m)\{\sum_{\mathbf{m}} I^{\mathbf{h},\mathbf{m}}\} \otimes \rho_{\mathcal{G}}^{\mathbf{v},m}[E]$$

$$= \rho^{\mathbf{h}} \otimes \rho_{\mathcal{G}}^{\mathbf{V}}[E] \tag{3.3}$$

$$\begin{aligned} \Longrightarrow I^H(E) &= \sum_S I^{\mathbf{h},S} \otimes \rho_{\mathcal{G}}^{\mathbf{V},S}[E] \\ &= \sum_S \left\{ \sum_{[\mathbf{m}]\in S} I^{\mathbf{h},[\mathbf{m}]} \otimes \rho_{\mathcal{G}}^{\mathbf{V},[\mathbf{m}]}[E] \right\}; \\ \rho_{\mathcal{G}}^{\mathbf{V},[\mathbf{m}]} \Leftrightarrow \sigma_{\mathbf{V}}([\mathbf{m}]) &= \left\{ \langle \mathbf{V}^2 \rangle^{[\mathbf{m}]} \right\}^{1/2} \\ \rho_{\mathcal{G}}^{\mathbf{V},S} \Leftrightarrow \sigma_{\mathbf{V}}(S) &= \left[\left\{ \sum_{[\mathbf{m}]\in S} d([\mathbf{m}]) \right\}^{-1} \sum_{[\mathbf{m}]\in S} d([\mathbf{m}]) \langle \mathbf{V}^2 \rangle^{[\mathbf{m}]} \right]^{1/2} \end{aligned} \tag{3.4}$$

The first two equations in (3.3) just define $\rho^m(E)$ taking into account that $V^{[0][2]}$ part is negligible. The third equality follows easily from (2.44). The fourth equality in (3.3) follows from the fact that $\mathbf{h}$ and $\mathbf{V}$ are orthogonal to each other and in the CLT limit the $\rho^{\mathbf{h}+\mathbf{V},\mathbf{m}}(E)$ will be a Gaussian with all the moments defined in terms of the centroid $\langle \mathbf{h}+\mathbf{V} \rangle^{\mathbf{m}} = \langle \mathbf{h} \rangle^{\mathbf{m}} = \epsilon(\mathbf{m})$ and variance $\langle (\mathbf{h}+\mathbf{V})^2 \rangle^{\mathbf{m}} = \langle \mathbf{h}^2 \rangle^{\mathbf{m}} + \langle \mathbf{V}^2 \rangle^{\mathbf{m}}$ which are additive with no cross term between $\mathbf{h}$ and $\mathbf{V}$; thus the CLT result given in (2.28) is applied locally. Then the local convolution form given by the fifth and sixth equalities is immediate. The seventh equality follows from the assumption of constancy of fixed-$\mathbf{m}$ variances. This leads to the result that I^H is a convolution of the NIP density $I^{\mathbf{h}}$ with the spreading Gaussian produced by $\mathbf{V}$ (in each S-subspace). Now carrying (3.3) over each S-subspace, one has the final convolution result given by (3.4); note that the S-subspaces are non-interacting. An additional fact, not mentioned before but is used in (3.3) is the feature of constancy of fixed-$\mathbf{m}$

widths. This is a well known result in SAT ([Pa-78, Wo-86] give examples) and in [Fr-83b, Fr-89a, Fr-94] it is explicitly verified that the spreading widths for $\mathbf{m}$'s that belong to fixed-S subspaces fluctuate very little from each other (the fluctuation is $\lesssim 3\%$) and its origin lies in an ensemble representation of $\mathbf{V}$ [Fr-89a, Fr-94]. Table 3.1 gives the average fixed-S spreading widths $\sigma_{\mathbf{V}}$ ((3.4) gives the definition of $\sigma_{\mathbf{V}}(S)$) in various parts of the periodic table. The results show that the widths are $\sim 6-8\ MeV$ for lighter nuclei ($A \lesssim 60$) and $\sim 2\ MeV$ for rare earth and actinide nuclei; the numbers are obtained using (2.71).

The convolution result given by (3.3) and (3.4) tacitly assumes that the internal structure of $\mathbf{V}$ does not play any role in generating smoothed state densities. All it does is to produce a *scale* which is the average spreading variance. If this is so, then all realistic interactions (in a given shell) should be highly correlated. This led us to calculate $\zeta_{\mathbf{V_1}-\mathbf{V_2}}$ for various ds-shell interactions. The results are given in the Table 3.2. As can be seen from Table 3.2, except for BARE-G and MSDI interactions, which are exceptional (BARE-G has no renormalization and MSDI is phenomenological), rest of the intearctions are highly correlated. The mass dependent UNIV-SD and BONN-J interactions are somewhat different from the rest of the interactions (PW, CW, KB, KLS-R, VY, K+12FP). Thus the results in the table indirectly justify the assumption that $\mathbf{V}$ produces a constant spreading width. This conclusion which is based on correlation coefficients, is consistent with the recent claim of Zucker and collaborators [Ab-91] who argued that as long as $V^{[0]}$ is taken care of properly, the saturation properties of nuclei can be described by any realistic interaction.

Table 3.1 Spreading widths $\sigma_{\mathbf{V}}$ (in MeV) for state densities in various parts of the periodic table. Given also in the table are also the centroid shifts $\epsilon_{\mathbf{V}:J_z^2}$ (in MeV) and spreading widths $\sigma_{\mathbf{V}:J_z^2}$ (in MeV) for spin-cutoff densities.

Space	Interaction	$(m_p, m_n, S)^\dagger$	$\sigma_{\mathbf{V}}$	$\epsilon_{\mathbf{V}:J_z^2}$	$\sigma_{\mathbf{V}:J_z^2}$
(ds)	KUO-67[i]	(2,4,0)	6.687	−0.644	6.146
		(4,4,0)	8.442	−0.837	7.800
		(6,6,0)	9.570	−0.942	8.840
	UNIV-SD[ii]	(2,4,0)	6.701	−0.681	6.171
		(4,4,0)	8.242	−0.861	7.627
		(6,6,0)	8.923	−0.921	8.254
(fp)	MWH2[iii]	(3,7,0)	5.905	−0.213	5.582
		(6,10,0)	7.846	−0.315	7.435
		(10,10,0)	8.565	−0.344	8.136
	FPM13[iv]	(3,7,0)	5.725	−0.282	5.419
		(6,10,0)	7.309	−0.391	6.928
		(10,10,0)	7.788	−0.417	7.399
(ds, fp)	KUO-7[v]	(4,4,0)	7.567	−1.077	6.993
		(4,4,1)	8.624	−1.107	8.212
		(4,4,2)	9.318	−0.995	8.993
		(6,6,0)	8.560	−1.222	7.933
		(6,6,1)	10.107	−1.219	9.583
		(6,6,2)	11.325	−1.253	10.866
		(8,8,0)	7.567	−1.007	6.993
		(8,8,1)	9.606	−1.134	9.006
		(8,8,2)	11.318	−1.237	10.809
#1	SDI[vi]	(10,10,0)	2.005	0.043	1.946
		(16,17,0)	2.071	0.030	2.013
	P + Q.Q[vi]	(10,10,0)	2.079	0.068	2.016
		(16,17,0)	2.022	0.072	1.965
#2	SDI[vi]	(10,16,0)	1.835	0.038	1.790
		(11,19,0)	1.905	0.040	1.861
	P + Q.Q[vi]	(10,16,0)	1.594	0.054	1.553
		(11,19,0)	1.640	0.058	1.598

[i][Ku-67]; [ii][Wi-84]; [iii][Mc-70]; [iv][Ri-91]; [v][Ku-71]; [vi]Appendix B
#1 $(2d_{5/2}1h_{11/2}2d_{3/2}3s_{1/2})^{m_p} \oplus (1h_{9/2}1i_{13/2}3p_{3/2}2f_{5/2}3p_{1/2})^{m_n}$;
#2 $(1h_{9/2}1i_{13/2}2f_{7/2})^{m_p} \oplus (2g_{9/2}1j_{15/2}1i_{11/2}3d_{5/2})^{m_n}$; † see Table 3.3.

Table 3.2 Correlation coefficients between V part of different *ds*-shell interactions

interaction #1	interaction #2	$\zeta_{V_1-V_2}$	interaction #1	interaction #2	$\zeta_{V_1-V_2}$
BARE-G[i]	KB[ii]	0.88	CW	KLS-R	0.98
	PW[iii]	0.87		VY	0.97
	CW[iv]	0.89		UNIV-SD	0.94
	KLS-R[v]	0.86		BONN-J	0.94
	VY[vi]	0.84		MSDI	0.81
	UNIV-SD[vii]	0.87		K+12FP	0.98
	BONN-J[viii]	0.85	KLS-R	VY	0.98
	MSDI[ix]	0.73		UNIV-SD	0.98
	K + 12FP[x]	0.87		BONN-J	0.98
KB	PW	0.99		MSDI	0.80
	CW	0.98		K +12FP	0.97
	KLS-R	0.99	VY	UNIV-SD	0.93
	VY	0.97		BONN-J	0.93
	UNIV-SD	0.92		MSDI	0.80
	BONN-J	0.92		K + 12FP	0.96
	MSDI	0.81	UNIV-SD	BONN-J	0.96
	K+12FP	0.98		MSDI	0.81
PW	CW	0.99		K+12FP	0.92
	KLS-R	0.98	BONN-J	MSDI	0.92
	VY	0.97		K+12FP	0.92
	UNIV-SD	0.92	MSDI	K+12FP	0.81
	BONN-J	0.92			
	MSDI	0.81			
	K+12FP	0.98			

All the calculations are carried out in five (m_p, m_n) spaces. The V parts of various interactions are obtained using (2.56, 2.57). The correlation coefficient $\zeta_{V_1-V_2}$ is defined by $\zeta_{V_1-V_2} = \langle V_1 V_2 \rangle^{m_p,m_n} / \{\langle V_1{}^2 \rangle^{m_p,m_n} \langle V_2{}^2 \rangle^{m_p,m_n}\}^{1/2}$ and all the traces are calculated using (2.71). The values of (m_p, m_n) are not shown in the table as ζ is found to be essentially independent of (m_p, m_n).

[i][*ds*-shell part of bare G-matrix elements of Hamada - Johnston potential obtained with $\hbar\omega = 12.5\ MeV$ [Ku-65]] ; [ii][the $3p-1h$ renormalized interaction from Hamada - Johnston potential with $\hbar\omega = 12.5\ MeV$ [Ku-65]] ; [iii][Pr-72] ; [iv][Va-77] ; [v][Ka-69] ; [vi][Va-77] ; [vii][Wi-84] ; [viii][Ji-92] ; [ix][Br-77] ; [x][Ha-71].

3.1.3 Convolution forms for spin-cutoff and occupancy densities

The convolution form (given by 3.3, 3.4) for state densities extended to spin-cutoff and occupancy densities $I^H_{J^2_Z}(E)$ and $I^H_{n_\alpha}(E)$ respectively [Fr-89b, Fr-94],

$$I^H_K(E) = \langle\langle K\delta(H-E)\rangle\rangle^m$$

$$= \sum_S I^{\mathrm{h},S}_K \otimes \rho^{\mathbf{V},S}_{K:\mathcal{G}}[E]\,;\quad K = J^2_Z \ \ or \ \ n_\alpha$$

$$\rho^{\mathbf{V},S}_K(x) = \frac{\langle K\delta(V-x)\rangle^{m,S}}{\langle K\rangle^{m,S}}\ ;$$

$$\rho^{\mathbf{V},S}_{K:\mathcal{G}}(E) \ \Leftrightarrow \ \left\{\begin{array}{lcl} \epsilon_{\mathbf{V}:K}(S) & = & \left\{\sum_{[\mathrm{m}]\in S} d([\mathrm{m}])\langle K\mathbf{V}\rangle^{[\mathrm{m}]}\right\} \Big/ \left\{\sum_{[\mathrm{m}]\in S} d([\mathrm{m}])\langle K\rangle^{[\mathrm{m}]}\right\} \\ \sigma_{\mathbf{V}:K}(S) & = & \left[\left\{\sum_{[\mathrm{m}]\in S} d([\mathrm{m}])\langle K\mathbf{V}^2\rangle^{[\mathrm{m}]}\right\} \Big/ \left\{\sum_{[\mathrm{m}]\in S} d([\mathrm{m}])\langle K\rangle^{[\mathrm{m}]}\right\}\right. \\ & & \left. -\{\epsilon_{\mathbf{V}:K}(S)\}^2\right]^{1/2} \end{array}\right. \tag{3.5}$$

The K - centroids $\epsilon_{\mathbf{V}:K}(S)$ (in fact centroid shifts with respect to the $\rho^{\mathbf{V}}_{\mathcal{G}}$ centroid $\epsilon_{\mathbf{V}} = \langle\mathbf{V}\rangle = 0$) and widths $\sigma_{\mathbf{V}:K}(S)$ define the $\rho^{\mathbf{V},S}_{K:\mathcal{G}}(E)$ spreading Gaussian densities. One can rewrite (3.5) in a slightly different form by using the unitary configurations $[\mathrm{m}]$ from the beginning,

$$\begin{aligned} I^H_K(E) &= \sum_S \left\{\sum_{[\mathrm{m}]\in S} I^{H,[\mathrm{m}]}_K(E)\right\} \\ &= \sum_S \left\{\sum_{[\mathrm{m}]\in S} I^{\mathrm{h},[\mathrm{m}]}_K \otimes \rho^{\mathbf{V},[\mathrm{m}]}_{K:\mathcal{G}}[E]\right\}; \\ \rho^{\mathbf{V},[\mathrm{m}]}_K(y) &= \langle K\delta(\mathbf{V}-y)\rangle^{[\mathrm{m}]}/\langle K\rangle^{[\mathrm{m}]}\,; \end{aligned}$$

$$\rho^{\mathbf{V},[\mathbf{m}]}_{K:\mathcal{G}} \Leftrightarrow \begin{cases} \epsilon_{\mathbf{V}:K}([\mathbf{m}]) &= \langle K\mathbf{V}\rangle^{[\mathbf{m}]}/\langle K\rangle^{[\mathbf{m}]} \\ \sigma_{\mathbf{V}:K}([\mathbf{m}]) &= \left[\langle K\mathbf{V}^2\rangle^{[\mathbf{m}]}/\langle K\rangle^{[\mathbf{m}]} - \{\epsilon_{\mathbf{V}:K}([\mathbf{m}])\}^2\right]^{1/2} \end{cases} \tag{3.6}$$

The form given in (3.6) for I^H_K is employed in Chapter 4 for reasons that are explained there. Modifications of the results given in (3.5, 3.6) in the cases $\langle K\rangle^{\mathbf{m}} = 0$ is straightforward. For the occupancy densities $K = n_\alpha$ it is easily seen that the centroid shifts $\epsilon_{\mathbf{V}:n_\alpha}$ are zero and in addition the widths $\sigma_{\mathbf{V}:n_\alpha}$ are very close to $\sigma_{\mathbf{V}}$; (2.72) enables one to calculate $\sigma_{\mathbf{V}:n_\alpha}([\mathbf{m}])$ and $\sigma_{\mathbf{V}:n_\alpha}(S)$. For the spin-cutoff densities $I^H_{J^2_Z}(E)$, the centroid shifts $\epsilon_{\mathbf{V}:J^2_Z}$ are not zero and they can be calculated using (2.71). Similarly the spin-cutoff spreading variances can be calculated using (2.71 - 2.73). Table 3.1 gives the average fixed-S spin-cutoff centroid shifts $\epsilon_{\mathbf{V}:J^2_Z}$ and spreading widths $\sigma_{\mathbf{V}:J^2_Z}$. One striking result that follows from Table 3.1 is that the spin-cutoff variances are consistently smaller than the state density variances and the difference is $\sim 10\%$. This result is used in Chapter 4.

3.1.4 Moment methods and convolution forms for NIP state, spin-cutoff and occupancy densities

In order to apply (3.3) - (3.6), it is essential to have good methods for constructing NIP densities $I^h(E)$ and their S - decompositions; methods for calculating the centroids and variances of the spreading functions are already given. In principle one can construct NIP densities exactly by using spherical orbits and spherical configurations, i.e. by employing the well known direct counting method [Hi-69]. However this method suffers from several problems: (i) the method becomes very slow with increasing number of spherical orbits,

typically, say the number of orbits ≥ 6; (ii) the method will not yield information about the underlying structures that generate the NIP densities; (iii) it will not give any explanation to the connection between the CLT Gaussian form and Bethe's exponential $exp\sqrt{aE}$ form for the densities. Moment methods (based on calculating the moments of the distributions and then using Edgeworth expansion (2.8)) cure these problems and enables one to construct the NIP densities rapidly and produce smoothed forms for the densities. The moment methods are easy to apply since NIP densities defined over a particular unitary configuration can be written as a multiple convolution of the densities defined over each unitary orbit. From now onwards, in this section, without loss of generality, $h = \mathbf{h}$.

With the decomposition (3.1) of the spectroscopic space, the NIP state density $I^h(E)$ and its decompositions are (assuming that there are L unitary orbits) [Fr-89a, Fr-94],

$$I^{h,m}(E) = \langle\langle \delta(h-E)\rangle\rangle^m = d(m)\langle \delta(h-E)\rangle^m = \sum_{[\mathbf{m}]} \langle\langle \delta(h-E)\rangle\rangle^{[\mathbf{m}]}$$

$$= \left[\sum_{[\mathbf{m}]} I^{h,[\mathbf{m}]}(E)\right] = \sum_S \left\{ \sum_{[\mathbf{m}]\in S} I^{h,[\mathbf{m}]}(E)\right\} = \sum_S I^{h,S}(E) \qquad (3.7)$$

$$I^{h,[\mathbf{m}]}(E) = I^{h\boldsymbol{\alpha}}_{N_{\boldsymbol{\alpha}}} \otimes I^{h\boldsymbol{\beta}}_{N_{\boldsymbol{\beta}}} \otimes ..... \otimes I^{h\mathbf{L}}_{N_{\mathbf{L}}}\ [E] \qquad (3.8)$$

In deriving (3.8), the following decomposition of the NIP hamiltonian is used: $h = \sum \epsilon_\alpha n_\alpha = \sum_\alpha h_\alpha = \sum_{\boldsymbol{\alpha}} h\boldsymbol{\alpha} = \sum_{\boldsymbol{\alpha}} \left\{ \sum_{\alpha\in\boldsymbol{\alpha}} h_\alpha \right\}$. The first four central moments $\mathcal{M}_r$ of single unitary orbit densities $I^{h\boldsymbol{\alpha}}_{N_{\boldsymbol{\alpha}}}$ can be obtained using (2.63, 2.64, 2.67). The convolution form in (3.8) implies that the cumulants of $I^{h,[\mathbf{m}]}$ are sum of the cumulants of $I^{h\boldsymbol{\alpha}}_{N_{\boldsymbol{\alpha}}}$. Applying the CLT, the Edgeworth corrected

Gaussian representation for $I^{h,[\mathrm{m}]}(E)$ can be constructed and hence $I^{h,S}(E)$ and $I^{h,m}(E)$. Eqs. (3.7, 3.8) extend to the more complicated expectation value densities $I^h_K(E)$. For example the occupancy density and its decompositons are [Fr-89b, Fr-94]

$$I^{h,m}_{n_\alpha}(E) = \langle\langle n_\alpha \delta(h-E)\rangle\rangle^m = \sum_{[\mathrm{m}]} \langle\langle n_\alpha \delta(h-E)\rangle\rangle^{[\mathrm{m}]} = \sum_{[\mathrm{m}]} I^{h,[\mathrm{m}]}_{n_\alpha}(E)$$

$$= \sum_S \left\{ \sum_{[\mathrm{m}]\in S} I^{h,[\mathrm{m}]}_{n_\alpha}(E) \right\} = \sum_S I^{h,S}_{n_\alpha}(E); \tag{3.9}$$

$$I^{h,[\mathrm{m}]}_{n_\alpha}(E) = I^{h\boldsymbol{\alpha}}_{N_{\boldsymbol{\alpha}};n_\alpha} \otimes I^{h\boldsymbol{\beta}}_{N_{\boldsymbol{\beta}}} \otimes \ldots\ldots \otimes I^{h_{\mathbf{t}}}_{N_{\mathbf{t}}} \otimes \ldots\ldots \otimes I^{h_{\mathbf{L}}}_{N_{\mathbf{L}}}\ [E] \quad \text{for } \alpha \in \boldsymbol{\alpha}. \tag{3.10}$$

In applying the convolution result (3.10) for orbit $\tau \in \mathbf{t}$, the suffix n_τ in the R.H.S. of (3.10) should be attached to $I^{h_{\mathbf{t}}}_{N_{\mathbf{t}}}$, i.e. $I^{h_{\mathbf{t}}}_{N_{\mathbf{t}}} \to I^{h_{\mathbf{t}}}_{N_{\mathbf{t}};n_\tau}$ and $I^{h\boldsymbol{\alpha}}_{N_{\boldsymbol{\alpha}};n_\alpha} \to I^{h\boldsymbol{\alpha}}_{N_{\boldsymbol{\alpha}}}$. The moments of $I^{h\boldsymbol{\alpha}}_{N_{\boldsymbol{\alpha}};n_\alpha}(E)$ follow by the parametric differentiation of the moments of $I^{h\boldsymbol{\alpha}}_{N_{\boldsymbol{\alpha}}}(E)$ as given by (2.34). Thus once again applying CLT, Edgeworth corrected Gaussian representation for $I^{h,[\mathrm{m}]}_{n_\alpha}(E)$ can be constructed and hence $I^{h,S}_{n_\alpha}(E)$ and $I^{h,m}_{n_\alpha}(E)$. Extension of (3.9) to J^2_Z operator is immediate,

$$I^{h,m}_{J^2_Z}(E) = \langle\langle J^2_Z \delta(h-E)\rangle\rangle^m = \sum_S I^{h,S}_{J^2_Z}(E) = \sum_S \left[\sum_{[\mathrm{m}]\in S} I^{h,[\mathrm{m}]}_{J^2_Z}(E) \right] \tag{3.11}$$

The moments of $I^{h,[\mathrm{m}]}_{J^2_Z}(E)$ follow from the convolution result given in (3.8) with $h \to h + \lambda J_Z$ and carrying out double parametric differention of resulting moments as given by (2.35). Alternatively noting that $J_Z = \sum_\alpha J_Z(\alpha)$ and $\langle J^2_Z\rangle = \sum_\alpha \langle J^2_Z(\alpha)\rangle$, one can apply the convolution result (3.10) for $J^2_Z(\alpha)$ (in place of n_α) and this then will yield the moments of $I^{h,[\mathrm{m}]}_{J^2_Z}(E)$.

3.1.5 Summary of convolution results and conventions for pn systems

To summarize, in SAT-LSS as given by (3.3) - (3.6) the state, spin-cutoff and occupancy densities are sum of partial non-interacting fixed-S densities with density for each S taking a convolution form. Given $H = \mathbf{h} + \mathbf{V}$, the fixed-$S$ densities are convolution of NIP densities produced by $\mathbf{h}$ with the spreading Gaussuian produced by $\mathbf{V}$. The spreading Gaussians are determined by first two moments viz. by centroids and variances. In addition the moment method also allows to construct NIP densities as there are further convolution forms for partial NIP densities as given by (3.7 - 3.11). Our purpose in this chapter is to test (in a comprehensive manner) two important aspects of SAT-LSS and they are: (i) establishing that $V^{[0][2]}$ is small for intearctions all across the periodic table; (ii) test of moment methods for constructing the NIP densities and their S - decompositions. The results of these studies are given in Sects. 3.2 and 3.3 respectively. In the examples given in Sects 3.2 and 3.3 as well as in Chapters 3 - 6 pn systems are dealt with or in other words the pn formalism (but not the isospin formalism) is used. All the results given in Chapter 2 and in Sect. 3.1 apply directly to the pn case with the following conventions. The conventions given below are used throughout the thesis unless otherwise specified.

For pn systems, with protons and neutrons occupying spherical orbits α with angular momentum j_α, the following conventions are used. Let us assume that there are k_p number of proton orbits and k_n number of neutron orbits. Then the orbit label α takes values $\alpha = 1, 2, ..., k_p + k_n$ with α = 1,2,...k_p being protron orbits α(p) and $\alpha = k_p + 1,\ k_p + 2$,...$k_p + k_n$ being neutron

orbits α(n) as shown for example in Fig. 3.1. A pn configuration $(\mathbf{m_p}, \mathbf{m_n})$ $= (m_p^1, m_p^2, ..., m_p^{k_p}, m_n^1, m_n^2, ..., m_n^{k_n})$ then corresponds to the configuration $\mathbf{m}$ $= (m_1, m_2, ...m_{k_p+k_n})$ with $m_1 = m_p^1$, $m_2 = m_p^2, ..., m_{k_p} = m_p^{k_p}$, $m_{k_p+1} = m_n^1$, $m_{k_p+2} = m_n^2, ..., m_{k_p+k_n} = m_n^{k_n}$, where $m_p^{\alpha(p)}$ and $m_n^{\alpha(n)}$ are proton and neutron numbers in orbits α(p) and $\alpha(n)$ respectively and m_α is number of particles in the orbit α. Similarly defined are the SPE ϵ_α, the orbit degeneracies N_α, $N_{\boldsymbol{\alpha}}$, $V_{\alpha\beta}$, $V_{\boldsymbol{\alpha\beta}}$ etc. In the pn case, the eigenstates of h are given by the spherical configurations $\mathbf{m} = (\mathbf{m_p}, \mathbf{m_n})$ with energies $\epsilon(\mathbf{m_p}, \mathbf{m_n}) = \epsilon(\mathbf{m}) = \sum m_\alpha \epsilon_\alpha$ and dimensionalities $d(\mathbf{m_p}, \mathbf{m_n}) = d(\mathbf{m}) = \prod_\alpha \begin{pmatrix} N_\alpha \\ m_\alpha \end{pmatrix}$. Let us consider the example of 4 protons and 6 neutrons in the space defined by the spherical orbits $1d_{5/2}$, $2s_{1/2}$, $1d_{3/2}$, $1f_{7/2}$, $2p_{3/2}$, $2p_{1/2}$, $1f_{5/2}$. With the conventions defined above, $\alpha = 1, 2, 3, 4, 5, 6, 7, 8, 9, 10, 11, 12, 13, 14$ correspond to $1d_{5/2}$, $2s_{1/2}$, $1d_{3/2}$, $1f_{7/2}$, $2p_{3/2}$, $2p_{1/2}$, $1f_{5/2}$, $1d_{5/2}$, $2s_{1/2}$, $1d_{3/2}$, $1f_{7/2}$, $2p_{3/2}$, $2p_{1/2}$ and $1f_{5/2}$ orbits respectively; the first seven orbits are for protons and the next seven are for neutrons. The configuration (4,0,0,0,0,0,0,6,0,0,0,0,0,0) correspond to $(1d_{5/2})^{4p}(1d_{5/2})^{6n}$ and similarly (3,0,1,0,0,0,0,4,0,0,2,0,0,0) correspond to $(1d_{5/2})^{3p}(1d_{3/2})^{1p}(1d_{5/2})^{4n}(1f_{7/2})^{2n}$ etc. Also $N_\alpha = 6, 2, 4, 8, 4, 2, 6, 6, 2, 4, 8, 4, 2, 6$ for $\alpha = 1, 2, 3, ..., 14$. Finally it should be added that for the case of unitary orbits in pn case, the unitary orbits should be chosen such that the spherical orbits belong to a unitary orbit are all either proton orbits or neutron orbits; Fig. 3.1 and the footnotes to Table 3.3 ahead give examples. In the example considered above, choosing ds and fp orbits to be unitary orbits, $\boldsymbol{\alpha} = 1, 2, 3, 4$ correspond to ds, fp, ds and fp with $N_{\boldsymbol{\alpha}} = 12, 20, 12, 20$ respectively; the first two orbits are for protons and the next two are for neutrons. The unitary configuration [4,0,6,0] corresponds to $(ds)^{4p}(ds)^{6n}$ and similarly [3,1,4,2] corresponds to $(ds)^{3p}(fp)^{1p}(ds)^{4n}(fp)^{2n}$ etc.

3.2 Test of the smallness of $V^{[0][2]}$ part of various interactions

In this section, a large variety of nuclear hamiltonians ($H = h(1) + V(2)$) are considered in spectroscopic spaces relevant for nuclei in various parts of the periodic table (*ds*, *fp*, *ds-fp*, *ds-fp-sdg* etc.) and employing a norm that defines sizes of operators (footnote #3 in Chapter 1), it is shown that $V^{[0][2]}$, the non-NIP like part of $V^{[0]}$, is indeed small in all cases considered. Similar results are obtained in [Fr-83b, Fr-89a] by considering some limited examples and the present exercise aims at completeness; results of this section are first reported in [Ko-92b]. Given the one plus two-body hamiltonian $H = h(1) + V(2)$ defined by the SPE ϵ_α and TBME $V^J_{\alpha\beta\gamma\delta}$, using (2.56, 2.57) the decomposition $H = \left\{h(1) + V^{[0]}\right\} + \mathbf{V}$ is carried out with $V^{[0]}$ defined by $V_{\alpha\beta}$ matrix elements (2.50). As described in Sect. 3.1, $H \rightarrow \mathbf{h} + \mathbf{V}$; $h(1) + V^{[0]} \rightarrow \mathbf{h} = \left[h^{[0][0]} + V^{[0][0]}\right] + \left[h^{[0][1]} + V^{[0][1]}\right]$ provided $V^{[0][2]}$ is neglected. The decompositon of $h(1) + V^{[0]}$ into unitary tensor parts follows from (2.58) with the transcription $\mathcal{E}_\alpha \rightarrow \epsilon_\alpha$, $C_{\alpha\beta} \rightarrow V_{\alpha\beta}$, $\mathcal{E}_{\boldsymbol{\alpha}} \rightarrow \epsilon_{\boldsymbol{\alpha}}$, $C_{\boldsymbol{\alpha\beta}} \rightarrow V_{\boldsymbol{\alpha\beta}}$, $\mathcal{E}^{[1]}_\alpha \rightarrow \epsilon^{[1]}_\alpha$ and $\mathcal{A}^{[1]} \rightarrow H^{[0][1]}$.

In order to establish that the $V^{[0][2]}$ part of $\{h + V^{[0]}\}$ is small compared to the $\{h^{[0][1]} + V^{[0][1]}\}$ part ($\{h^{[0][0]} + V^{[0][0]}\}$ part of $\mathbf{h}$ behaves as a scalar (number) with respect to unitary configurations and hence this part need not be considered in the calculation of norms), the unitary norm [Fr-72, Fr-83b] which gives the measure of the size of an operator is employed. In the present case, the fixed unitary configuration norm $|\mathcal{O}|_{[\mathbf{m}]}$ of an operator $\mathcal{O}$ (which do not have $[\mathbf{0}]$ tensor part) is defined simply by $|\mathcal{O}|^2_{[\mathbf{m}]} = \langle \mathcal{O}^\dagger \mathcal{O} \rangle^{[\mathbf{m}]}$; the unitary configuration trace on the R.H.S. follows from the results given in Sect. 2.6.

The explicit propagation equations for the squares of norms of $h^{[0][1]}$, $V^{[0][1]}$, $H^{[0][1]} = h^{[0][1]} + V^{[0][1]}$ and $V^{[0][2]}$ are given by,

$$\begin{aligned}
\left|h^{[0][1]}\right|^2_{[\mathrm{m}]} &= \sum_{\boldsymbol{\alpha}} \frac{m_{\boldsymbol{\alpha}} m^{\times}_{\boldsymbol{\alpha}}}{N_{\boldsymbol{\alpha}\boldsymbol{\alpha}}} \sum_{\alpha} N_{\alpha} \left\{\epsilon^{[1]}_{\alpha}\right\}^2 \\
\left|V^{[0][1]}\right|^2_{[\mathrm{m}]} &= \sum_{\boldsymbol{\alpha}} \frac{m_{\boldsymbol{\alpha}} m^{\times}_{\boldsymbol{\alpha}}}{N_{\boldsymbol{\alpha}\boldsymbol{\alpha}}} \sum_{\alpha} N_{\alpha} \left\{\zeta^{[1]}_{\alpha}([\mathrm{m}])\right\}^2 \\
\left|H^{[0][1]}\right|^2_{[\mathrm{m}]} &= \sum_{\boldsymbol{\alpha}} \frac{m_{\boldsymbol{\alpha}} m^{\times}_{\boldsymbol{\alpha}}}{N_{\boldsymbol{\alpha}\boldsymbol{\alpha}}} \sum_{\alpha} N_{\alpha} \left\{\xi^{[1]}_{\alpha}([\mathrm{m}])\right\}^2 \\
\left|V^{[0][2]}\right|^2_{[\mathrm{m}]} &= \sum_{\boldsymbol{\alpha}\geq\boldsymbol{\beta}} \frac{m_{\boldsymbol{\alpha}\boldsymbol{\beta}} m^{\times}_{\boldsymbol{\alpha}\boldsymbol{\beta}}}{N_{\boldsymbol{\alpha}\boldsymbol{\beta}\boldsymbol{\alpha}\boldsymbol{\beta}}} [1+\delta_{\boldsymbol{\alpha}\boldsymbol{\beta}}]^{-1} \sum_{\substack{\alpha\in\boldsymbol{\alpha} \\ \beta\in\boldsymbol{\beta}}} (V^{[0][2]}_{\alpha\beta})^2 N_{\alpha\beta}
\end{aligned} \tag{3.12}$$

It is essential to recognize that the different $[\boldsymbol{\nu}]$ tensor parts of $h + V^{[0]}$ are orthogonal to each other with respect to the fixed-$[\mathrm{m}]$ norm defined above. In general for one plus two-body operators $\mathcal{A} = \sum_{[\boldsymbol{\nu}]} \mathcal{A}^{[\boldsymbol{\nu}]}$ and $\mathcal{B} = \sum_{[\boldsymbol{\nu}]} \mathcal{B}^{[\boldsymbol{\nu}]}$,

$$\langle \mathcal{A}\mathcal{B} \rangle^{[\mathrm{m}]} = \langle \mathcal{A}^{[0]}\mathcal{B}^{[0]} \rangle^{[\mathrm{m}]} + \langle \mathcal{A}^{[1]}\mathcal{B}^{[1]} \rangle^{[\mathrm{m}]} + \langle \mathcal{A}^{[2]}\mathcal{B}^{[2]} \rangle^{[\mathrm{m}]}. \tag{3.13}$$

Applying (3.13), gives the important result that in $h + V^{[0]} \rightarrow H^{[0][1]} + V^{[0][2]}$, $V^{[0][2]}$ is orthogonal to $H^{[0][1]}$ and therefore the smallness of $V^{[0][2]}$ can be established by comparing the norm of $H^{[0][1]} + V^{[0][2]}$ with that of $V^{[0][2]}$. Finally, fixed-S norms are defined in terms of fixed-$[\mathrm{m}]$ norms as follows,

$$|K|^2_S = \left[\sum_{[\mathrm{m}]\in S} d([\mathrm{m}])\right]^{-1} \left[\sum_{[\mathrm{m}]\in S} d([\mathrm{m}]) |K|^2_{[\mathrm{m}]}\right] \tag{3.14}$$

where $K = h^{[0][1]}$, $V^{[0][1]}$, $H^{[0][1]}$ or $V^{[0][2]}$.

The unitary decomposition and calculation of norms are carried out for the following cases and they span the entire periodic table:

(*i*) The ds-shell interactions :

(a) Chung Wildenthal interaction (given in [Va-77]) (CW) with ^{17}O energies (−4.15, 0.93, −3.28) MeV for ($1d_{5/2}$, $1d_{3/2}$, $2s_{1/2}$) orbits.

(b) Preedom Wildenthal interaction [Pr-72] (PW) with ^{17}O energies (−4.15, 0.93, −3.28) MeV for ($1d_{5/2}$, $1d_{3/2}$, $2s_{1/2}$) orbits.

(c) Universal−sd interaction (UNIV-SD) of Wildenthal [Wi-84] where the two-body matrix elements have A-dependence $(18/A)^{0.3}$ and the SPE are (−3.948, 1.647, −3.164) MeV for ($1d_{5/2}$, $1d_{3/2}$, $2s_{1/2}$) orbits.

(d) Interaction (BONN-J) derived from Bonn-A potential by Jiang et al [Ji-92]. The SPE are (0.000, 5.080, 0.870) MeV for ($1d_{5/2}$, $1d_{3/2}$, $2s_{1/2}$) orbits.

(e) Pairing plus quadrupole - quadrupole (P + Q.Q) interaction (given in Appendix B) with ^{17}O energies (−4.15, 0.93, −3.28) MeV for ($1d_{5/2}$, $1d_{3/2}$, $2s_{1/2}$) orbits.

(*ii*) fp-shell interactions :

(a) The McGrory, Wildenthal and Halbert interaction as modified by Sharma and Bhatt (MWH2) [Mc-70] with ^{41}Ca energies (−8.364, −6.264, −1.864, −4.464) MeV for ($1f_{7/2}$, $2p_{3/2}$, $1f_{5/2}$, $2p_{1/2}$) orbits.

(b) FPM13 interaction of Richter et al [Ri-91] where TBME have the scale factor $(42/A)^{0.35}$ and SPE are (−8.364, −6.333, −2.154, −4.407) MeV for ($1f_{7/2}$, $2p_{3/2}$, $1f_{5/2}$, $2p_{1/2}$) orbits.

(*iii*) ($2p_{3/2}$, $1f_{5/2}$, $2p_{1/2}$, $1g_{9/2}$) space interaction KBB which is a modified version of the KUO interaction [Ku-69]; the SPE are (0.000, 0.780, 1.080,

3.000) MeV respectively.

(*iv*) ($1f_{7/2}$, $1f_{5/2}$, $2p_{3/2}$, $2p_{1/2}$, $1d_{5/2}$, $1d_{3/2}$, $2s_{1/2}$) space with Kuo interaction KUO-7; the $7(ds-fp)$ - orbit part of the KUO-10 orbit interaction defined in the 10-orbit ($1f_{7/2}$, $1f_{5/2}$, $2p_{3/2}$, $2p_{1/2}$, $1d_{5/2}$, $1d_{3/2}$, $2s_{1/2}$, $1p_{3/2}$, $1p_{1/2}$, $1s_{1/2}$) space [Ku-71]. The SPE (in MeV) are (9.380, 15.570, 11.400, 13.410, −4.150, 0.930, −3.280) respectively for the above seven fp and ds orbits. They derive from the p-h spectrum of ^{16}O as given in [Sp-65]; see also the discussion following KUO-12 interaction.

(*v*) ($1d_{5/2}$, $2s_{1/2}$, $1d_{3/2}$, $1f_{7/2}$, $2p_{3/2}$, $1f_{5/2}$, $2p_{1/2}$, $1g_{9/2}$, $2d_{5/2}$, $1g_{7/2}$, $3s_{1/2}$, $2d_{3/2}$) space with KUO interaction KUO-12; 12-orbit (ds, fp, sdg) part of the KUO-15 orbit interaction defined in the 15-orbit ($1s_{1/2}$, $1p_{3/2}$, $1p_{1/2}$, $1d_{5/2}$, $2s_{1/2}$, $1d_{3/2}$, $1f_{7/2}$, $2p_{3/2}$, $1f_{5/2}$, $2p_{1/2}$, $1g_{9/2}$, $2d_{5/2}$, $1g_{7/2}$, $3s_{1/2}$, $2d_{3/2}$) space [Ku-71]. The SPE (in MeV) are (−4.150, −3.820, 0.930, 7.210, 9.230, 13.400, 11.240, 17.780, 22.460, 21.780, 23.780, 24.380). The energies of the first 7-orbits derive from the energies of the p-h spectrum of ^{16}O as given in [Sp-65]. The $g_{9/2}$ orbit is put 1 MeV above $f_{5/2}$ orbit, ($g_{7/2}$ − $g_{9/2}$) separation is chosen to be 4 MeV and the energies of $2d_{5/2}$, $3s_{1/2}$ and $2d_{3/2}$ orbits are chosen to be that of ^{116}Sn as given in [Bo-85]. In addition the $ds-fp$ separation is increased by Δ_1 MeV and $fp-sdg$ separation by Δ_2 MeV where the origin and the values of (Δ_1, Δ_2) are given in the footnote below [1].

[1] While dealing with ds-shell nuclei with KUO-10 orbit interaction and ds and fp-shell nuclei with KUO-15 orbit interaction, for many purposes one can eliminate the closed (for $S=0$ configurations) s and p shells. However this introduces renormalization of the resulting 7 and 12 orbit interaction hamiltonians. The one of consequence in the present exercise is the renormalization of h. Let us consider the 10 to 7 orbit reduction with s, p, ds and fp defining the unitary orbits $\alpha = 1, 2, 3$ and 4 respectively (for both protons and neutrons). By eliminating s and p orbits, one should take into account the $ds-fp$ splitting produced

(*vi*) Rare-earth nuclei with Surface Delta Interaction (SDI) and P + Q.Q interaction; definitions of these interactions are given in Appendix B. The SPE are from zero deformation Nilsson energies [Bo-75]. For example, the SPE for the rare-earth nucleus $^{168}_{68}Er_{100}$ are (41.523, 42.194, 43.100, 44.554, 44.841) MeV and (48.475, 49.137, 49.910, 51.410, 51.778, 52.826) MeV for ($1g_{7/2}$, $2d_{5/2}$, $1h_{11/2}$, $2d_{3/2}$, $3s_{1/2}$) proton orbits and ($2f_{7/2}$, $1h_{9/2}$, $1i_{13/2}$, $3p_{3/2}$, $2f_{5/2}$, $3p_{1/2}$) neutron orbits respectively. Formulas for the strengths of SDI and P + Q.Q interactions are given in Appendix B.

(*vii*) Actinide nuclei with SDI and P + Q.Q interactions. The SPE are from zero deformation Nilsson energies [Bo-75]. For example, the SPE for the actinide nucleus $^{239}_{92}U_{147}$ are (42.745, 43.555, 43.786, 46.445, 47.023, 48.163) MeV and (48.825, 50.362, 50.445, 51.569, 52.601, 53.225, 53.667) MeV for ($1h_{9/2}$, $1i_{13/2}$, $2f_{7/2}$, $2f_{5/2}$, $2p_{3/2}$, $2p_{1/2}$) proton orbits and ($2g_{9/2}$,

---

by interactions of valence (ds, fp) particles with s^4p^{12} core and also the single particle splittings produced by this interaction. Both these quantities follow easily [Fr-94] from $V_{\alpha\beta}$ and $V_{\alpha\beta}$ by using (2.58). The $ds - fp$ separation Δ is given by $\Delta = 2(V_{\mathbf{1}_p\mathbf{4}_p} - V_{\mathbf{1}_p\mathbf{3}_p}) + 6(V_{\mathbf{2}_p\mathbf{4}_p} - V_{\mathbf{2}_p\mathbf{3}_p}) + 2(V_{\mathbf{1}_n\mathbf{4}_n} - V_{\mathbf{1}_n\mathbf{3}_p}) + 6(V_{\mathbf{2}_n\mathbf{4}_p} - V_{\mathbf{2}_n\mathbf{3}_p})$. Similarly the s.p. energies $\epsilon^{[\mathbf{1}]}_\beta$ produced by the interaction of valence particles with s^4p^{12} core are given by $h^{[\mathbf{1}]} = \sum_\beta \epsilon^{[\mathbf{1}]}_\beta n_\beta$; $\epsilon^{[\mathbf{1}]}_\beta = 2\epsilon^{[\mathbf{1}],s}_\beta(pp) + 6\epsilon^{[\mathbf{1}],p}_\beta(pp) + 2\epsilon^{[\mathbf{1}],s}_\beta(pn) + 6\epsilon^{[\mathbf{1}],p}_\beta(pn)$. With KUO -10 orbit interaction $\Delta = 7.83\ MeV$ and $\epsilon^{[\mathbf{1}]}_\beta = -1.73, 3.31, -1.43, -0.55, 4.30, -4.01, -2.68\ MeV$ for the orbits $d_{5/2}$, $d_{3/2}$, $s_{1/2}$, $f_{7/2}$, $f_{5/2}$, $p_{3/2}$, $p_{1/2}$ respectively. Similarly by extending the above results for the 15-orbit case give $ds - fp$ separation $\Delta_1 = 5.66\ MeV$ and fp-sdg separation $\Delta_2 = 3.38\ MeV$. The $\epsilon^{[\mathbf{1}]}_\beta$ for ($d_{5/2}$, $s_{1/2}$, $d_{1/2}$) orbits are (−0.75, −1.35, 1.80) MeV, for ($f_{7/2}$, $p_{3/2}$, $f_{5/2}$, $p_{1/2}$) orbits are (0.24, −3.25, 2.70, −2.59) MeV and for ($g_{9/2}$, $d_{5/2}$, $g_{7/2}$, $s_{1/2}$, $d_{3/2}$) orbits are (1.12, −3.45, 3.12, −3.77, −1.98) MeV. The SPE produced by the interaction should be added to the primary energy which, in oscillator shell n, should be $(n + 3/2)\hbar\omega/2$. However the resulting SPE which become ϵ_α for 7 and 12-orbit interactions are not close to the ^{17}O energies given in [Sp-65]. Therefore in the present calculations these energies are replaced by ^{17}O energies and the Δ's produced by the interaction. These then give the $\epsilon^{[\mathbf{1}]}_\alpha$ in Table 3.5 for KUO-7 and KUO-12 interactions. It is useful to note that the Δ's play no role in the norms calculations presented in Table 3.6.

$1j_{15/2}$, $1i_{11/2}$, $3d_{5/2}$, $2g_{7/2}$, $4s_{1/2}$, $3d_{3/2}$) neutron orbits respectively. Formulas for the strengths of SDI and P + Q.Q interactions are given in Appendix B.

Results of the unitary decompositions (carried out in pn spaces) are cataloged in Tables 3.3 - 3.5 and Figs. 3.2a - 3.2c. In Tables 3.3, 3.4 the SPE ϵ_{α} and TBME $V_{\alpha\beta}$ respectively that shifts the location of unitary configurations [m] (the unitary orbits are defined in the footnote of Table 3.3) are given. Although they play no role in the present investigation (i.e. establishing that $V^{[0][2]}$ part is negligible), it is useful to point out that they contribute to the backshifting of the state density. Table 3.5 gives the primary traceless SPE $\epsilon_{\alpha}^{[1]}$ and the renormalized (due to $V(2)$) energies $\xi_{\alpha}^{[1]}$; the later depend on [m] and examples for some selected [m] are shown in the table. It is striking to note that in almost all cases (exceptions being P + Q.Q interaction and in other cases those with $j = 1/2$ orbit) the renormalized energies are obtained essentially by shifting the primary energies, i.e. the $\epsilon_{\alpha}^{[1]}$ and the induced energies given by $\xi_{\alpha}^{[1]}([\mathrm{m}])$ are highly correlated. In Figs. 3.2a - 3.2c, the $V_{\alpha\beta}$ matrix elements of $V^{[0]}$ and $V^{[0][2]}$ are compared for the pp and pn parts of various interactions (the results for SDI and P + Q.Q interactions are given in Appendix B; here $V_{\alpha\beta}^{[0][2]}$ is negligible by definition). It is seen from the figures that $V_{\alpha\beta}^{[0][2]}$ fluctuates around zero and most strikingly $V_{\alpha\beta}^{[0][2]}$ are seen to follow closely $V_{\alpha\beta}$. Thus one can conclude that $V_{\alpha\beta}^{[0][2]}$ are essentially zero (hence $V^{[0][2]}$ can be neglected) in general. In order to quantify the above observations, norms (3.12, 3.14) of various parts of $h + V^{[0]}$ are calculated and the results are given in Table 3.6. It is seen from the last column of Table 3.6 that irrespective of the space and the interaction, in all the cases considered, the error in the norm of the operator $(h^{[0][1]} + V^{[0][1]} + V^{[0][2]})$ is negligible 2%

Table 3.3 The unitary orbit α, the number of states N_α in the unitary orbit α and the mean single particle energy ϵ_α with respect to each unitary orbit are listed[†].

Space	Interaction	α	N_α	ϵ_α (MeV)
(ds)[a]	CW	1	12	−2.312
	PW	1	12	−2.312
	UNIV-SD	1	12	−1.952
	BONN-J	1	12	1.838
(fp)[b]	MWH2	1	20	−5.604
	FPM13	1	20	−5.699
#1[c]	KBB	1	22	1.675
(ds,fp)[d]	KUO-7	1	20	12.034
		2	12	−2.312
(ds,fp,sdg)[e]	KUO-12	1	12	−2.312
		2	20	9.874
		3	30	21.027
#2[f]	SDI*	1	20	42.663
		2	12	43.100
		3	30	50.038
		4	14	49.910
	P + Q.Q	1	20	42.663
		2	12	43.100
		3	30	50.038
		4	14	49.910
#3[g]	SDI**	1	30	44.694
		2	14	43.555
		3	42	51.070
		4	16	50.362
	P + Q.Q	1	30	44.694
		2	14	43.555
		3	42	51.070
		4	16	50.362

Table 3.3 (cont'd)

#1 $(2p_{3/2}\ 1f_{5/2}\ 2p_{1/2}\ 1g_{9/2})$

#2 $(1g_{7/2},\ 2d_{5/2},\ 1h_{11/2},\ 2d_{3/2},\ 3s_{1/2})^{m_p} \oplus (2f_{7/2},\ 1h_{9/2},\ 1i_{13/2},\ 3p_{3/2},\ 2f_{5/2},\ 3p_{1/2})^{m_n}$

#3 $(1h_{9/2},\ 1i_{13/2},\ 2f_{7/2},\ 2f_{5/2},\ 2p_{3/2},\ 2p_{1/2})^{m_p}$, $(2g_{9/2},\ 1j_{15/2},\ 1i_{11/2},\ 3d_{5/2},\ 2g_{7/2},\ 4s_{1/2},\ 3d_{3/2})^{m_n}$

a The spherical orbits $(1d_{5/2},\ 1d_{3/2},\ 2s_{1/2})$, define the unitary orbit $\alpha = 1$ with $s = 0$. The proton and neutron unitary orbits are same.

b The spherical orbits $(1f_{7/2},\ 2p_{3/2},\ 1f_{5/2},\ 2p_{1/2})$ define the unitary orbit $\alpha = 1$ with $s = 0$. The proton and neutron unitary orbits are same.

c The spherical orbits $(2p_{3/2},\ 1f_{5/2},\ 2p_{1/2},\ 1g_{9/2})$ define the unitary orbit $\alpha = 1$ with $s = 0$. The proton and neutron unitary orbits are same.

d The spherical orbits $(1f_{7/2},\ 1f_{5/2},\ 2p_{3/2},\ 2p_{1/2})$ and $(1d_{5/2},\ 1d_{3/2},\ 2s_{1/2})$ define the unitary orbits $\alpha = 1$ and 2 with $s = 0$ and 1 respectively. The proton and neutron unitary orbits are same.

e The spherical orbits $(1d_{5/2},\ 2s_{1/2},\ 1d_{3/2})$, $(1f_{7/2},\ 2p_{3/2},\ 1f_{5/2},\ 2p_{1/2})$ and $(1g_{9/2},\ 2d_{5/2},\ 1g_{7/2},\ 3s_{1/2},\ 2d_{3/2})$ define the unitary orbits $\alpha = 1$, 2 and 3 with $s = 0$, 1 and 2 respectively. The proton and neutron unitary orbits are same.

f The spherical orbits $(1g_{7/2},\ 2d_{5/2},\ 2d_{3/2},\ 3s_{1/2})$, $(1h_{11/2})$ define $\alpha = 1$, 2 for protons and $(2f_{7/2},\ 1h_{9/2},\ 3p_{3/2},\ 2f_{5/2},\ 3p_{1/2})$, $(1i_{13/2})$ define $\alpha = 3,4$ for neutrons. All unitary orbits have $s = 0$.

g The spherical orbits $(1h_{9/2},\ 2f_{7/2},\ 2f_{5/2},\ 2p_{3/2},\ 2p_{1/2})$, $(1i_{13/2})$ define $\alpha = 1$, 2 for protons and $(2g_{9/2},\ 1i_{11/2},\ 3d_{5/2},\ 2g_{7/2},\ 4s_{1/2},\ 3d_{3/2})$, $(1j_{15/2})$ define $\alpha = 3,4$ for neutrons. All unitary orbits have $s = 0$.

* In this case, values are given for ${}^{168}_{68}Er_{100}$. For other rare-earth nuclei the scale factor $41/A^{1/3}$ should be used.

** In this case, values are given for ${}^{239}_{92}U_{147}$. For other actinide nuclei the scale factor $41/A^{1/3}$ should be used.

† References for various interactions are given in the text.

Table 3.4 The unitary orbits (α and β) indices, two particle unitary orbit dimensionality $\check{N}_{\alpha\beta}$ and the $V_{\alpha\beta}$ that defines the $V^{[0][0]}$ for several 2-body interactions (pp, nn and pn parts are given separately) in different spaces are tabulated[†].

Space Interaction	α	β	pp		nn		pn	
			$\check{N}_{\alpha\beta}$	$V_{\alpha\beta}$ (MeV)	$\check{N}_{\alpha\beta}$	$V_{\alpha\beta}$ (MeV)	$\check{N}_{\alpha\beta}$	$V_{\alpha\beta}$ (MeV)
(ds)[a]								
CW	1	1	66	−0.144	66	−0.144	144	−1.430
PW	1	1	66	−0.070	66	−0.070	144	−1.407
UNIV-SD*	1	1	66	−0.308	66	−0.308	144	−1.775
BONN-J	1	1	66	−0.347	66	−0.347	144	−1.519
(fp)[b]								
MWH2	1	1	190	−0.005	190	−0.005	400	−0.637
FPM13**	1	1	190	−0.106	190	−0.106	400	−0.720
#1[c]								
KBB	1	1	231	0.016	231	0.016	484	0.444
(ds,fp)[d]								
KUO-7 orbit	1	1	190	−0.439	190	−0.439	400	−1.102
	1	2	240	−0.484	240	−0.484	240	−1.277
	2	2	66	−0.707	66	−0.707	144	−1.778
(ds,fp,sdg)[e]								
KUO-12 orbit	1	1	66	−0.514	66	−0.514	144	−1.307
	1	2	240	−0.353	240	−0.353	240	−0.949
	1	3	360	−0.269	360	−0.269	360	−0.688
	2	2	190	−0.323	190	−0.323	400	−0.821
	2	3	600	−0.245	600	−0.245	600	−0.638
	3	3	435	−0.226	435	−0.226	900	−0.558

Table 3.4 (cont'd)

Space Interaction	α	β	pp		nn		pn	
			$\check{N}_{\alpha\beta}$	$V_{\alpha\beta}$ (MeV)	$\check{N}_{\alpha\beta}$	$V_{\alpha\beta}$ (MeV)	$\check{N}_{\alpha\beta}$	$V_{\alpha\beta}$ (MeV)
$\#2^{J,***}$								
P + Q.Q	1	1	190	0.010	–	–	–	–
	1	2	240	0.000	–	–	–	–
	2	2	66	0.008	–	–	–	–
	3	3	–	–	435	0.016	–	–
	3	4	–	–	420	0.000	–	–
	4	4	–	–	91	0.017	–	–
	1	3	–	–	–	–	600	0.000
	1	4	–	–	–	–	280	0.000
	2	3	–	–	–	–	360	0.000
	2	4	–	–	–	–	168	0.000
$\#3^{g,***}$								
P + Q.Q	1	1	435	0.006	–	–	–	–
	1	2	420	0.006	–	–	–	–
	2	2	91	0.005	–	–	–	–
	3	3	–	–	861	0.009	–	–
	3	4	–	–	672	0.000	–	–
	4	4	–	–	120	0.011	–	–
	1	3	–	–	–	–	1200	0.000
	1	4	–	–	–	–	480	0.000
	2	3	–	–	–	–	588	0.000
	2	4	–	–	–	–	224	0.000

* The quantities are to be multiplied by $(18/A)^{0.3}$

** The quantities are to be multiplied by $(42/A)^{0.35}$

*** The strength G_p, G_n, G^Q_{pp}, G^Q_{nn}, G^Q_{pn} define the P + Q.Q interaction are given in the text. $V_{\alpha\beta}$ for pn part of the interaction is zero (see Appendix B).

† See footnote of Table 3.3 for other details.

For SDI, analytical expressions for $V_{\alpha\beta}$ are available (see Appendix B).

Table 3.5 The unitary one-body part $\epsilon_\alpha^{[1]}$ of NIP hamiltonian h and the renormalized single particle energies $\xi_\alpha^{[1]}([\mathbf{m}])$ (defined by (2.58)), for protons and neutrons, that depend on unitary configurations are compared for each spherical orbit α in different spaces for various interactions. The corresponding pn unitary orbit configurations $[\mathbf{m}_p, \mathbf{m}_n]$ are also given[†].

Space $[\mathbf{m}_p]$ $[\mathbf{m}_n]$	Interaction	α	$\epsilon_\alpha^{[1]}$ (MeV)	$\xi_{\alpha;p}^{[1]}$ (MeV)	$\xi_{\alpha;n}^{[1]}$ (MeV)
$(\mathbf{ds})^a$	UNIV-SD	1	−1.996	−2.458	−2.458
[4]		2	3.599	3.810	3.810
[4]		3	−1.211	−0.246	−0.246
[6]		1	−1.996	−2.691	−2.691
[6]		2	3.599	3.991	3.991
		3	−1.211	0.249	0.249
[6]	BONN-J	1	−1.838	−2.730	−2.730
[6]		2	3.242	4.425	4.425
		3	−0.968	−0.660	−0.660
$(\mathbf{fp})^b$	MWH2	1	3.740	4.298	4.298
[10]		2	−2.760	−3.016	−3.016
[10]		3	−0.660	−0.950	−0.950
		4	1.140	1.072	1.072
	FPM13	1	−2.665	−2.821	−2.821
[2]		2	−0.634	−0.499	−0.499
[2]		3	3.545	3.642	3.642
		4	1.292	1.620	1.620
		1	−2.665	−3.317	−3.317
[8]		2	−0.634	−0.002	−0.002
[8]		3	3.545	3.938	3.938
		4	1.292	1.458	1.458
$\#1^c$	KBB	1	−1.675	−1.845	−1.845
[8]		2	−0.895	−2.574	−2.574
[8]		3	−0.595	−0.775	−0.775
		4	1.325	2.437	2.437

Table 3.5 (cont'd)

Space $[\mathbf{m}_p]$ $[\mathbf{m}_n]$	Interaction	α^*	$\epsilon_\alpha^{[1]}$ (MeV)	$\xi_{\alpha;p}^{[1]}$ (MeV)	$\xi_{\alpha;n}^{[1]}$ (MeV)
(ds,fp)^d	KUO-7	1	−1.838	−2.039	−2.008
[4 0]		2	3.242	3.460	3.387
[2 2]		3	−0.968	−0.803	−0.750
		4	−2.664	−3.231	−3.275
		5	3.526	3.794	3.656
		6	−0.664	−0.310	−0.098
		7	1.366	2.159	2.328
[5 1]		1	−1.838	−2.161	−2.161
[5 1]		2	3.242	3.575	3.575
		3	−0.968	−0.666	−0.666
		4	−2.664	−3.629	−3.629
		5	3.526	3.856	3.856
		6	−0.664	0.074	0.074
		7	1.366	2.803	2.803
(ds,fp,sdg)^e	KUO-12	1	−1.838	−2.060	−2.060
		2	−0.968	−0.645	−0.645
		3	3.242	3.413	3.413
		4	−2.664	−3.341	−3.341
		5	−0.664	0.048	0.048
[6 0 0]		6	3.526	3.596	3.596
[6 0 0]		7	1.366	2.480	2.480
		8	−3.247	−3.824	−3.824
		9	1.253	1.384	1.384
		10	0.753	1.393	1.393
		11	2.753	2.265	2.265
		12	3.353	3.564	3.564

Table 3.5 (cont'd)

Space $[\mathbf{m}_p]$ $[\mathbf{m}_n]$	Interaction	α^*	$\epsilon_\alpha^{[1]}$ (MeV)	$\xi_{\alpha;p}^{[1]}$ (MeV)	$\xi_{\alpha;n}^{[1]}$ (MeV)
	KUO-12	1	−1.838	−2.407	−2.437
		2	−0.968	−0.102	−0.075
		3	3.242	3.662	3.693
		4	−2.664	−4.296	−4.304
		5	−0.664	1.000	0.875
[12 4 2]		6	3.526	3.717	3.832
[12 10 0]		7	1.366	4.032	3.970
		8	−3.247	−5.100	−5.007
		9	1.253	1.963	1.685
		10	0.753	1.860	2.110
		11	2.753	3.014	2.545
		12	3.353	4.580	4.498

* For UNIV-SD, BONN-J interactions α = 1, 2 and 3 correspond to $1d_{5/2}$, $1d_{3/2}$ and $2s_{1/2}$ spherical orbits respectively.

For MWH2 interaction α = 1, 2, 3 and 4 correspond to $1f_{5/2}$, $1f_{7/2}$, $2p_{3/2}$ and $2p_{1/2}$ spherical orbits respectively; for FPM13 interaction α = 1, 2, 3 and 4 correspond to $1f_{7/2}$, $2p_{3/2}$, $1f_{5/2}$ and $2p_{1/2}$ spherical orbits respectively.

For KBB interaction α = 1, 2, 3 and 4 correspond to $2p_{3/2}$, $1f_{5/2}$, $2p_{1/2}$ and $1g_{9/2}$ spherical orbits respectively.

For KUO-7 orbit interaction α = 1, 2, 3, 4, 5, 6 and 7 correspond to $1f_{7/2}$, $1f_{5/2}$, $2p_{3/2}$, $2p_{1/2}$, $1d_{5/2}$, $1d_{3/2}$ and $2s_{1/2}$, spherical orbits respectively.

For KUO-12 orbit interaction α = 1, 2, 3, 4, 5, 6, 7, 8, 9, 10, 11 and 12 correspond to $1d_{5/2}$, $2s_{1/2}$, $1d_{3/2}$, $1f_{7/2}$, $2p_{3/2}$, $1f_{5/2}$, $2p_{1/2}$, $1g_{9/2}$, $2d_{5/2}$, $1g_{7/2}$, $3s_{1/2}$ and $2d_{3/2}$ spherical orbits respectively.

† For other symbols in the table, see footnotes of Table 3.3.

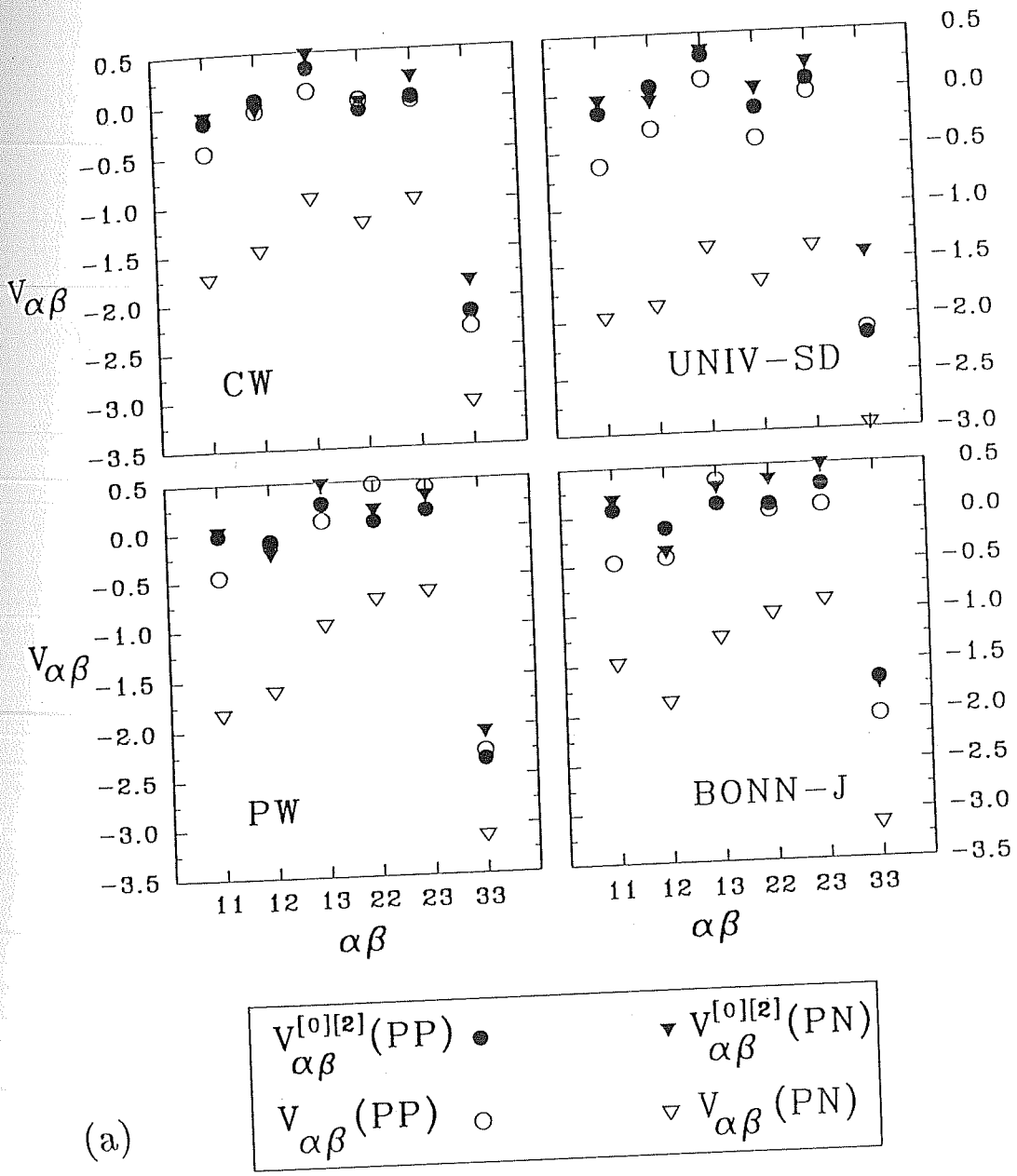
Results for rare-earth and actinide nuclei with SDI and P + Q.Q interactions are not shown as for SDI, the SPE renormalization is zero, i.e. $\xi_\alpha^{[1]} = \epsilon_\alpha^{[1]}$ and the renormalization is negligibly small for P + Q.Q interaction.

Figure 3.2

(a) $V_{\alpha\beta}$ matrix elements of $V^{[0]}$ and $V^{[0][2]}$ vs $(\alpha\beta)$ for various ds-shell interactions. Results are shown for pp and pn parts of the interactions (note that pp and nn parts are identical). The definition of the index α (and β) is given in the footnote to Table 3.5. The $V_{\alpha\beta}$ and $V_{\alpha\beta}^{[0][2]}$ are in MeV units. Text and the footnotes to Tables 3.3, 3.5 give further details.

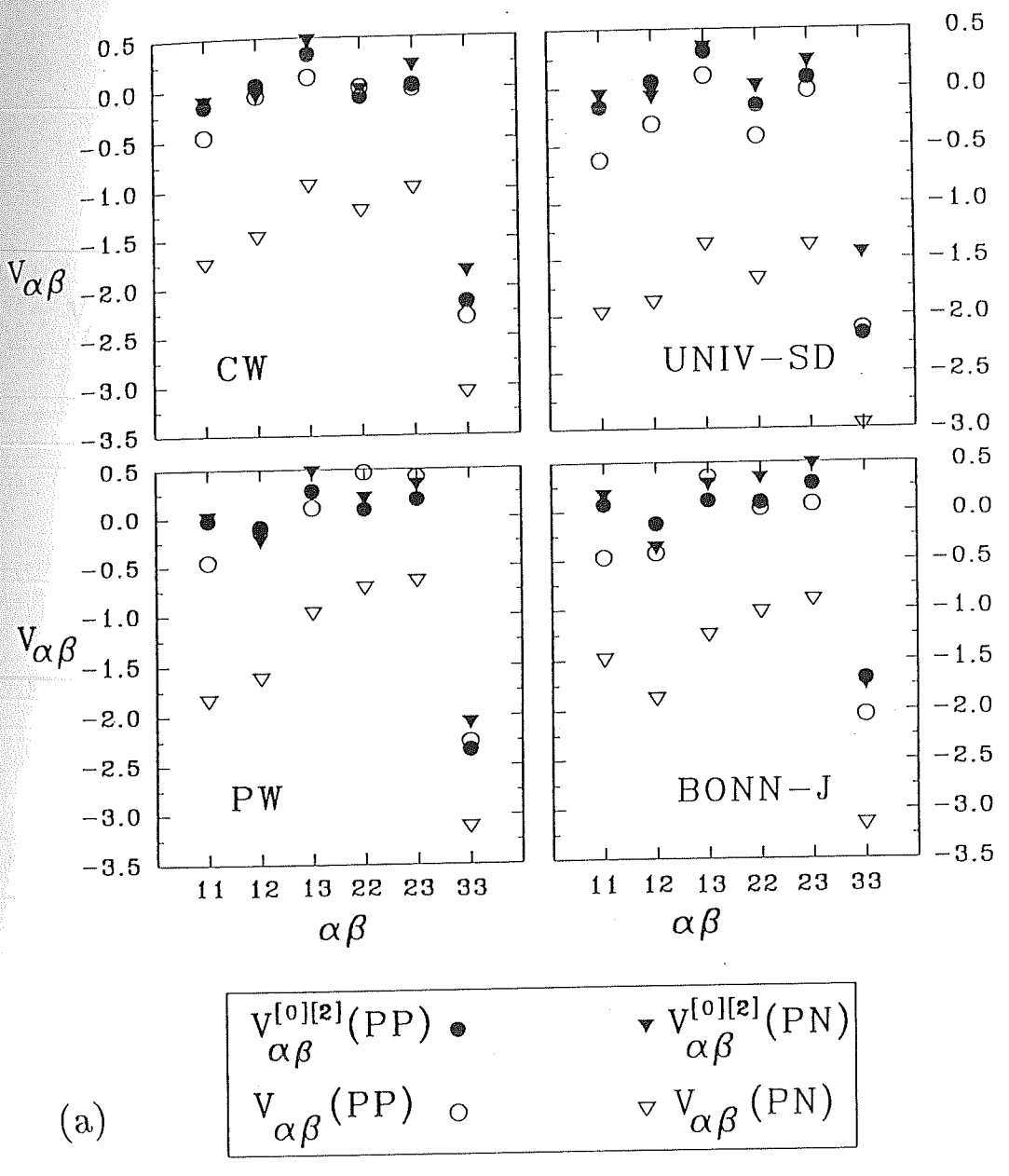
(b) $V_{\alpha\beta}$ matrix elements of $V^{[0]}$ and $V^{[0][2]}$ vs $(\alpha\beta)$ for various fp-shell interactions. Results are shown for pp and pn parts of the interactions (note that pp and nn parts are identical). The definition of the index α (and β) is given in the footnote to Table 3.5. The $V_{\alpha\beta}$ and $V_{\alpha\beta}^{[0][2]}$ are in MeV units. Text and the footnotes to Tables 3.3, 3.5 give further details.

(c) $V_{\alpha\beta}$ matrix elements of $V^{[0]}$ and $V^{[0][2]}$ vs β for various α values for KUO-10 orbit interaction in ($1f_{7/2}$, $1f_{5/2}$, $2p_{3/2}$, $2p_{1/2}$, $1d_{5/2}$, $1d_{3/2}$, $2s_{1/2}$, $1p_{3/2}$, $1p_{1/2}$, $1s_{1/2}$) space with spherical orbit indices α = 1,2,...., 10 respectively for protons (and neutrons). Results are shown for pp and pn parts of the interactions (note that pp and nn parts are identical). The $V_{\alpha\beta}$ and $V_{\alpha\beta}^{[0][2]}$ are in MeV units. See text and footnote to Tables 3.3, 3.5 for further details. The orbits ($1f_{7/2}$, $1f_{5/2}$, $2p_{3/2}$, $2p_{1/2}$), ($1d_{5/2}$, $1d_{3/2}$, $2s_{1/2}$), ($1p_{3/2}$, $1p_{1/2}$) and ($1s_{1/2}$) define the unitary orbits $\boldsymbol{\alpha}$ = 1, 2, 3 and 4 for protons (and neutrons). The $V_{\alpha\beta}$ and $V_{\alpha\beta}^{[0][2]}$ for the KUO - 7 orbit interactions are same as that of KUO - 10 orbit interaction with $\alpha, \beta \in 1f_{7/2}$, $1f_{5/2}$, $2p_{3/2}$, $2p_{1/2}$, $1d_{5/2}$, $1d_{3/2}$, $2s_{1/2}$ and therefore they can be read off from the figure.

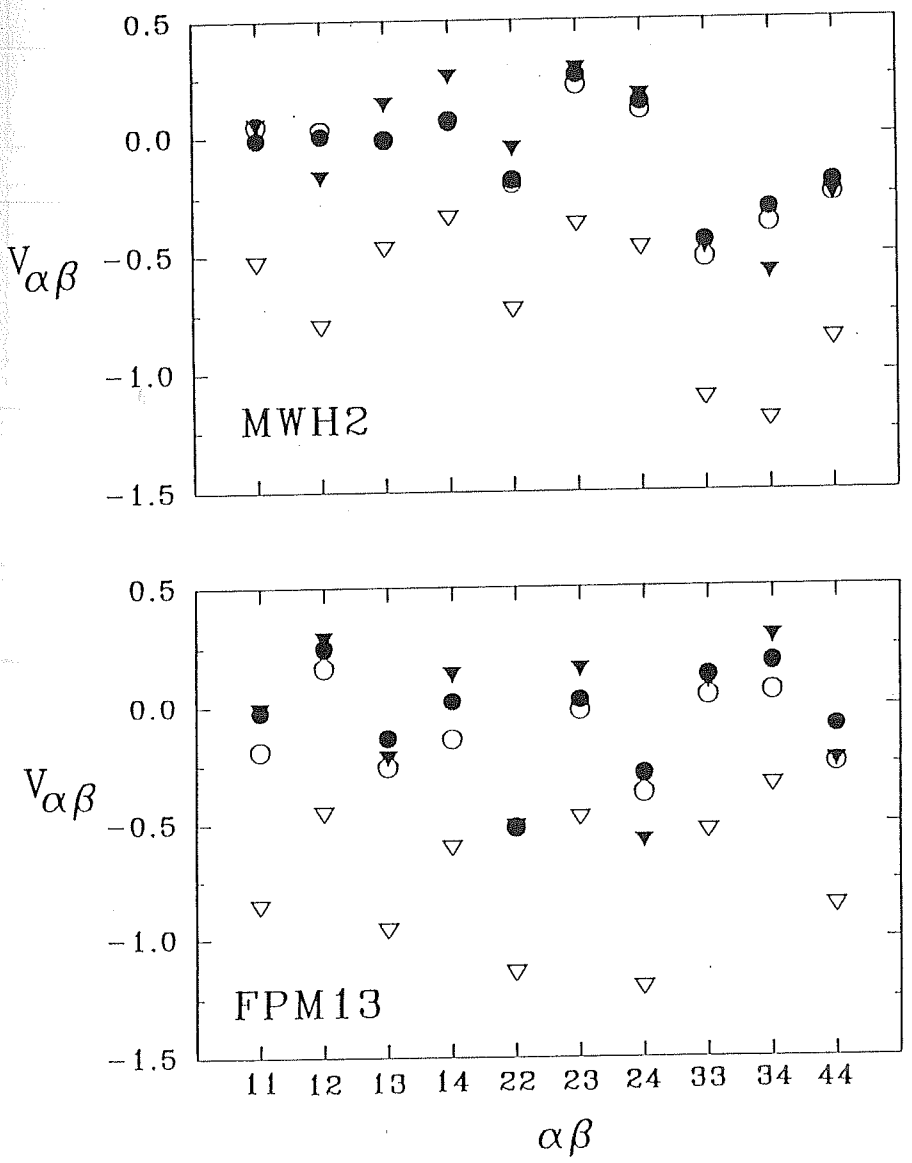

CW
UNIV−SD
PW
BONN−J
$V_{\alpha\beta}$
$\alpha\beta$
11 12 13 22 23 33
$V^{[0][2]}_{\alpha\beta}$(PP)
$V^{[0][2]}_{\alpha\beta}$(PN)
$V_{\alpha\beta}$(PP)
$V_{\alpha\beta}$(PN)

(a)

ds−SHELL INTERACTIONS

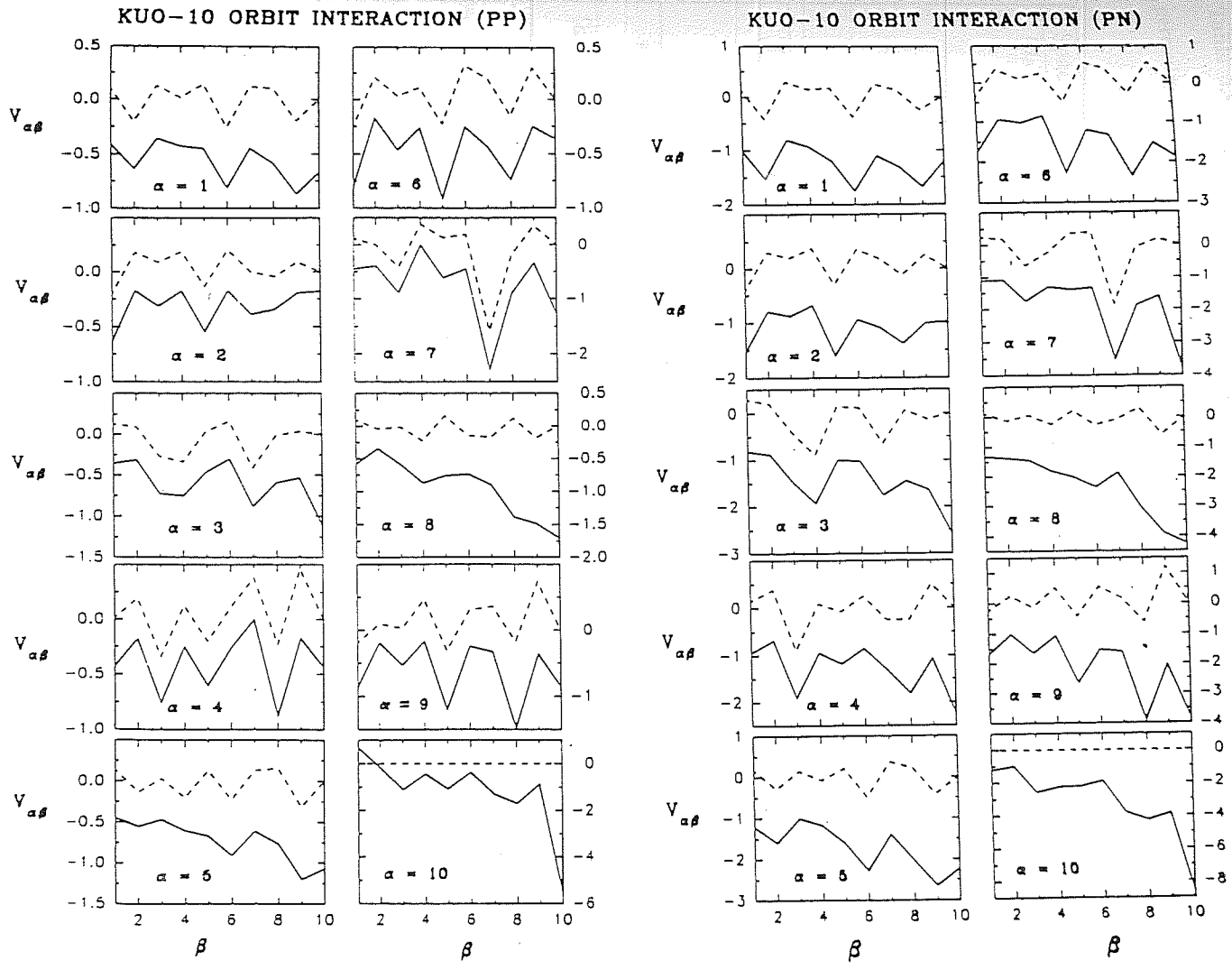


(a)



(b)

$V_{\alpha\beta}^{[0][2]}(PP)$ ●	▼ $V_{\alpha\beta}^{[0][2]}(PN)$
$V_{\alpha\beta}(PP)$ ○	▽ $V_{\alpha\beta}(PN)$


KUO−10 ORBIT INTERACTION (PP)
KUO−10 ORBIT INTERACTION (PN)
$V_{\alpha\beta}$
α = 1
α = 2
α = 3
α = 4
α = 5
α = 6
α = 7
α = 8
α = 9
α = 10
β
β

(c)

Table 3.6 Norms (in MeV) of various tensor parts of $h + V^{[0]}$. Last column gives the percentage error in the norm of $H^{[0][1]} + V^{[0][2]}$ when $V^{[0][2]}$ is put to zero †.

Space	interaction	(m_p, m_n, S)	$\|h^{[0][1]}\|$	$\|V^{[0][1]}\|$	$\|H^{[0][1]}\|$	$\|V^{[0][2]}\|$	Error
$(ds)^a$	PW	(4,6,0)	5.75	4.55	10.01	1.66	1.37%
		(8,8,0)	5.58	7.33	12.55	1.55	0.77%
	UNIV-SD	(4,6,0)	6.36	1.65	7.16	1.16	1.32%
		(8,8,0)	6.17	2.51	7.50	1.02	0.93%
	BONN-J	(4,4,0)	5.58	1.42	6.94	1.43	2.13%
		(6,8,0)	5.75	2.76	8.41	1.53	1.65%
	P + Q.Q	(4,4,0)	5.58	0.58	5.50	0.43	0.30%
		(4,6,0)	5.75	0.75	5.66	0.41	0.26%
$(fp)^b$	MWH2	(6,6,0)	8.12	0.63	8.72	1.24	1.01%
		(10,10,0)	8.86	1.20	9.99	1.49	1.11%
	FPM13	(6,6,0)	7.79	1.23	8.74	1.21	0.96%
		(10,10,0)	8.50	2.18	10.21	1.38	0.92%
$\#1^c$	KBB	(4,6,0)	3.53	1.97	5.23	0.89	1.44%
		(8,8,0)	4.08	3.78	7.43	1.21	1.32%
$(ds, fp)^d$	KUO-7	(4,4,0)	5.58	0.56	6.04	1.66	3.78%
		(4,4,2)	6.27	0.85	6.84	1.57	2.64%
		(6,6,0)	5.92	0.94	6.72	1.88	3.91%
		(6,6,2)	6.86	1.45	7.91	2.00	3.21%
$(ds, fp, sdg)^e$	KUO-12	(6,6,0)	5.92	0.58	6.31	1.39	0.69%
		(6,6,1)	6.43	0.82	6.91	1.43	2.15%
		(6,6,2)	6.81	0.93	7.33	1.46	1.99%
		(6,6,3)	7.10	0.98	7.65	1.48	1.87%
		(6,6,4)	7.33	1.00	7.89	1.48	1.76%
		(18,22,0)	8.14	4.75	11.46	1.35	0.69%
		(18,22,1)	8.49	4.80	11.87	1.43	0.72%
		(18,22,2)	8.81	4.84	12.25	1.51	0.76%
$\#2^f$	SDI	(14,10,0)	4.74	0.00	4.74	0.04	$\sim 0.00\%$
		(22,24,0)	4.94	0.00	4.94	0.04	$\sim 0.00\%$
	P + Q.Q	(14,10,0)	4.74	0.14	4.87	0.09	0.02%
		(24,25,0)	4.80	0.27	5.04	0.09	0.02%
$\#3^g$	SDI	(8,16,0)	6.33	0.00	6.33	0.03	$\sim 0.00\%$
		(10,21,0)	6.77	0.00	6.77	0.03	$\sim 0.00\%$
	P + Q.Q	(8,16,0)	6.33	0.12	6.41	0.08	0.01%
		(13,21,0)	7.00	0.16	7.12	0.09	0.01%

† see footnotes of Table 3.3 and text for details

or less when $V^{[0][2]}$ is dropped; only in the case KUO-7 interaction in (ds, fp) space, the error is $\sim 3\%$.

In conclusion, it is clearly confirmed, by the results shown in Table 3.6, that the $V^{[0][2]}$ part of the interaction can be neglected irrespective of which part of the periodic table one is dealing with, as seen from the results obtained for variety of interactions that span the entire periodic table. Thus the generality of one of the important assumptions made in the level density theory with interactions as given by (3.3), (3.4) is established. Finally it is worth remarking that the negligible renormalization of SPE produced by SDI and P + Q.Q interactions and that the corresponding $V^{[0][2]}$ part is negligible show that these phenomenological interactions built into them one of the important requirements for the applicability of the level density theory with interactions.

3.3 Tests of moment methods for NIP state, spin-cutoff and occupancy densities

In order to test, in large spaces, the moment theory given in Sect. 3.1.4 for NIP state, spin-cutoff and occupancy densities and their S-decompositions, a case of twelve protons ($m_p = 12$) and twelve neutrons ($m_n = 12$) in sixteen spherical orbits is considered with $S\hbar\omega = 0$ to $4\hbar\omega$ excitations. The s.p. orbits are ($\alpha = 1-16$) $1s_{1/2}$, $1p_{3/2}$, $1p_{1/2}$, $1d_{5/2}$, $2s_{1/2}$, $1d_{3/2}$, $1f_{7/2}$, $2p_{3/2}$, $1f_{5/2}$, $2p_{1/2}$, $1g_{9/2}$, $2d_{5/2}$, $1g_{7/2}$, $3s_{1/2}$, $2d_{1/2}$, $1h_{11/2}$ and the corresponding SPE (in MeV) are 0.0, 8.076, 12.206, 16.388, 20.596, 21.851, 24.752, 29.431, 31.208, 32.201, 33.116, 38.213, 40.383, 41.297, 42.238, 41.454 respectively. The SPE follow from Seeger energies for neutrons; Ref. [Hi-69] gives the Seeger energies. The spherical orbits are divided into eight unitary orbits (α = 1-8) and they are

$[1s_{1/2}]$, $[1p_{3/2},\ 1p_{1/2}]$, $[1d_{5/2},\ 2s_{1/2},\ 1d_{3/2}]$, $[1f_{7/2}]$, $[2p_{3/2},\ 1f_{5/2},\ 2p_{1/2}]$, $[1g_{9/2}]$, $[2d_{5/2},\ 1g_{7/2},\ 3s_{1/2},\ 2d_{3/2}]$, and $[1h_{11/2}]$. The corresponding s values and parities $(s(\pi))$ are $0(+)$, $1(-)$, $2(+)$, $3(-)$, $3(-)$, $4(+)$, $4(+)$ and $5(-)$ respectively (in the above choice, parity is uniquely defined for a given s and therefore parity is dropped in the remaining part of this section; in principle one can take $s = 4$ for $1h_{11/2}$ orbit but then one has to decompose the space according to s and π). Results for state, spin-cutoff and occupancy densities are given in Figs. 3.3a - 3.3f. In the figures the exact results are obtained by direct counting method (i.e. by using spherical configurations $(\mathbf{m}_p,\ \mathbf{m}_n)$). Results shown in Figs. 3.3a - 3.3f are first reported in [Ko-92a].

Comparison with direct counting results

The state densities and their decompositions are well described by the moment methods as shown in Fig. 3.3a and they confirm that the earlier results by Smith [Sm-87; also Ko-91] for identical particles (Smith dealt with 36 neutrons in 31 spherical orbits) extend to the realistic case with protons and neutrons. As can be seen from Fig. 3.3a, the essentially Gaussian densities for a given S add up to give exponential form (as in Bethe's Fermi gas theory; Eq. (C.1) of Appendix C ahead) for the state densities and this has its origin in the fact that at the energy where a given S-density peaks, the density for a higher S (which is displaced with respect to the lower S density) dominates and this continues. It should be mentioned that calculations for pn systems without S-decompositons (therefore they do not tell much about origin of the exponential form of the state density) are given in [Ha-80]. Fig. 3.3b shows that moment methods give good description of spin-cutoff densities and their S-decompositions. The quality of agreement is similar to that of state

Figure 3.3

(a) Comparison of exact counting results with moment theory for state densities $I(E)$ and the corresponding S-decompositions $I^{h,S}(E)$. The exact results are averaged over 2 MeV bins. $I(E)$ is in MeV^{-1} units and shown in the figure is $\ell og(I(E))$ vs E. Text gives details regarding special orbits, s values, unitary orbits etc.

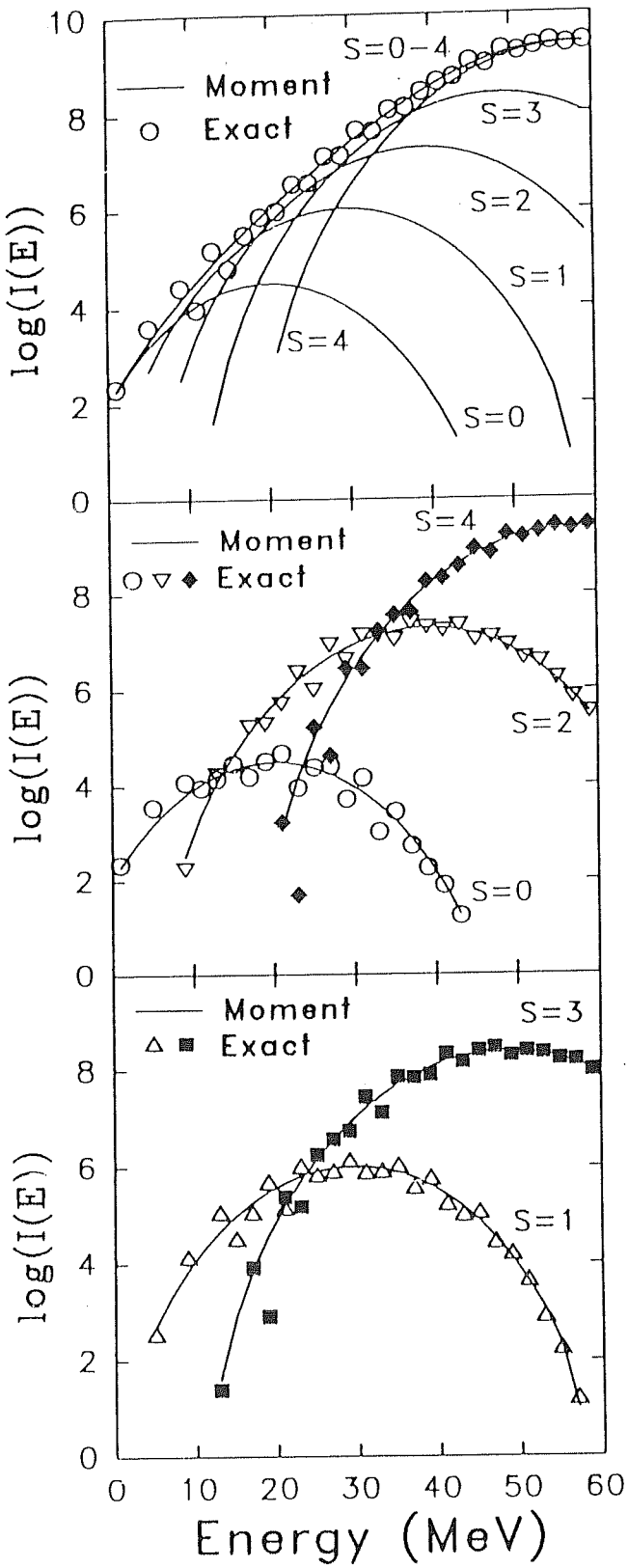
(b) Same as Fig. 3.3a but for J_Z^2 - densities $I^h_{J_Z^2}(E)$ and $I^{h,S}_{J_Z^2}(E)$.

(c) Same as Fig. 3.3a but for n_α - densities $I^h_{n_\alpha}(E)$ and $I^{h,S}_{n_\alpha}(E)$; $\alpha = 1d_{5/2}$ proton orbit. The results are same for $1d_{5/2}$ neutron orbit.

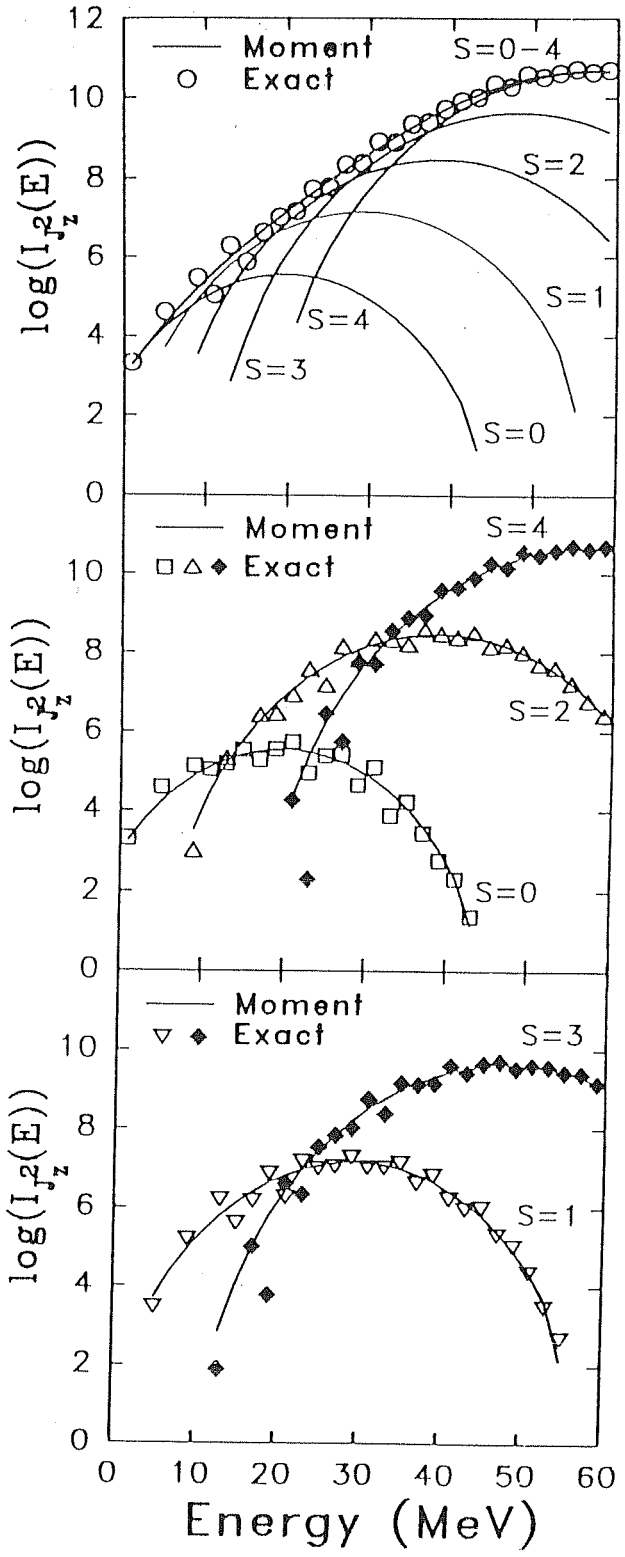
(d) Same as Fig. 3.3c but for $\alpha = 1f_{7/2}$ proton orbit.

(e) Comparison of moment theory results with exact results (averaged over 2 MeV bins) for state densities ($I(E)$), spin-cutoff factors ($\langle J_Z^2\rangle^E$) and occuaption number $\langle n_\alpha\rangle^E$. The $\langle n_\alpha\rangle^E$ results are given for proton orbits $1d_{5/2}$ and $1f_{7/2}$. The results are same for corresponding neutron orbits. Shown in the figure are also the comparison of moment method results with fermi gas forms (see text) for $I(E)$ and $\langle J_Z^2\rangle^E$.

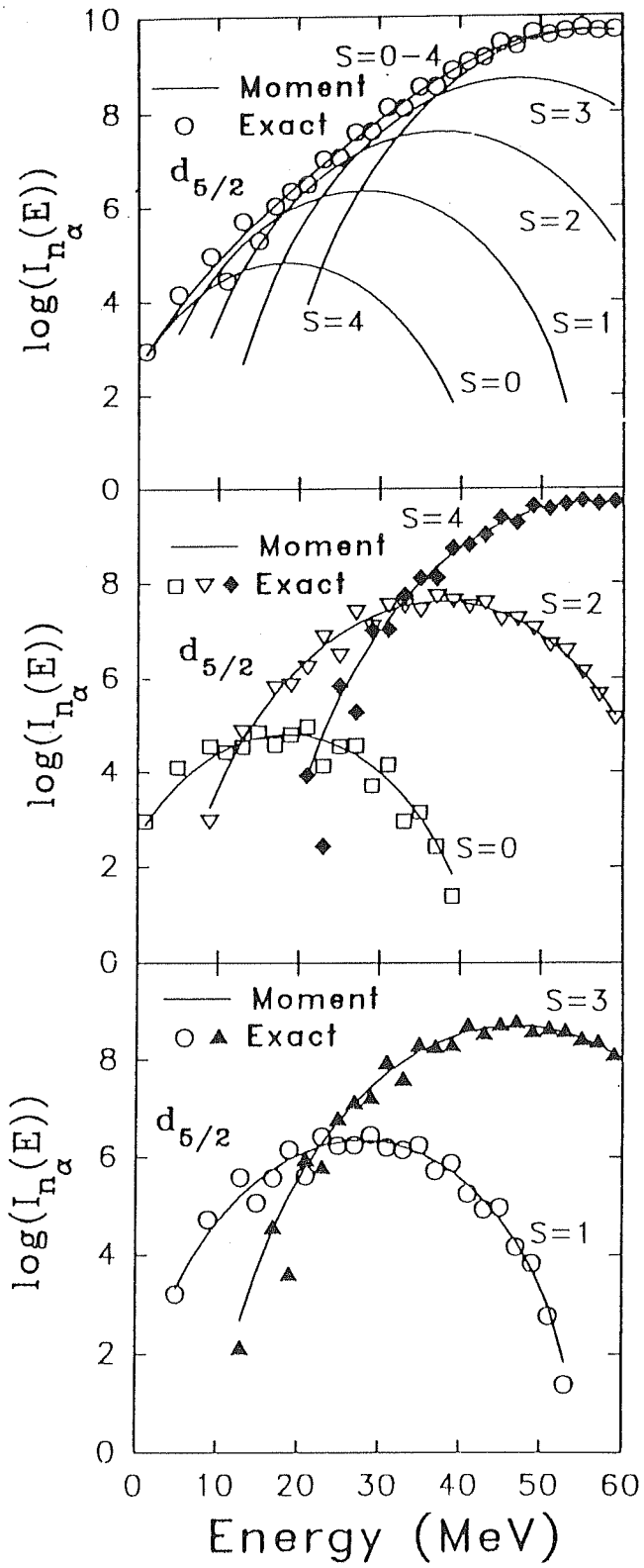
(f) Comparison of fractional occupancies (for protons) $n_{\epsilon_\alpha}(E)$ calculated using moment theory with Fermi-Dirac form (3.16) for $E = 5$, 21 and 41 MeV. The SPE ϵ_α are given in the text for the orbits α used in the calculations. The results are same for neutrons.



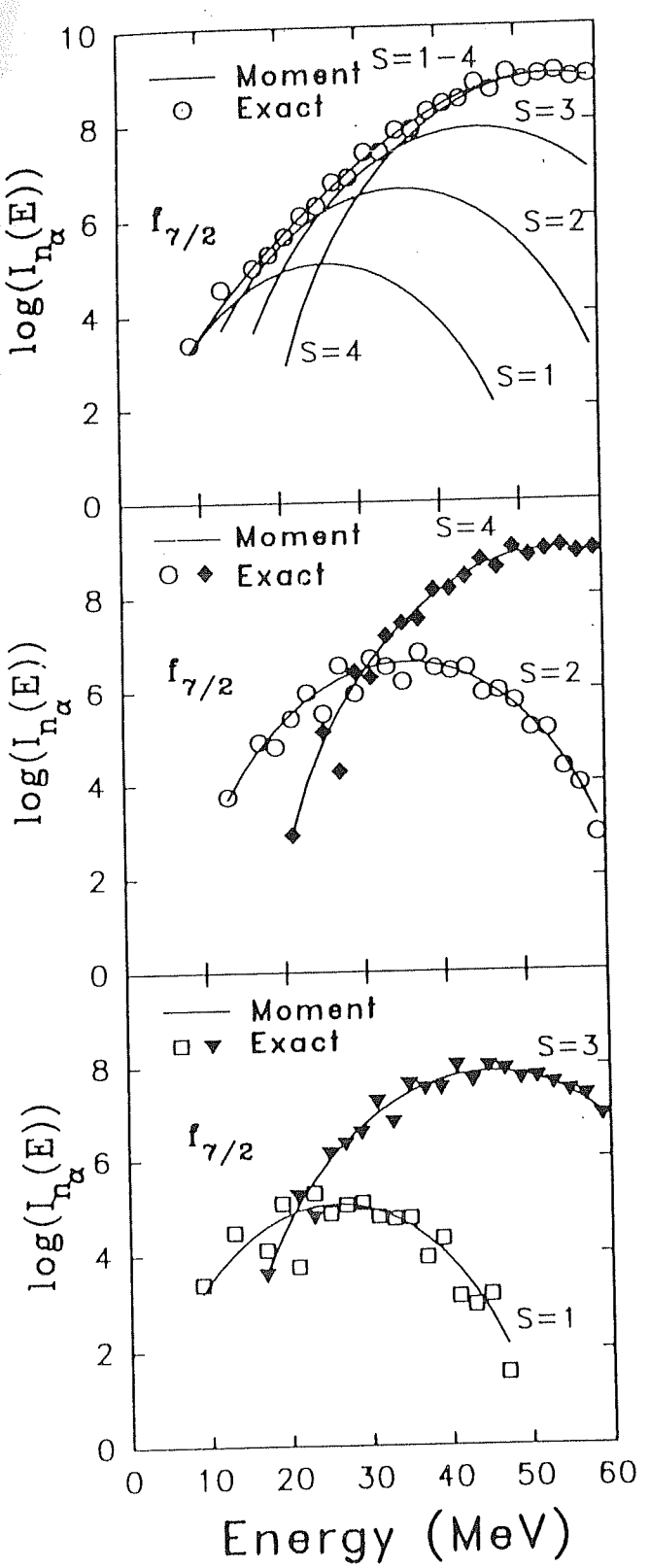
(a)


Moment
Exact
S=0-4
S=2
S=1
S=4
S=3
S=0
Moment
Exact
S=4
S=2
S=0
Moment
Exact
S=3
S=1
log(I_Jz^2(E))
Energy (MeV)
0
10
20
30
40
50
60
0
2
4
6
8
10
12

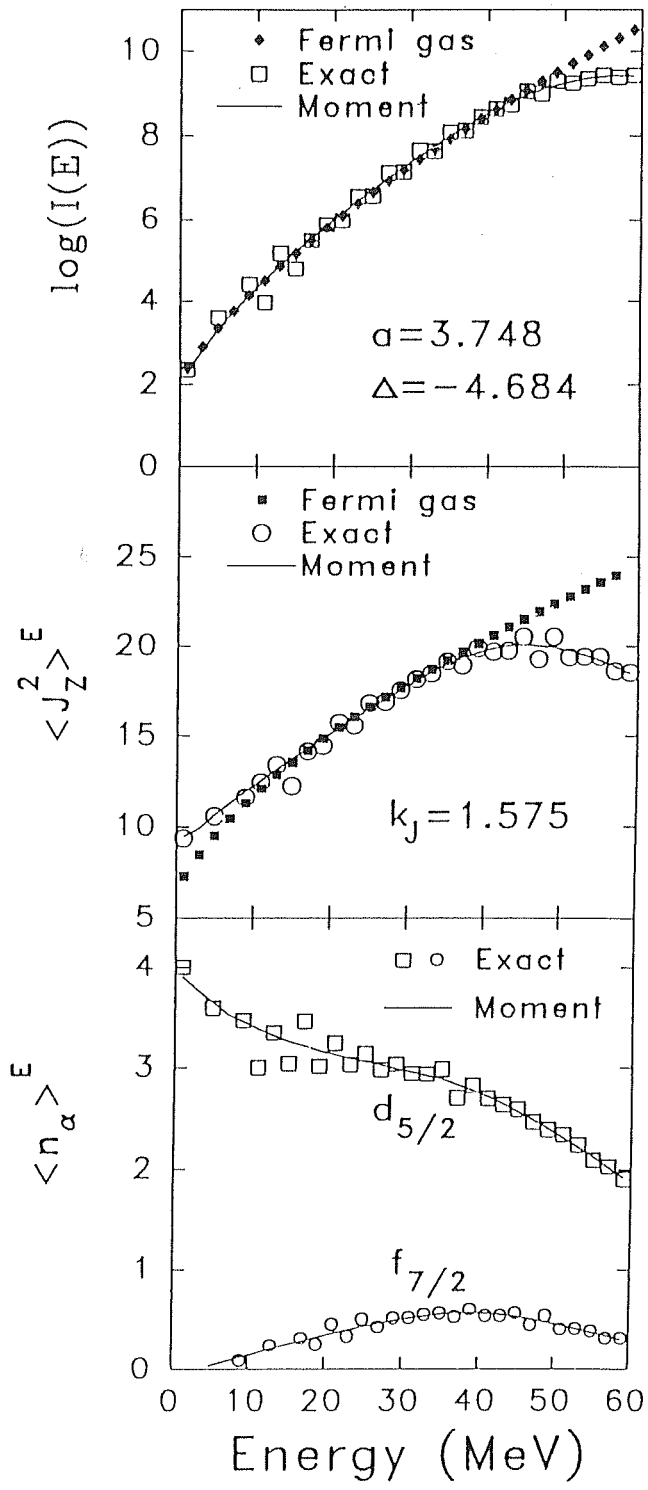
(b)



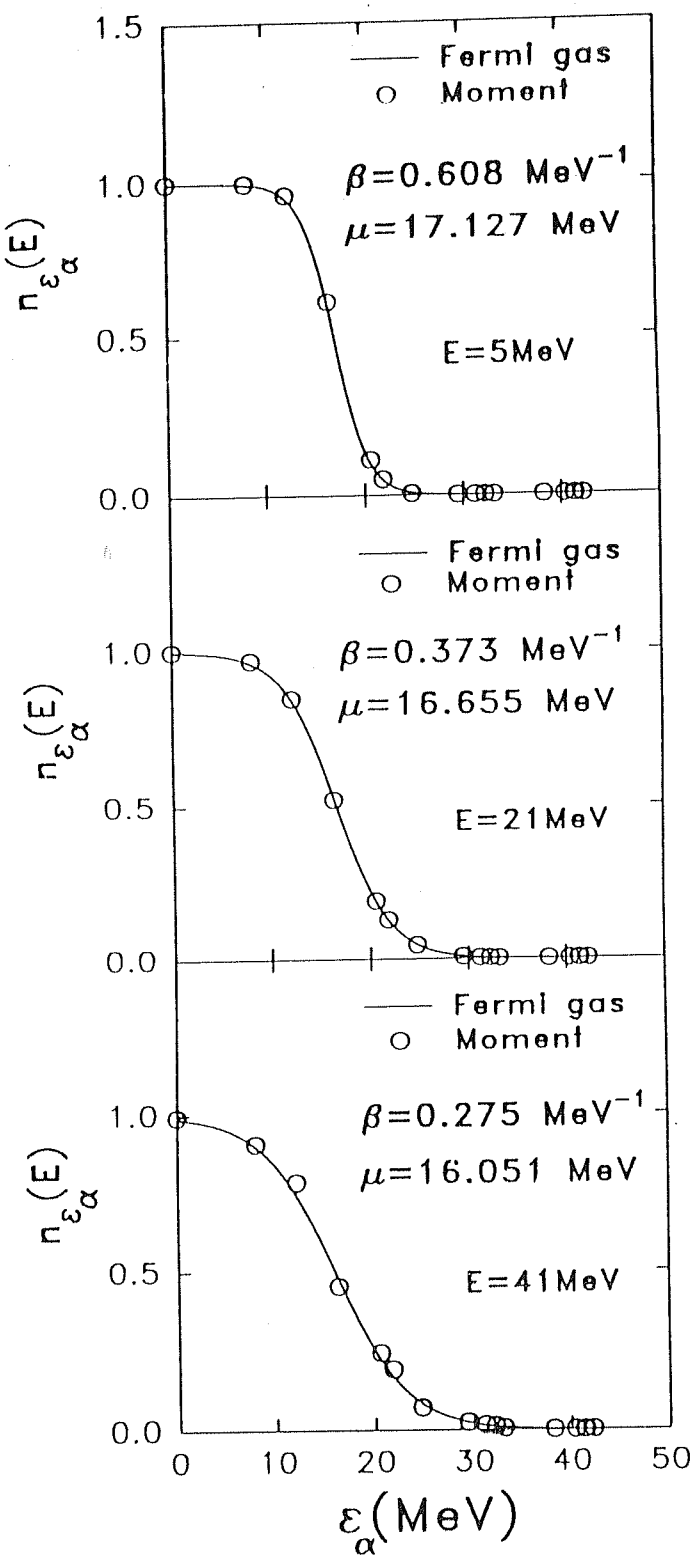
(c)


Moment
Exact
S=1-4
S=3
S=2
S=4
S=1
$f_{7/2}$
$\log(I_{n\alpha}(E))$
Moment
Exact
S=4
S=2
$f_{7/2}$
$\log(I_{n\alpha}(E))$
Moment
Exact
S=3
S=1
$f_{7/2}$
$\log(I_{n\alpha}(E))$
0
2
4
6
8
10
0
10
20
30
40
50
60
Energy (MeV)

(d)


Fermi gas
Exact
Moment
log(I(E))
a=3.748
Δ=−4.684
Fermi gas
Exact
Moment
$\langle J_z^2 \rangle^E$
k_J=1.575
Exact
Moment
$\langle n_\alpha \rangle^E$
$d_{5/2}$
$f_{7/2}$
Energy (MeV)

(e)


Fermi gas
Moment
β=0.608 MeV⁻¹
μ=17.127 MeV
E=5MeV
Fermi gas
Moment
β=0.373 MeV⁻¹
μ=16.655 MeV
E=21MeV
Fermi gas
Moment
β=0.275 MeV⁻¹
μ=16.051 MeV
E=41MeV
n_εα(E)
ε_α(MeV)
0.0
0.5
1.0
1.5
0
10
20
30
40
50

(f)

densities. Here once again the total spin-cutoff densities have exponential form. The centroids ϵ (in MeV) of $I^{h,S}_{J^2_Z}(E)$ densities are 264.2, 273.81, 283.35, 292.85 and 302.32 for $S = 0$, 1, 2, 3 and 4 respectively. Thus each state density is shifted by $\simeq 10\ MeV$ from its neighbor and this explains the exponential behavior of J^2_Z - density as seen in Fig. 3.3b. The average (σ (in MeV), γ_1, γ_2) values for the unitary orbit configurations that belong to a given S are (5.86, −0.01, −0.13), (6.06, −0.01, −0.13), (6.22, −0.01, −0.12), (6.35, −0.01, −0.12) and (6.46, −0.02, −0.12) for S = 0, 1, 2, 3 and 4 respectively. For the state densities $I^S(E)$, $\gamma_1 \simeq -0.01$, $\gamma_2 \simeq -0.13$ while (ϵ, σ) (in MeV) take the values (264.71, 6.17), (274.17, 6.31), (283.63, 6.43), (293.08, 6.54) and (302.52, 6.62) for S = 0, 1, 2, 3 and 4 respectively. The widths σ for $I^{h,S}_{J^2_Z}(E)$ are consistently smaller than the widths for $I^{h,S}(E)$ and same is true for centroids. The (γ_1, γ_2) values given above confirm the action of CLT for NIP state and spin-cutoff densities. The quality of agreements seen from J^2_Z-density extends to occupancy densities and in Figs. 3.3c, 3.3d the results for $1d_{5/2}$ and $1f_{7/2}$ densities are shown. As an example, the centroids (in MeV) of $I^{h,S}_{n_\alpha}(E)$ for $1d_{5/2}$ orbit are 262.88, 272.34, 281.80, 291.25 and 300.68 for S = 0, 1, 2, 3 and 4 respectively. The centroids shift ($\simeq 10\ MeV$) with respect to S explains the exponential increase in $I^{h,S}_{n_\alpha}(E)$ with E. The average (σ (in MeV), γ_1, γ_2) values for the unitary orbit configurations that belong to a given S (for $d_{5/2}$ occupancy density) are (5.88, 0.0, −0.16), (6.03, −0.01, −0.16), (6.16, −0.02, −0.16), (6.27, −0.03, −0.15) and (6.36, −0.03, −0.15) for $S = 0$, 1, 2, 3 and 4 respectively. In order to further test the results for J^2_Z and n_α - densities, spin-cutoff factors and occupation numbers are calculated as ratios of densities,

$$\sigma^2_J(E) = \langle J^2_Z \rangle^E = I^h_{J^2_Z}(E)/I^h(E)$$

$$\langle n_\alpha \rangle^E = I^h_{n_\alpha}(E)/I^h(E) \tag{3.15}$$

and the corresponding results are shown in Fig. 3.3e. One sees that moment methods describe $\langle J_Z^2 \rangle^E$ and $\langle n_\alpha \rangle^E$ in large spaces very well. The variation in $\langle J_Z^2 \rangle^E$ and $\langle n_\alpha \rangle^E$ with E can be understood by replacing the fixed-S densities by Gaussians and using the fact the (ϵ, σ) values for $I^{h,S}(E)$ densities are smaller (the deviations are larger for $1d_{5/2}$ densities) than the corresponding values for $I^{h,S}_K(E)$ densities; $K = J_Z^2$ or n_α with $\alpha = 1d_{5/2}$. Calculations for $\langle J_Z^2 \rangle^E$ and $\langle n_\alpha \rangle^E$ for 'nucleons' are reported in [Ko-91] while in the present exercise more realistic pn system is dealt with. It should be added that calculations for different (m_p, m_n) sets are carried out and also with different SPE for protons and neutrons and the results are found to be similar to the results shown in Figs. 3.3a - 3.3e.

Comparison with Fermi gas forms

It is important to understand how close the moment method results are to the NIP forms as the later forms are widely used in literature in analyzing data (Appendix C gives a summary of various Fermi gas forms). Recently comparison of Fermi gas forms with exact results are given by Grimes [Gr-88] and they are not of much use as the Fermi forms are not compared with a theory that can be extended easily to the interacting particle case. The same is true with the recursive method for calculating NIP state densities and spin-cutoff factors proposed by Jacquemin and Kataria [Ja-86] and the Monte Carlo method proposed by Cerf [Ce-94]. For state densities of pn systems, the back-shifted Fermi gas form [Hu-72; Eq. (C.1)] is given by $I(E) = (\sqrt{\pi}/12) exp\{(2\sqrt{a(E-\Delta)})/(a^{1/4}(E-\Delta)^{5/4})\}$. In Fig. 3.3e, the fit of the back shifted Fermi gas form with the moment method results is shown

and the deduced value of the level density parameter "a" and the back shifting energy "Δ" are $a = 3.75\ MeV^{-1}$ and $\Delta = -4.68\ MeV$. The Fermi form fits very well upto 45 MeV and beyond that one has to enlarge the single particle space to get good agreements. As it is well known in the Fermi gas theory [Hu-72, Gi-65; Appendix C] the spin-cutoff factors take the form $\sigma_J^2(E) = \langle J_Z^2 \rangle^E = k_J \sqrt{a(E-\Delta)}$ where k_J is taken to be a free parameter ($k_J \propto A^{2/3}$). With the (a, Δ) values determined from the fit to state densities, the calculated $\langle J_Z^2 \rangle^E$ values are fitted to the above form and the results are shown in Fig. 3.3e. The value of k_J is determined to be 1.58. One sees that the Fermi gas form shows departures at lower energies ($E < 10MeV$), as well as at higher energies ($E > 40MeV$). Thus the Fermi gas form cannot be used at lower energies and the discrepancy at higher energies is due to the truncation of the single particle space to sixteen orbits. The parameters (a, Δ, k_J) obtained above are somewhat larger than the values commonly used for real nuclei, i.e. $a \simeq A/8$ to $A/10\ MeV^{-1}$, $|\Delta| \simeq 2\ MeV$ and $k_J \simeq 0.1A^{2/3}$.

From the calculated occupation numbers it is possible to deduce [Sm-87] thermodynamic temperature ($\beta(E)$) and chemical potential ($\mu(E)$) by fitting the fractional occupancies $n_{\epsilon_\alpha}(E)$ to the Fermi-Dirac form,

$$n_{\epsilon_\alpha}(E) = \frac{< n_\alpha >^E}{(2j_\alpha + 1)} = \frac{1}{1 + exp[\beta(E)\{\epsilon - \mu(E)\}]} \qquad (3.16)$$

At various energies E, the calculated occupation numbers $\langle n_\alpha \rangle^E$ for the spherical orbits α (with SPE ϵ_α) are fitted to (3.16) and the inverse temperature β and the chemical potential μ are deduced and the results are shown in Fig. 3.3f for $E = 5\ MeV$, 21 MeV and 41 MeV. One sees that occupancies have excellent agreement with Fermi-Dirac form (3.16). With increase in energy as normally one expects, the chemical potential decreases and temperature (β^{-1})

increases; $(\beta(E),\ \mu(E))$ are (in MeV^{-1}, MeV) (0.61, 17.13), (0.37, 16.66) and (0.28, 16.05) for $E = 5$, 21 and 41 MeV respectively. The calculated $(\beta(E),\ \mu(E))$ values are seen to follow closely the approximate Fermi gas expressions $\beta(E) = A/\sqrt{E}$ and $\mu(E)\beta(E) = A' + B'\sqrt{E}$; A, A' and B' are free parameters [2]. Thus it is seen that occupation numbers yield values for thermodynamic temperature. Obviously its extension to the case with interactions is of immense value (Smith [Sm-87] made some preliminary studies of the same; however he did not give any large scale NIP example). Thus the results given in Figs. 3.3a - 3.3f conclusively establish that one has a good theory in moment methods for constructing state, spin-cutoff and occupancy densities, their S-decompositions and for calculating spin-cutoff factors and occupation numbers in large spaces for NIP systems. The agreements shown for S-decompositons of $\langle J_Z^2\rangle^E$ and $\langle n_\alpha\rangle^E$ densities are essential for applying Eqs. (3.3) - (3.6).

3.4 Summary

Two important tests of SAT-LSS are performed in a comprehensive manner and they are described in Sects. 3.2 and 3.3. The test of smallness of $V^{[0][2]}$ demonstrates that one of the conditions for validity of the convolution forms given in (3.3 - 3.6) where the densities are expressed as a convolution of NIP densities (due to $\mathbf{h}$) with spreading Gaussians produced by $\mathbf{V}$, is well satisfied by nuclear effective interactions. The detailed tests of the moment methods for NIP state, spin-cutoff and occupancy densities clearly show that the moment

[2] $\beta = \frac{\partial}{\partial E}\ell n\, I(E)$ and $\mu_p\beta = \frac{-\partial}{\partial m_p}\ell n(I(E))$, where $m_p = \sum n^p_{\epsilon_\alpha}(E)$ is proton number. The $\mu_n\beta$ is similarly defined. From the Fermi gas theory $I(E) \sim A_0 e^{B_0\sqrt{E}}$. The form given above for $\mu\beta$ follows by taking $\frac{\partial A_0}{\partial m_p}$ and $\frac{\partial B_0}{\partial m_p}$ to be constants.

methods are well suited, having the desired structures, for constructing the NIP densities which are one of the convolution factors in the IP theory given by (3.3 - 3.6). Further tests of SAT-LSS come from actual data analysis. Towards this end, in the next chapter a systematic analysis of fp-shell level densities and spin-cutoff factors data is carried out.

Chapter 4

Analysis of Level Density Data for fp-Shell Nuclei: Systematic Calculations Using SAT-LSS

4.1 Preview

Level density calculations for 8 fp-shell nuclei $\{^{55}_{25}Mn_{30}, ^{56}_{26}Fe_{30}, ^{59}_{27}Co_{32}, ^{60}_{27}Co_{33}, ^{60}_{28}Ni_{32}, ^{62}_{28}Ni_{34}, ^{63}_{29}Cu_{34}, ^{65}_{29}Cu_{36}\}$ are carried out using SAT-LSS and the results are described in this chapter. The various conditions that led to the selection of the above eight nuclei are given in Sect. 4.2.1. In order to proceed with the calculations, one needs to have a reference energy, a set of s.p. orbits (and their energies) and a two-body interaction. The problem of reference energy is briefly described in Sect. 4.2.2 and the choice of s.p. orbits, SPE and two-body interaction is given in Sect. 4.2.3. All the calculations are carried out using surface delta interaction (SDI) with one strength parameter G. The theoretical calculations involve evaluating the spreading variances and the moments for constructing NIP densities as described in Sect. 3.1. For these two, it is necessary to group the spherical orbits into unitary orbits and the choice of

unitary orbits for the above two calculations need not be the same. In general the later should be finer than the former. The unitary configurations in the former case define the classes [1] as described in [Fr-94] and using the classes and (3.4 - 3.6), the state and spin-cutoff densities are constructed. The choice of unitary orbits and the corresponding classes are given in Sect. 4.2.4. In Sect. 4.2.5, the empirical fact that in general spin-cutoff variances $\sigma^2_{\mathbf{V}:J_z^2}$ are smaller compared to state density variances $\sigma^2_{\mathbf{V}}$ by $\sim 10\%$ is verified for the eight fp-shell nuclei. This result is used in the calculation of level densities in order to reduce computer time. The calculational procedure is outlined in Sect. 4.2.6. The results of the calculation of the level densities and spin-cutoff factors and their comparison with the experimental data are given in Sect. 4.3 for the six nuclei ^{55}Mn, ^{56}Fe, ^{59}Co, ^{60}Co, ^{60}Ni, ^{62}Ni and ^{63}Cu employing the space spanned over the eight spherical orbits ($1d_{5/2}$, $2s_{1/2}$, $1d_{3/2}$, $1f_{7/2}$, $2p_{3/2}$, $1f_{5/2}$, $2p_{1/2}$, $1g_{9/2}$) and in Sect. 4.4 for the nuclei ^{62}Ni, ^{63}Cu and ^{65}Cu employing the space spanned over the ten spherical orbits ($1d_{5/2}$, $2s_{1/2}$, $1d_{3/2}$, $1f_{7/2}$, $2p_{3/2}$, $1f_{5/2}$, $2p_{1/2}$, $1g_{9/2}$, $1g_{7/2}$, $2d_{5/2}$). Using ^{63}Cu nucleus as an example, it is clearly demonstrated in Sect. 4.3 that for $A > 60$ nuclei it is essential to go beyond the eight orbit space and therefore in the calculations presented in Sect. 4.4, the space of ten spherical orbits is employed. Finally a summary is given in Sect. 4.5. The results given in this chapter are first reported in [Ko-94c].

[1] Classes are defined by the unitary configurations in (3.4 - 3.6). These unitary configurations are generated by the largest possible unitary orbits (orbits α in Fig. 3.1) consistent with the definition of the S - quantum number. In fact it is the fluctuation in the spreading widths of spherical configurations that belong to a given class is small but not for the configurations that belong to a given S. It should be noted that the class variances involve partial variances unlike the fixed-S variances. Classes are introduced in [Fr-94] as they appear to provide a basis for the constant width approximation in terms of an ensemble representation of the hamiltonian.

4.2 Selection of nuclei, choice of orbits and the hamiltonian and the procedure for calculations

4.2.1 Choice of fp-shell nuclei

The experimental data for level densities and spin-cutoff factors come from four different sources and they are : (1) direct counting of levels; (2) neutron/proton resonance experiments; (3) charged particle spectra; (4) Ericson fluctuation measurements. Details of these methods are given in Appendix C. The first method gives level densities at few (2 or 3) low-lying energies (say $E \sim 2 - 4\,MeV$), the second method gives the level density at resonance energy (proton resonance experiments give densities at say 2 nearby energies), the third method gives values for level density parameters (a and Δ) say valid upto 20-25 MeV excitation and the fourth one gives level densities at a few (3 or 4) energies at high excitation energy (say around 20 MeV). Theoretical calculations need a reference energy (Sect. 4.2.2) and there is also a free parameter (G; see Sect. 4.2.3 and Appendix B) in the interaction. The low-energy data is used in fixing the reference energy and then the resonance data gives a value for G. The purpose here is not just to derive a value for G but also to verify whether one can extrapolate the predictions much beyond the resonance energy (i.e. beyond say 10 MeV and upto say $20 - 25\,MeV$ excitation). To verify this one needs data from sources (3) and/or (4). Thus, in the selection of the nuclei, for analysis with the theory given in Sect. 4.3.1, we impose the restriction that the nucleus under question should have level density data from {(1) and/or (2)} and {(3) and/or (4)}. With this restriction, there are only eight fp-shell nuclei, as given in Table 4.1, that can be analyzed. The

data for the eight nuclei listed in Table 4.1 are compiled in Appendix C.

Table 4.1 Sources of data for fp-shell nuclei. The sources (1) - (4) are defined in the text.

Nucleus	Sources of data
^{55}Mn	(1), (2), (4)
^{56}Fe	(1), (3), (4)
^{59}Co	(1), (2), (3)
^{60}Co	(2), (4)
^{60}Ni	(1), (2), (3), (4)
^{62}Ni	(1), (2), (3)
^{63}Cu	(1), (2), (3)
^{65}Cu	(1), (2), (3)

4.2.2 Reference energy

The calculated state density yields a smoothed spectrum via the distribution function $F(E) = \int_{-\infty}^{E} I(x)dx$. Given a sequence of levels with angular momentum J_1, J_2, J_3, ...J_r, inverting the equation $F(E) = \sum_{k=1}^{r-1}(2J_k+1)+(2J_r+1)/2$ gives the energy E_r of the r^{th} level. With $N_r = \sum_{k=1}^{r}(2J_k+1)$ denoting total number of states including and upto the r^{th} level, one has to solve the equation

$$\left[N_r - \frac{(2J_r+1)}{2}\right] = \int_{-\infty}^{\overline{E_r}} I(E)\,dE \tag{4.1}$$

to obtain the smoothed energy $\overline{E_r}$. For sequence of levels with fixed parity (say π), extension of (4.1) is straightforward by replacing $I(E)$ by $I^{\pi}(E)$, N_r by N_r^{π} and J_r by J_r^{π}. Using this method one can calculate the ground state energy and then measure all the energies with respect to this energy. Then comparison of calculated and experimental densities is immediate. However, as the fluctuations in low-energy domain are not "quantum chaotic", one should match the energy of a high lying level with the corresponding calculated energy

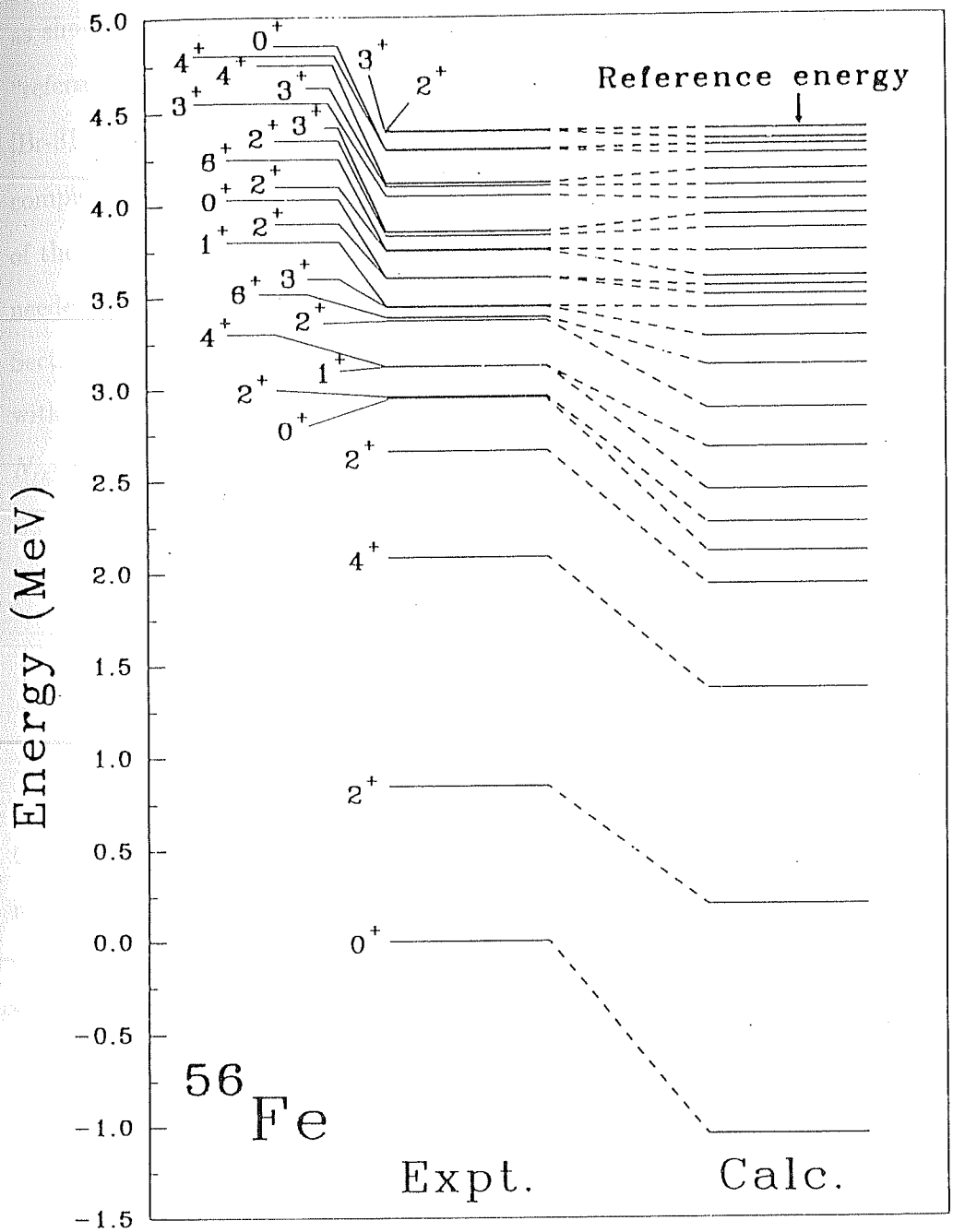


Fig. 4.1 Comparison of calculated smoothed spectrum with experimental spectrum for ^{56}Fe. Figure gives an example of reference energy selection.

as shown in Fig. 4.1 and then measure all the energies with respect to this "reference energy". There are several variants of the reference energy selection [Br-81, Fr-94]. Thus in order to proceed to the level density calculations, complete set of low-lying levels (upto a high enough energy) and the J^{π}_{ref} value of the last level (reference level) in the sequence (with energy $E_{ref}(J^{\pi}_{ref})$) are needed. This data for the eight nuclei mentioned in Table 4.1 are given in Sect. 4.3. Using $I(E) = \sum_{[\mathrm{m}]} I^{[\mathrm{m}]}(E) = \sum_{[\mathrm{m}]} d([\mathrm{m}])\rho^{[\mathrm{m}]}(E)$ as given by (3.2) with $\rho^{[\mathrm{m}]}(E)$ taken to be a Edgeworth corrected Gaussian (2.8) leads to (with N_{ref} giving the number of states upto and including the reference level),

$$\left[N_{ref} - \tfrac{1}{2}(2J_{ref}+1)\right] = \sum_{[\mathrm{m}]} d([\mathrm{m}]) \int_{-\infty}^{\overline{E}_{ref}} \rho^{[\mathrm{m}]}(E)dE \ ;$$

$$\int_{-\infty}^{\overline{E}_{ref}} \rho^{[\mathrm{m}]}(E)\, dE = \frac{1}{2} erfc\left[\frac{\epsilon([\mathrm{m}]) - \overline{E}_{ref}}{\sqrt{2}\sigma([\mathrm{m}])}\right] - \eta\varrho(z)\left\{\left[\frac{k_3([\mathrm{m}])}{6} He_2(z)\right] + \left[\frac{k_4([\mathrm{m}])}{24} He_3(z) + \frac{[k_3([\mathrm{m}])]^2}{72} He_5(z)\right]\right\} \ ;$$

$$z = (\overline{E}_{ref} - \epsilon([\mathrm{m}]))/\sigma([\mathrm{m}]) \qquad (4.2)$$

Given the values of $(N_{ref},\ J^{\pi}_{ref})$ one can solve [2] (4.2) to obtain $\overline{E}_{ref}$ and match it with the experimental energy $E_{ref}(J^{\pi}_{r})$.

4.2.3 Choice of the single particle orbits and the two-body interaction

s.p. orbits and SPE

For the calculation of the level densities, eight single particle shell model orbits are chosen (for both protons and neutrons) and they are $1d_{5/2}$, $2s_{1/2}$,

[2] A simple formula for the error function is as follows [Ab-64, p. 297,299]: $erfc(z) = 1 - erf(z)$, $erfc(-z) = 1 + erf(z) = 2 - erfc(z)$; $z > 0$, $erf(x) = 1 - (a_1 t + a_2 t^2 + a_3 t^3 + a_4 t^4 + a_5 t^5)e^{-x^2} + \epsilon(x)$; $t = \frac{1}{1+px}$, $|\epsilon(x)| \leq 1.5 \times 10^{-7}$; $p = 0.3275911$, $a_1 = 0.254829592$, $a_2 = -0.284496736$, $a_3 = 1.421413741$, $a_4 = -1.453152027$, $a_5 = 1.061405429$.

$1d_{3/2}$, $1f_{7/2}$, $2p_{3/2}$, $1f_{5/2}$, $2p_{1/2}$ and $1g_{9/2}$. Thus (s^4p^{12}) is taken as the closed core and the space consists of ds - shell, fp-shell and $g_{9/2}$ orbit. The SPE given in [Sp-65] are used in the calculations and for the above eight orbits they are (in MeV) (−4.15, −3.28, 0.93, 1.55, 3.57, 7.74, 5.58, 8.74) respectively. They give the ds, fp and $g_{9/2}$ centroid energies to be −2.311, 4.214, and 8.74 MeV respectively. The $ds-fp$ and $fp-g_{9/2}$ separations then are $\Delta_{ds-fp} = 6.53\,MeV$ and $\Delta_{fp-g_{9/2}} = 4.53\,MeV$. However the interaction V produces a further renormalization of Δ_{ds-fp} and $\Delta_{fp-g_{9/2}}$ as we are considering s^4p^{12} to be a closed core; the renormalization arises (as discussed in footnote #1 of Chapter 3) due to the interaction of a particle in (ds), (fp) and $g_{9/2}$ shells with the core. The $ds - fp$ and $fp - g_{9/2}$ separations due to renormalization are calculated (given in footnote #1 of Chapter 3) using Kuo 15-orbit interaction and they are $\delta\Delta^{Kuo}_{sd-fp} = 5.66\ MeV$ and $\delta\Delta^{Kuo}_{fp-g_{9/2}} = 3.38\ MeV$. However as SDI is used for V in the present calculations, it is plausible that one need not use the above values for $\delta\Delta$. A number of level density calculations are carried out, to test the effects due to variations in $\delta\Delta$ (Sect. 4.3 gives an important

Table 4.2 Quantum numbers and energies of s.p. orbits

orbit #	s	n	ℓ	j	$\epsilon_j\ (MeV)$
#1	0	0	2	5/2	-1.838
#2	0	1	0	1/2	-0.968
#3	0	0	2	3/2	3.242
#4	1	0	3	7/2	-2.664
#5	1	1	1	3/2	-0.644
#6	1	0	3	5/2	3.526
#7	1	1	1	1/2	1.366
#8	2	0	4	9/2	0.000

$\overline{\Delta}_{ds-fp} = 11.03\,MeV$ $\overline{\Delta}_{fp-g_{9/2}} = 6.53\,MeV$

discussion regarding these calculations) for all the eight fp-shell nuclei and found that it is best to use $\delta\Delta_{ds-fp} = 4.5\,MeV$ and $\delta\Delta_{fp-g_{9/2}} = 2\,MeV$. With this, the adopted (denoted by $\overline{\Delta}$) values of Δ_{ds-fp} and $\Delta_{fp-g_{9/2}}$ are $\overline{\Delta}_{ds-fp} = 11.03\,MeV$ and $\overline{\Delta}_{fp-g_{9/2}} = 6.53\,MeV$. The resulting zero centered SPE and the separations $\overline{\Delta}$, used in the calculations, are given in Table 4.2.

Two-body interaction V

The two-body interaction that has been chosen for the present calculations is the Surface Delta Interaction (SDI) with one strength parameter G as given by (B.3, B.4). Thus we have a one parameter interaction. The choice of SDI is made on the basis of its simplicity and because of the important property that SDI does not renormalize SPE (details are given in Appendix B). It is known from earlier calculations [Ko-91, Fr-94] of level densities and state densities for ^{168}Er and ^{234}U that the state density $I(E)$ (and so also the level density) varies rapidly with G. Since the value of G has to be fixed by fitting to experimental data, some knowledge of variation of $I(E)$ with G for fp-shell nuclei is essential. This variation is investigated with ^{56}Fe and ^{60}Ni as examples and the results are shown in Fig. 4.2. One sees a rapid variation in $I(E)$ with G for a given E. Thus G can be determined with precision by using level density data.

4.2.4 Unitary orbits for spreading variances and NIP calculations

For calculating state and spin-cutoff density variances, the eight spherical orbits given in Table 4.2 for protons (and neutrons) are divided into three unitary orbits (denoted by UOV). The UOV orbits and the corresponding s values are

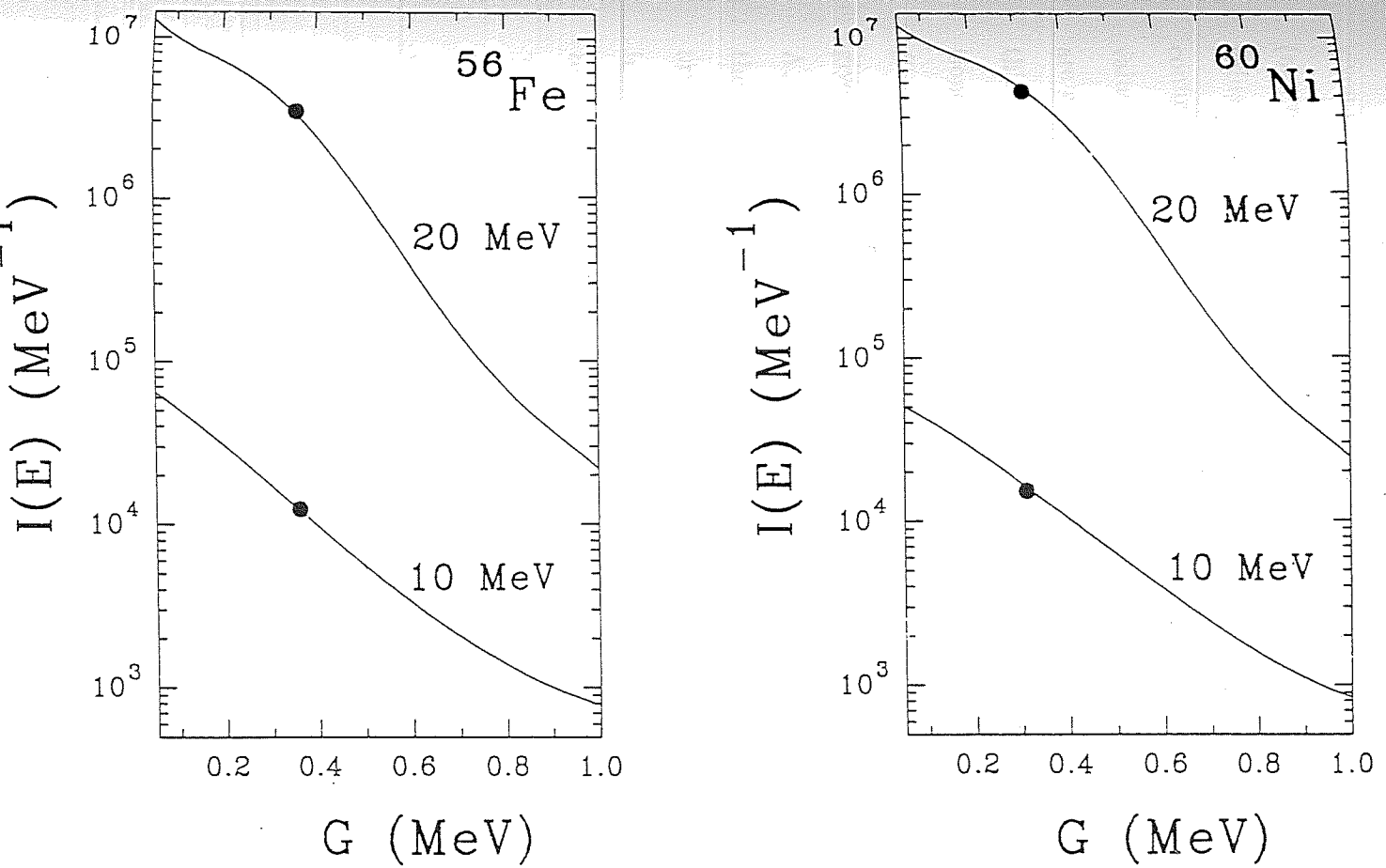


Fig. 4.2 State density $I(E)$ vs G for ^{56}Fe and ^{60}Ni at $E = 10\ MeV$ and $20\ MeV$. The value of G used in the level density calculations is shown by filled circles.

given in Table 4.3. Given a fp-shell nucleus, the proton and neutron numbers (m_p, m_n) outside the s^4p^{12} core can be easily counted. The smallest total S value allowed for the nucleus is given by $S_{min} = m_p + m_n - 24$. Given a unitary configuration $[\mathbf{m}_p, \mathbf{m}_n]$ defined over the UOV given in Table 4.3, the total S value $S_{TOT}([\mathbf{m}_p, \mathbf{m}_n]) = \sum_{i=1}^{3}(\mathbf{m}_p)_i s_i + \sum_{i=1}^{3}(\mathbf{m}_n)_i s_i$. Then the $S\hbar\omega$ excitations are given by $S = S([\mathbf{m}_p, \mathbf{m}_n]) = S_{TOT}([\mathbf{m}_p, \mathbf{m}_n]) - S_{min}$. The calculations in this chapter are restricted to $2\hbar\omega$ excitations, i.e. $S \leq 2$. As already mentioned before, the classes are defined by $[\mathbf{m}_p, \mathbf{m}_n]$. There are one $S = 0$, four $S = 1$ and ten $S = 2$ classes. The S values and the corresponding classes are given in Table 4.4. In Table 4.4 whenever Λ_{-1} is not shown, it implies that Λ_{-1} orbit is full. Similarly Λ_1 orbit is not shown whenever it is empty. For the calculation of the NIP densities $I^{\mathbf{h}}(E)$, and $I^{\mathbf{h}}_{J_Z^2}(E)$, three UOV unitary orbits are further divided into five unitary orbits (denoted by UON) as given in Table 4.5. For each nucleus, the number of unitary configurations defined by UON unitary orbits for each of the 15 classes are given in Table 4.6. From Tables 4.4 and 4.6 it is seen that for spreading variance calculations there are 11 configurations for +ve parity states and for both parities 15 configurations while for NIP calculations and in the final sum (using (3.4 - 3.6)) involving convolution of NIP and spreading Gaussian densities there are $\sim$ 1500 configurations for both parities. However, with spherical orbits for both UOV and UON orbits, there will be $\sim 10^4$ configurations and then one has to calculate $\sim 10^4$ spreading variances unlike only 15 with UOV unitary orbits.

Table 4.3 Unitary orbits (UOV) for spreading variance calculations. Given in the table are also the s values of and symbols for each unitary orbit.

UOV #	Spherical orbits	s value	symbol
#1	$d_{5/2}$, $s_{1/2}$, $d_{3/2}$	0	Λ_{-1}
#2	$f_{7/2}$, $p_{3/2}$, $f_{5/2}$, $p_{1/2}$	1	Λ_0
#3	$g_{9/2}$	2	Λ_1

Table 4.4 Class structures. Table 4.3 defines the symbol Λ_i.

S	Class Structure	Class No.
0	$(\Lambda_0)^{m_p}(\Lambda_0)^{m_n}$	#1
1	$(\Lambda_0)^{m_p}(\Lambda_{-1})^{m_n-1}(\Lambda_1)^{1_n}$	#2
	$(\Lambda_0)^{m_p}(\Lambda_{-1})^{-1_n}(\Lambda_0)^{m_n+1}$	#3
	$(\Lambda_{-1})^{m_p-1}(\Lambda_1)^{1_p}(\Lambda_0)^{m_n}$	#4
	$(\Lambda_{-1})^{-1_p}(\Lambda_0)^{m_p+1}(\Lambda_0)^{m_n}$	#5
2	$(\Lambda_0)^{m_p}(\Lambda_0)^{m_n-2}(\Lambda_1)^{2_n}$	#6
	$(\Lambda_0)^{m_p}(\Lambda_{-1})^{-1_n}(\Lambda_0)^{m_n}(\Lambda_1)^{1_n}$	#7
	$(\Lambda_0)^{m_p}(\Lambda_{-1})^{-2_n}(\Lambda_0)^{m_n+2}$	#8
	$(\Lambda_0)^{m_p-1}(\Lambda_1)^{1_p}(\Lambda_0)^{m_n-1}(\Lambda_1)^{1_n}$	#9
	$(\Lambda_0)^{m_p-1}(\Lambda_1)^{1_p}(\Lambda_{-1})^{-1_n}(\Lambda_0)^{m_n+1}$	#10
	$(\Lambda_0)^{m_p-2}(\Lambda_1)^{2_p}(\Lambda_0)^{m_n}$	#11
	$(\Lambda_{-1})^{-1_p}(\Lambda_0)^{m_p+1}(\Lambda_0)^{m_n-1}(\Lambda_1)^{1_n}$	#12
	$(\Lambda_{-1})^{-1_p}(\Lambda_0)^{m_p+1}(\Lambda_{-1})^{-1_n}(\Lambda_0)^{m_n+1}$	#13
	$(\Lambda_{-1})^{-1_p}(\Lambda_0)^{m_p}(\Lambda_1)^{1_p}(\Lambda_0)^{m_n}$	#14
	$(\Lambda_{-1})^{-2_p}(\Lambda_0)^{m_p+2}(\Lambda_0)^{m_n}$	#15

Table 4.5 Unitary orbits (UON) for NIP calculations. Given also are the s - values for each unitary orbit.

UON #	Spherical orbits	s
#1	$d_{5/2}, s_{1/2}$	0
#2	$d_{3/2}$	0
#3	$f_{7/2}$	1
#4	$p_{3/2}, f_{5/2}, p_{1/2}$	1
#5	$g_{9/2}$	2

Table 4.6 Number of unitary configuration for NIP calculations

Class #	Nucleus							
	^{55}Mn	^{56}Fe	^{59}Co	^{60}Co	^{60}Ni	^{62}Ni	^{63}Cu	^{65}Cu
#1	54	63	72	64	81	63	63	45
#2	54	63	72	72	81	72	72	54
#3	108	126	128	112	144	108	108	72
#4	45	54	63	56	72	63	56	45
#5	126	144	162	144	162	126	126	90
#6	54	63	72	72	81	81	81	63
#7	108	126	144	128	162	126	126	90
#8	162	189	168	144	189	135	135	81
#9	45	54	63	63	72	64	72	54
#10	90	108	112	98	128	96	108	72
#11	36	45	54	48	63	49	56	40
#12	126	144	162	162	162	144	144	108
#13	252	288	288	252	288	216	216	144
#14	108	126	144	128	162	126	126	90
#15	216	243	243	216	243	189	189	135

4.2.5 Ratio of J^2-density variance and state density variance

From the previous level density calculations for ^{28}Si, ^{168}Er, ^{181}W and ^{234}U nuclei [Ko-91, Ko-93a, Fr-94] it is found that in general the J^2-density variance is smaller, $\sim 90\%$ of the state density variance for all class members. Using this result will considerably reduce the computing time. On the machine

that is available to us it takes $\sim$ 80 hours for calculating $\sigma^2_{V;J_Z^2}$ for all the 15 classes listed in Table 4.4 against $\sim$ 4 minutes for calculating the spreading variances σ^2_V for the 15 classes. Thus the 8 - orbit calculations are impractical but however calculations are easy to carry out if the result $\sigma^2_{V;J_Z^2}/\sigma^2_V \sim 0.9$ is used. Before using this result in the present calculations, it should be verified for fp-shell nuclei. In order to do this, we have chosen a 7-orbit space consisting of ($2s_{1/2}$, $1d_{3/2}$, $1f_{7/2}$, $2p_{3/2}$, $1f_{5/2}$, $2p_{1/2}$, $1g_{9/2}$) spherical orbits and the corresponding unitary orbit numbers are (#1, #1, #2, #2, #2, #2, #3) respectively. Thus in the 7-orbit calculations Λ_{-1} of Table 4.3 contains only $2s_{1/2}$ and $1d_{3/2}$ orbits. It should be clear that there is a one to one correspondence between the 7-orbit and 8-orbit classes. For each of the 15 classes given in the Table 4.4 the ratio $\sigma^2_V/\sigma^2_{V;J_Z^2}$ is observed to be $\sim$ 1.09 and the results are given in Table 4.7; the 7-orbit calculations for each nucleus

Table 4.7 The ratio $\sigma^2_V/\sigma^2_{V;J_Z^2}$ for fp-shell nuclei in a 7-orbit calculation

Class #	$\sigma^2_V/\sigma^2_{V;J_Z^2}$							
	^{55}Mn	^{56}Fe	^{59}Co	^{60}Co	^{60}Ni	^{62}Ni	^{63}Cu	^{65}Cu
#1	1.11	1.11	1.10	1.11	1.10	1.11	1.11	1.11
#2	1.09	1.08	1.08	1.08	1.08	1.08	1.08	1.08
#3	1.09	1.09	1.08	1.09	1.08	1.08	1.08	1.08
#4	1.09	1.08	1.08	1.08	1.08	1.08	1.08	1.08
#5	1.09	1.09	1.09	1.09	1.09	1.09	1.09	1.09
#6	1.08	1.07	1.07	1.07	1.07	1.07	1.07	1.07
#7	1.07	1.07	1.07	1.07	1.07	1.07	1.07	1.07
#8	1.07	1.07	1.07	1.07	1.07	1.07	1.07	1.07
#9	1.07	1.07	1.07	1.07	1.07	1.07	1.07	1.07
#10	1.07	1.07	1.07	1.07	1.07	1.07	1.07	1.07
#11	1.08	1.08	1.07	1.07	1.07	1.07	1.07	1.07
#12	1.08	1.07	1.07	1.07	1.07	1.07	1.07	1.07
#13	1.08	1.08	1.08	1.08	1.08	1.08	1.07	1.07
#14	1.08	1.08	1.07	1.07	1.07	1.07	1.07	1.07
#15	1.08	1.08	1.08	1.08	1.08	1.08	1.08	1.08

takes $\sim$ 4 hours of computing time. In ^{56}Fe example full 8-orbit calculations for $\sigma^2_{\mathbf{V}:J^2_Z}$ are carried out for all the 15 classes given in Table 4.4. The 8-orbit $\sigma^2_{\mathbf{V}}/\sigma^2_{\mathbf{V}:J^2_Z}$ values for each of the 15 classes are found to be essentially identical (within 1%) to the 7-orbit numbers given in Table 4.7. This result permits us to use the results of Table 4.7 in 8-orbit calculations.

The results discussed above are employed in calculating the spreading variances as follows. Using propagation methods given in Sect. 2.6 the state density spreading variances $\sigma^2_{\mathbf{V}}$ are calculated for each of the 15 classes in 8-orbit case. Using the 8-orbit values for $\sigma^2_{\mathbf{V}}$ and the 7-orbit results (from Table 4.7) for $\sigma^2_{\mathbf{V}}/\sigma^2_{\mathbf{V}:J^2_Z}$, $\{\sigma^2_{\mathbf{V}:J^2_Z}\}_{8-orbit}$ is computed using $\sigma^2_{\mathbf{V}:J^2_Z} = \{\sigma^2_{\mathbf{V}}\}_{8-orbit} \times \left[\{\sigma^2_{\mathbf{V}}/\sigma^2_{\mathbf{V}:J^2_Z}\}_{7-orbit}\right]^{-1}$. These effective 8-orbit $\sigma^2_{\mathbf{V}:J^2_Z}$ values together with centroid shifts $\epsilon_{\mathbf{V}:J^2_Z}$ are used in constructing the spin-cutoff densities.

4.2.6 Procedure for calculations

Following the theory outlined in Sect. 3.1, for calculating level densities and spin-cutoff factors, first the unitary decomposition (with respect to the direct sum group defined by UOV orbits) of the hamiltonian ($h + V$; h defined by SPE in Table 4.2 and $V = G \times (SDI)$) and J^2 operator are carried out. Then, for each of the fifteen classes given in Table 4.4, the spreading variances $\sigma^2_{\mathbf{V}}([\mathbf{m}])$ and centroid shifts $\epsilon_{\mathbf{V}:J^2_Z}([\mathbf{m}])$ are obtained. Using the method described in Sect. 4.2.5 the spin-cutoff density variances $\sigma^2_{\mathbf{V}:J^2_Z}([\mathbf{m}])$ are calculated. Generating the configurations $\{\mathbf{m}\}$ defined by UON orbits for each of the 15 classes (defined by UOV orbits), the first four NIP density cumulants $\epsilon_{NIP}(\{\mathbf{m}\})$, $\sigma^2_{NIP}(\{\mathbf{m}\})$, $\gamma_1^{NIP}(\{\mathbf{m}\})$ and $\gamma_2^{NIP}(\{\mathbf{m}\})$ are calculated (the number of $\{\mathbf{m}\}$ in a $[\mathbf{m}]$ is given in Table 4.6) both for NIP state and spin-cutoff

densities. The $I^h \otimes \rho^V$ convolution, for each $\{\mathbf{m}\} \in [\mathbf{m}]$, is carried out by adding the I^h and ρ^V cumulants (in the present exercise ρ^V is a Gaussian). Using the first four cumulants (ϵ, σ^2, γ_1, γ_2) thus obtained, the fixed $\{\mathbf{m}\}$ densities are written as Edgeworth corrected Gaussian densities (2.8). The above exercise is carried out for positive parity configurations in case of even-even or odd-odd nuclei and for negative parity configurations in case of even-odd or odd-even nuclei in our set. All the calculations use $S = 0 \oplus S = 2$ space. The ratio of these fixed-parity spin-cutoff and state densities give the fixed parity spin-cutoff factors. This information is then converted into total level densities and spin-cutoff factors by using (C.8, C.12, C.13).

In the actual calculations, starting with the reference energy data (E_{ref}, J^{π}_{ref}, N_{ref}) given ahead in Sect. 4.3 and a value for the SDI strength G ($G \simeq 25/A$ MeV), $N^{\pi}(E)$ is calculated at various energies E and then (4.2) is used to obtain $\overline{E}_{ref}$. Then the ground state energy in the calculation is $E_{GS} = \overline{E}_{ref} - E_{ref}$. Now $I^{\pi}(E)$ is calculated at around 10 MeV excitation where resonance or some other data for $I_{\ell}(E)$ is available (we call it $I_{\ell;href}(E)$). The $I^{\pi}(E)$ is converted into $I_{\ell}(E)$ and compared with $I_{\ell;href}(E)$. The value of G is varied until the calculated $I_{\ell}(E)$ is within say 5% of the $I_{\ell;href}(E)$. Using the G-value thus obtained, $I_{\ell}(E)$, $I(E)$ and $\sigma_J(E)$ are calculated for E from 4 to 25 MeV excitation and compared with data.

Good agreements with data alone do not justify that the calculations are proper. It is essential that (i) in the low-energy domain (say $E \lesssim 6\,MeV$) the $S = 0$ densities should be much larger than the $S = 2$ densities ($I(E) = I_{S=0}(E) + I_{S=2}(E)$) and (ii) the value of G should be in a meaningful domain (low-energy spectroscopic calculations yield $G \simeq 25/A$ MeV). In fact the

Δ_{ds-fp} and $\Delta_{fp-g_{9/2}}$ separations (one set for all nuclei) given in Sect 4.2.3 are chosen such that for all the fp-shell nuclei under consideration the condition (i) above is satisfied and to get good agreement with data $G \simeq 20/A\ MeV$ is used. Table 4.8 shows the S-decomposititon of the state densities at various

Table 4.8 S-decomposition of state densities. For a given nucleus and a given energy, the first entry is for $I^{\pi}_{\ell;S=0}(E)$ and the second for $I^{\pi}_{\ell;S=2}(E)$. The parity $\pi = +$ for even-even nuclei and $\pi = -$ for even-odd or odd-even nuclei respectively. In Sect. 4.3.6 ahead $^{63}Cu(a)$ and $^{63}Cu(b)$ calculations are defined.

E (MeV)	^{55}Mn	^{56}Fe	^{59}Co	^{60}Co	^{60}Ni	$^{63}Cu\ (a)$	$^{63}Cu\ (b)$
4.0	24	9	26	258	14	26	6
	7	2	4	47	1	6	25
8.0	338	140	350	2608	216	333	93
	144	42	97	988	23	136	513
12.0	3100	1479	3244	18546	2256	3002	1021
	2109	692	1613	14322	511	2304	7379
16.0	20121	11171	22046	97501	17057	19813	7934
	23607	8694	19914	150780	8015	28196	78174
20.0	96461	27442	113900	393590	97154	99534	45869
	204080	28022	187940	1201100	92063	260010	631190

energies for the six nuclei $\{^{55}Mn, ^{56}Fe, ^{59}Co, ^{60}Co, ^{60}Ni, ^{63}Cu\}$. In the case of ^{63}Cu using densities corresponding to $^{63}Cu\ (b)$ in Table 4.8, one gets excellent agreement with data as described in Sect. 4.3.6 ahead. However here the $S = 2$ densities are much larger than $S = 0$ densities. Thus these calculations cannot be considered to be good (similar problems exist in the preliminary calculations for ^{56}Fe reported in [Ja-92]). However this is not the case with the $^{63}Cu\ (a)$ calculations though here the agreements are only satisfactory as shown in Fig. 4.10 ahead.

4.3 8-orbit results for ^{55}Mn, ^{56}Fe, ^{59}Co, ^{60}Co, ^{60}Ni and ^{63}Cu

Following Sect. 4.2, level densities and spin-cutoff factors are calculated for the eight nuclei $\{^{55}Mn,\ ^{56}Fe,\ ^{59}Co,\ ^{60}Co,\ ^{60}Ni,\ ^{62}Ni,\ ^{63}Cu,\ ^{65}Cu\}$. It is found that $A > 60$ nuclei, the space defined by the eight orbits $\{1d_{5/2},\ 2s_{1/2},\ 1d_{3/2},\ 1f_{7/2},\ 2p_{3/2},\ 1f_{5/2},\ 2p_{1/2},\ 1g_{9/2}\}$ is not adequate. For the three nuclei ^{62}Ni, ^{63}Cu and ^{65}Cu, the calculated densities differ from data values by a factor 2-3 and it is clearly seen that in these cases to get good agreements one has to necessarily violate the conditions (i) and (ii) given in Sect. 4.2.6. The problems encountered here are discussed in some detail with the ^{63}Cu example in Sect 4.3.6. Because of the problem mentioned above, detailed calculations are carried out only for the six nuclei $\{^{55}Mn,\ ^{56}Fe,\ ^{59}Co,\ ^{60}Co,\ ^{60}Ni,\ ^{63}Cu\}$ and compared with data in Sects. 4.3.1 – 4.3.6. It appears that the solution to the problems encountered with $A > 60$ nuclei can be solved only by expanding the space, i.e. by including $(2d_{5/2},\ 1g_{7/2})$ orbits or in other words by performing 10-orbit calculations for these nuclei. This aspect is discussed in Sect. 4.3.6 and the results of 10-orbit calculations are given in Sect. 4.4. All the calculations reported in Sects. 4.3.1 – 4.3.6 and 4.4 are performed using the package LVLDN_INT [Ha-92].

4.3.1 Nucleus ^{55}Mn

The low-energy data which is used in fixing the reference energy are given in Table 4.9. Also shown in the table are E_{ref}, J^{π}_{ref} and N_{ref} values and with these values,

Table 4.9 Low energy data for reference energy calculation

E (MeV)	J^π	Ref
0.0	$5/2^-$	[Nu-85]
0.126	$7/2^-$	[Nu-85]
0.984	$9/2^-$	[Nu-85]
1.290	$1/2^-$	[Le-78]
1.292	$11/2^-$	[Nu-85]
1.293	$1/2^-$	[Nu-85]
1.528	$3/2^-$	[Nu-85]
$E_{ref} = 1.528\ MeV$		$J^\pi_{ref} = 3/2^-$
	$N_{ref} = 44$	

the GS energy is calculated, with a trial value of G, using the method outlined in Sect. 4.2.2. The value of G is varied such that the total level density $I_\ell(E)$ at $E = 10\ MeV$ becomes close to the values obtained from the experimental (proton resonance) data compiled by Iljinov et al (Table C.1) which is $3000 \pm 800\, MeV^{-1}$. With $G = 0.365\, MeV$ the calculated value of $I_\ell(E)$ at $10\ MeV$ is $3200\ MeV^{-1}$. The values of σ^2_{V}, $\sigma^2_{\mathrm{V};J^2_{\mathrm{Z}}}$ and $\epsilon_{\mathrm{V};J^2_{\mathrm{Z}}}$ calculated with $G = 0.365\, MeV$ are $17.2\ MeV^2$, $15.5\ MeV^2$ and $0.015\ MeV$ respectively for $S = 0$ configuration, $\sim 25\ MeV^2$, $\sim 23\ MeV^2$ and $\sim 0.01\ MeV$ respectively for $S = 1$ configurations, $\sim 33\ MeV^2$, $\sim 30\ MeV^2$ and $\sim 0.02\ MeV$ respectively for $S = 2$ configurations. With the class variances and centroid shifts, $I(E)$, $I_\ell(E)$ and $\sigma_J(E)$ are calculated at various energies using the procedures given in Sect. 4.2.6 and the results are compared with data in Figs. 4.3, 4.4. From Fig. 4.3, it is seen that the agreement between data and calculations is good upto $\sim 16\, MeV$ and the departures appear to be significant beyond say $22\ MeV$. The calculated spin-cutoff factors are in excellent agreement with Katsanos et al data (Table C.2). The calculated state densities are fitted to the Lang LeCouteur (LLC) and back shifted Fermi gas forms (C.1, C.3, C.4) and the parameters (a, Δ) obtained from best fit are given in Table 4.10.

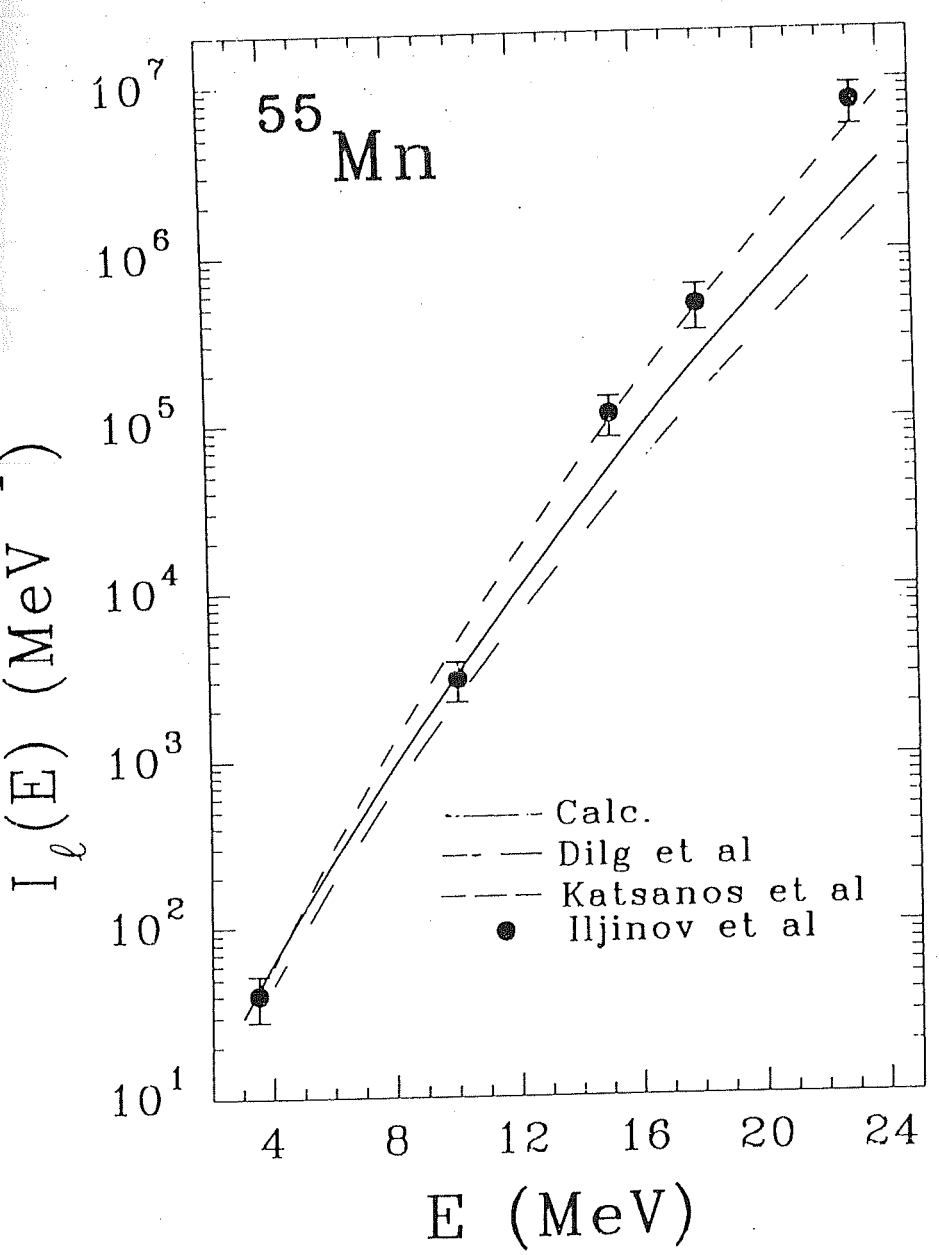


Fig. 4.3 Total level density $I_\ell(E)$ vs E for ^{55}Mn. References to data (Dilg et al, Katsanos et al, Iljinov et al) and the actual data values are given in Appendix C.

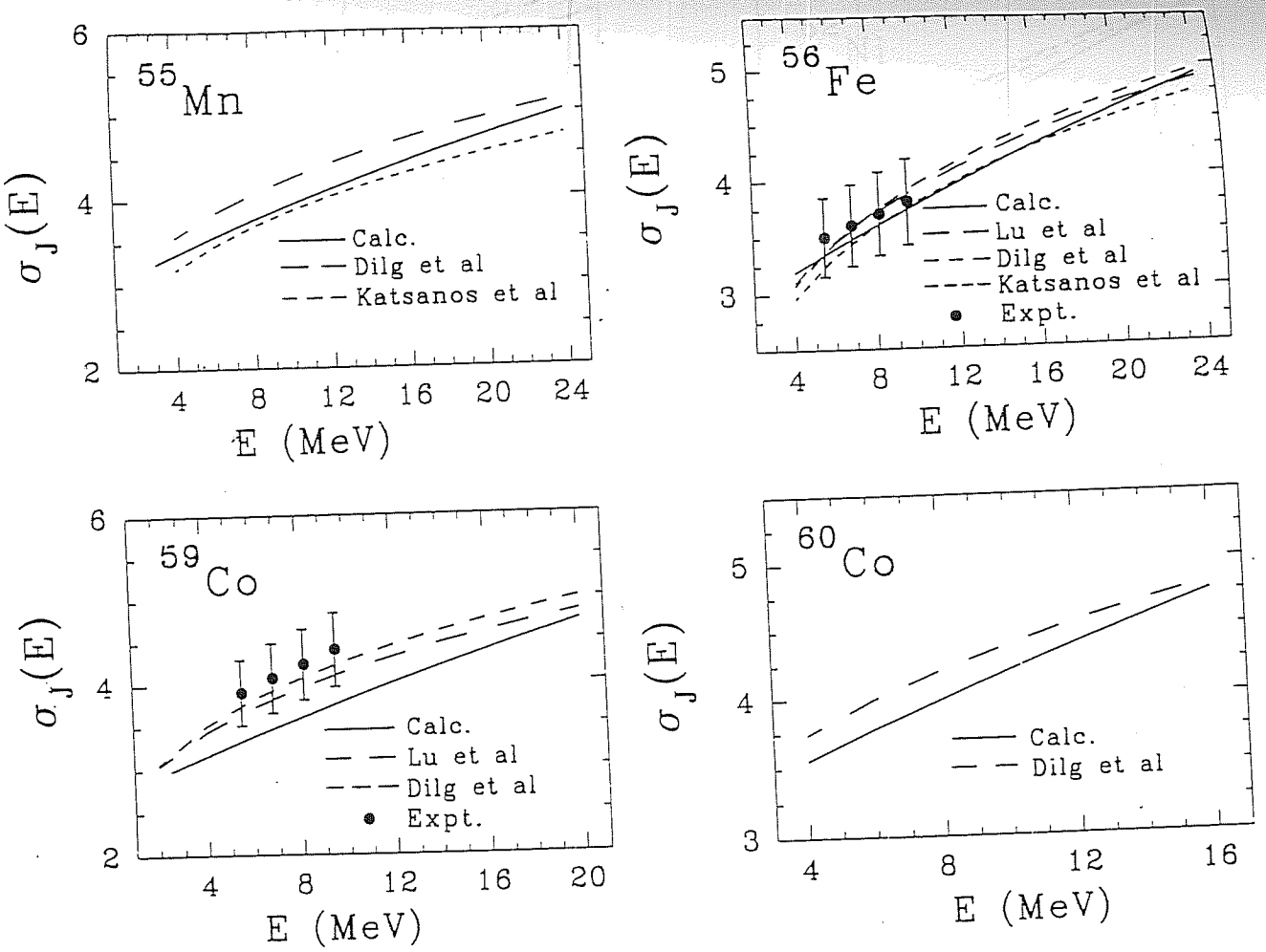


Fig. 4.4 Square root of spin-cutoff factor $\sigma_J(E)$ vs E for ^{55}Mn, ^{56}Fe, ^{59}Co, ^{60}Co, ^{60}Ni, ^{62}Ni, ^{63}Cu, ^{65}Cu. References to experimental data, data due to Dilg et al, Katsanos et al and Lu et al and actual data values are given in Appendix C.

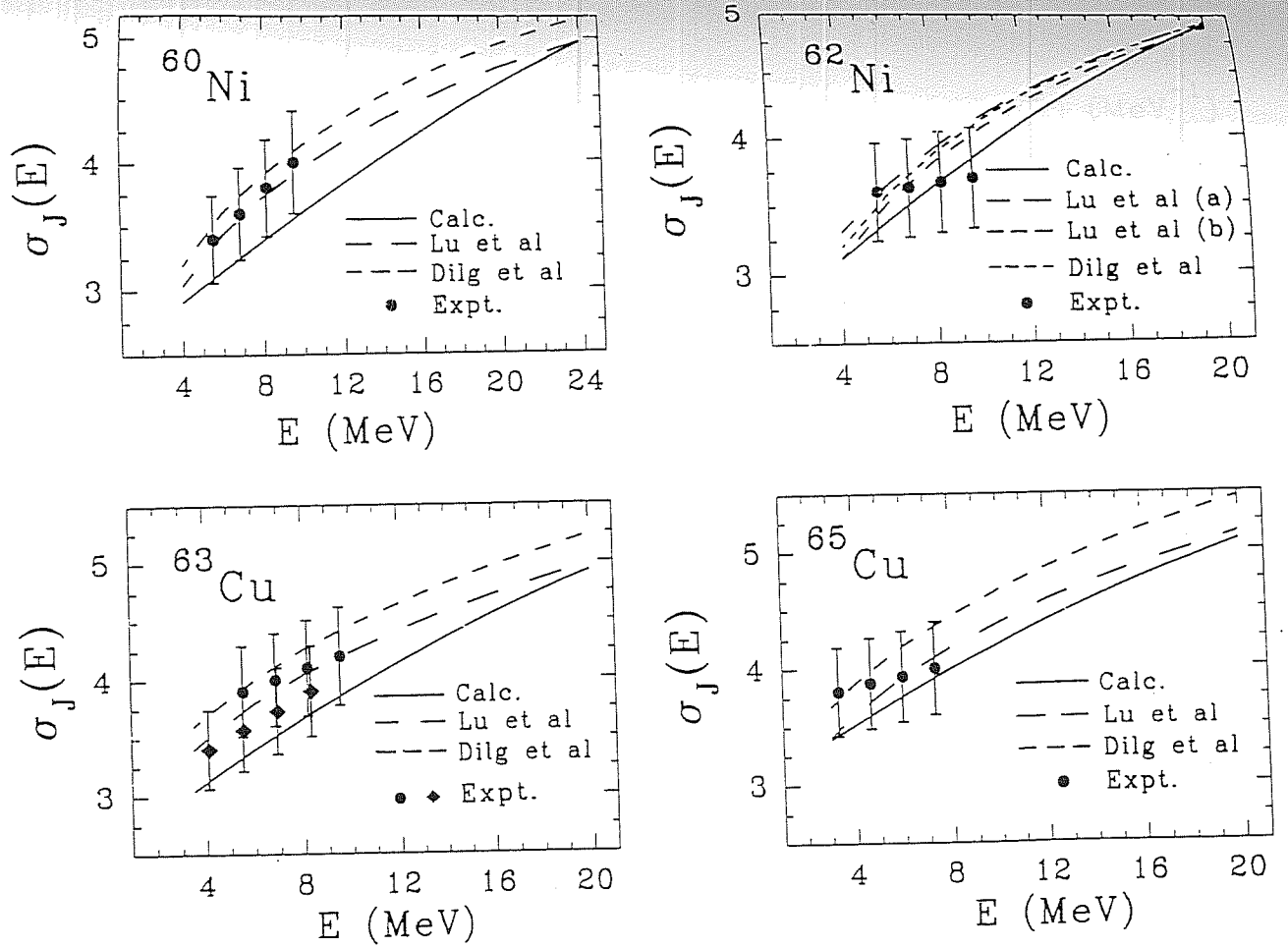

60Ni
62Ni
63Cu
65Cu
σJ(E)
E (MeV)
Calc.
Lu et al
Lu et al (a)
Lu et al (b)
Dilg et al
Expt.

Fig. 4.4 (cont'd)

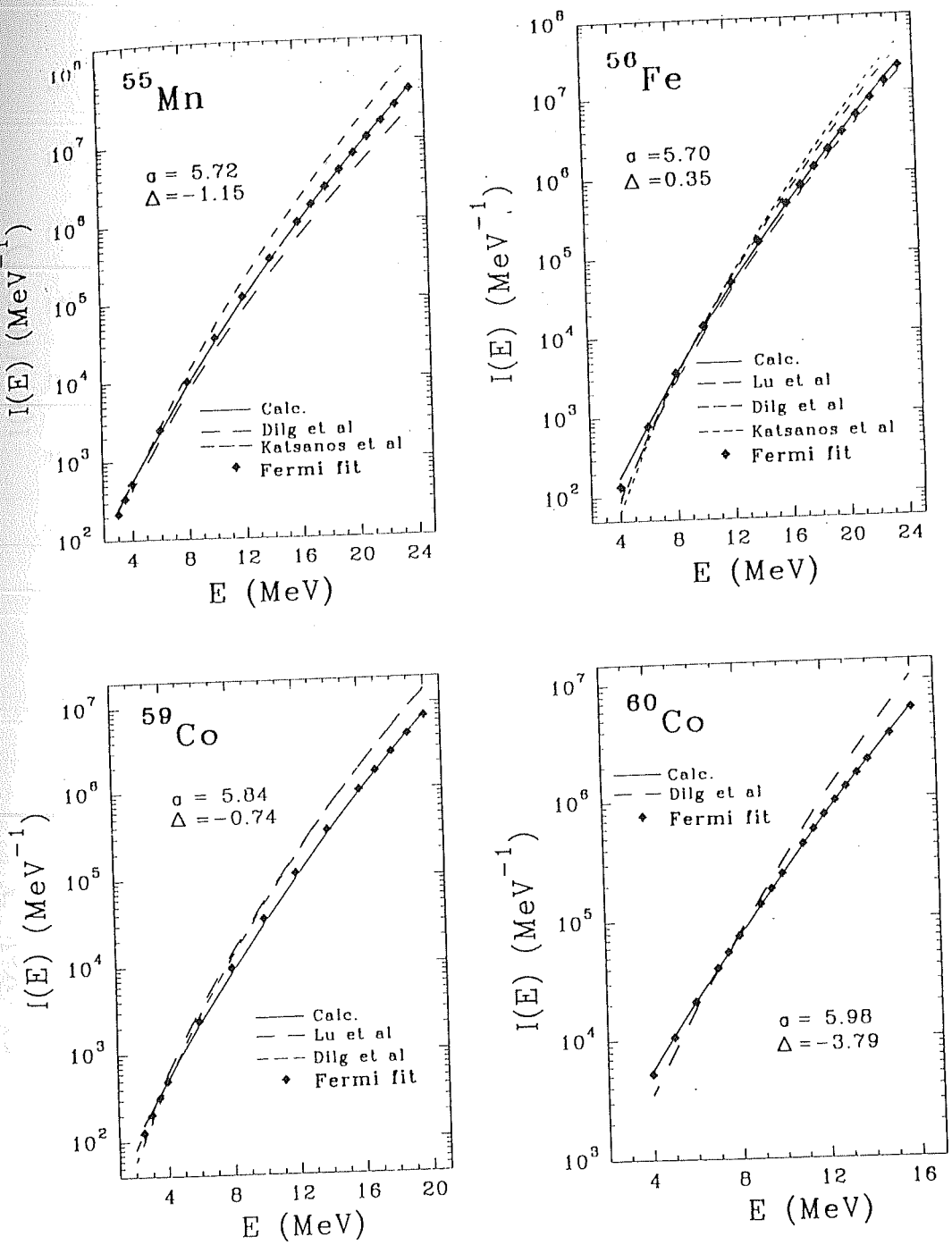


Fig. 4.5 State density $I(E)$ vs E. Filled diamonds in the figure correspond to Fermi gas fit to the calculated state density; as described in the text, the Lang LeCouteur Fermi gas formula is used in the fits. The calculated $I(E)$ is also compared with Dilg et al, Katsanos et al and Lu et al data. The Dilg et al, Katsanos et al and Lu et al data are tabulated in Appendix C.

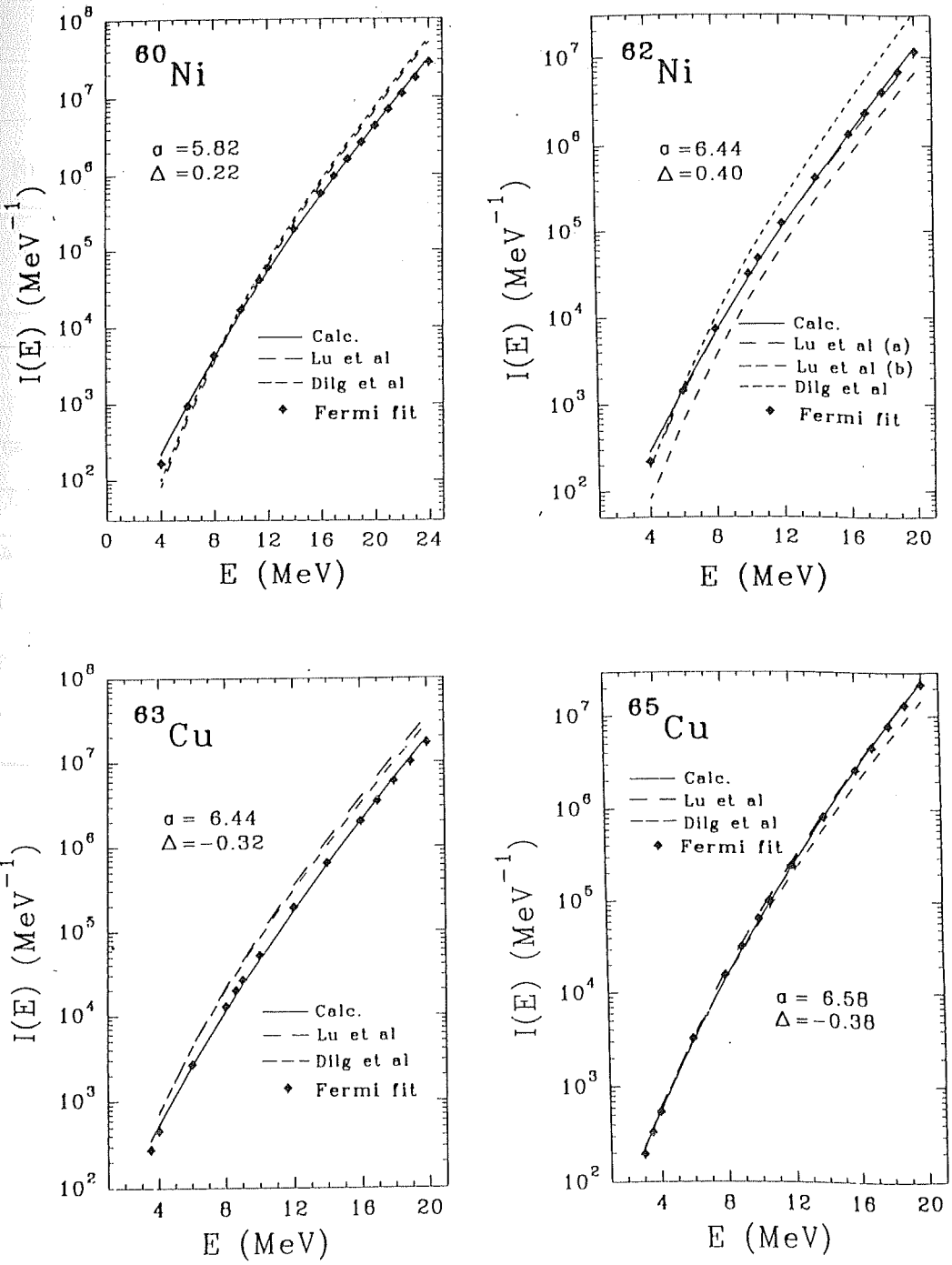

60Ni
a =5.82
Δ =0.22
Calc.
Lu et al
Dilg et al
Fermi fit
I(E) (MeV⁻¹)
E (MeV)
62Ni
a =6.44
Δ =0.40
Calc.
Lu et al (a)
Lu et al (b)
Dilg et al
Fermi fit
I(E) (MeV⁻¹)
E (MeV)
63Cu
a = 6.44
Δ =−0.32
Calc.
Lu et al
Dilg et al
Fermi fit
I(E) (MeV⁻¹)
E (MeV)
65Cu
Calc.
Lu et al
Dilg et al
Fermi fit
a = 6.58
Δ =−0.38
I(E) (MeV⁻¹)
E (MeV)

Fig. 4.5 (cont'd)

Table 4.10 Fermi gas parameters

Nucleus	Dilg et al		Katsanos et al		Present Calculation	
	a (MeV^{-1})	Δ (MeV)	a (MeV^{-1})	Δ (MeV)	a (MeV^{-1})	Δ (MeV)
^{55}Mn	5.45	-1.20	6.30	-0.50	5.52^{*}	-1.15^{*}
					$5.74^{@}$	$-0.85^{@}$

* for Lang LeCouteur Fermi gas form @ for back shifted Fermi gas form

As can be seen from Fig. 4.5 the calculated densities are well represented by the LLC Fermi gas form. Only the LLC Fermi gas fit is shown in the figure as we are comparing our results with Dilg et al and Katsanos et al (a, Δ) values and these authors deduced (a, Δ) values using LLC form. As can be seen from Table 4.10 the deduced (a, Δ) values are compatible more with Dilg et al values than the Katsanos et al values.

4.3.2 Nucleus ^{56}Fe

The low-energy data which is used in fixing the reference energy are given in Table 4.11. Also shown in the table are E_{ref}, J^{π}_{ref} and N_{ref} values and with these values, the GS energy is calculated with a trial value of G using the method outlined in Sect. 4.2.2. The value of G is obtained such that it fits reasonably well with (there is no resonance data for ^{56}Fe) the Dilg et al ($1385\ MeV^{-1}$), Lu et al ($1064\ MeV^{-1}$) and Katsanos et al ($1476\ MeV^{-1}$) data for $I_{\ell}(E)$ at 10 MeV excitation. At this energy the calculated $I_{\ell}(E) = 1304\,MeV^{-1}$ for $G = 0.36\,MeV$. For example, $\sigma^2_{\mathbf{V}}$, $\sigma^2_{\mathbf{V};J^2_z}$ and $\epsilon_{\mathbf{V};J^2_z}$ calculated with $G = 0.36\,MeV$ are 18.7 MeV^2, 16.9 MeV^2 and 0.006 MeV respectively for $S = 0$ configuration, $\sim$ 25 MeV^2, $\sim$ 23 MeV^2 and $\sim$ 0.01 MeV respectively for $S = 1$ configurations and $\sim 34\ MeV^2$, $\sim 32\ MeV^2$

Table 4.11 Low energy data for reference energy calculation

E (MeV)	J^π	Ref	E (MeV)	J^π	Ref
0.0	0^+	[Le-78]	3.607	0^+	[Le-78]
0.847	2^+	[Le-78]	3.748	2^+	[Nu-77]
2.085	4^+	[Le-78]	3.756	6^+	[Le-78]
2.658	2^+	[Le-78]	3.832	2^+	[Le-78]
2.942	0^+	[Le-78]	3.857	3^+	[Le-78]
2.960	2^+	[Le-78]	4.049	3^+	[Nu-77]
3.120	1^+	[Le-78]	4.100	3^+	[Nu-77]
3.123	4^+	[Le-78]	4.120	4^+	[Le-78]
3.372	2^+	[Le-78]	4.293	4^+	[Nu-77]
3.388	6^+	[Le-78]	4.302	0^+	[Nu-77]
3.445	3^+	[Le-78]	4.395	3^+	[Le-78]
3.449	1^+	[Le-78]	4.401	2^+	[Nu-77]
3.602	2^+	[Le-78]			

$E_{ref} = 4.401\ MeV$ $\qquad J^\pi_{ref} = 2^+$

$N_{ref} = 147$

Table 4.12 Fermi gas parameters

Nucleus	Lu et al		Dilg et al		Katsanos et al		Present Calculation	
	a (MeV^{-1})	Δ (MeV)	a (MeV^{-1})	Δ (MeV)	a (MeV^{-1})	Δ (MeV)	a (MeV^{-1})	Δ (MeV)
^{56}Fe	5.70	0.70	6.15	1.10	6.40	1.50	5.7* 5.72@	0.35* 0.64@

* for Lang LeCouteur Fermi gas form @ for back shifted Fermi gas form

and $\sim 0.02\ MeV$ respectively for $S = 2$ configurations. With these variances and centroid shifts $I(E)$, $I_\ell(E)$ and $\sigma_J(E)$ are calculated upto 24 MeV, using the procedure outlined in Sect. 4.2.6 and the results are compared with data in Figs. 4.6, 4.4. Fig. 4.6 shows that the calculations are in excellent agreement with data right upto 24 MeV. The low-lying data (upto 6 MeV) from direct

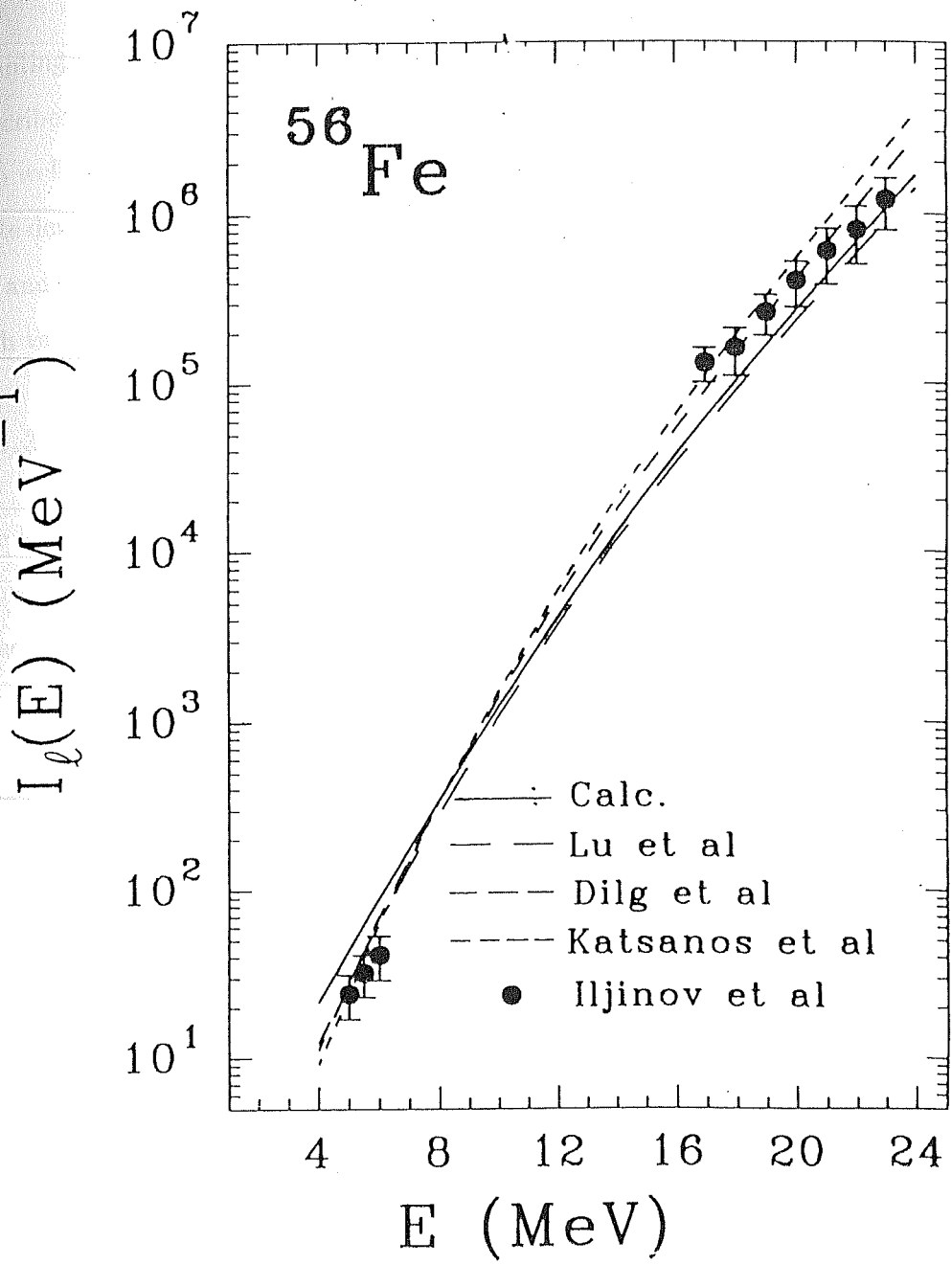


Fig. 4.6 Total level density $I_\ell(E)$ vs E for ^{56}Fe. References to data (Lu et al, Dilg et al, Katsanos et al, Iljinov et al) and the actual data values are given in Appendix C.

counting and high lying data from Ericson fluctuation (17-23 MeV) are well described. Similarly, as can be seen from Fig. 4.4 the spin-cutoff factors are also well described; $\sigma_J(E) \sim 3.2 - 4.5$ for $E = 4 - 20\,MeV$. The calculated state densities are well represented by the LLC Fermi gas form as shown in Fig. 4.5 and the deduced (a, Δ) values, given in Table 4.12, are in close agreement with values due to Lu et al who used the charge particle data.

4.3.3 Nucleus ^{59}Co

The low-energy data which is used in fixing the reference energy are given in Table 4.13. Also shown in the table are E_{ref}, J^{π}_{ref} and N_{ref} values and with these values,

Table 4.13 Low energy data for reference energy calculation

E (MeV)	J^{π}	Ref
0.0	$7/2^-$	[Nu-83]
1.099	$3/2^-$	[Nu-83]
1.190	$9/2^-$	[Nu-83]
1.292	$3/2^-$	[Nu-83]
1.434	$1/2^-$	[Nu-83]
1.460	$11/2^-$	[Nu-83]
1.482	$5/2^-$	[Nu-83]
1.745	$7/2^-$	[Nu-83]
2.062	$7/2^-$	[Le-78]
2.088	$5/2^-$	[Nu-83]
$E_{ref} = 2.088\ MeV$		$J^{\pi}_{ref} = 5/2^-$
	$N_{ref} = 68$	

the GS energy is calculated, with a trial value of G, using the method outlined in Sect. 4.2.2. The value of G is varied such that the total level density $I_\ell(E)$ at $E = 10\ MeV$ becomes close to the values obtained from the experimental

(proton resonance) data compiled by Iljinov et al (Table C.7) which is $3000 \pm 900\, MeV^{-1}$. With $G = 0.339\, MeV$ the calculated value of $I_\ell(E)$ at $10\ MeV$ is $3045\ MeV^{-1}$. The state and spin-cutoff variances ($\sigma^2_{\mathbf{V}}$, $\sigma^2_{\mathbf{V}:J_z^2}$) and the centroid shifts $\epsilon_{\mathbf{V}:J_z^2}$ are calculated with $G = 0.339\, MeV$. With these variances and centroid shifts $I(E)$, $I_\ell(E)$ and $\sigma_J(E)$ are calculated at various energies using the procedures given in Sect. 4.2.6 and the results are compared with data in Figs. 4.7, 4.4. It is seen from Fig. 4.7 that the calculations extrapolate the densities from 10 MeV well upto 20 MeV. The calculated spin-cutoff factors (Fig. 4.4) are somewhat smaller (say by 20%) than the experimental values. The $I(E)$ is well represented by LLC Fermi gas form with $(a, \Delta) = (5.84\, MeV^{-1}, -0.74\, MeV)$ as shown in Fig. 4.5 and the deduced a values, as can be seen from Table 4.14 are somewhat smaller than the Lu et al and Dilg et al values.

Table 4.14 Fermi gas parameters

Nucleus	Lu et al		Dilg et al		Present Calculation	
	a (MeV^{-1})	Δ (MeV)	a (MeV^{-1})	Δ (MeV)	a (MeV^{-1})	Δ (MeV)
^{59}Co	6.20	-0.80	6.31	-0.47	5.84^* $5.77^@$	-0.74^* $-0.74^@$

* for Lang LeCouteur Fermi gas form @ for back shifted Fermi gas form

4.3.4 Nucleus ^{60}Co

Complete low-energy data for ^{60}Co nucleus is available only upto $0.79\, MeV$ [Nu-86b]. As this energy is extremely low, it is not good to consider this energy to be the reference energy. Therefore in this case a different prescription (as

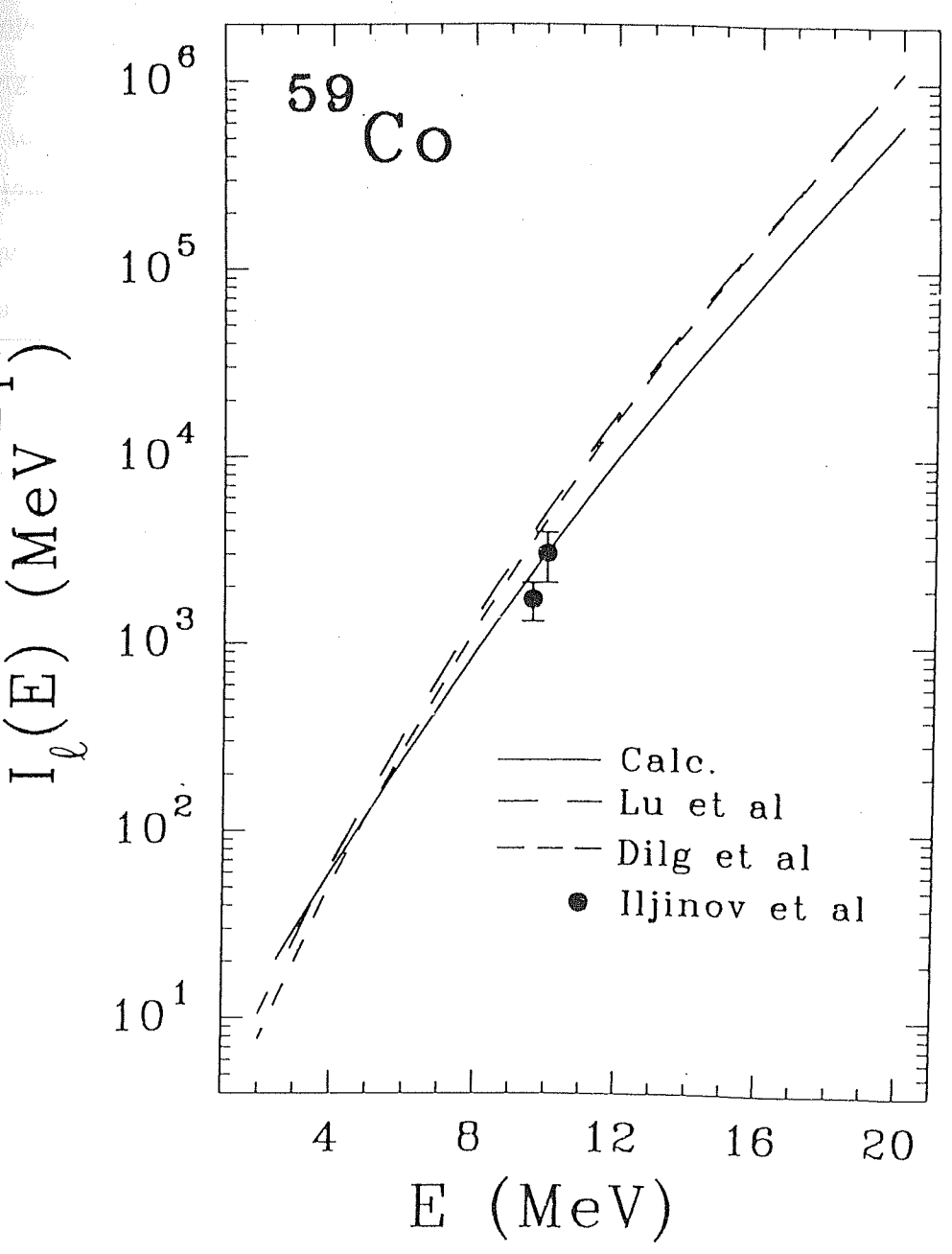


Fig. 4.7 Total level density $I_\ell(E)$ vs E for ^{59}Co. References to data (Lu et al, Dilg et al, Iljinov et al) and the actual data values are given in Appendix C.

compared to the method outlined in Sect. 4.2.2 is used) for fixing the reference energy. Using the Dilg et al data for level densities (Table C.11), at 4 MeV the total number of positive parity states $N^{+}(E_{ref} = 4\,MeV)$ is determined to be 1796. Starting with a value of G, the reference energy ($\overline{E}_{ref}$) is determined using $N^{+}(E_{ref})$ value. The value of G is then varied to reproduce the $I_{\ell}(E)$ value of Dilg et al at 8 MeV excitation ($I_{\ell}(E = 8\,MeV) = 7337\,MeV^{-1}$) and also the neutron resonance density at the resonance energy 7.491 MeV ($I_{\ell}(E = 7.491\,MeV) = 4389 \pm 627\,MeV^{-1}$). To get agreements it is found that a rather low value (compared to $20/A$ MeV) of G has to be used. As this is not proper (G should be normally $25/A$ MeV), the value of G is fixed to be $G = 0.31\,MeV$. Then with the above described method of fixing the reference energy, the $I_{\ell}(E)$ at $E = 8\,MeV$, $7.491\,MeV$ are found to be smaller by a factor 2 and at higher energies by a factor of $3 - 4$ (see the inset to Fig. 4.8). In order to produce satisfactory agreements, the calculated ground state has to be moved up by 1 MeV. The results obtained for $I_{\ell}(E)$, $I(E)$ and $\sigma_{J}(E)$ with $G = 0.31\,MeV$ by the above mentioned correction for GS location, are shown in Figs. 4.8, 4.4.

The source of error in locating properly the GS could be that there is a back shifting as we are using SDI for an odd-odd nucleus. Alternatively this may be due to the fact that level densities at low-energies are quite high for odd-odd nuclei compared to its even-even or odd-A neighbor and with SDI it may not be possible to reproduce these densities. It is worth pointing out that ^{60}Co is the only odd-odd nucleus that is so far analyzed using SAT-LSS [3]. The problems that can be encountered when dealing with odd-odd nuclei should

[3] Behkami and Huizenga [Be-73], in their analysis of fp - shell level density and spin-cutoff factor data using Fermi gas (NIP) theory with pairing, also considered the same set of nuclei listed in Table 4.1 but 'without' ^{60}Co nucleus.

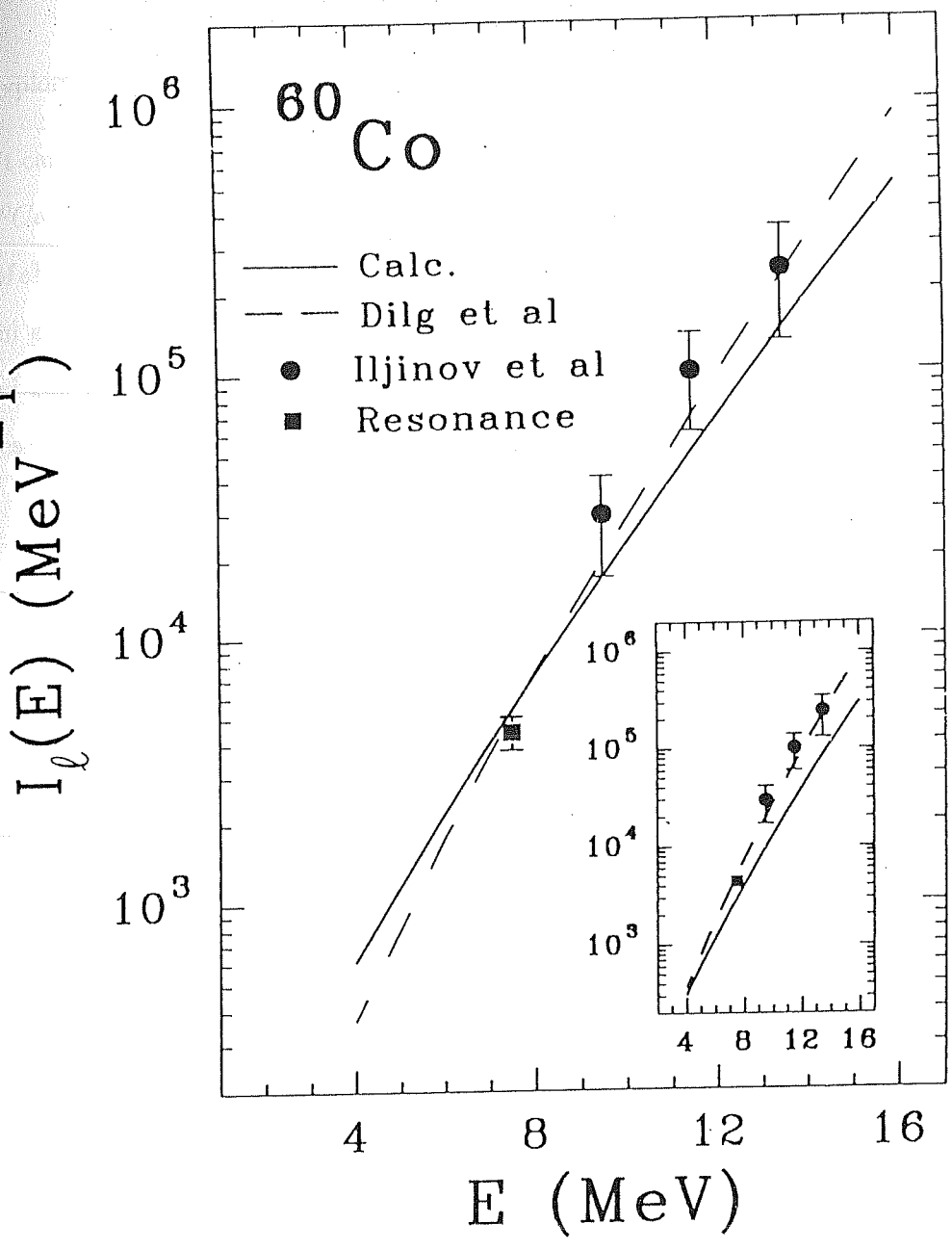


Fig. 4.8 Total level density $I_\ell(E)$ vs E for ^{60}Co. References to data (Dilg et al, Iljinov et al, Resonance) and the actual data values are given in Appendix C. The results shown in the inset figure correspond to the calculation where the ground state is not moved (text gives details).

be explored further.

It can be seen from Figs. 4.8, 4.4, the level densities and spin-cutoff factors for ^{60}Co are well described by the IP theory (level densities are calculated upto 16 MeV). The calculated state densities ($I(E)$) are well represented by the Fermi gas forms as shown in Fig. 4.5. The deduced (a, Δ) values with LLC Fermi gas form are not compatible, as shown in Table 4.15, with Dilg et al values obtained by fitting the low-energy data and the neutron resonance data.

Table 4.15 Fermi gas parameters

Nucleus	Dilg et al		Present Calculation	
	a (MeV^{-1})	Δ (MeV)	a (MeV^{-1})	Δ (MeV)
^{60}Co	6.86	−2.16	5.98*	−3.79*
			5.99@	−3.53@

* for Lang LeCouteur Fermi gas form @ for back shifted Fermi gas form

4.3.5 Nucleus ^{60}Ni

For ^{60}Ni nucleus there is complete low-energy data [Le-78] upto 4.007 MeV, however there are several levels between $3.32 - 4.01$ MeV for which the spins and parities are not assigned as can be seen from Table 4.16. In principle one can use, 3.318 MeV level as reference energy as all levels below are identified with J^{π} values assigned. As we are dealing with an even-even nucleus, for these the level densities at low-energies being low, it is always better to use as high a reference energy as possible. Therefore all the levels upto 4.007 MeV shown in Table 4.16 are used but with degeneracies assigned to levels with no J^{π} assignments by using the so called information theory method [Sm-87].

According to the information theory the total number of states $I^{\pi}(E)dE$ at energy E is given by,

$$I^{\overline{\pi}}(E)dE = \frac{\sum_{J\,(\text{known } J'\text{s or all } J'\text{s}),\,\pi=\overline{\pi}} (2J+1)P_{J\pi}}{\sum_{J\,(\text{known } J'\text{s or all } J'\text{s}),\,\pi} P_{J\pi}}$$

$$P_{J\pi} = C_J P_{\pi}$$

$$C_J = \frac{(2J+1)}{\sqrt{8\pi}\sigma_J^3} exp\, -\frac{(J+1/2)^2}{2\sigma_J^2}$$

$$P_{\pi} = 1 \quad \text{desired parity}$$

$$P_{\pi} = \tfrac{1}{2} \quad \text{for unknown parity}$$

$$P_{\pi} = 0 \quad \text{for opposite parity .} \qquad (4.3)$$

In applying (4.3), it should be kept in mind that J-summation is over the known J's if some J assignmments are known and otherwise it is over all J's (i.e. $J = 0$ to ∞). Eq. (4.3) is applied with $\sigma_J = 3$ which is a typical value for ^{60}Ni at low-energies as can be seen from Fig. 4.4. The final reference energy is given in Table 4.16 and with this reference energy the GS is calculated using a trial value for G and the method outlined in Sect. 4.2.2. The neutron resonance data (Table C.13) is found to give a value of $G < 0.3$ (much lower than $20/A\ MeV$) and therefore a search for a value of G (not much lower than $20/A\ MeV$) is made which gives overall good description of $I_\ell(E)$ data from 4 $-$ 24 MeV and the value found is $G = 0.31\,MeV$. The calculated $I_\ell(E)$, $I(E)$ and $\sigma_J(E)$ are compared with data in Figs. 4.9, 4.4. The ^{60}Ni nucleus is the only nucleus in our set that has level density data from all the four sources mentioned in Sect. 4.2.2. As can be seen from Fig. 4.9, the calculations

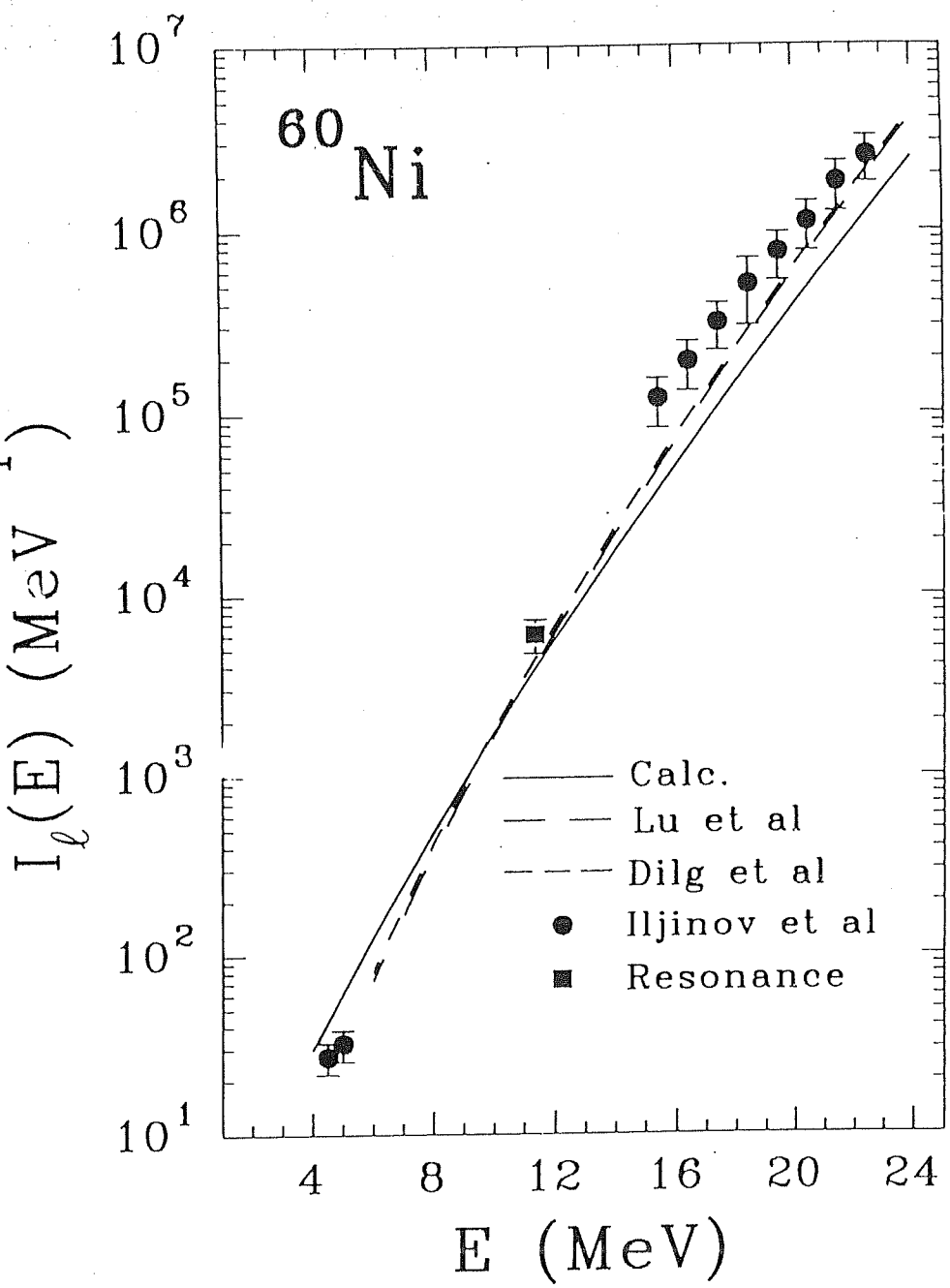


Fig. 4.9 Total level density $I_\ell(E)$ vs E for ^{60}Ni. References to data (Lu et al, Dilg et al, Iljinov et al, Resonance) and the actual data values are given in Appendix C.

with $G = 0.31\ MeV$ describe the data in the $4 - 24\ MeV$ energy range. The deviations at energies $> 16\ MeV$ are not more than a factor 2. The calculated spin-cutoff factor values (Fig. 4.4) are somewhat smaller than data values. The results for ^{60}Ni confirm that the IP theory describes the data in a wide energy range.

Table 4.16 Low energy data for reference energy calculation

E (MeV)	J	π	$I^+(E)dE$	Ref
0.0	0	+	1	[Le-78]
1.333	2	+	5	[Le-78]
2.159	2	+	5	[Le-78]
2.285	0	+	1	[Le-78]
2.506	4	+	9	[Le-78]
2.626	3	+	7	[Le-78]
3.120	4	+	9	[Le-78]
3.124	2	+	5	[Le-78]
3.186	3	+	7	[Le-78]
3.194	1	+	3	[Le-78]
3.269	2	+	5	[Le-78]
3.319	0	+	1	[Le-78]
3.381	unknown	unknown	3.74	[Le-78]
3.394	2	+	5	[Le-78]
3.533	0	+	1	[Le-78]
3.588	0	+	1	[Le-78]
3.620	unknown	unknown	3.74	[Le-78]
3.623	unknown	unknown	3.74	[Le-78]
3.671	4	+	9	[Le-78]
3.700	unknown	unknown	3.74	[Le-78]
3.731	unknown	unknown	3.74	[Le-78]
3.736	2	+	5	[Le-78]
3.738	unknown	unknown	3.74	[Le-78]
3.741	unknown	unknown	3.74	[Le-78]
3.871	unknown	unknown	3.74	[Le-78]
3.875	2	+	5	[Le-78]
3.887	unknown	unknown	3.74	[Le-78]
3.895	unknown	unknown	3.74	[Le-78]
3.925	3	+	7	[Le-78]
4.007	2	+	5	[Le-78]

$E_{ref} = 4.007\ MeV$ $\qquad$ $J^{\pi}_{ref} = 2^+$

$N_{ref} = 133.5$

Once again the state density $I(E)$ is well represented by LLC Fermi gas forms as can be seen from Fig. 4.5. The deduced $(a;\ \Delta)$ values are somewhat smaller than Lu et al (from charge particle spectra) and Dilg et al values, as shown in Table 4.17 but yet the calculated $I(E)$ is quite close to Lu et al and Dilg et al curves (Fig. 4.5).

Table 4.17 Fermi gas parameters

Nucleus	Lu et al		Dilg et al		Present Calculation	
	a (MeV^{-1})	Δ (MeV)	a (MeV^{-1})	Δ (MeV)	a (MeV^{-1})	Δ (MeV)
^{60}Ni	6.40	1.30	6.42	1.14	5.82* 5.84@	0.22* 0.51@

* for Lang LeCouteur Fermi gas form @ for back shifted Fermi gas form

4.3.6 Nucleus ^{63}Cu

The low-energy data for fixing the reference energy is taken from [Nu-91],

Table 4.18 Low lying data for reference energy calculation

E (MeV)	J^π	Ref
0.0	$3/2^-$	[Nu-91]
0.670	$1/2^-$	[Nu-91]
0.962	$5/2^-$	[Nu-91]
1.327	$7/2^-$	[Nu-91]
1.412	$5/2^-$	[Nu-91]
1.547	$3/2^-$	[Nu-91]
1.861	$7/2^-$	[Nu-91]
2.011	$3/2^-$	[Nu-91]
2.081	$5/2^-$	[Nu-91]
2.093	$7/2^-$	[Nu-91]
2.208	$9/2^-$	[Nu-91]
2.337	$5/2^-$	[Nu-91]
$E_{ref} = 2.337\ MeV$	$N_{ref} = 74$	$J^\pi_{ref} = 5/2^-$

With the $(E_{ref}, J^{\pi}_{ref}, N_{ref})$ given in the table and a trial value of G the GS energy is determined. Then G is varied to get best possible description of data. An attempt to fix the value of G using the proton resonance data $I_\ell(E) = 2100 \pm 600\, MeV^{-1}$ at $E = 8.6 MeV$ gives a value $G < 0.27\, MeV$ (note that $25/A = 0.397$ for ^{63}Cu) which is not in the acceptable range (this value of G violates the conditions laid down in Sect. 4.2.6 for the goodness of a calculation) and also with $G < 0.27\, MeV$ the $I_\ell(E)$ data above 10 MeV is not well described. With $G = 0.317$ MeV a reasonable description of data is obtained and the corresponding results are shown in Fig. 4.10 (labelled ^{63}Cu (a)). However if the resonance data has to be well represented and also that the description of $I_\ell(E)$ data beyond 10 MeV has to be good then one has to change the $\overline{\Delta}_{fp-g_{9/2}}$ spacing. By decreasing $\overline{\Delta}_{fp-g_{9/2}}$ spacing from 6.53 MeV to 4.53 MeV (given in Table 4.2) but still using $G = 0.317\, MeV$, one gets excellent agreement with data as shown in Fig 4.10 (labelled ^{63}Cu (b)). The decomposition of density into $S = 0$ and $S = 2$ parts clearly shows (Table 4.8) that the $S = 2$ densities dominate over the $S = 0$ densities in this case and therefore ^{63}Cu (b) calculations cannot be considered to be proper calculations. It is possible that most of the $S = 2$ intensity may be coming from excitation into $g_{9/2}$ orbit and then the calculations can be considered acceptable. Altenatively from the ^{63}Cu (b) results one can argue that the decrease in $\overline{\Delta}_{fp-g_{9/2}}$ may be a renormalization effect as we are restricting to 8-orbits. Thus the ^{63}Cu example shows the deficiencies of the choices made regarding s.p. orbits, their s values and $\overline{\Delta}$ spacings for $A > 60$ nuclei. One can resolve these puzzles by performing 10-orbit calculations (by including $2d_{5/2}$ and $1g_{7/2}$ orbits).

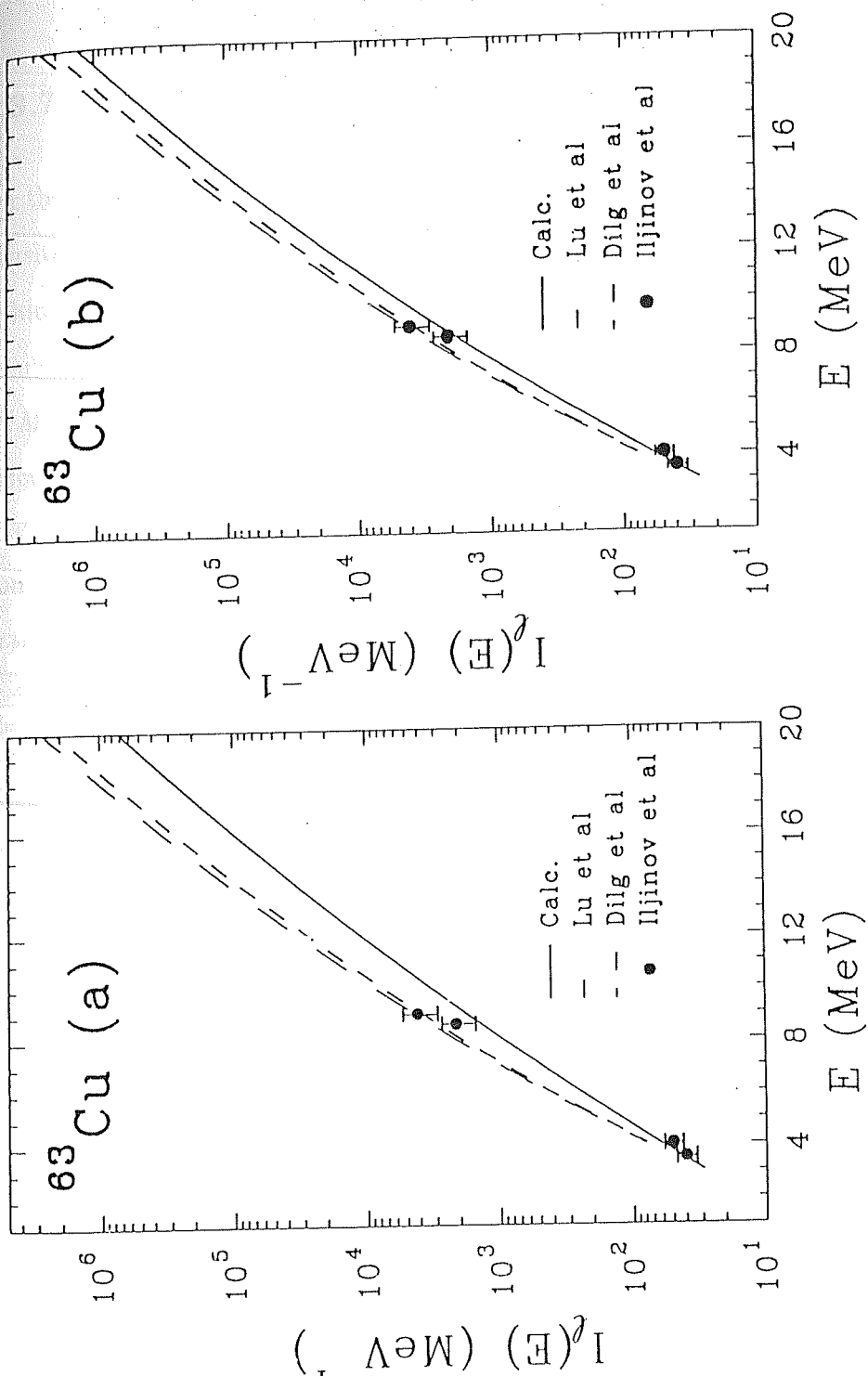


Fig. 4.10 Total level density $I_\ell(E)$ vs E for ^{63}Cu. References to data (Lu et al, Dilg et al, Iljinov et al) and the *actual data values are given in Appendix C.* The ^{63}Cu (a) and ^{63}Cu (b) calculations are described in the text.

4.3.7 Summary of 8-orbit calculations

For the first time, for a series of fp-shell nuclei, systematic calculations for level densities, state densities and spin-cutoff factors are performed using SAT-LSS (which is a IP theory [4]) and compared with data in Sects. 4.3.1 - 4.3.6. It is seen from Sect. 4.3, the description of the data is excellent for the three nuclei $\{^{55}Mn,\ ^{56}Fe,\ ^{59}Co\}$ and satisfactory for the two nuclei $\{^{60}Co,\ ^{60}Ni\}$. The calculations determine the SDI strength 'G' to be $G \sim 20/A\ MeV$. It is noted that the resulting spreading variances in $S = 0$ case are in general smaller compared to the variances produced by 'renormalized' effective fp-shell interactions. The ^{63}Cu example demonstrates that the 8-orbit calculations have

[4]Starting from Bethe's $exp\sqrt{aE}$ Fermi gas form for level densities, besides deriving various modifications of the Bethe form mainly via various parametrization of the level density parameter 'a' and back shifting parameter 'Δ' [Ig-83, Ka-80; Appendix C], inclusion of pairing via a temperature dependent gap equation [Hu-72, Be-73; Appendix C] and collective effects via a convolution which gives enhancement of level densities by collective enhancement factor given by the partition function of the collective hamiltonians [Ig-83, Ar-91, Ko-93b], there are various attempts to develop a interacting particle level density theory. They are: (i) via Casimir operators of groups as done in the case of Wigner SU(4) by Bloch [Bl-54], Elliott $SU(3)$ by Kanestrom [Ka-66a, Ha-83] and single j - shell pairing [Pa-93]; (ii) employing the CLT results of SAT as given in Chapter 2, a preliminary attempt in this direction is due to Ayik and Ginnochio [Ay-74b] and a more elaborate study is due to Grimes and collabortators [Gr-83] (these studies suffer from the problems mentioned in the beginning of Sect. 3.1). In addition also there is [Ha-82b] the phenomenological version of the theory given in Sect. 3.1; (iii) development of a theory analogous to what was described in Sect. 3.1 but employing a GOE to represent interactions (i.e. $V(2)$) and this work is due to Sato and Yashida [Sa-87a]. It should be noted that GOE is not a model for densities and it is good only for fluctuations. However extension of this work by Pluhar and Weidenmuller [Pl-88], where ensembles similar to what was described in Appendix A are considered but once again by representing the block matrices by GOE, is of importance. The results of this work combined with the model in Appendix A might yield a usable theory for dealing with the important problem of $S = 0 \oplus 2$ mixing (in fact for $S = 0 \oplus 2 \oplus 4 \oplus ....$ mixing) in SAT-LSS; (iv) the so called static path approximation (SPA) due to Bertsch and others [La-88, Al-93] which makes use of the Hubbard-Stratonovich transformation and ideally suited for P + Q.Q interaction. Though this approach is promising, so far no data analysis is carrried out using this method; (v) the Monte Carlo (path integral) method, which is also based on the Hubbard-Stratonovich linearization, for the shell model as being developed by Koonin and collaborators [Jo-92, Ko-94d]. The studies using this method are so far restricted to $0\hbar\omega$ spaces.

problems when applied to $A > 60$ nuclei. It appears that the spectroscopic space has to be enlarged by opening up $(2d_{5/2}, 1g_{7/2})$ orbits. Because of this, in the present section $\{^{62}Ni, ^{65}Cu\}$ nuclei are not analyzed although they are in the selected set given in Table 4.1. The results of the 10-orbit calculations for ^{62}Ni and $^{63,65}Cu$ nuclei are described in the following section.

4.4 Level Density Calculations for fp-shell Nuclei : 10-Orbit Results

Results of ten orbit calculations, with $(2d_{5/2}, 1g_{7/2})$ orbits added to the eight orbits considered in the previous section, for the three nuclei ^{62}Ni, $^{63,65}Cu$ are reported in this chapter. Expansion of the single particle space indeed cures the problems for $A > 60$ nuclei that are highlighted in the previous section with ^{63}Cu example. The ten orbit results are in good agreement with data as can be seen from Sects. 4.4.2 - 4.4.4 ahead. Sect. 4.4.1 gives the choice of s values, single particle energies and centriod separation of unitary orbits and other calculational details.

4.4.1 Choice of s values, single particle energies and centroid separations

Choice of s values

The orbits $(2d_{5/2}, 1g_{7/2})$ are added so that the density at $E > 10\,MeV$ grows and with this, with a reasonable value of G (strength of SDI) and keeping $S = 0$ description to be dominant upto and above E_{ref}, the data is well explained for the three nuclei ^{62}Ni, $^{63,65}Cu$ as can be seen from Sect. 4.4.2 - 4.4.4. The important question that one has to face is that of the s value for the

$2d_{5/2}$, $1g_{7/2}$ orbits. One possible choice is to assign $\bar{s} = 2$ for the three orbits $(1g_{9/2}, 2d_{5/2}, 1g_{7/2})$ with $\bar{s} = 0$ and 1 for (ds) and (fp) orbits respectively as

Table 4.19 Unitary orbits for spreading variance calculations

UOV #	Spherical orbits	s value	symbol
#1	$d_{5/2}$, $s_{1/2}$, $d_{3/2}$	0	Λ_{-1}
#2	$f_{7/2}$, $p_{3/2}$, $f_{5/2}$, $p_{1/2}$	1	Λ_0
#3	$g_{9/2}$	2	Λ_1
#4	$d_{5/2}$, $g_{7/2}$	3	Λ_2

Table 4.20 Class structures (for $+ve$ parity states in ^{62}Ni and $-ve$ parity states in $^{63,65}Cu$). In the last three columns, the numbers in the first row for each nucleus and each class correspond to the ratio $\sigma^2_{\mathrm{V}}/\sigma^2_{\mathrm{V}:J^2_z}$ and the number in the second row give the numbers of UON configurations[†].

S	Class Structure	Class #	^{62}Ni	^{63}Cu	^{65}Cu
0	$(\Lambda_0)^{m_p}(\Lambda_0)^{m_n}$	#1	1.11	1.11	1.12
			63	63	45
2	$(\Lambda_0)^{m_p}(\Lambda_0)^{m_n-2}(\Lambda_1)^{2_n}$	#2	1.07	1.07	1.07
			81	81	63
	$(\Lambda_0)^{m_p}(\Lambda_{-1})^{-1_n}(\Lambda_0)^{m_n}(\Lambda_1)^{1_n}$	#3	1.07	1.07	1.07
			126	126	90
	$(\Lambda_0)^{m_p}(\Lambda_{-1})^{-2_n}(\Lambda_0)^{m_n+2}$	#4	1.07	1.07	1.06
			135	135	81
	$(\Lambda_0)^{m_p-1}(\Lambda_1)^{1_p}(\Lambda_0)^{m_n-1}(\Lambda_1)^{1_n}$	#5	1.07	1.07	1.07
			64	72	54
	$(\Lambda_0)^{m_p-1}(\Lambda_1)^{1_p}(\Lambda_{-1})^{-1_n}(\Lambda_0)^{m_n+1}$	#6	1.07	1.07	1.07
			96	108	72
	$(\Lambda_0)^{m_p-2}(\Lambda_1)^{2_p}(\Lambda_0)^{m_n}$	#7	1.07	1.07	1.07
			49	56	40
	$(\Lambda_{-1})^{-1_p}(\Lambda_0)^{m_p+1}(\Lambda_0)^{m_n-1}(\Lambda_1)^{1_n}$	#8	1.07	1.07	1.08
			144	144	108
	$(\Lambda_{-1})^{-1_p}(\Lambda_0)^{m_p+1}(\Lambda_{-1})^{-1_n}(\Lambda_0)^{m_n+1}$	#9	1.08	1.07	1.08
			216	216	144
	$(\Lambda_{-1})^{-1_p}(\Lambda_0)^{m_p}(\Lambda_1)^{1_p}(\Lambda_0)^{m_n}$	#10	1.07	1.07	1.07
			126	126	90
	$(\Lambda_{-1})^{-2_p}(\Lambda_0)^{m_p+2}(\Lambda_0)^{m_n}$	#11	1.08	1.08	1.08
			189	189	135

Table 4.20 Cont'd

S	Class Structure	Class #	^{62}Ni	^{63}Cu	^{65}Cu
3	$(\Lambda_0)^{m_p}(\Lambda_0)^{m_n-2}(\Lambda_1)^{1_n}(\Lambda_2)^{1_n}$	#12	1.07	1.07	1.07
			81	81	63
	$(\Lambda_0)^{m_p}(\Lambda_{-1})^{m_n-1}(\Lambda_2)^{1_n}$	#13	1.07	1.07	1.07
			126	126	90
	$(\Lambda_0)^{m_p-1}(\Lambda_1)^{1_p}(\Lambda_0)^{m_n-1}(\Lambda_2)^{1_n}$	#14	1.07	1.07	1.07
			64	72	54
	$(\Lambda_0)^{m_p-1}(\Lambda_2)^{1_p}(\Lambda_0)^{m_n-1}(\Lambda_1)^{1_n}$	#15	1.07	1.07	1.07
			64	72	54
	$(\Lambda_0)^{m_p-1}(\Lambda_2)^{1_p}(\Lambda_{-1})^{-1_n}(\Lambda_0)^{m_n+1}$	#16	1.07	1.07	1.07
			96	108	72
	$(\Lambda_0)^{m_p-2}(\Lambda_1)^{1_p}(\Lambda_2)^{1_p}(\Lambda_0)^{m_n}$	#17	1.07	1.07	1.07
			49	56	40
	$(\Lambda_{-1})^{-1_p}(\Lambda_0)^{m_p+1}(\Lambda_0)^{m_n-1}(\Lambda_2)^{1_n}$	#18	1.07	1.07	1.08
			144	144	108
	$(\Lambda_{-1})^{-1_p}(\Lambda_0)^{m_p}(\Lambda_2)^{1_p}(\Lambda_0)^{m_n}$	#19	1.07	1.10	1.07
			126	126	90
4	$(\Lambda_0)^{m_p}(\Lambda_0)^{m_n-2}(\Lambda_2)^{2_n}$	#20	1.07	1.07	1.07
			81	81	63
	$(\Lambda_0)^{m_p-1}(\Lambda_2)^{1_p}(\Lambda_0)^{m_n-1}(\Lambda_2)^{1_n}$	#21	1.07	1.07	1.07
			64	72	54
	$(\Lambda_0)^{m_p-2}(\Lambda_2)^{2_p}(\Lambda_0)^{m_n}$	#22	1.07	1.07	1.07
			49	56	40

† In the table whenever Λ_{-1} is not shown, it implies that Λ_{-1} orbit is full. Similarly Λ_0, Λ_1 and Λ_2 orbits are not shown whenever they are empty.

in the previous section. Let us denote ds, fp and ($1g_{9/2}$, $2d_{5/2}$, $1g_{7/2}$,) orbits as unitary orbits $\overline{\Lambda}_{-1}$, $\overline{\Lambda}_0$, $\overline{\Lambda}_1$ respectively. With this choice, the calculated density is not found to be acceptable as $\bar{S} = 2$ intensity even at E_{ref} and below is nearly 100%. The reason for this is that the $\bar{S} = 2$ class variances become larger by about 20% compared to the corresponding variances without ($2d_{5/2}$, $1g_{7/2}$) orbits. This then leads to the natural choice of $s = 2$ for $1g_{9/2}$ as before and $s = 3$ for ($2d_{5/2}$, $1g_{7/2}$) orbits. This is consistent with the fact that $1g_{9/2}$ orbit is well separated from ($2d_{5/2}$, $1g_{7/2}$) orbits to form the magic number 50. With this choice there are four unitary orbits (UOV) for variance calculations as given in Table 4.19. Then for example, a $S = 2$ class $(\overline{\Lambda}_0)^{-2p}$

$(\overline{\Lambda}_1)^{2p} \rightarrow (\Lambda_0)^{-2p}\,(\Lambda_1)^{2p} \oplus (\Lambda_0)^{-2p}\,(\Lambda_1)^{1p}\,(\Lambda_2)^{1p} \oplus (\Lambda_0)^{-2p}\,(\Lambda_2)^{2p}$ with $S = 2,\ 3$ and 4 respectively. Thus we are led to $S = 4$ calculations in the 10-orbit case. The corresponding classes (one $S = 0$, ten $S = 2$, eight $S = 3$ and three $S = 4$) are given in Table 4.20.

Single particle energies and choice of centroid separations

The s.p. energies for the ds, fp and $1g_{9/2}$ orbits are same as in the 8-orbit calculations. The $1g_{7/2}$ orbit energy is chosen to be 4 MeV above the $1g_{9/2}$ orbit and the $2d_{5/2} - 1g_{7/2}$ separation is chosen to be 0.68 MeV as in ^{116}Sn calculations [Bo-85]. With this choice, the resulting traceless single particle energies and the centroid separations (which are referred to as $\overline{\Delta}^{(1)}$ below), are given in Table 4.21. With the centroid separation $\overline{\Delta}^{(1)}$ given below, it is

Table 4.21 Quantum numbers and energies of s.p. orbits

orbit #	s	n	ℓ	j	ϵ_j (MeV)
#1	0	0	2	5/2	−1.838
#2	0	1	0	1/2	−0.968
#3	0	0	2	3/2	3.242
#4	1	0	3	7/2	−2.664
#5	1	1	1	3/2	−0.644
#6	1	0	3	5/2	3.526
#7	1	1	1	1/2	1.366
#8	2	0	4	9/2	0.000
#9	3	1	2	5/2	0.389
#10	3	0	4	7/2	−0.291

$$\overline{\Delta}^{(1)}_{sd-fp} = 11.03\,MeV \quad \overline{\Delta}^{(1)}_{fp-g_{9/2}} = 6.53\,MeV \quad \overline{\Delta}^{(1)}_{g_{9/2}-\{d_{5/2},g_{7/2}\}} = 4.29\,MeV$$

$$\overline{\Delta}^{(2)}_{sd-fp} = 11.03\,MeV \quad \overline{\Delta}^{(2)}_{fp-g_{9/2}} = 5.78\,MeV \quad \overline{\Delta}^{(2)}_{g_{9/2}-\{d_{5/2},g_{7/2}\}} = 3.29\,MeV$$

found that, for ^{62}Ni and ^{63}Cu the calculated densities are usually small by a factor 2 and therefore the $\overline{\Delta}^{(1)}_{fp-g_{9/2}}$ is decreased by 0.75 MeV and $\overline{\Delta}^{(1)}_{g_{9/2}-\{d_{5/2},g_{7/2}\}}$

by 1 MeV and with this choice (denoted as $\overline{\Delta}^{(2)}$ in Table 4.21), together with reasonable value for G, good agreements with data are obtained and also the $S = 0$ description upto and above E_{ref}; in the case of ^{65}Cu, $\overline{\Delta}^{(1)}$ choice is found to be good. The S-decomposition of the densities is given in Table 4.22.

Table 4.22 S-decomposition of state densities. For a given nucleus and a given energy, the four entries are (in MeV^{-1}) for $I^{\pi}_{\ell;S=0}(E)$, $I^{\pi}_{\ell;S=2}(E)$, $I^{\pi}_{\ell;S=3}(E)$ and $I^{\pi}_{\ell;S=4}(E)$ respectively. The parity $\pi = +$ for ^{62}Ni and $\pi = -$ for $^{63,65}Cu$. The $^{65}Cu(a)$ and $^{65}Cu(b)$ are described in Sect. 4.4.4.

E (MeV)	^{62}Ni	^{63}Cu	$^{65}Cu(a)$	$^{65}Cu(b)$
$E^{\dagger}_{ref}$	13	6	2	6
	5	3	5	2
	1	0	1	0
	0	0	0	0
$E^{\dagger}_{res}$	915	422	611	1259
	982	408	2808	2034
	220	92	915	258
	7	3	43	3
16.0	14263	18962	8444	15021
	33048	50868	69794	56811
	10863	18678	31741	12108
	549	1115	2362	342

† For ^{62}Ni, $E_{ref} = 4.055\,MeV$, $E_{res} = 10.597\,MeV$; For ^{63}Cu, $E_{ref} = 2.337\,MeV$, $E_{res} = 8.6\,MeV$; For ^{65}Cu, $E_{ref} = 2.329\,MeV$, $E_{res} = 10.65\,MeV$

Calculational details

The $\sigma^2_{\mathrm{V}}/\sigma^2_{\mathrm{V};J^2_Z}$ ratio is fixed in the following way. The $S = 0$ and $S = 2$ classes in the 8 and 10-orbit calculations are identical. Therefore for these classes the results given in Table 4.7 for the $\sigma^2_{\mathrm{V}}/\sigma^2_{\mathrm{V};J^2_Z}$ ratio are used. For the

$S = 3$ and $S = 4$ classes, the value for the corresponding $S = 2$ classes that has same number of protons and neutrons in $ds(\Lambda_{-1})$ and $fp(\Lambda_0)$ unitary orbits is taken (for example for $(\Lambda_0^{-2_n})$ $(\Lambda_1^{2_n})$, $(\Lambda_0^{-2_n})$ $(\Lambda_1^{1_n})$ $(\Lambda_2^{1_n})$, $(\Lambda_0^{-2_n})$ $(\Lambda_2^{-2_n})$ which have $S = 2$, 3 and 4 respectively, the $\sigma_V^2/\sigma_{V:J_z^2}^2$ is taken to be that of $(\Lambda_0^{-2_n})$ $(\Lambda_1^{2_n})$ class). The final values for all the classes are given in Table 4.20.

For the calculation of NIP densities, the choice that is made for the UON unitary orbits is given in Table 4.23. The number of unitary configurations defined by UON for each nucleus for each of the 22 classes are given in Table 4.20. All other calculational procedures are same as in Sect. 4.2.

Table 4.23 Unitary orbits for NIP calculations

UON #	Spherical orbits	s
#1	$d_{5/2}, s_{1/2}$	0
#2	$d_{3/2}$	0
#3	$f_{7/2}$	1
#4	$p_{3/2}$, $f_{5/2}$, $p_{1/2}$	1
#5	$g_{9/2}$	2
#6	$d_{5/2}, g_{7/2}$	3

4.4.2 Nucleus ^{62}Ni

For ^{62}Ni nucleus there is complete low-energy data [Nu-90] upto 4.055 MeV, however there are several levels between $3.258 - 4.055$ MeV for which the spins and parities are not assigned as can be seen from Table 4.24. In principle it is possible to use 3.258 MeV level as reference energy as all levels below this energy are identified with J^π values assigned. For even-even nuclei, as for these nuclei the level densities at low-energies being low, it is always better to use as high a reference energy as possible. Therefore all the levels upto 4.055 MeV

shown in Table 4.26 are used but with degeneracies assigned to levels with no J and/or π assignments by using information theory method described in Sect. 4.3.5. In applying (4.3) the value of spin-cutoff factor has been taken to be 3.0. The final (E_{ref}, N_{ref} and J^{π}_{ref}) values are given

Table 4.24 Low energy data for reference energy calculation

E (MeV)	J	π	$I^{+}(E)dE$	Ref
0.00	0	+	1	[Nu-90]
1.173	2	+	5	[Nu-90]
2.049	0	+	1	[Nu-90]
2.302	2	+	5	[Nu-90]
2.336	4	+	9	[Nu-90]
2.891	0	+	1	[Nu-90]
3.059	2	+	5	[Nu-90]
3.158	2	+	5	[Nu-90]
3.177	4	+	9	[Nu-90]
3.258	2	+	5	[Nu-90]
3.262	(2,4)	+	6.81	[Nu-90]
3.270	1,2	+	4.14	[Nu-90]
3.277	4	+	9	[Nu-90]
3.370	1,2	+	4.14	[Nu-90]
3.378	unknown	unknown	3.74	[Nu-90]
3.462	1,2,3,4	+	6.07	[Nu-90]
3.486	unknown	unknown	3.74	[Nu-90]
3.500	2	+	5	[Nu-90]
3.519	2	+	5	[Nu-90]
3.523	2,3	+	6.00	[Nu-90]
3.757	3	−	0.00	[Nu-90]
3.844	unknown	unknown	3.74	[Nu-90]
3.849	0,1,2	+	3.71	[Nu-90]
3.853	2	+	5	[Nu-90]
3.860	1,2	+	4.14	[Nu-90]
3.967	unknown	+	7.48	[Nu-90]
3.973	2	+	5	[Nu-90]
3.998	4	+	9	[Nu-90]
4.019	6	+	13	[Nu-90]
4.036	unknown	+	7.48	[Nu-90]
4.055	4	+	9	[Nu-90]

$E_{ref} = 4.055\ MeV$ $\qquad$ $J^{\pi}_{ref} = 4^{+}$

$N_{ref} = 167.2$

in Table 4.24. With this reference energy data and the unitary orbit centroid separation as given by $\overline{\Delta}^{(2)}$ in Table 4.21, the GS is calculated using a trial value for G. The level density ($4552\ MeV^{-1}$) at the neutron resonance energy $10.597\ MeV$ is reproduced with $G = 0.305\,MeV$. The values of $\sigma^2_{\mathbf{V}}$, $\sigma^2_{\mathbf{V}:J^2_z}$ and $\epsilon_{\mathbf{V}:J^2_z}$ calculated with $G = 0.305\,MeV$ are $12.8\ MeV^2$, $11.6\ MeV^2$ and $0.004\ MeV$ respectively for $S = 0$ configuration, $\sim 17\ MeV^2$, $\sim 16\ MeV^2$ and $\sim 0.01\ MeV$ respectively for $S = 1$ configurations, $\sim 22\ MeV^2$, $\sim 21\ MeV^2$ and $\sim 0.02\ MeV$ respectively for $S = 2$ configurations, $\sim 22\ MeV^2$, $\sim 20\ MeV^2$ and $\sim 0.01\ MeV$ respectively for $S = 3$ configurations, $\sim 20\ MeV^2$, $\sim 18\ MeV^2$ and $\sim 0.001\ MeV$ respectively for $S = 4$ configurations. The calculated $I_\ell(E)$, $I(E)$ and $\sigma_J(E)$ are compared with data in Figs. 4.11, 4.4. As can be seen from Fig. 4.11, the calculations with $G = 0.305\,MeV$ describe the data in the $4 - 20\ MeV$ energy range (the Lu et al (b) curve is consistently low compared to the calculated curve). The calculated spin-cutoff factor values (Fig. 4.4) are somewhat smaller than data values at low-energies. The results for ^{62}Ni confirm that the IP theory describes the data in a wide energy range. The state density $I(E)$ is well represented by LLC Fermi gas forms as can be seen from Fig. 4.5. The deduced (a, Δ) values are given in Table 4.25.

Table 4.25 Fermi gas parameters

Nucleus	Lu et al (a)		Lu et al (b)		Dilg et al		Present Calculation	
	a (MeV^{-1})	Δ (MeV)	a (MeV^{-1})	Δ (MeV)	a (MeV^{-1})	Δ (MeV)	a (MeV^{-1})	Δ (MeV)
^{62}Ni	6.40	0.5	6.40	1.30	7.27	1.07	6.44* 6.45@	0.40* 0.67@

* for Lang LeCouteur Fermi gas form @ for back shifted Fermi gas form

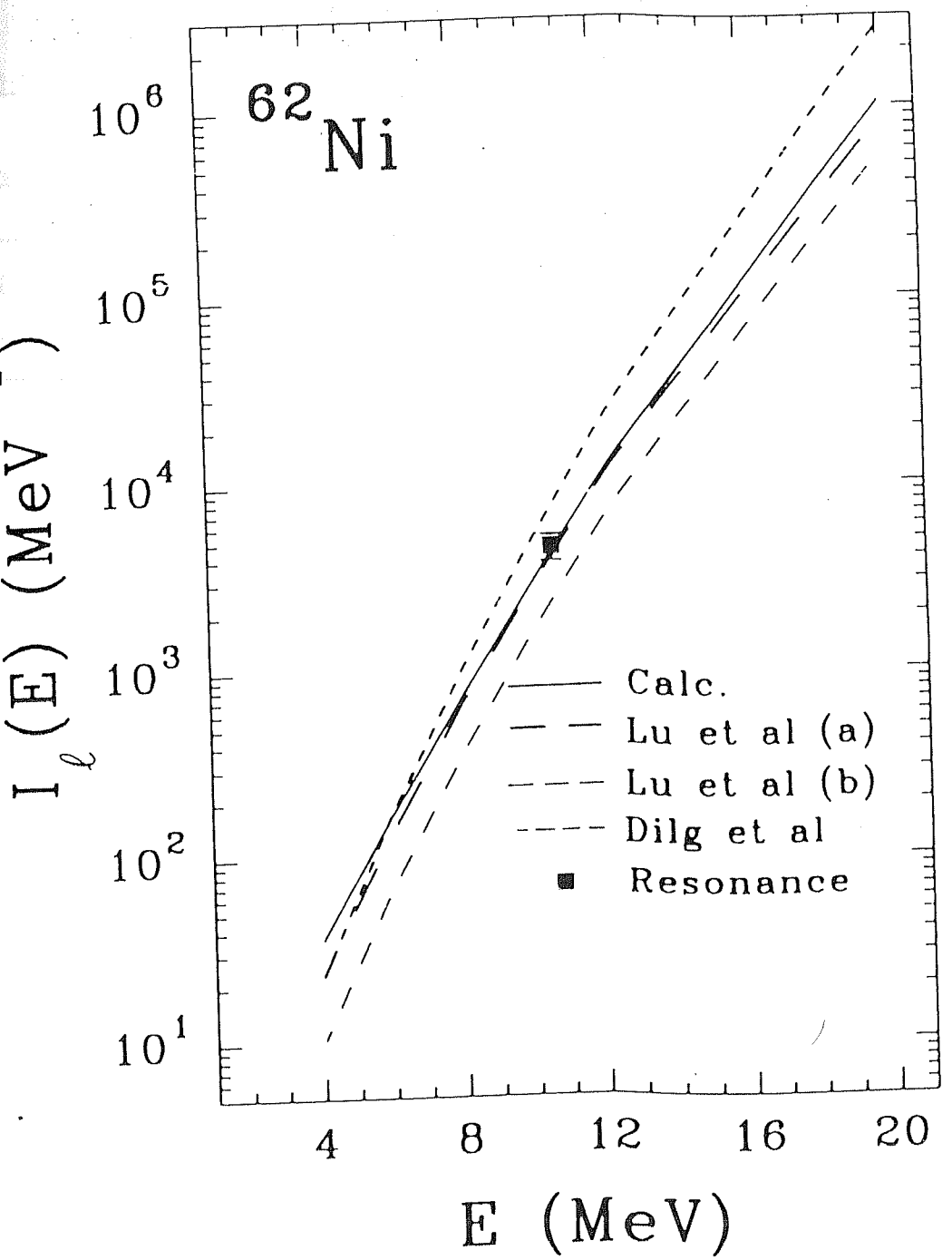


Fig. 4.11 Total level density $I_\ell(E)$ vs E for ^{62}Ni. References to data (Lu et al (a), Lu et al (b), Dilg et al, Resonance) and the actual data values are given in Appendix C.

4.4.3 Nucleus ^{63}Cu

With the low-energy data given in Sect. 4.3.6, centroid separation given by $\overline{\Delta}^{(2)}$ in Table 4.21 and the proton resonance data ($E_{res} = 8.6\,MeV$, $I_\ell(E) = 2100\,MeV^{-1}$) determine the value of G to be 0.305 MeV. Using this deduced value of G the calculated values of $I(E)$, $I_\ell(E)$ and $\sigma_J(E)$ are compared with data in Figs. 4.12, 4.4. Beyond the resonance energy of 8.6 MeV, the calcualted values are found to be lower, by about 40%, compared to data. The spin-cutoff factors change from $\sigma_J(E) = 3$ to 4 as E changes from 4 to 12 MeV while the data values are around 4 with an error of $10 - 20\%$. The Fermi gas fits to the calculated $I(E)$ and the deduced values of (a, Δ) are given in Fig. 4.5 and Table 4.26 respectively.

Table 4.26 Fermi gas parameters

Nucleus	Lu et al		Dilg et al		Present Calculation	
	a (MeV^{-1})	Δ (MeV)	a (MeV^{-1})	Δ (MeV)	a (MeV^{-1})	Δ (MeV)
^{63}Cu	6.60	-0.50	6.24	-0.77	6.44*	-0.32*
					6.45@	-0.06@

* for Lang LeCouteur Fermi gas form @ for back shifted Fermi gas form

Thus ^{62}Ni and ^{63}Cu are reasonably well described by using the centroids separation as given by $\overline{\Delta}^{(2)}$ in Table 4.21. The $\overline{\Delta}^{(1)}$ set is found to give densities to be too low, compared to data, to be acceptable.

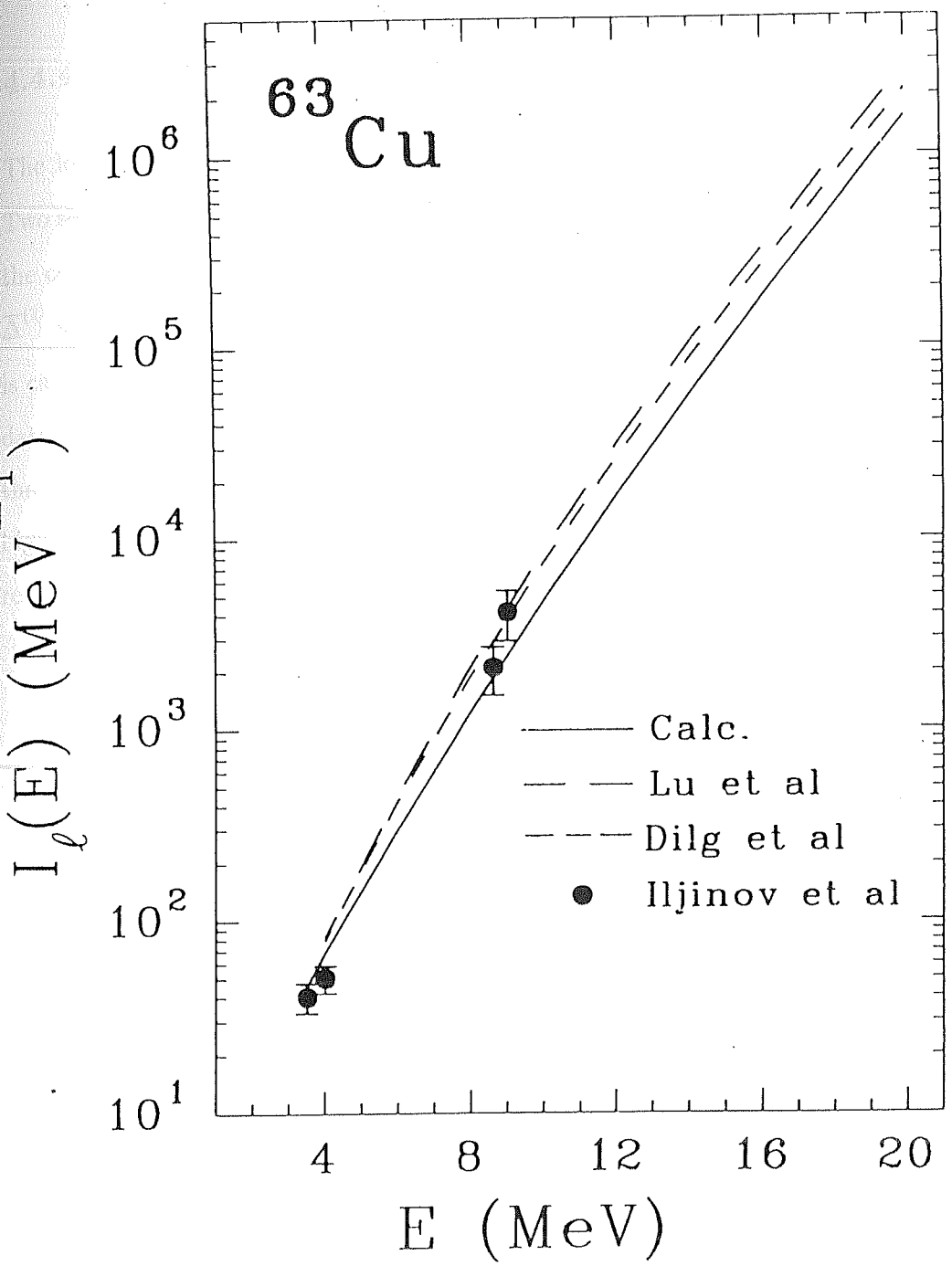


Fig. 4.12 Total level density $I_\ell(E)$ vs E for ^{63}Cu. References to data (Lu et al, Dilg et al, Iljinov et al) and the actual data values are given in Appendix C.

4.4.4 Nucleus ^{65}Cu

The low-energy data for fixing the reference energy is taken from [Nu-86a]. Two sets of calculations are performed for ^{65}Cu. In the first set of calculations, the centroid separations are chosen to be same as in ^{62}Ni and ^{63}Cu cases, i.e. $\overline{\Delta}^{(2)}$ set given in Table 4.21 is used. This set (the corresponding calculation is called ^{65}Cu (a)), the low-energy data given in Table 4.27 and the resonance data ($E_{res} = 10.65\,MeV$, $I_\ell(E_{res}) = 6854 \pm 2056\,MeV^{-1}$) are used to determine the value of G. The deduced value is $G = 0.315\,MeV$ and even with this high value of G (compared to 0.305 MeV used in ^{62}Ni and ^{63}Cu cases), the resonance

Table 4.27 Low lying data for reference energy calculation

E (MeV)	J^π	Ref
0.0	$3/2^-$	[Nu-86a]
0.77	$1/2^-$	[Nu-86a]
1.115	$5/2^-$	[Nu-86a]
1.481	$7/2^-$	[Nu-86a]
1.623	$5/2^-$	[Nu-86a]
1.725	$3/2^-$	[Nu-86a]
2.094	$7/2^-$	[Nu-86a]
2.107	$5/2^-$	[Nu-86a]
2.213	$1/2^-$	[Nu-86a]
2.278	$7/2^-$	[Nu-86a]
2.329	$3/2^-$	[Nu-86a]
$E_{ref} = 2.329\ MeV$		$J^\pi_{ref} = 3/2^-$
	$N_{ref} = 58$	

density is predicted to be $\sim 9000\ MeV^{-1}$ which is just within the error bar of the resonance density $6854 \pm 2056\ MeV^{-1}$. As a consequence, at $E \gtrsim 16\,MeV$ the calculated $I_\ell(E)$ differ from Dilg et al data by a factor 2. However it is in close agreement with Lu et al data as shown in Fig. 4.13. In order to

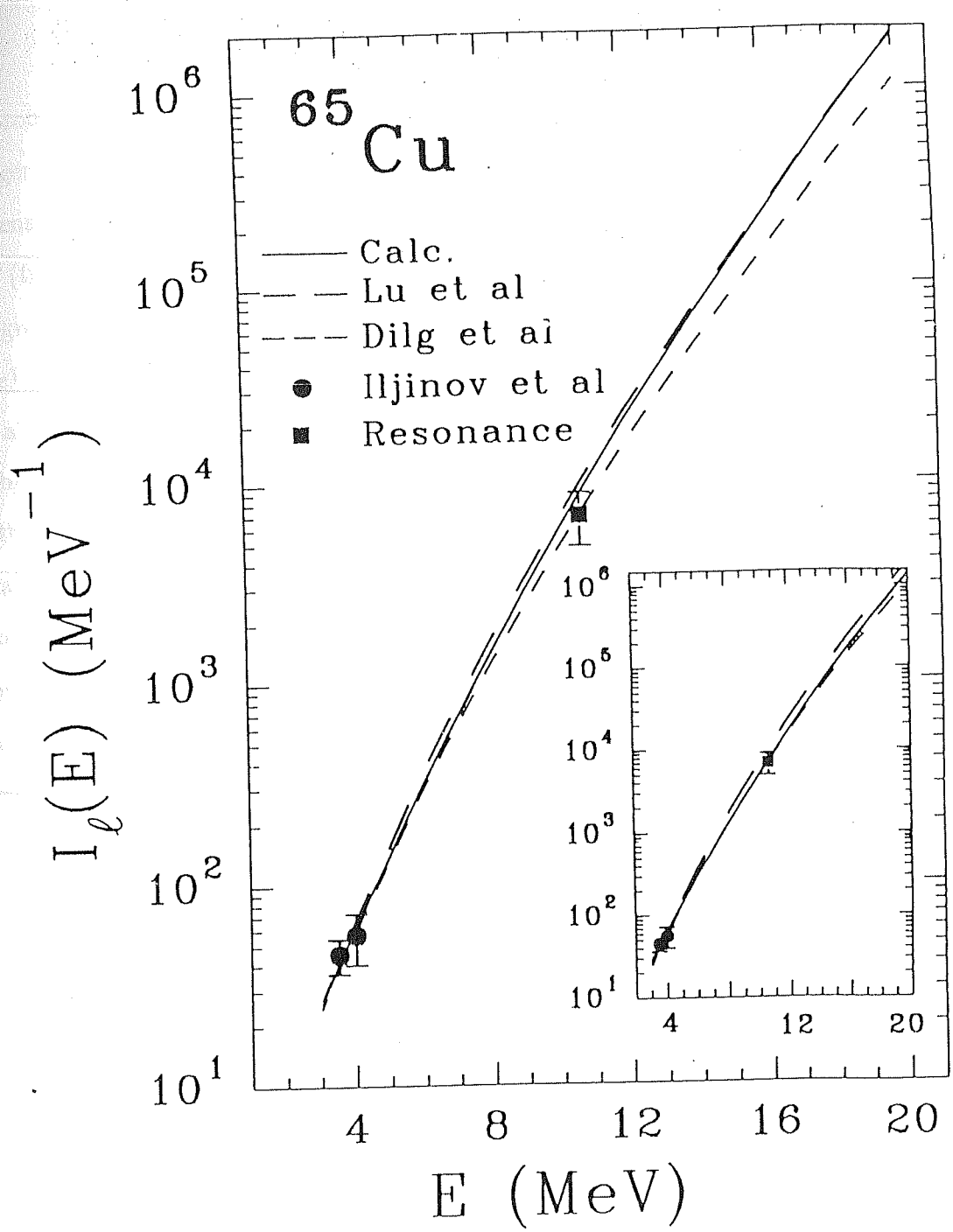


Fig. 4.13 Total level density $I_\ell(E)$ vs E for ^{65}Cu. References to data (Lu et al, Dilg et al, Iljinov et al, Resonance) and the actual data values are given in Appendix C. The results shown in the inset figure correspond to ^{65}Cu (b) calculations described in the text.

reproduce the resonance density value of 6800 MeV^{-1}, one has to use a much larger G value and also the $S = 2$ intensities become much larger than $S = 0$ intensities at low-energies which cannot be accepted. However using a different set (the corresponding calculation is called ^{65}Cu (b)) of centroid separations, as given by the set $\overline{\Delta}^{(1)}$ in Table 4.21, the value of G is determined to be 0.3 MeV. With this the resonance density is reproduced rather well as also Dilg et al data upto 20 MeV. However, here the deviations from Lu at al data is by about 40% as shown in the inset figure of Fig. 4.13. To be consistent with ^{62}Ni and ^{63}Cu calculations, the $^{65}Cu(a)$ results are accepted to be the final results. Therefore for $^{65}Cu(a)$ calculation, the results for $\sigma_J(E)$ vs E are shown in Fig. 4.4 and also the Fermi gas fits are made for $I(E)$ obtained in this case. The deduced values of (a, Δ) are given in Table 4.28 and the fit is shown in Fig. 4.5.

Table 4.28 Fermi gas parameters

Nucleus	Lu et al		Dilg et al		Present Calculation ^{65}Cu (a)	
	a (MeV^{-1})	Δ (MeV)	a (MeV^{-1})	Δ (MeV)	a (MeV^{-1})	Δ (MeV)
^{65}Cu	6.60	−0.50	6.24	−0.77	6.58*	−0.38*
					6.60@	−0.13@

* for Lang LeCouteur Fermi gas form @ for back shifted Fermi gas form

4.5 Summary

First systematic calculations, of level densities and spin-cutoff factors for all nuclei in a given region of the periodic table, in SAT-LSS framework are presented in this chapter with fp-shell nuclei as example. With the 8 - orbit

calculations for the five nuclei ^{55}Mn, ^{56}Fe, ^{59}Co, ^{60}Co, ^{60}Ni (described in Sect. 4.3) and 10 - orbit calculations for the three nuclei ^{62}Ni, ^{63}Cu, ^{65}Cu (described in 4.4), it is clearly demonstrated (as can be seen from Figs. 4.3 - 4.13) that SAT-LSS describes the level densities and spin-cutoff factors data rather well and that it is a powerful tool in analyzing and predicting statistical properties of nuclei. The calculations determine a magnitude parameter of the interaction - the strength G which is found to be $\sim 20/A\ MeV$ for all the nuclei is compatible with the values deduced from low-energy spectroscopy. The theory is seen to provide an excellent extrapolation from the resonance energy ($\sim 8\ MeV$) to $\sim 20\ MeV$ excitation and interpolation between the reference energy ($\sim 3-4\ MeV$) and the resonance energy. The calculated spin-cutoff factors and their energy variations (deriving from $J_Z^2 - \mathbf{V}^2$ correlations) are in good accord with the values deduced from data.

Chapter 5

Non-Interacting Particle Strength Densities for One-Body Transition Operators

5.1 Introduction

Going beyond state (level) and expectation value densities, the present chapter and the following chapter deal with bivariate strength densities and in particular Gamow - Teller (GT) strength densities are constructed for calculating GT summed strengths and β-decay rates; the bivariate strength density $\mathbf{I}^H_{\mathcal{O}}(E,E')$ as stated in Chapter 2, for a transition operator $\mathcal{O}$ and hamiltonian H is the transition strength weighted by the state densities at initial and final energies. The present work is based on the convolution result for strength densities in SAT-LSS. Using some plausible arguments and applying the bivariate Gaussian form (2.15) for $\mathbf{I}^H_{\mathcal{O}}$ locally, it was shown by French et al [Fr-87a, Fr-88b] that the IP strength density takes a simple bivariate convolution form, $\mathbf{I}^H_{\mathcal{O}}(E,E') = \sum_S \mathbf{I}^{\mathbf{h},S}_{\mathcal{O}} \otimes \rho^{\mathbf{V},S}_{\mathcal{O};BIV-\mathcal{G}}[E,E']$. Leaving aside the question of determining the five parameters (two centroids, two variances and

the bivariate correlation coefficient) of $\rho^{\mathbf{V}}_{\mathcal{O};BIV-g}$, one needs good methods for constructing $\mathbf{I}^{\mathbf{h}}_{\mathcal{O}}$ and its S - decompositions in large spaces. This chapter deals with the problem of constructing NIP densities $\mathbf{I}^{\mathbf{h}}_{\mathcal{O}}$ and the next chapter deals with the IP convolution. Therefore without loss of generality, from now on $\mathbf{h}$ is replaced by h. A theory for constructing NIP strength densities, for a general transition operator, is worked out in [Fr-88b] by employing s.p. *states* both for defining the eigen states of h and the transition operator; the NIP strength density takes a bivariate convolution form where one of the factors is a NIP state density and the other a δ function. An alternative formalism is developed in the present chapter using spherical/unitary orbits and spherical tensor form for the transition operators. Here the NIP strength density is written as a superposition of unitary configuration partial densities (they in turn give the S - decompositions required for incorporating interactions) and the partial strength densities are constructed in terms of their low order bivariate moments as Edgeworth corrected Gaussians (2.21) - i.e. CLT is used for the partial strength densities. In statistical spectroscopy studies, bivariate densities are directly constructed in terms of the bivariate moments (i.e. moment method is used) and applied for the first time in [Ko-84a, Ko-85]. The moment method, though approximate (it is exact with spherical configurations) is much faster as the number of unitary orbits is usually much smaller than the corresponding s.p. states. The results of the present chapter are restricted to one-body transition operators. In the next chapter the NIP strength densities for $GT(\beta^-)$ operator are employed in constructing the corresponding IP densities and with this a method for calculating β-decay rates for neutron excess fp-shell nuclei which play an important role in the evolution of massive presupernova stars [Au-90, Au-94], is developed and applied. We will now give

a preview.

Sects. 5.2 and 5.3 give preliminaries regarding one-body transition operators $\mathcal{O}^k_\mu$ of spherical tensor rank-k and the NIP strength densities $\mathbf{I}^h_{\mathcal{O}}$ respectively. In Sect. 5.4 exact expression for $\mathbf{I}^h_{\mathcal{O}}$ is derived using spherical configurations $\mathbf{m}$. The S decomposition of $\mathbf{I}^h_{\mathcal{O}}$ and further decomposition into partial unitary configuration densities $\mathbf{I}^{h;[\mathbf{m}],[\mathbf{m}']}_{\mathcal{O}}$ are introduced in Sect. 5.5. In Sect. 5.6, trace propagation formulas for the bivariate strength density moments M_{rs} for $r+s \leq 4$, for $\mathbf{I}^h_{\mathcal{O}}$ in m-particle scalar spaces are given; they are used in studying some general features of $\mathbf{I}^h_{\mathcal{O}}$. In Sect. 5.7, derived are the trace propagation formulas for the various fixed - $[\mathbf{m}]$ basic traces that determine the bivariate moments $M_{rs}([\mathbf{m}],[\mathbf{m}'])$ for $r+s \leq 2$, of $\mathbf{I}^{h;[\mathbf{m}],[\mathbf{m}']}_{\mathcal{O}}$. In Sect. 5.8 a numerical test, in a large shell model space example, for the goodness of bivariate Gaussian representation for the partial NIP strength densities $\mathbf{I}^{h;[\mathbf{m}],[\mathbf{m}']}_{\mathcal{O}}$ is described. Finally a summary is given in Sect. 5.9. The results given in this chapter are first reported in [Ko-94a].

5.2 One-body transition operators

A general one-body transition operator $\mathcal{O}^k_\mu$ and some of its properties are,

$$
\begin{aligned}
\mathcal{O}^k_\mu &= \sum \epsilon^{(k)}_{\alpha\beta} \left(a^\dagger_\alpha \tilde{a}_\beta \right)^k_\mu = \sum \epsilon^{(k)}_{\alpha\beta} \mathcal{O}^k_{\alpha\beta;\mu} \ , \\
\left(\mathcal{O}^k_\mu \right)^\dagger &= \sum (-1)^{j_\alpha - j_\beta} \epsilon^{(k)}_{\alpha\beta} (-1)^\mu \left(a^\dagger_\beta \tilde{a}_\alpha \right)^k_{-\mu} \ , \\
\left(\mathcal{O}^\dagger \right)^k_\mu &= \sum \epsilon^{(k)}_{\alpha\beta} (-1)^{j_\alpha - j_\beta} \left(a^\dagger_\beta \tilde{a}_\alpha \right)^k_\mu \ , \\
\left(\mathcal{O}^k_\mu \right)^\dagger &= (-1)^\mu \left(\mathcal{O}^\dagger \right)^k_{-\mu} \ ,
\end{aligned}
$$

$$\sum_{\mu} \left(\mathcal{O}^k_\mu\right)^\dagger \mathcal{O}^k_\mu \;=\; \left(\mathcal{O}^\dagger\right)^k \cdot \mathcal{O}^k \,. \tag{5.1}$$

In (5.1) $\epsilon^{(k)}_{\alpha\beta}$ are parameters that define $\mathcal{O}^k_\mu$ and for hermitian $\mathcal{O}$ (i.e. $\left(\mathcal{O}^k_\mu\right)^\dagger = (-1)^\mu \mathcal{O}^k_{-\mu}$) one has $\epsilon^{(k)}_{\beta\alpha} = (-1)^{j_\alpha - j_\beta}\epsilon^{(k)}_{\alpha\beta}$. For later convenience $\mathcal{O}^k_\mu$ are divided into four categories and they are

$$\begin{aligned}
[A]: \quad \mathcal{O}^k_\mu &= \sum \epsilon^{(k)}_{\alpha\beta} \left(a^\dagger_{\alpha_x} \tilde{a}_{\beta_y}\right)^k_\mu \;; \qquad x, y = \text{p or n} \\
[B]: \quad \mathcal{O}^k_\mu &= \alpha_p \left(\mathcal{O}^k_\mu\right)_p + \alpha_n \left(\mathcal{O}^k_\mu\right)_n \\
[C]: \quad \mathcal{O}^k_\mu &= \sum \epsilon^{(k)}_{\alpha_p\beta_n} \left(a^\dagger_{\alpha_p} \tilde{a}_{\beta_n}\right)^k_\mu \\
[D]: \quad \mathcal{O}^k_\mu &= \sum \epsilon^{(k)}_{\alpha_n\beta_p} \left(a^\dagger_{\alpha_n} \tilde{a}_{\beta_p}\right)^k_\mu
\end{aligned} \tag{5.2}$$

In (5.2), α_p and α_n are parameters. The operator $\mathcal{O}^k_\mu$ under category [A] belongs to identical particle system (protons or neutrons) while the remaining three are for pn systems. Note that electromagnetic operators belong to category [B] while $GT(\beta^+)$ and $GT(\beta^-)$ operators belong to categories [C] and [D] respectively. For example, explicit expressions for $GT(\beta^\pm)$ operator and the corresponding $\epsilon^{(k)}_{\alpha\beta}$'s are,

$$\mathcal{O}_{GT(\beta^\pm)} = \sum \epsilon^{(1)}_{\alpha(n'\ell'\frac{1}{2}j'),\beta(n\ell\frac{1}{2}j)} \left(a^\dagger_{\alpha_x} a_{\beta_y}\right)^1_\mu \;;$$

$$x = \text{n}, \quad y = \text{p} \quad \text{for} \quad \beta^+ \text{ and } x = \text{p}, \quad y = \text{n} \quad \text{for} \quad \beta^- \,,$$

$$\epsilon^{(1)}_{\alpha\beta} = \epsilon^{(1)}_{\alpha(n'\ell'\frac{1}{2}j'),\beta(n\ell\frac{1}{2}j)}$$

$$= \delta_{\ell\ell'}\delta_{nn'} \sqrt{\frac{2j+1}{3}} \frac{[j(j+1) + 3/4 - \ell(\ell+1)]}{\sqrt{j(j+1)}} \;; \quad \text{for} \quad j = j'$$

$$\epsilon^{(1)}_{\alpha\beta} = \epsilon^{(1)}_{\alpha(n'\ell'\frac{1}{2}j'),\beta(n\ell\frac{1}{2}j)} = \delta_{\ell\ell'}\delta_{nn'}(\pm)\sqrt{\frac{8\ell(\ell+1)}{3(2\ell+1)}} \;;$$

$$\pm \quad \text{for} \quad j = \ell \pm \frac{1}{2} \quad \text{and} \quad j' = \ell \mp \frac{1}{2} \tag{5.3}$$

In (5.3), (n, n') denote the oscillator radial quantum numbers, i.e. for oscillator shell N, $2n+\ell = N$. The delta functions in (5.3) for $\epsilon^{(1)}_{\alpha\beta}$ show that the $\mathcal{O}_{GT(\beta\pm)}$ operator is S-conserving when S quantum number is defined by the oscillator $n\hbar\omega$ excitations. Appendix D gives the explicit expressions for electromagnetic multiple operators and the corresponding $\epsilon^{(k)}_{\alpha\beta}$'s.

5.3 NIP strength densities

Given a NIP hamiltonian $h = \sum \epsilon_\alpha n_\alpha$ and a transition operator $\mathcal{O}^k_\mu$, explicit definitions of the strength $R^h_{\mathcal{O}}(E, E')$ and the strength density $\mathbf{I}^h_{\mathcal{O}}(E, E')$ follow from (2.36) and (2.37); in these equations, a factor $(2k+1)$ is used for convenience. In the NIP case the eigenstates are labelled by spherical configurations $\mathbf{m}$ with energies $\epsilon(\mathbf{m}) = \sum \epsilon_\alpha m_\alpha$ and degeneracies $d(\mathbf{m}) = \prod_\alpha \begin{pmatrix} N_\alpha \\ m_\alpha \end{pmatrix}$. Then $\mathbf{I}^h_{\mathcal{O}}(E, E')$ is given by

$$\mathbf{I}^h_{\mathcal{O}}(E,E') = (2k{+}1)^{-1} \sum_{\mathbf{m},\mathbf{m}',\mu} \sum_{\substack{\gamma \in \mathbf{m} \\ \gamma' \in \mathbf{m}'}} \left| \langle \mathbf{m}'\gamma' | \mathcal{O}^k_\mu | \mathbf{m}\gamma \rangle \right|^2 \delta(E{-}\epsilon(\mathbf{m}))\delta(E'{-}\epsilon(\mathbf{m}')) \tag{5.4}$$

In order to construct the total NIP density $\mathbf{I}^h_{\mathcal{O}}(E, E')$ and carry out its S - decompositions, strength densities are generated using : (i) spherical configurations, p or n or (p and n); (ii) scalar m - particle space, p or n; (iii) unitary configurations, p or n or (p and n). These three cases are dealt with in Sects. 5.4, 5.6 and 5.7 respectively.

5.4 Exact expression for $\mathbf{I}^h_{\mathcal{O}}$: spherical configurations

5.4.1 Identical particles

In order to derive the exact formula for $\mathbf{I}^h_{\mathcal{O}}$, first one should recognize that in (5.4) the summation over $(\mathbf{m}, \mathbf{m}')$ configurations disappears (i.e. when one is using spherical configuration decomposition of the m - particle spaces) as they are uniquely defined by E and E' respectively; from now on in this section, the summation over $(\mathbf{m}, \mathbf{m}')$ is dropped. As the transition operators that are being considered are of one-body $(a^\dagger_\alpha a_\beta)$ type, in general there are two types of strengths possible which are denoted by $\Delta = 0$ $(\mathbf{m} = \mathbf{m}')$ and 1 $(\mathbf{m} \neq \mathbf{m}')$ respectively. In both cases as we shall see ahead, the strength density is reduced to a trace over the initial configuration $(\mathbf{m})$. First the case of identical particles is considered; here one is using only category [A] operators of (5.2).

In $\Delta = 0$ case $\mathbf{m}' = \mathbf{m}$, i.e. the initial and final configurations are same. Then only the part $\left[\sum_\mu \epsilon^{(k)}_{\alpha\alpha} \mathcal{O}^k_{\alpha\alpha;\mu}\right]$ of $\mathcal{O}^k_\mu$ will contribute to the strength,

$$\mathbf{I}^h_{\mathcal{O}}(E,E') = (2k+1)^{-1} d(\mathbf{m}) \left\langle \left(\sum_\alpha \epsilon^{(k)}_{\alpha\alpha} \mathcal{O}^\dagger_{\alpha\alpha}\right)^k \cdot \left(\sum_{\alpha'} \epsilon^{(k)}_{\alpha'\alpha'} \mathcal{O}^k_{\alpha'\alpha'}\right) \right\rangle^{\mathbf{m}} \times \delta(E - \epsilon(\mathbf{m}))\delta(E' - \epsilon(\mathbf{m})) \tag{5.5}$$

The trace in (5.5) is evaluated by decomposing $\left(\sum_\alpha \epsilon^k_{\alpha\alpha} \mathcal{O}^\dagger_{\alpha\alpha}\right)^k \cdot \left(\sum_{\alpha'} \epsilon^k_{\alpha'\alpha'} \mathcal{O}^k_{\alpha'\alpha'}\right)$ into one and two-body parts and only the TBME of the type $V^{k'}_{\alpha\beta\alpha\beta}$ will contribute to the configuration trace. The resulting SPE ϵ'_α and TBME $V^{k'}_{\alpha\beta\alpha\beta}$ are $\epsilon'_\alpha = \sum_\alpha \left[\left\{\epsilon^{(k)}_{\alpha\alpha}\right\}^2 / N_\alpha\right] n_\alpha$ and $V^{k'}_{\alpha\beta\alpha\beta} = 2(-1)^{j_\alpha + j_\beta - k'} \epsilon^{(k)}_{\alpha\alpha} \epsilon^{(k)}_{\beta\beta} \begin{Bmatrix} j_\alpha & j_\alpha & k \\ j_\beta & j_\beta & k' \end{Bmatrix}$.

Using these and evaluating the fixed-$\mathbf{m}$ trace in (5.5), gives

$$\mathbf{I}^h_{\mathcal{O}}(E,E') = d(\mathbf{m})\delta(E-\epsilon(\mathbf{m}))\delta(E'-\epsilon(\mathbf{m}))\times$$
$$\left\{\left[\sum_\alpha \frac{\left\{\epsilon^{(k)}_{\alpha\alpha}\right\}^2}{N_\alpha} m_\alpha(\mathbf{m})\right] + \left[\sum_{\alpha>\beta} 2(\epsilon^{(k)}_{\alpha\alpha}\epsilon^{(k)}_{\beta\beta})\delta_{k,0}\times m_\alpha(\mathbf{m})m_\beta(\mathbf{m})\right] + \right.$$
$$\left.\left[\sum_\alpha 2\frac{\left\{\epsilon^{(k)}_{\alpha\alpha}\right\}^2}{N_{\alpha\alpha}}\left[\sum_{k'=0,2,4,..}(-1)^{1+k'}(2k'+1)\left\{\begin{array}{ccc} j_\alpha & j_\alpha & k \\ j_\alpha & j_\alpha & k'\end{array}\right\}\right] m_{\alpha\alpha}(\mathbf{m})\right]\right\} \tag{5.6}$$

Simplifying the summation involving the six-j symbol in (5.6) leads to, for $k\neq 0$, the following compact expression for $\mathbf{I}^h_{\mathcal{O}}(E,E')$,

$$\mathbf{I}^h_{\mathcal{O}}(E,E') = d(\mathbf{m})\sum_\alpha \left\{\epsilon^{(k)}_{\alpha\alpha}\right\}^2 \{m_\alpha(\mathbf{m})m^{\times}_\alpha(\mathbf{m})N^{-1}_{\alpha\alpha}\}\delta(E-\epsilon(\mathbf{m}))\delta(E-E') \tag{5.7}$$

In (5.7), $m_\alpha(\mathbf{m})$ gives number of particles in orbit α for the configuration $\mathbf{m}$ and similarly $m^{\times}_\alpha(\mathbf{m})$ is defined.

In $\Delta=1$ case only the terms $a^\dagger_\alpha a_\beta$ with $\alpha\neq\beta$ will contribute i.e. in the configuration $\mathbf{m}$, a particle in orbit β is destroyed and a particle in orbit α (with $\alpha\neq\beta$) is created, leading to $\mathbf{m}'$. Then $\mathbf{m}'$ is uniquely defined by $\mathbf{m}$ and (α,β); $\mathbf{m}'=\mathbf{m}\times\left(1^\dagger_\alpha 1_\beta\right)$. Alternatively given the initial configuration $\mathbf{m}$ and final configuration $\mathbf{m}'$, a unique $\mathcal{O}^k_{\alpha\beta}$ term will contribute to the strength. With this, $\mathbf{I}^h_{\mathcal{O}}(E,E')$ is given by

$$\mathbf{I}^h_{\mathcal{O}}(E,E') = (2k+1)^{-1}d(\mathbf{m})\left\{\epsilon^{(k)}_{\alpha\beta}\right\}^2\left\langle\left(\mathcal{O}^\dagger_{\alpha\beta}\right)^{(k)}\cdot\mathcal{O}^k_{\alpha\beta}\right\rangle^{\mathbf{m}}\times$$
$$\delta(E-\epsilon(\mathbf{m})\delta(E'-\epsilon[(\mathbf{m}')=(\mathbf{m})\times(1^\dagger_\alpha 1_\beta)]) \tag{5.8}$$

The configuration scalar part of $\left(\mathcal{O}^\dagger_{\alpha\beta}\right)^k\cdot\mathcal{O}^k_{\alpha\beta}$ is $(2k+1)n_\beta m^{\times}_\alpha/N_{\beta\alpha}$ and with this the formula for $\mathbf{I}^h_{\mathcal{O}}$ in (5.8) is,

$$\mathbf{I}^h_{\mathcal{O}}(E,E') = d(\mathbf{m})\left\{\epsilon^{(k)}_{\alpha\beta}\right\}^2\{m_\beta(\mathbf{m})\}\{m^{\times}_\alpha(\mathbf{m})\}\left[N_{\beta\alpha}\right]^{-1}\times$$

Using these and evaluating the fixed-$\mathbf{m}$ trace in (5.5), gives

$$\mathbf{I}^h_{\mathcal{O}}(E,E') = d(\mathbf{m})\delta(E-\epsilon(\mathbf{m}))\delta(E'-\epsilon(\mathbf{m}))\times$$
$$\left\{\left[\sum_\alpha \frac{\left\{\epsilon^{(k)}_{\alpha\alpha}\right\}^2}{N_\alpha} m_\alpha(\mathbf{m})\right] + \left[\sum_{\alpha>\beta} 2(\epsilon^{(k)}_{\alpha\alpha}\epsilon^{(k)}_{\beta\beta})\delta_{k,0}\times m_\alpha(\mathbf{m})m_\beta(\mathbf{m})\right] + \right.$$
$$\left.\left[\sum_\alpha 2\frac{\left\{\epsilon^{(k)}_{\alpha\alpha}\right\}^2}{N_{\alpha\alpha}}\left[\sum_{k'=0,2,4,..}(-1)^{1+k'}(2k'+1)\left\{\begin{array}{ccc} j_\alpha & j_\alpha & k \\ j_\alpha & j_\alpha & k'\end{array}\right\}\right] m_{\alpha\alpha}(\mathbf{m})\right]\right\} \tag{5.6}$$

Simplifying the summation involving the six-j symbol in (5.6) leads to, for $k\neq 0$, the following compact expression for $\mathbf{I}^h_{\mathcal{O}}(E,E')$,

$$\mathbf{I}^h_{\mathcal{O}}(E,E') = d(\mathbf{m})\sum_\alpha \left\{\epsilon^{(k)}_{\alpha\alpha}\right\}^2 \{m_\alpha(\mathbf{m})m^{\times}_\alpha(\mathbf{m})N^{-1}_{\alpha\alpha}\}\delta(E-\epsilon(\mathbf{m}))\delta(E-E') \tag{5.7}$$

In (5.7), $m_\alpha(\mathbf{m})$ gives number of particles in orbit α for the configuration $\mathbf{m}$ and similarly $m^{\times}_\alpha(\mathbf{m})$ is defined.

In $\Delta=1$ case only the terms $a^\dagger_\alpha a_\beta$ with $\alpha\neq\beta$ will contribute i.e. in the configuration $\mathbf{m}$, a particle in orbit β is destroyed and a particle in orbit α (with $\alpha\neq\beta$) is created, leading to $\mathbf{m}'$. Then $\mathbf{m}'$ is uniquely defined by $\mathbf{m}$ and (α,β); $\mathbf{m}' = \mathbf{m}\times\left(1^\dagger_\alpha 1_\beta\right)$. Alternatively given the initial configuration $\mathbf{m}$ and final configuration $\mathbf{m}'$, a unique $\mathcal{O}^k_{\alpha\beta}$ term will contribute to the strength. With this, $\mathbf{I}^h_{\mathcal{O}}(E,E')$ is given by

$$\mathbf{I}^h_{\mathcal{O}}(E,E') = (2k+1)^{-1}d(\mathbf{m})\left\{\epsilon^{(k)}_{\alpha\beta}\right\}^2\left\langle\left(\mathcal{O}^\dagger_{\alpha\beta}\right)^{(k)}\cdot\mathcal{O}^k_{\alpha\beta}\right\rangle^{\mathbf{m}}\times$$
$$\delta(E-\epsilon(\mathbf{m})\delta(E'-\epsilon[(\mathbf{m}')=(\mathbf{m})\times(1^\dagger_\alpha 1_\beta)]) \tag{5.8}$$

The configuration scalar part of $\left(\mathcal{O}^\dagger_{\alpha\beta}\right)^k\cdot\mathcal{O}^k_{\alpha\beta}$ is $(2k+1)n_\beta n^{\times}_\alpha/N_{\beta\alpha}$ and with this the formula for $\mathbf{I}^h_{\mathcal{O}}$ in (5.8) is,

$$\mathbf{I}^h_{\mathcal{O}}(E,E') = d(\mathbf{m})\left\{\epsilon^{(k)}_{\alpha\beta}\right\}^2\{m_\beta(\mathbf{m})\}\{m^{\times}_\alpha(\mathbf{m})\}\left[N_{\beta\alpha}\right]^{-1}\times$$

$$\delta(E-\epsilon(\mathbf{m}))\delta\left(E'-\epsilon\left[(\mathbf{m}')=(\mathbf{m})\times\left(1^{\dagger}_{\alpha}1_{\beta}\right)\right]\right)\,. \tag{5.9}$$

Combining (5.7, 5.9), the general expression for the exact NIP density $\mathbf{I}^h_{\mathcal{O}}$ is,

$$\begin{aligned}\mathbf{I}^h_{\mathcal{O}}(E,E') &= d(\mathbf{m})\sum_{\alpha,\beta}\left\{\epsilon^{(k)}_{\alpha\beta}\right\}^2\{m_\beta(\mathbf{m})\}\{m^{\times}_\alpha(\mathbf{m})\}N^{-1}_{\beta\alpha}\times \\ &\quad \delta(E-\epsilon(\mathbf{m}))\delta(E'-\epsilon\left[(\mathbf{m}')=(\mathbf{m})\times\left(1^{\dagger}_{\alpha}1_{\beta}\right)\right])\,. \end{aligned}\tag{5.10}$$

5.4.2 pn systems

For pn systems, and for transition operators that belong to category [B] of (5.2), $\mathcal{O}^k_\mu = e_p(\mathcal{O}^k_\mu)_p + e_n(\mathcal{O}^k_\mu)_n$ and the strength density involve $(\mathcal{O}^k_\mu)^\dagger(\mathcal{O}^k_\mu) = e^2_p(\mathcal{O}^k_\mu)^\dagger_p(\mathcal{O}^k_\mu)_p + e^2_n(\mathcal{O}^k_\mu)^\dagger_n(\mathcal{O}^k_\mu)_n + e_pe_n(\mathcal{O}^k_\mu)^\dagger_p(\mathcal{O}^k_\mu)_n + e_ne_p(\mathcal{O}^k_\mu)^\dagger_n(\mathcal{O}^k_\mu)_p$ with a trace over $(\mathbf{m}_p, \mathbf{m}_n)$. Obviously for $k \neq 0$, the pn cross terms will vanish as they cannot be reduced to a configuration scalar. Then, with only the pp and nn terms surviving, the expression for $\mathbf{I}^h_{\mathcal{O}}$ is given by (5.10) with the conventions defined in Sect. 3.1.5 for the orbit (α) indices. For pn one-body transition operators that belong to categories [C] and [D] (5.2), only the $\Delta = 1$ case discussed in Sect. 5.4.1 will be relevant as here $\alpha \neq \beta$ (one of them being a proton index and other a neutron index). Therefore just as above, in this case also (5.10) will give the exact NIP strength density with the conventions for the orbit indices (α) given in Sect. 3.1.5.

Thus for all the four categories of one-body operators given in (5.2), the exact $\mathbf{I}^h_{\mathcal{O}}$ can be constructed using (5.10) and the conventions given in Sect. 3.1.5 for orbit indices.

5.5 S-decomposition of strength densities

The strength density $\mathbf{I}^h_{\mathcal{O}}(E,E')$ can be decomposed into unitary orbit densities and also into fixed-S densities which will then allow us to apply the IP formalism for strength densities ([Fr-87a, Fr-88b, Ko-94b]) in very large spaces. To this end (5.4) is rewritten as,

$$\begin{aligned}
\mathbf{I}^{h;m}_{\mathcal{O}}(E,E') &= \sum_{[\mathbf{m}],[\mathbf{m}']} \left[\sum_{\mathbf{m}\in[\mathbf{m}],\,\mathbf{m}'\in[\mathbf{m}']} |\overline{\langle\, \mathbf{m}'|\mathcal{O}^k|\mathbf{m}\rangle}\,|^2 I^{h,\mathbf{m}}(E) I^{h,\mathbf{m}'}(E') \right] \\
&= \sum_{[\mathbf{m}],[\mathbf{m}']} [\mathbf{I}^{h;[\mathbf{m}],[\mathbf{m}']}_{\mathcal{O}}(E,E')] \\
&= \sum_{S,S'} \mathbf{I}^{h;\,S,S'}_{\mathcal{O}}(E,E') \;; \\
\mathbf{I}^{h;\,S,S'}_{\mathcal{O}}(E,E') &= \sum_{\substack{[\mathbf{m}]\,\in\, S \\ [\mathbf{m}']\,\in\, S'}} \mathbf{I}^{h;[\mathbf{m}],[\mathbf{m}']}_{\mathcal{O}}(E,E') \;; \\
I^{h;\mathbf{m}}(E) &= d(\mathbf{m})\delta(E-\epsilon(\mathbf{m})) \\
|\overline{\langle\, \mathbf{m}'|\mathcal{O}^k|\mathbf{m}\rangle}\,|^2 &= (2k+1)^{-1} \sum_{\gamma,\gamma',\mu} \frac{|\langle\, \mathbf{m}'\gamma'|\mathcal{O}^k_\mu|\mathbf{m}\gamma\rangle\,|^2}{d(\mathbf{m})d(\mathbf{m}')}
\end{aligned} \tag{5.11}$$

Eq. (5.11) applies directly to pn case. The first two equalities in (5.11) define the unitary configuration partial strength densities $\mathbf{I}^{h;[\mathbf{m}],[\mathbf{m}']}_{\mathcal{O}}$ and the next two equalities define the S - decomposition, i.e. $\mathbf{I}^{h;S,S'}_{\mathcal{O}}$. The bivariate moments $\mathbf{M}_{PQ}$ of the unitary orbit strength densities $\mathbf{I}^{[\mathbf{m}],[\mathbf{m}']}_{\mathcal{O}}(E,E')$ are,

$$\begin{aligned}
\mathbf{M}_{PQ}([\mathbf{m}],[\mathbf{m}']) &= [d([\mathbf{m}])]^{-1} \times \\
&\qquad \sum_{\substack{\mathbf{m}\,\in\,[\mathbf{m}] \\ \mathbf{m}'\,\in\,[\mathbf{m}']}} |\overline{\langle\, \mathbf{m}'|\mathcal{O}^k|\mathbf{m}\rangle}\,|^2 \times [d(\mathbf{m})d(\mathbf{m}')\epsilon^P(\mathbf{m})\epsilon^Q(\mathbf{m}')] \\
&= (2k+1)^{-1} \sum_\mu \langle (\mathcal{O}^k_\mu)^\dagger \mathbf{P}([\mathbf{m}'])h^Q \mathcal{O}^k_\mu h^P \rangle^{[\mathbf{m}]}
\end{aligned}$$

$$= [(2k+1)d([\mathbf{m}])]^{-1} \sum_{\mu,\gamma,\gamma'} \langle [\mathbf{m}]\gamma | \left(\mathcal{O}^k_\mu\right)^\dagger | [\mathbf{m}']\gamma' \rangle \langle [\mathbf{m}']\gamma' | h^Q \mathcal{O}^k_\mu h^P | [\mathbf{m}]\gamma \rangle \ ;$$

$$\mathbf{P}([\mathbf{m}'])|[\mathbf{m}]\gamma\rangle = |[\mathbf{m}']\gamma\rangle \delta_{[\mathbf{m}],[\mathbf{m}']} \tag{5.12}$$

In (5.12), $\mathbf{P}([\mathbf{m}'])$ is a projection operator. The first equality in (5.12) together with (5.10) (i.e. using the exact NIP density) one can numerically calculate the bivariate moments $\mathbf{M}_{PQ}$. However using the second and third equalities in (5.12), it is possible to derive propagation equations for the $\mathbf{M}_{PQ}$ traces directly in terms of (without using spherical configurations) the unitary configuration labels. We will do this in the next two sections. It must be mentioned that the $\mathbf{M}_{PQ}$ defined in (5.12) are not normalized and in order to construct an Edgeworth (bivariate) representation of $\mathbf{I}_{\mathcal{O}}^{[\mathbf{m}],[\mathbf{m}']}(E,E')$ one should use the normalized moments M_{PQ},

$$M_{PQ}([\mathbf{m}],[\mathbf{m}']) = \mathbf{M}_{PQ}([\mathbf{m}],[\mathbf{m}'])/\mathbf{M}_{00}([\mathbf{m}],[\mathbf{m}']) \tag{5.13}$$

$$\mathbf{I}_{\mathcal{O}}^{[\mathbf{m}],[\mathbf{m}']}(E,E') = \mathbf{M}_{00}([\mathbf{m}],[\mathbf{m}'])\rho_{\mathcal{O}}^{[\mathbf{m}],[\mathbf{m}']}(E,E'), \tag{5.14}$$

where ρ is normalized bivariate density. Explicit expression for bivariate Edgeworth corrected Gaussian is given in (2.21).

As an example using $GT(\beta^-)$ operator and choosing the s.p. orbits $[1d_{5/2}, 2s_{1/2}, 1d_{3/2}]$ and $[1f_{7/2}, 2p_{3/2}, 1f_{5/2}, 2p_{1/2}]$ to be the unitary orbits (denoted by # 1, 2) for both protons and neutrons and SPE (in MeV) to be Seeger [Hi-69] energies 16.388, 20.596, 21.851, 24.752, 29.431, 31.208, 32.201 respectively for the seven spherical orbits, the bivariate reduced cumulants k_{rs} are calculated for the strength densities $\mathbf{I}_{\mathcal{O}(GT)}^{h;[\mathbf{m}],[\mathbf{m}']}$ with $(m_p,m_n) = (4,6) \rightarrow (m'_p,m'_n) = (5,5)$ and $S = S' = 0$, 1 and 2. Here Eqs. (5.3, 5.10, 5.12, 5.13, 2.18) are used. It is seen that the bivariate cumulants k_{rs} for $r+s \geq 3$ are usually small. With $\{m_1,m_2,m_3,m_4\}$ denoting a unitary configuration with m_1 protons in $\#1, m_2$

protons in #2, m_3 neutrons in #1 and m_4 neutrons in #2 ($m_p = m_1 + m_2$, $m_n = m_3 + m_4$), the cumulants k_{rs} for $r+s \geq 3$ are: for $[4,0,6,0] \rightarrow [5,0,5,0]$ with $S = 0 \rightarrow S' = 0$, $k_{03} = 0.008$, $k_{04} = -0.11$, $k_{12} = 0.006$, $k_{13} = -0.07$, $k_{21} = 0.005$, $k_{22} = -0.09$, $k_{30} = -0.007$, $k_{31} = -0.08$ and $k_{40} = -0.11$; for $[4,0,5,1] \rightarrow [4,1,5,0]$ with $S = 1 \rightarrow S' = 1$, $k_{03} = -0.01$, $k_{04} = -0.14$, $k_{12} = 0.0004$, $k_{13} = -0.07$, $k_{21} = 0.0004$, $k_{22} = -0.07$, $k_{30} = -0.01$, $k_{31} = -0.07$ and $k_{40} = -0.14$; for $[3,1,5,1] \rightarrow [4,1,4,1]$ with $S = 2 \rightarrow S' = 2$, $k_{03} = -0.02$, $k_{04} = -0.16$, $k_{12} = -0.02$, $k_{13} = -0.14$, $k_{21} = -0.02$, $k_{22} = -0.15$, $k_{30} = -0.02$, $k_{31} = -0.14$ and $k_{40} = -0.16$. In this example the widths are $\simeq 6 - 7$ MeV and the correlation coefficients $\zeta = k_{11} \simeq 0.8$.

5.6 Scalar strength density bivariate moments: identical particles

In the scalar (m - particle average case) only the identical particle case is relevant with category [A] operators given in (5.2). As here $[\mathbf{m}] = m = [\mathbf{m}']$, the bivarite moments $\mathbf{M}_{PQ}([\mathbf{m}],[\mathbf{m}'])$ are written as $\mathbf{M}_{PQ}(m)$. The moments $\mathbf{M}_{PQ}(m)$ are expressible in terms of $\widetilde{M}_{PQ}(m)$ which are defined by $\widetilde{M}_{PQ}(m) = (2k+1)^{-1} \sum_{\mu} \langle ((\mathcal{O}^k_\mu)^\dagger \tilde{h}^Q \mathcal{O}^k_\mu) \tilde{h}^P \rangle^m$; $h = \sum \epsilon_\alpha n_\alpha \Longrightarrow \tilde{h} = \sum \tilde{\epsilon}_\alpha n_\alpha$ and $\tilde{\epsilon}_\alpha = \epsilon_\alpha - \bar{\epsilon}$, $\bar{\epsilon} = (\sum N_\alpha \epsilon_\alpha)/N$ as given in (2.49). Propagation formulas for $\widetilde{M}_{PQ}$ are derived, though tedious but straight forward, using the methods given in detail in Sects. 2.5 - 2.6. With $\mathbf{X}_{PQ}(i)$ denoting the i-body part of $(2k+1)^{-1} \sum_{\mu} (\mathcal{O}^k_\mu)^\dagger \tilde{h}^Q \mathcal{O}^k_\mu \tilde{h}^P$ and $Z_{PQ}(i) = \langle \mathbf{X}_{PQ}(i) \rangle^i$, the trace propagation formulas for $\widetilde{M}_{PQ}$ for $P+Q \leq 2$ are,

$$\widetilde{M}_{00}(m) = M_{00} = \frac{mm^{\times}}{[N]_2} Z_{00}(1) \; ; \; Z_{00}(1) = \sum_{\alpha,\beta} \left\{ \epsilon^{(k)}_{\alpha\beta} \right\}^2 \qquad (5.15)$$

$$\widetilde{M}_{10}(m) = \widetilde{M}_{01}(m) = \frac{mm^{\times}(m^{\times}-m)}{[N]_3} Z_{PQ}(1) \; ;$$

$$Z_{10}(1) = Z_{01}(1) = \sum_{\alpha,\beta} \left\{\epsilon_{\alpha\beta}^{(k)}\right\}^2 \tilde{\epsilon}_{\alpha} \tag{5.16}$$

$$\widetilde{M}_{PQ}(m) = \left[\frac{mm^{\times}}{[N]_2} + \frac{[m]_2[m^{\times}]_2}{[N]_4}\right] Z_{PQ}(1) + \left[\frac{[m]_2[m^{\times}]_2}{[N]_4}\right] Z_{PQ}(2) \; ; \; P+Q=2,$$

$$Z_{20}(1) = Z_{02}(1) = \sum_{\alpha,\beta} \left\{\epsilon_{\alpha\beta}^{(k)}\right\}^2 \tilde{\epsilon}_{\alpha}^2$$

$$Z_{20}(2) = Z_{02}(2) = -5\sum_{\alpha,\beta} \left\{\epsilon_{\alpha\beta}^{(k)}\right\}^2 \tilde{\epsilon}_{\alpha}^2 - 2\sum_{\alpha,\beta} \left\{\epsilon_{\alpha\beta}^{(k)}\right\}^2 \tilde{\epsilon}_{\alpha}\tilde{\epsilon}_{\beta} .$$

$$+ \left[\sum_{\alpha,\beta} \left\{\epsilon_{\alpha\beta}^{(k)}\right\}^2\right] \left[\sum_{\tau} \tilde{\epsilon}_{\tau}^2 N_{\tau}\right]$$

$$Z_{11}(1) = \sum_{\alpha,\beta} \left\{\epsilon_{\alpha\beta}^{(k)}\right\}^2 \tilde{\epsilon}_{\alpha}\tilde{\epsilon}_{\beta}$$

$$Z_{11}(2) = -4\sum_{\alpha,\beta} \left\{\epsilon_{\alpha\beta}^{(k)}\right\}^2 \tilde{\epsilon}_{\alpha}^2 - 3\sum_{\alpha,\beta} \left\{\epsilon_{\alpha\beta}^{(k)}\right\}^2 \tilde{\epsilon}_{\alpha}\tilde{\epsilon}_{\beta} + \left[\sum_{\alpha,\beta} \left\{\epsilon_{\alpha\beta}^{(k)}\right\}^2\right] \left[\sum_{\tau} \tilde{\epsilon}_{\tau}^2 N_{\tau}\right] \tag{5.17}$$

For $P+Q=3,4$ the basic inputs $Z_{PQ}(i)$ are given in Tables 5.1, 5.2 and they together with the following propagation formulas will determine $\widetilde{M}_{PQ}(m)$ for $P+Q=3,4$,

$$\widetilde{M}_{PQ}(m) = \left\{\frac{3[m]_2[m^{\times}]_2(m^{\times}-m)}{[N]_5} + \frac{mm^{\times}(m^{\times}-m)}{[N]_3}\right\} Z_{PQ}(1)$$

$$+ \left\{\frac{[m]_2[m^{\times}]_2(m^{\times}-m)}{[N]_5}\right\} Z_{PQ}(2) \; ; \; P+Q=3 \tag{5.18}$$

$$\widetilde{M}_{PQ}(m) = \left\{\frac{mm^{\times}}{[N]_2} + \frac{[m]_2[m^{\times}]_2}{[N]_4} + \frac{2[m]_3[m^{\times}]_3}{[N]_6}\right\} Z_{PQ}(1)$$

$$+ \left\{\frac{[m]_2[m^{\times}]_2}{[N]_4} + \frac{2[m]_3[m^{\times}]_3}{[N]_6}\right\} Z_{PQ}(2) + \left\{\frac{[m]_3[m^{\times}]_3}{[N]_6}\right\} Z_{PQ}(3) \; ; \; P+Q=4 \tag{5.19}$$

Table 5.1 Basic inputs $Z_{PQ}(i) = \sum_{r=1}^{4} a_r A_r$ for $\widetilde{M}_{PQ}(m)$ moments with $P+Q = 3$. The a_r's and A_r's are given in the table.

(P,Q)	i	a_r			
		$r=1$	$r=2$	$r=3$	$r=4$
(3,0)	1	1	0	0	0
(3,0)	2	−9	−6	3	1
(2,1)	1	0	1	0	0
(2,1)	2	−6	−9	3	1

$$A_1 = \sum_{\alpha,\beta} \left\{\epsilon_{\alpha\beta}^{(k)}\right\}^2 \widetilde{\epsilon}_{\alpha}^3 \qquad A_2 = \sum_{\alpha,\beta} \left\{\epsilon_{\alpha\beta}^{(k)}\right\}^2 \widetilde{\epsilon}_{\alpha}^2 \widetilde{\epsilon}_{\beta}$$

$$A_3 = \left[\sum_{\alpha,\beta} \left\{\epsilon_{\alpha\beta}^{(k)}\right\}^2 \widetilde{\epsilon}_{\alpha}\right] \left[\sum_{\tau} \widetilde{\epsilon}_{\tau}^2 N_{\tau}\right] \quad A_4 = \left[\sum_{\alpha,\beta} \left\{\epsilon_{\alpha\beta}^{(k)}\right\}^2\right] \left[\sum_{\tau} \widetilde{\epsilon}_{\tau}^3 N_{\tau}\right]$$

Given the expression for $\widetilde{M}_{PQ}(m)$, the $\mathbf{M}_{PQ}(m)$ moments are easy to write down,

$$\mathbf{M}_{PQ}(m) = \sum_{r=0-P, s=0-Q} \binom{P}{r} \binom{Q}{s} \widetilde{M}_{rs}(m) (m\bar{\epsilon})^{P+Q-r-s} \tag{5.20}$$

Using the relationship between the normalized moments $M_{PQ} = \mathbf{M}_{PQ}/\mathbf{M}_{00}$, the central moments $\mathcal{M}_{PQ}$ and the cumulants k_{PQ} together with (5.15 - 5.20) one is in a position to construct a bivariate Edgeworth representation (2.21) for $\mathbf{I}_{\mathcal{O}}^{h,m}$. Before going to the next section, it should be mentioned that the formulas in (5.15 - 5.20) are verified numerically by using the first equality in (5.12) and (5.10). The scalar propagation equations and the moments $\mathbf{M}_{PQ}(m)$ for

Table 5.2 Basic inputs $Z_{PQ}(i) = \sum_{r=1}^{8} a_r A_r$ for $\widetilde{M}_{PQ}(m)$ moments with $P+Q = 4$. The a_r's and A_r's are given in the table.

(P,Q)	i	a_r							
		$r=1$	$r=2$	$r=3$	$r=4$	$r=5$	$r=6$	$r=7$	$r=8$
(4,0)	1	1	0	0	0	0	0	0	0
(4,0)	2	−17	−8	−6	6	0	4	1	0
(4,0)	3	80	64	36	−36	−12	−24	−8	3
(3,1)	1	0	1	0	0	0	0	0	0
(3,1)	2	−10	−15	−6	3	3	4	1	0
(3,1)	3	68	76	36	−30	−18	−24	−8	3
(2,2)	1	0	0	1	0	0	0	0	0
(2,2)	2	−8	−16	−7	2	4	4	1	0
(2,2)	3	64	80	36	−28	−20	−24	−8	3

$$A_1 = \sum_{\alpha,\beta} \left\{\epsilon_{\alpha\beta}^{(k)}\right\}^2 \tilde{\epsilon}_\alpha^4 \qquad A_2 = \sum_{\alpha,\beta} \left\{\epsilon_{\alpha\beta}^{(k)}\right\}^2 \tilde{\epsilon}_\alpha^3 \tilde{\epsilon}_\beta$$

$$A_3 = \sum_{\alpha,\beta} \left\{\epsilon_{\alpha\beta}^{(k)}\right\}^2 \tilde{\epsilon}_\alpha^2 \tilde{\epsilon}_\beta^2 \qquad A_4 = \left[\sum_{\alpha,\beta} \left\{\epsilon_{\alpha\beta}^{(k)}\right\}^2 \tilde{\epsilon}_\alpha^2\right] \left[\sum_{\tau} \tilde{\epsilon}_\tau^2 N_\tau\right]$$

$$A_5 = \left[\sum_{\alpha,\beta} \left\{\epsilon_{\alpha\beta}^{(k)}\right\}^2 \tilde{\epsilon}_\alpha \tilde{\epsilon}_\beta\right] \left[\sum_{\tau} \tilde{\epsilon}_\tau^2 N_\tau\right] \qquad A_6 = \left[\sum_{\alpha,\beta} \left\{\epsilon_{\alpha\beta}^{(k)}\right\}^2 \tilde{\epsilon}_\alpha\right] \left[\sum_{\tau} \tilde{\epsilon}_\tau^3 N_\tau\right]$$

$$A_7 = \left[\sum_{\alpha,\beta} \left\{\epsilon_{\alpha\beta}^{(k)}\right\}^2\right] \left[\sum_{\tau} \tilde{\epsilon}_\tau^4 N_\tau\right] \qquad A_8 = \left[\sum_{\alpha,\beta} \left\{\epsilon_{\alpha\beta}^{(k)}\right\}^2\right] \left[\sum_{\tau_1} \tilde{\epsilon}_{\tau_1}^2 N_{\tau_1} \sum_{\tau_2} \tilde{\epsilon}_{\tau_2}^2 N_{\tau_2}\right]$$

$P+Q \leq 4$ are useful for many purposes. For example the expressions (and the methods) for the scalar moments indicate the methods for deriving unitary configuration traces as given ahead in Sect. 5.7. Eqs. (5.15 - 5.20) allow us to study the asymptotic behavior of bivariate correlation coefficients and the higher order shape parameters defined by the bivariate cumulants k_{rs}. As an example let us consider the case of a random one-body hamiltonian $h = \sum \epsilon_\alpha n_\alpha$ with $N_\alpha = 1$ for any α and ϵ_α to be zero centered independent Gaussian random variables with unit variance. With $Y = \sum \left\{\epsilon_{\alpha\beta}^{(k)}\right\}^2$, assuming $\epsilon_{\alpha\alpha}^{(k)} = 0$ and using (5.15, 5.17), give $Z_{00}(1) = Y$, $Z_{20}(1) = Y$, $Z_{20}(2) = Y(N-5)$, $Z_{11}(1) = 0$ and $Z_{11}(2) = Y(N-4)$. In the dilute limit ($m \to \infty$, $N \to \infty$, $m/N \to 0$), they lead to the results that $\zeta(m) \simeq 1 - 1/m$. Therefore in general the NIP state density correlation coefficient will be large – with half a dozen to dozen particles $\zeta \simeq 0.8 - 0.9$ (see also the numerical example in Sect. 5.5). It should be added that it is easy to derive finite - N corrections to the $\zeta(m)$ expression given above. Using (5.15 - 5.20), numerical calculations of the shape parameters k_{rs} (for $r+s = 3, 4$) is straightforward and with k_{rs}, one can have estimates (in finite - (N, m) cases) for departures from the bivariate Gaussian nature; for example, as can be seen from Table 5.3, in the above model, with $N = 40$ and $m = 10$, $k_{11} = 0.87$, $k_{40} = -0.15$, $k_{31} = -0.13$, $k_{22} = 0.12$ and similarly with $N = 100$, $m = 20$ give $k_{11} = 0.94$, $k_{40} = -0.06$, $k_{31} = -0.06$, $k_{22} = 0.05$. A different model where $\epsilon_{\alpha\beta}^{(k)}$ are chosen to be Gaussian random variables was dealt with in [Fr-88b] and this model also gives $\zeta(m) \simeq 1 - 1/m$; Eqs. (5.15 - 5.20) reproduce the results of [Fr-88b] and in addition they give finite - N corrections for the bivariate cumulants.

Table 5.3 Bivariate cumulants (k_{rs}) in scalar space for a random one-body hamiltonian. In the table N is number of single particle states and m is number of particles. Note that in the model considered in the text, $k_{rs} = 0$ for $r + s$ odd.

	$N = 20$		
	$m = 4$	$m = 8$	$m = 10$
$k_{11} = \zeta$	0.70	0.80	0.80
k_{40}	−0.28	−0.31	−0.31
k_{31}	−0.20	−0.25	−0.26
k_{22}	−0.17	−0.23	−0.24
	$N = 40$		
	$m = 4$	$m = 10$	$m = 20$
$k_{11} = \zeta$	0.73	0.87	0.90
k_{40}	−0.13	−0.15	−0.15
k_{31}	−0.09	−0.13	−0.14
k_{22}	−0.08	−0.12	−0.13
	$N = 100$		
	$m = 10$	$m = 20$	$m = 50$
$k_{11} = \zeta$	0.89	0.94	0.96
k_{40}	−0.06	−0.06	−0.06
k_{31}	−0.05	−0.06	−0.06
k_{22}	−0.05	−0.05	−0.06

5.7 Unitary configuration strength density bivariate moments

5.7.1 Identical particles

In the unitary configuration case, propagation equations for the bivariate strength density moments $\widehat{M}_{PQ}([\mathrm{m}])$,

$$\widehat{M}_{PQ}([\mathrm{m}]) = (2k+1)^{-1}\langle\sum_{\mu}(\mathcal{O}^k_\mu)^\dagger h^Q \mathcal{O}^k_\mu h^P\rangle^{[\mathrm{m}]}, \tag{5.21}$$

with $P+Q \leq 2$ are derived and the results are given below. Their decomposition into partial strength moments $M_{PQ}([\mathbf{m}],[\mathbf{m}'])$ (5.12, 5.13) that define the partial strength densities $\mathbf{I}_{\mathcal{O}}^{h;[\mathbf{m}],[\mathbf{m}']}$ is straight forward and this is described in Sect. 5.7.3. All the discussion below is appropriate for identical particle systems and Sect. 5.7.2 deals with pn systems.

In order to derive propagation formulas for $\widehat{M}_{PQ}([\mathbf{m}])$ traces, the method employed is to first carry out the unitary decomposition (using the results of Sect. 2.5) of the operators $[\ (2K+1)^{-1}\sum_{\mu}(\mathcal{O}_{\mu}^{k})^{\dagger}\mathcal{O}_{\mu}^{k}\ ]$ which is denoted as $\mathcal{O}^{\dagger}\mathcal{O}$, and h^2. They will have $[\mathbf{0}] \oplus [\mathbf{1}] \oplus [\mathbf{2}]$ unitary tensor parts; only the diagonal TBME of $\mathcal{O}^{\dagger}\mathcal{O}$ contribute to the $\widehat{M}_{PQ}$ moments. The SPE and TBME of h^2 operator are (note that $h = h^{[\mathbf{0}]} + h^{[\mathbf{1}]}$, $h^{[\mathbf{0}]} = \sum_{\boldsymbol{\alpha}} \epsilon_{\boldsymbol{\alpha}}^{[\mathbf{0}]} n_{\boldsymbol{\alpha}}$, $h^{[\mathbf{1}]} = \sum \epsilon_{\alpha}^{[\mathbf{1}]} n_{\alpha}$, $\epsilon_{\boldsymbol{\alpha}}^{[\mathbf{0}]} = N_{\boldsymbol{\alpha}}^{-1} \sum_{\alpha\in\boldsymbol{\alpha}} \epsilon_{\alpha} N_{\alpha}$ and $\epsilon_{\alpha}^{[\mathbf{1}]} = \epsilon_{\alpha} - \epsilon_{\boldsymbol{\alpha}}^{[\mathbf{0}]}$),

$$\begin{aligned} (h^2)_{\text{1-body}} &= \sum \epsilon_{\alpha}^2 n_{\alpha} \\ (h^2)_{\text{2-body}} &\Leftrightarrow C^{J}_{\alpha\beta\alpha\beta} = C_{\alpha\beta} = 2\epsilon_{\alpha}\epsilon_{\beta}. \end{aligned} \tag{5.22}$$

Eqs. (2.58, 5.22) give the unitary decomposition of the h^2 operator,

$$\begin{aligned} (h^2)^{[\mathbf{0}]} &= \sum_{\boldsymbol{\alpha}} n_{\boldsymbol{\alpha}} n_{\boldsymbol{\alpha}}^{\times} N_{\boldsymbol{\alpha}\boldsymbol{\alpha}}^{-1} \left\{ \sum_{\alpha\in\boldsymbol{\alpha}} \epsilon_{\alpha}^2 N_{\alpha} \right\} \\ (h^2)^{[\mathbf{1}]} &= \sum_{\alpha} n_{\alpha} \left\{ \frac{(N_{\boldsymbol{\alpha}}^{\times} - n_{\boldsymbol{\alpha}})}{(N_{\boldsymbol{\alpha}} - 2)} \left[N_{\boldsymbol{\alpha}}^{-1} \sum_{\alpha'\in\boldsymbol{\alpha}} N_{\alpha'}(\epsilon_{\alpha}^2 - \epsilon_{\alpha'}^2) \right] \right\} \\ (h^2)^{[\mathbf{2}]} &= h^2 - (h^2)^{[\mathbf{0}]} - (h^2)^{[\mathbf{1}]} \end{aligned} \tag{5.23}$$

With $\mathcal{O}_{\mu}^{k}$ defined by $\epsilon_{\alpha\beta}^{(k)}$, the one and two-body parts of $\mathcal{O}^{\dagger}\mathcal{O}$ operator are,

$$(\mathcal{O}^{\dagger}\mathcal{O})_{\text{1-body}} = \sum_{\beta} \left[\left(\sum_{\alpha} \left\{ \epsilon_{\alpha\beta}^{(k)} \right\}^2 \right) N_{\beta}^{-1} \right] n_{\beta} \tag{5.24}$$

$$(\mathcal{O}^{\dagger}\mathcal{O})_{\text{2-body}} = \sum_{k'} \left[\epsilon_{\alpha\beta}^{(k)} \epsilon_{\gamma\delta}^{(k)} \left\{ \begin{array}{cc} j_\beta & j_\alpha \ k \\ j_\delta & j_\gamma \ k' \end{array} \right\} \times \right.$$

$$(-1)^{j_\alpha+j_\beta+j_\gamma+j_\delta+1}\sqrt{(1+\delta_{\beta\gamma})(1+\delta_{\alpha\delta})}\Big]$$

$$\frac{(a^\dagger_\beta a^\dagger_\gamma)^{k'}_\mu}{\sqrt{(1+\delta_{\beta\gamma})}}\frac{\left\{(a^\dagger_\delta a^\dagger_\alpha)^{k'}_\mu\right\}^\dagger}{\sqrt{(1+\delta_{\alpha\delta})}} \tag{5.25}$$

It is easily seen that for the traces under consideration, only the average two-particle matrix elements $C_{\alpha\beta}$ (2.50) of $(\mathcal{O}^\dagger\mathcal{O})_{\text{2-body}}$ will contribute (this is because h^2 operator has only $C_{\alpha\beta}$ part as given in (5.22)). Using (5.25) and the results $\sum_{k'=\text{even}}(2k'+1)\left\{\begin{array}{ccc} j_\alpha & j_\alpha & k \\ j_\alpha & j_\alpha & k' \end{array}\right\} = \frac{1}{2}$, $\sum_{k'}(2k'+1)\left\{\begin{array}{ccc} j_\alpha & j_\beta & k \\ j_\alpha & j_\beta & k' \end{array}\right\} = 1$ for $k \neq 0$ give $C_{\alpha\beta}$ of $\mathcal{O}^\dagger\mathcal{O}$ to be,

$$(\mathcal{O}^\dagger\mathcal{O})_{\text{2-body}} \Leftrightarrow C_{\alpha\beta} = -\left[\left\{\epsilon^{(k)}_{\alpha\beta}\right\}^2 + \left\{\epsilon^{(k)}_{\beta\alpha}\right\}^2\right] N^{-1}_{\alpha\beta} \tag{5.26}$$

Eqs. (2.58, 5.25 - 5.27) give the unitary decomposition of the $\mathcal{O}^\dagger\mathcal{O}$ operator,

$$\begin{aligned}
(\mathcal{O}^\dagger\mathcal{O})^{[0]} &= \sum_{\boldsymbol{\alpha},\boldsymbol{\beta}} n_{\boldsymbol{\alpha}} n^{\times}_{\boldsymbol{\beta}} N^{-1}_{\boldsymbol{\alpha\beta}} \times \left[\sum_{\alpha\in\boldsymbol{\alpha},\beta\in\boldsymbol{\beta}} \left\{\epsilon^{(k)}_{\beta\alpha}\right\}^2\right] \\
(\mathcal{O}^\dagger\mathcal{O})^{[1]} &= \sum_{\boldsymbol{\alpha},\boldsymbol{\beta};\ \alpha\in\boldsymbol{\alpha},\ \beta\in\boldsymbol{\beta}} n_\alpha \left\{\left(\frac{N_{\boldsymbol{\beta}} - n_{\boldsymbol{\beta}} - \delta_{\boldsymbol{\alpha\beta}}}{N_{\boldsymbol{\beta}} - 2\delta_{\boldsymbol{\alpha\beta}}}\right)\right. \\
&\times \left\{(N_\alpha N_{\boldsymbol{\alpha}})^{-1} \sum_{\alpha'\in\boldsymbol{\alpha}} (N_{\alpha'} \left\{\epsilon^{(k)}_{\beta\alpha}\right\}^2 - N_\alpha \left\{\epsilon^{(k)}_{\beta\alpha'}\right\}^2)\right\} \\
&- \left(\frac{n_{\boldsymbol{\beta}} - \delta_{\boldsymbol{\alpha\beta}}}{N_{\boldsymbol{\beta}} - 2\delta_{\boldsymbol{\alpha\beta}}}\right) \\
&\times \left.\left\{(N_\alpha N_{\boldsymbol{\alpha}})^{-1} \sum_{\alpha'\in\boldsymbol{\alpha}} (N_{\alpha'} \left\{\epsilon^{(k)}_{\alpha\beta}\right\}^2 - N_\alpha \left\{\epsilon^{(k)}_{\alpha'\beta}\right\}^2)\right\}\right\} \\
(\mathcal{O}^\dagger\mathcal{O})^{[2]} &= (\mathcal{O}^\dagger\mathcal{O}) - (\mathcal{O}^\dagger\mathcal{O})^{[0]} - (\mathcal{O}^\dagger\mathcal{O})^{[1]}
\end{aligned} \tag{5.27}$$

The $\widehat{M}_{PQ}([\mathbf{m}])$ traces with $P+Q \leq 2$ have the following decomposition involving $h^{[0]}$ and $h^{[1]}$,

$$\widehat{M}_{10}([\mathbf{m}]) = \langle\mathcal{O}^\dagger\mathcal{O}h\rangle^{[\mathbf{m}]} = \langle\mathcal{O}^\dagger\mathcal{O}h^{[1]}\rangle^{[\mathbf{m}]} + \langle\mathcal{O}^\dagger\mathcal{O}\rangle^{[\mathbf{m}]}\langle h^{[0]}\rangle^{[\mathbf{m}]}$$

$$
\begin{aligned}
\widehat{M}_{01}([\mathbf{m}]) &= \langle \mathcal{O}^\dagger h \mathcal{O}\rangle^{[\mathbf{m}]} = \langle \mathcal{O}^\dagger \mathcal{O} h^{[1]}\rangle^{[\mathbf{m}]} + \langle \mathcal{O}^\dagger [h^{[1]}, \mathcal{O}]\rangle^{[\mathbf{m}]} + \langle \mathcal{O}^\dagger h^{[0]} \mathcal{O}\rangle^{[\mathbf{m}]} \\
\widehat{M}_{20}([\mathbf{m}]) &= \langle \mathcal{O}^\dagger \mathcal{O} h^2\rangle^{[\mathbf{m}]} = \langle \mathcal{O}^\dagger \mathcal{O} (h^{[1]})^2\rangle^{[\mathbf{m}]} + \langle \mathcal{O}^\dagger \mathcal{O}\rangle^{[\mathbf{m}]} \langle (h^{[0]})^2\rangle^{[\mathbf{m}]} \\
&\quad + 2\langle \mathcal{O}^\dagger \mathcal{O} h^{[1]}\rangle^{[\mathbf{m}]} \langle h^{[0]}\rangle^{[\mathbf{m}]} \\
\widehat{M}_{11}([\mathbf{m}]) &= \langle \mathcal{O}^\dagger h \mathcal{O} h\rangle^{[\mathbf{m}]} = \langle \mathcal{O}^\dagger \mathcal{O} (h^{[1]})^2\rangle^{[\mathbf{m}]} + \langle \mathcal{O}^\dagger [h^{[1]}, \mathcal{O}] h^{[1]}\rangle^{[\mathbf{m}]} \\
&\quad + \langle \mathcal{O}^\dagger h^{[0]} \mathcal{O}\rangle^{[\mathbf{m}]} \langle h^{[0]}\rangle^{[\mathbf{m}]} + \langle \mathcal{O}^\dagger [h^{[1]}, \mathcal{O}]\rangle^{[\mathbf{m}]} \langle h^{[0]}\rangle^{[\mathbf{m}]} \\
&\quad + \langle \mathcal{O}^\dagger [h^{[0]}, \mathcal{O}] h^{[1]}\rangle^{[\mathbf{m}]} + 2\langle \mathcal{O}^\dagger \mathcal{O} h^{[1]}\rangle^{[\mathbf{m}]} \langle h^{[0]}\rangle^{[\mathbf{m}]} \\
\widehat{M}_{02}([\mathbf{m}]) &= \langle \mathcal{O}^\dagger h^2 \mathcal{O}\rangle^{[\mathbf{m}]} = \langle \mathcal{O}^\dagger \mathcal{O} (h^{[1]})^2\rangle^{[\mathbf{m}]} + 2\langle \mathcal{O}^\dagger [h^{[1]}, \mathcal{O}] h^{[1]}\rangle^{[\mathbf{m}]} \\
&\quad + \langle \mathcal{O}^\dagger [h^{[1]}, [h^{[1]}, \mathcal{O}]]\rangle^{[\mathbf{m}]} + \langle \mathcal{O}^\dagger (h^{[0]})^2 \mathcal{O}\rangle^{[\mathbf{m}]} \\
&\quad + 2\{\langle \mathcal{O}^\dagger [h^{[0]}, \mathcal{O}] h^{[1]}\rangle^{[\mathbf{m}]} + \langle \mathcal{O}^\dagger \mathcal{O} h^{[1]}\rangle^{[\mathbf{m}]} \langle h^{[0]}\rangle^{[\mathbf{m}]}\} \\
&\quad + 2\langle \mathcal{O}^\dagger h^{[0]} [h^{[1]}, \mathcal{O}]\rangle^{[\mathbf{m}]} \qquad (5.28)
\end{aligned}
$$

and therefore the basic traces needed for evaluating $\widehat{M}_{PQ}$ with $P+Q \leq 2$ are, $\langle \mathcal{O}^\dagger \mathcal{O}\rangle^{[\mathbf{m}]}$, $\langle \mathcal{O}^\dagger (h^{[0]})^P \mathcal{O}\rangle^{[\mathbf{m}]}$, $\langle \mathcal{O}^\dagger \mathcal{O} h^{[1]}\rangle^{[\mathbf{m}]}$, $\langle \mathcal{O}^\dagger [h^{[1]}, \mathcal{O}]\rangle^{[\mathbf{m}]}$, $\langle \mathcal{O}^\dagger [h^{[0]}, \mathcal{O}]\rangle^{[\mathbf{m}]}$, $\langle \mathcal{O}^\dagger \mathcal{O} (h^{[1]})^2\rangle^{[\mathbf{m}]}$, $\langle \mathcal{O}^\dagger [h^{[1]}, \mathcal{O}] h^{[1]}\rangle^{[\mathbf{m}]}$, $\langle \mathcal{O}^\dagger [h^{[0]}, \mathcal{O}] h^{[1]}\rangle^{[\mathbf{m}]}$, $\langle \mathcal{O}^\dagger [h^{[1]}, [h^{[1]}, \mathcal{O}]]\rangle^{[\mathbf{m}]}$, $\langle \mathcal{O}^\dagger h^{[0]} [h^{[1]}, \mathcal{O}]\rangle^{[\mathbf{m}]}$ and $\langle (h^{[0]})^P\rangle^{[\mathbf{m}]}$. Propagation equations for these eleven basic traces are derived using the unitary decompositions given by (5.23, 5.27).

For $\langle \mathcal{O}^\dagger \mathcal{O}\rangle^{[\mathbf{m}]}$ trace, only $(\mathcal{O}^\dagger \mathcal{O})^{[0]}$ contributes (due to invariance properties of traces) and then the trace propagation formula is,

$$
\langle \mathcal{O}^\dagger \mathcal{O}\rangle^{[\mathbf{m}]} = \sum_{\boldsymbol{\alpha},\boldsymbol{\beta}} m_{\boldsymbol{\alpha}} m^{\times}_{\boldsymbol{\beta}} N^{-1}_{\boldsymbol{\alpha}\boldsymbol{\beta}} \left\{ \sum_{\alpha\in\boldsymbol{\alpha},\beta\in\boldsymbol{\beta}} \left\{ \epsilon^{(k)}_{\beta\alpha} \right\}^2 \right\} \qquad (5.29)
$$

The decomposition of $\langle \mathcal{O}^\dagger \mathcal{O}\rangle^{[\mathbf{m}]}$ into partial traces involving intermediate $[\mathbf{m}']$ configurations is immediate; $[\mathbf{m}'] = [\mathbf{m}] \times \left(1^\dagger_{\boldsymbol{\beta}} 1_{\boldsymbol{\alpha}}\right)$. Therefore, using (5.29),

the propagation formula for $\langle \mathcal{O}^\dagger (h^{[0]})^P \mathcal{O} \rangle^{[\mathbf{m}]}$ is given by,

$$\langle \mathcal{O}^\dagger (h^{[0]})^P \mathcal{O} \rangle^{[\mathbf{m}]} = \sum_{\boldsymbol{\alpha},\boldsymbol{\beta}} \left\{ m_{\boldsymbol{\alpha}} m^{\times}_{\boldsymbol{\beta}} N^{-1}_{\boldsymbol{\alpha}\boldsymbol{\beta}} \times \sum_{\alpha\in\boldsymbol{\alpha},\beta\in\boldsymbol{\beta}} \left\{ \epsilon^{(k)}_{\beta\alpha} \right\}^2 \right\} \times \left\{ \sum_{\boldsymbol{\tau}} \epsilon^{[\mathbf{0}]}_{\boldsymbol{\tau}} m'_{\boldsymbol{\tau}} \right\}^P \delta\left([\mathbf{m}'], [\mathbf{m}] \times (1^\dagger_{\boldsymbol{\beta}} 1_{\boldsymbol{\alpha}}) \right) \quad (5.30)$$

In order to derive the formula for $\langle \mathcal{O}^\dagger \mathcal{O} h^{[1]} \rangle^{[\mathbf{m}]}$, it should be recognized that only $(\mathcal{O}^\dagger \mathcal{O})^{[1]}$ part of $\mathcal{O}^\dagger \mathcal{O}$ contributes to the trace (as $[\boldsymbol{\nu}] \times [\mathbf{1}]$ yields $[\mathbf{0}]$ only with $[\boldsymbol{\nu}] = [\mathbf{1}]$). Using $(\mathcal{O}^\dagger \mathcal{O})^{[1]})$ given in (5.27) and $h^{[1]}$ given above (5.22) together with (5.16) immediately produces,

$$\langle \mathcal{O}^\dagger \mathcal{O} h^{[1]} \rangle^{[\mathbf{m}]} = \sum_{\boldsymbol{\alpha}\boldsymbol{\beta}} \left\{ \left[m_{\boldsymbol{\alpha}} m^{\times}_{\boldsymbol{\alpha}\boldsymbol{\beta}} N^{-1}_{\boldsymbol{\alpha}\boldsymbol{\alpha}\boldsymbol{\beta}} \right] \sum_{\alpha\in\boldsymbol{\alpha},\beta\in\boldsymbol{\beta}} \left\{ \epsilon^{(k)}_{\beta\alpha} \right\}^2 \epsilon^{[1]}_{\alpha} - \left[m_{\boldsymbol{\alpha}\boldsymbol{\beta}} m^{\times}_{\boldsymbol{\alpha}} N^{-1}_{\boldsymbol{\alpha}\boldsymbol{\alpha}\boldsymbol{\beta}} \right] \times \sum_{\alpha\in\boldsymbol{\alpha},\beta\in\boldsymbol{\beta}} \left\{ \epsilon^{(k)}_{\alpha\beta} \right\}^2 \epsilon^{[1]}_{\alpha} \right\} \quad (5.31)$$

It is interesting to note that the scalar propagation formula (5.16) for $\langle \mathcal{O}^\dagger \mathcal{O} \tilde{h} \rangle^m$ symbolically translates into (5.31). This rather important and interesting connection between scalar traces and unitary configurations traces is not yet fully understood. Using the result that $[h^{[1]}, \mathcal{O}] = \mathcal{O}'$ with $\mathcal{O}'$ defined by $\left\{ \epsilon^{(k)}_{\alpha\beta} \right\}'$s where $[h^{[1]}, \mathcal{O}] = \mathcal{O}' \Rightarrow \left\{ \epsilon^{(k)}_{\alpha\beta} \right\}' = \epsilon^{(k)}_{\alpha\beta} (\epsilon^{[1]}_{\alpha} - \epsilon^{[1]}_{\beta})$ and (5.29), give directly the formulas (changing $\left\{ \epsilon^{(k)}_{\beta\alpha} \right\}^2$ in (5.29) into $\left\{ \epsilon^{(k)}_{\beta\alpha} \right\} \left\{ \epsilon^{(k)}_{\beta\alpha} \right\}'$) for $\langle \mathcal{O}^\dagger [h^{[1]}, \mathcal{O}] \rangle^{[\mathbf{m}]}$ and $\langle \mathcal{O}^\dagger [h^{[0]}, \mathcal{O}] \rangle^{[\mathbf{m}]}$,

$$\langle \mathcal{O}^\dagger [h^{[1]}, \mathcal{O}] \rangle^{[\mathbf{m}]} = \sum_{\boldsymbol{\alpha},\boldsymbol{\beta}} m_{\boldsymbol{\alpha}} m^{\times}_{\boldsymbol{\beta}} N^{-1}_{\boldsymbol{\alpha}\boldsymbol{\beta}} \left\{ \sum_{\alpha\in\boldsymbol{\alpha},\beta\in\boldsymbol{\beta}} \left\{ \epsilon^{(k)}_{\beta\alpha} \right\}^2 (\epsilon^{[1]}_{\beta} - \epsilon^{[1]}_{\alpha}) \right\} \quad (5.32)$$

$$\langle \mathcal{O}^\dagger [h^{[0]}, \mathcal{O}] \rangle^{[\mathbf{m}]} = \sum_{\boldsymbol{\alpha},\boldsymbol{\beta}} m_{\boldsymbol{\alpha}} m^{\times}_{\boldsymbol{\beta}} N^{-1}_{\boldsymbol{\alpha}\boldsymbol{\beta}} \left\{ \sum_{\alpha\in\boldsymbol{\alpha},\beta\in\boldsymbol{\beta}} \left\{ \epsilon^{(k)}_{\beta\alpha} \right\}^2 (\epsilon^{[0]}_{\beta} - \epsilon^{[0]}_{\boldsymbol{\alpha}}) \right\} \quad (5.33)$$

In order to derive the expression for $\langle \mathcal{O}^\dagger \mathcal{O} (h^{[1]})^2 \rangle^{[m]}$, the SPE and TBME of $\mathcal{O}^\dagger \mathcal{O}$ and $(h^{[1]})^2$ operators as given by (5.22) and (5.24 - 5.26) and the corresponding unitary decompositions given by (5.23) and (5.27) respectively are used. The trace orthogonality equation (3.13) and the trace propagation equations (2.71, 2.72) give,

$$\begin{aligned}
\langle \mathcal{O}^\dagger \mathcal{O} (h^{[1]})^2 \rangle^{[m]} &= \left[\sum_{\boldsymbol{\alpha}} [\mathcal{E}_{\boldsymbol{\alpha}}(\{h^{[1]}\}^2)] m_{\boldsymbol{\alpha}} + \sum_{\boldsymbol{\alpha} \geq \boldsymbol{\beta}} [C_{\boldsymbol{\alpha}\boldsymbol{\beta}}(\{h^{[1]}\}^2)] m_{\boldsymbol{\alpha}\boldsymbol{\beta}} \right] \\
&\times \left[\sum_{\boldsymbol{\alpha}} [\mathcal{E}_{\boldsymbol{\alpha}}(\mathcal{O}^\dagger \mathcal{O})] m_{\boldsymbol{\alpha}} + \sum_{\boldsymbol{\alpha} \geq \boldsymbol{\beta}} [C_{\boldsymbol{\alpha}\boldsymbol{\beta}}(\mathcal{O}^\dagger \mathcal{O})] m_{\boldsymbol{\alpha}\boldsymbol{\beta}} \right] \\
&+ \sum_{\boldsymbol{\alpha}} m_{\boldsymbol{\alpha}} m^{\times}_{\boldsymbol{\alpha}} N^{-1}_{\boldsymbol{\alpha}\boldsymbol{\alpha}} \left[\sum_{\alpha \in \boldsymbol{\alpha}} N_\alpha \times \right. \\
&\left\{ [\mathcal{E}^{[1]}_\alpha \{(h^{[1]})^2\}] + \sum_{\boldsymbol{\beta}} (m_{\boldsymbol{\beta}} - \delta_{\boldsymbol{\alpha}\boldsymbol{\beta}}) [\mathcal{E}^{[1];\boldsymbol{\beta}}_\alpha \{(h^{[1]})^2\}] \right\} \\
&\times \left. \left\{ [\mathcal{E}^{[1]}_\alpha (\mathcal{O}^\dagger \mathcal{O})] + \sum_{\beta \in \boldsymbol{\beta}} (m_{\boldsymbol{\beta}} - \delta_{\boldsymbol{\alpha}\boldsymbol{\beta}}) [\mathcal{E}^{[1];\boldsymbol{\beta}}_\alpha (\mathcal{O}^\dagger \mathcal{O})] \right\} \right] \\
&+ \sum_{\boldsymbol{\alpha} \geq \boldsymbol{\beta}} m_{\boldsymbol{\alpha}\boldsymbol{\beta}} m^{\times}_{\boldsymbol{\alpha}\boldsymbol{\beta}} N^{-1}_{\boldsymbol{\alpha}\boldsymbol{\beta}\boldsymbol{\alpha}\boldsymbol{\beta}} \\
&\times \left[\left\{ \sum_{\alpha \in \boldsymbol{\alpha}, \beta \in \boldsymbol{\beta}} [C_{\alpha\beta}(\{h^1\}^2)][C_{\alpha\beta}(\mathcal{O}^\dagger \mathcal{O})] N_{\alpha\beta} (1 + \delta_{\alpha\beta}) \right\} (1 + \delta_{\boldsymbol{\alpha}\boldsymbol{\beta}})^{-1} \right]. \qquad (5.34)
\end{aligned}$$

Trace propagation formulas for $\langle \mathcal{O}^\dagger [h^{[1]}, \mathcal{O}] h^{[1]}) \rangle^{[m]}$ and $\langle \mathcal{O}^\dagger [h^{[0]}, \mathcal{O}] h^{[1]}) \rangle^{[m]}$ follow from the use of (5.31) and the $\mathcal{O}'$ operator defined above (5.32),

$$\begin{aligned}
\langle \mathcal{O}^\dagger [h^{[1]}, \mathcal{O}] h^{[1]}) \rangle^{[m]} &= \sum_{\boldsymbol{\alpha}, \boldsymbol{\beta}} \left\{ \left[m_{\boldsymbol{\alpha}} m^{\times}_{\boldsymbol{\alpha}\boldsymbol{\beta}} N^{-1}_{\boldsymbol{\alpha}\boldsymbol{\alpha}\boldsymbol{\beta}} \sum_{\alpha \in \boldsymbol{\alpha},\, \beta \in \boldsymbol{\beta}} \left\{ \epsilon^{(k)}_{\beta\alpha} \right\}^2 \epsilon^{[1]}_\alpha (\epsilon^{[1]}_\beta - \epsilon^{[1]}_\alpha) \right] \right. \\
&+ \left. \left[m_{\boldsymbol{\alpha}\boldsymbol{\beta}} m^{\times}_{\boldsymbol{\alpha}} N^{-1}_{\boldsymbol{\alpha}\boldsymbol{\alpha}\boldsymbol{\beta}} \sum_{\alpha \in \boldsymbol{\alpha},\, \beta \in \boldsymbol{\beta}} \left\{ \epsilon^{(k)}_{\alpha\beta} \right\}^2 \epsilon^{[1]}_\alpha (\epsilon^{[1]}_\beta - \epsilon^{[1]}_\alpha) \right] \right\} \qquad (5.35)
\end{aligned}$$

$$\langle \mathcal{O}^\dagger [h^{[0]}, \mathcal{O}] h^{[1]}) \rangle^{[\mathrm{m}]} = \sum_{\boldsymbol{\alpha},\boldsymbol{\beta}} \left\{ \left[m_{\boldsymbol{\alpha}} m^{\times}_{\boldsymbol{\alpha\beta}} N^{-1}_{\boldsymbol{\alpha\alpha\beta}} \sum_{\alpha\in\boldsymbol{\alpha},\, \beta\in\boldsymbol{\beta}} \left\{ \epsilon^{(k)}_{\beta\alpha} \right\}^2 \epsilon^{[1]}_{\alpha} (\epsilon^{[0]}_{\boldsymbol{\beta}} - \epsilon^{[0]}_{\boldsymbol{\alpha}}) \right] \right.$$

$$\left. + \left[m_{\boldsymbol{\alpha\beta}} m^{\times}_{\boldsymbol{\alpha}} N^{-1}_{\boldsymbol{\alpha\alpha\beta}} \sum_{\alpha\in\boldsymbol{\alpha},\, \beta\in\boldsymbol{\beta}} \left\{ \epsilon^{(k)}_{\alpha\beta} \right\}^2 \epsilon^{[1]}_{\alpha} (\epsilon^{[0]}_{\boldsymbol{\beta}} - \epsilon^{[0]}_{\boldsymbol{\alpha}}) \right] \right\} \tag{5.36}$$

The expression for $\langle \mathcal{O}^\dagger [h^{[1]}, [h^{[1]}, \mathcal{O}]] \rangle^{[\mathrm{m}]}$ is obtained by recognizing that $[h^{[1]}, [h^{[1]}, \mathcal{O}]] \Rightarrow [h^{[1]}, \mathcal{O}'] \Rightarrow \mathcal{O}''$ defined by $\left(\epsilon^{(k)}_{\alpha\beta}\right)'' = \epsilon^{(k)}_{\alpha\beta} \left(\epsilon^{[1]}_{\alpha} - \epsilon^{[1]}_{\beta}\right)^2$ and then using (5.29),

$$\langle \mathcal{O}^\dagger [h^{[1]}, [h^{[1]}, \mathcal{O}]] \rangle^{[\mathrm{m}]} = \sum_{\boldsymbol{\alpha\beta}} \left\{ m_{\boldsymbol{\alpha}} m^{\times}_{\boldsymbol{\beta}} N^{-1}_{\boldsymbol{\alpha\beta}} \right\} \sum_{\alpha\in\boldsymbol{\alpha},\, \beta\in\boldsymbol{\beta}} \left\{ \epsilon^{(k)}_{\beta\alpha} \right\}^2 \{ \epsilon^{[1]}_{\beta} - \epsilon^{[1]}_{\alpha} \}^2 \tag{5.37}$$

The expression for $\langle \mathcal{O}^\dagger h^{[0]} [h^{[1]}, \mathcal{O}] \rangle^{[\mathrm{m}]}$ follows easily from the $\left(\epsilon^{(k)}_{\alpha\beta}\right)'$ of $[h^{[1]}, \mathcal{O}]$ and (5.30),

$$\langle \mathcal{O}^\dagger h^{[0]} [h^{[1]}, \mathcal{O}] \rangle^{[\mathrm{m}]} = \sum_{\boldsymbol{\alpha},\boldsymbol{\beta}} \left\{ m_{\boldsymbol{\alpha}} m^{\times}_{\boldsymbol{\beta}} N^{-1}_{\boldsymbol{\alpha\beta}} \right\} \left[\sum_{\alpha\in\boldsymbol{\alpha},\, \beta\in\boldsymbol{\beta}} \left\{ \epsilon^{(k)}_{\beta\alpha} \right\}^2 (\epsilon^{[1]}_{\beta} - \epsilon^{[1]}_{\alpha}) \right]$$

$$\times \left[\left\{ \sum_{\boldsymbol{\tau}} \epsilon^{[0]}_{\boldsymbol{\tau}} m'_{\boldsymbol{\tau}} \right\} \delta \left([\mathrm{m}'], [\mathrm{m}] \times \left(1^{\dagger}_{\boldsymbol{\beta}} 1_{\boldsymbol{\alpha}} \right) \right) \right]. \tag{5.38}$$

Finally, the expression for $\langle (h^{[0]})^P \rangle^{[\mathrm{m}]}$ is,

$$\langle (h^{[0]})^P \rangle^{[\mathrm{m}]} = \left\{ \sum_{\boldsymbol{\alpha}} m_{\boldsymbol{\alpha}} \epsilon^{[0]}_{\boldsymbol{\alpha}} \right\}^P \tag{5.39}$$

It should be mentioned that the formulas (5.29 - 5.39) are verified numerically by using (5.12) and (5.10).

5.7.2 pn systems

For pn one-body transition operators that belong to categories $[B]$, $[C]$ or $[D]$ (5.2) and with pn unitary configurations ($[\mathrm{m}] \rightarrow [\mathrm{m_p}, \mathrm{m_n}]$), the results in

(5.29 - 5.39) will apply when the conventions given in Sect. 3.1.5 are used. It should be stressed that the order of the indices in $\epsilon^{(k)}_{\alpha\beta}$ should be kept as they are given in Eqs. 5.22 - 5.39 and without this, the results for operators belonging to categories $[C]$ and $[D]$ will be wrong (the phase relation $\epsilon^{(k)}_{\alpha\beta} = (-1)^{j_\alpha - j_\beta}\epsilon^{(k)}_{\beta\alpha}$ is valid only when α, $\beta \in$ p or n; its extension to the case with $\alpha \in$ p, $\beta \in$ n or $\alpha \in$ n $\beta \in$ p is immediate). For pn one-body transition operators that belong to categories $[B]$, $[C]$ or $[D]$ (5.2) and with pn unitary configurations ($[\mathbf{m}] \rightarrow [\mathbf{m_p}, \mathbf{m_n}]$), the results in (5.29 - 5.39) will apply when the conventions given in Sect. 3.1.5 are used. As an example the TBME for $GT(\beta^{\pm})$ operator can be written down using (5.25),

$$\begin{aligned} V^{k'}_{\alpha_p\beta_n\gamma_p\delta_n}(GT(\beta^-)) &= -\epsilon^{(1)}_{\alpha_p\delta_n}\epsilon^{(1)}_{\gamma_p\beta_n}\left\{\begin{array}{ccc} j_\beta & j_\gamma & k=1 \\ j_\delta & j_\alpha & k' \end{array}\right\} \\ V^{k'}_{\alpha_n\beta_p\gamma_n\delta_p}(GT(\beta^-)) &= (-1)^{j_\alpha+j_\beta+j_\gamma+j_\delta+1}\epsilon^{(1)}_{\beta_p\gamma_n}\epsilon^{(1)}_{\delta_p\alpha_n}\left\{\begin{array}{ccc} j_\alpha & j_\delta & k=1 \\ j_\gamma & j_\beta & k' \end{array}\right\} \end{aligned} \tag{5.40}$$

The phase relation

$$\epsilon^{(1)}_{\alpha_p\delta_n} = (-1)^{j_\alpha - j_\delta}\epsilon_{\delta_p\alpha_n} \tag{5.41}$$

immediately shows that $V^{k'}_{\alpha_n\beta_p\gamma_n\delta_p}(GT(\beta^-)) = V^{k'}_{\alpha_p\beta_n\gamma_p\delta_n}(GT(\beta^-))$ as required. The TBME for $(GT(\beta^+))$ operator follow easily from the second equation in (5.40),

$$V^{k'}_{\alpha_p\beta_n\gamma_p\delta_n}(GT(\beta^+)) = (-1)^{j_\alpha+j_\beta+j_\gamma+j_\delta+1}\epsilon^{(1)}_{\beta_n\gamma_p}\epsilon^{(1)}_{\delta_n\alpha_p}\left\{\begin{array}{ccc} j_\alpha & j_\delta & k=1 \\ j_\gamma & j_\beta & k' \end{array}\right\} \tag{5.42}$$

Finally note that $\epsilon^{(1)}_{\alpha_n\beta_p}$ also satisfies the phase relation (5.41); $\epsilon^{(1)}_{\alpha_n\beta_p} = (-1)^{j_\alpha - j_\beta}\epsilon^{(1)}_{\beta_n\alpha_p}$.

5.7.3 Partial $\mathbf{M}_{PQ}([\mathbf{m}],[\mathbf{m}'])$ moments

Given the initial configuration [m], the $\epsilon^{(k)}_{\alpha\beta}$ terms appearing in (5.29 - 5.39) immediately define the projection operator $\mathbf{P}([\mathbf{m}'])$ in (5.12) or in other words uniquely the [m'] configuration; $[\mathbf{m}'] = [\mathbf{m}] \times \left(1^{\dagger}_{\alpha} 1_{\beta}\right)$. It is easy to obtain $\mathbf{M}_{PQ}([\mathbf{m},\mathbf{m}'])$ moments by calculating $\widehat{M}_{PQ}([\mathbf{m}])$ moments for different $\epsilon^{(k)}_{\alpha\beta}$ terms separately. We will illustrate this with an example. Let us consider $GT(\beta^-)$ operator in a 7-orbit shell model space consisting of ds and fp-shells with ds-shell as one unitary orbit and fp-shell as another unitary orbit. Then there are two unitary orbits for protons and two for neutrons labelled as $\boldsymbol{\alpha} = 1,2,3$ and 4 respectively. From the definition of $\epsilon^{(k)}_{\alpha\beta}$ given in (5.3), it is clear that the partial moments are non-zero only for $S = S'$. In other words, for non-zero partial moments both α(p) and β(n) should belong to ds-shell or both should belong to fp-shell in this particular example. Therefore for a unitary configuration $[m_1, m_2, m_3, m_4]$, where $m_1 \in \boldsymbol{\alpha} = 1$, $m_2 \in \boldsymbol{\alpha} = 2$, $m_3 \in \boldsymbol{\alpha} = 3$ and $m_4 \in \boldsymbol{\alpha} = 4$, the possible final configurations are $[m_1+1, m_2, m_3-1, m_4]$ and $[m_1, m_2+1, m_3, m_4-1]$ where for the first configuration $\epsilon^{(k)}_{\alpha\beta}$ with $\alpha \in \boldsymbol{\alpha} = 1$ and $\beta \in \boldsymbol{\beta} = 3$ will contribute while for the second configuration $\epsilon^{(k)}_{\alpha\beta}$ with $\alpha \in \boldsymbol{\alpha} = 2$ and $\beta \in \boldsymbol{\beta} = 4$ will contribute. Therefore by putting $\epsilon^{(k)}_{\alpha\beta} = 0$ for $\alpha \in \boldsymbol{\alpha} = 2$, $\beta \in \boldsymbol{\beta} = 4$, gives $\widehat{M}_{PQ}([\mathbf{m}])/\widehat{M}_{00}([\mathbf{m}]) = \mathbf{M}_{PQ}([m_1, m_2, m_3, m_4], [m_1+1, m_2, m_3-1, m_4])/\ \mathbf{M}_{00}([m_1, m_2, m_3, m_4], [m_1+1, m_2, m_3-1, m_4])$ and similarly by putting $\epsilon^{(k)}_{\alpha\beta} = 0$ for $\alpha \in \boldsymbol{\alpha} = 1$, $\beta \in \boldsymbol{\beta} = 3$, gives $\widehat{M}_{PQ}\left([m_1, m_2, m_3, m_4]\right)/\widehat{M}_{00}\left([m_1, m_2, m_3, m_4]\right) = \mathbf{M}_{PQ}([m_1, m_2, m_3, m_4], [m_1, m_2+1, m_3, m_4-1])/\mathbf{M}_{00}([m_1, m_2, m_3, m_4], [m_1, m_2+1, m_3, m_4-1])$. With the same numerical example considered in Sect. 5.5 (i.e. $m_p = 4, m_n = 6 \rightarrow m_p = 5, m_n = 5$), and using the above equality between $\widehat{M}_{PQ}([\mathbf{m}])$ and

$\mathbf{M}_{PQ}([\mathbf{m}],[\mathbf{m}'])$ it is explicitly verified that (5.29 - 5.39) reproduce exactly the numbers given by (5.12, 5.10, 5.3).

5.8 Test of moment method for constructing $\mathbf{I}^h_{\mathcal{O}(GT)}$

The results of Sects. 5.4 and 5.5 allow one to construct the exact NIP strength density $\mathbf{I}^h_{\mathcal{O}}$ for one-body transition operators and the results of Sect. 5.7 via superposition of partial strength densities $\mathbf{I}^{h;[\mathbf{m}],[\mathbf{m}']}_{\mathcal{O}}$ represented by bivariate Gaussians with their five parameters calculated directly (without recourse to spherical configurations) in terms of bivariate moments $\mathbf{M}_{PQ}([\mathbf{m}],[\mathbf{m}'])$. In order to test the moment method (which is rapid and produces a smooth density) in *large spaces*, a numerical test is carried out using $GT(\beta^-)$ operator. Using the same s.p. orbits and SPE as given in the numerical example of Sect. 5.5 and the unitary orbits to be $[1d_{5/2}]$, $[2s_{1/2},1d_{3/2}]$, $[f_{7/2}]$ and $[2p_{3/2},1f_{5/2},2p_{1/2}]$ with $\boldsymbol{\alpha} = 1,2,3$ and 4 respectively for protons and similarly for neutrons with $\boldsymbol{\alpha} = 5,6,7$ and 8 respectively, the NIP strength density is calculated for $(m_p,m_n) = (4,6) \Rightarrow (m'_p,m'_n) = (5,5)$ with $S = 0,1$ and 2 (note that $s = 0$ for ds and $s = 1$ for fp-shell orbits). In this example there are 385 (35 $S = 0$, 116 $S = 1$ and 234 $S = 2$) unitary configurations against 5748 spherical configurations. The exact density is calculated using the formalism given in Sect. 5.4; this is denoted by $\mathbf{I}^h_{\mathcal{O}(GT);Ex}$. The strength density as superposition of bivariate Edgeworth corrected Gaussian representation (2.21) for the partial $\mathbf{I}^{h;[\mathbf{m}],[\mathbf{m}']}_{\mathcal{O}(GT)}$ densities is constructed using the results in Sects. 5.4, 5.5 (i.e. using the exact density to calculate k_{rs} with $r+s = 3,4$); the resulting

Figure 5.1

NIP strength densities $\mathbf{I}^{h}_{\mathcal{O}(GT)}$ and their S-decompositions for $GT(\beta^{-})$ transition operator. The densities $\mathbf{I}^{h}_{\mathcal{O}(GT)}$ are in MeV^{-2} units. Shown in the figures are $\ell og(\mathbf{I}^{h}_{\mathcal{O}(GT)}(E,E'))$ for E and E' upto 40 MeV:

(a) $S=0$ exact density $\mathbf{I}^{h,S=0}_{\mathcal{O}(GT(\beta^{-}));Ex}$,

(b) $\mathbf{I}^{h,S=0}_{\mathcal{O}(GT(\beta^{-}));\mathcal{G}}$,

(c) $S=1$ exact density $\mathbf{I}^{h,S=1}_{\mathcal{O}(GT(\beta^{-}));Ex}$,

(d) $\mathbf{I}^{h,S=1}_{\mathcal{O}(GT(\beta^{-}));\mathcal{G}}$,

(e) $S=2$ exact density $\mathbf{I}^{h,S=2}_{\mathcal{O}(GT(\beta^{-}));Ex}$,

(f) $\mathbf{I}^{h,S=2}_{\mathcal{O}(GT(\beta^{-}));\mathcal{G}}$,

(g) Exact total $(S=0\oplus 1\oplus 2)$ density, $\mathbf{I}^{h}_{\mathcal{O}(GT(\beta^{-}));Ex}$,

(h) Total $(S=0\oplus 1\oplus 2)$ density $\mathbf{I}^{h}_{\mathcal{O}(GT(\beta^{-}));\mathcal{G}}$,

(i) Total $(S=0\oplus 1\oplus 2)$ density $\mathbf{I}^{h}_{\mathcal{O}(GT(\beta^{-}));Ed}$.

See text for the definitions of the bivariate densities $\mathbf{I}^{h}_{\mathcal{O}(GT);\mathcal{G}}$ and $\mathbf{I}^{h}_{\mathcal{O}(GT);Ed}$ and also for all the calculational details.

S=0
5.0
3.75
2.5
1.25
0
E'(MeV)
E (MeV)
40.0
32.0
24.0
16.0
8.0
0
(a)
S=0
5.0
3.75
2.5
1.25
0
E'(MeV)
E (MeV)
40.0
32.0
24.0
16.0
0
(b)

log $(I^{h;s}(E,E')_{\partial(GT);Ex})$
S = 1
7.0
5.25
3.5
1.75
0
E'(MeV)
E (MeV)
8.0
16.0
24.0
32.0
40.0
(c)
log $(I^{h;s}(E,E')_{\partial(GT);q})$
S = 1
7.0
5.25
3.5
1.75
0
E'(MeV)
E (MeV)
8.0
16.0
24.0
32.0
40.0
(d)

S=2
8.0
6.0
4.0
2.0
0
E (MeV)
E'(MeV)
40.0
32.0
24.0
16.0
8.0
0
(e)
S=2
8.0
6.0
4.0
2.0
0
E (MeV)
E'(MeV)
40.0
32.0
24.0
16.0
8.0
0
(f)

TOTAL
8.0
6.0
4.0
2.0
0
E (MeV)
E'(MeV)
0
8.0
16.0
24.0
32.0
40.0
(g)
(h)
(i)

density is denoted by $\mathbf{I}^{h}_{\mathcal{O}(GT);Ed}$. The strength density as a superposition of bivariate Gaussian forms for $\mathbf{I}^{h;[\mathbf{m}],[\mathbf{m}']}_{\mathcal{O}(GT)}$ densities is constructed using the results of Sect. 5.7; the resulting density is denoted by $\mathbf{I}^{h}_{\mathcal{O}(GT);\mathcal{G}}$. In the construction of bivariate Gaussian or Edgeworth form, care has been taken to treat the singularities properly (this situation arises for example if correlation coefficient is unity). Choosing a bin size of 4 $MeV \times 4\ MeV$ (this choice of the bin size follows from [Dr-77b]), histograms for $\mathbf{I}^{h}_{\mathcal{O}(GT);Ex}$, $\mathbf{I}^{h}_{\mathcal{O}(GT);Ed}$ and $\mathbf{I}^{h}_{\mathcal{O}(GT);\mathcal{G}}$ and their S - decompositions are constructed and some of the results are shown in Figs. 5.1a - 5.1i. It is clear from the figures that the bivariate Gaussian representation of $\mathbf{I}^{h;[\mathbf{m}],[\mathbf{m}']}_{\mathcal{O}(GT)}$ describes the exact results for total density as well as their S - decompositions. It should be added that in the cases when k_{rs} with $r+s = 3,4$ are needed (i.e. departures from bivariate Gaussian are important), these higher order cumulants can be calculated using (5.10) for a random sampling of $([\mathbf{m}],[\mathbf{m}'])$ configurations and use them in determining the cumulants for all the $([\mathbf{m}],[\mathbf{m}'])$ configurations (there are various ways one can divide the unitary configurations into classes or groups). Alternatively it is also possible to use the estimates for k_{rs} as given by the scalar trace formulas of Sect. 5.6 and discussed for example following (5.20). Finally it should be mentioned that agreements similar to what are shown in Figs. 5.1a - 5.1i are also obtained for $GT(\beta^{+})$ operator.

5.9 Summary

Complete formalism for constructing NIP strength densities, which enter into IP strength densities as one of the convolution factors, and their unitary orbit decompositions is worked out for one-body transition operators and tested in a

large space example. The formalism given in Sects. 5.4 - 5.7 together with the spreading densities generated by interactions, is employed in the next chapter to give a method for calculating β-decay rates for massive presupernova stars.

Chapter 6

Interacting Particle Bivarite GT Strength Densities in SAT-LSS and β-Decay Rates for Some $A > 60$ fp-Shell Nuclei Relevant for Presupernova Stars

6.1 Introduction

Given a one plus two-body hamiltonian (H) and a transition operator ($\mathcal{O}$), in SAT-LSS the smoothed form of the IP transition strength densities ($\mathbf{I}^H_{\mathcal{O}}(E_i, E_f)$) in general takes a bivariate convolution form [Fr-87a, Fr-88b] with the NIP strength density being convoluted with a spreading bivariate Gaussian due to interactions. The construction of IP bivariate strength densities, allows one to address a wide variety of nuclear physics and nucler astrophysics problems; earlier applications, of the convolution form, in nuclear physics are given in [Fr-87a, Fr-88b, Po-91]. Applying the construction, explicitly in terms of the (partial) bivariate moments, of the IP bivariate strength densities, for the first

time to the problems of interest in nuclear astrophysics (it is well known [Wo-80a, Wo-80b, Ra-84, Pi-94], that knowledge of level densities, partition functions, orbit occupancy numbers, β-decay strength densities and other related statistical quantities is essential for a quantitative study of various problems in nuclear astrophysics – therefore SAT-LSS is ideally suited for applications in this important area of physics), this chapter deals with the construction of β-decay Gamow - Teller (GT) strength distributions and in particular for $A > 60$ neutron excess fp-shell nuclei that are of interest in presupernova evolution calculations. The β-decay rates for these nuclei play a very important role [Be-79, Au-90] in determining the structure of the core of massive presupernova stars and hence on their subsequent evolution towards gravitational collapse and supernova explosion phases.

The earlier calculations of β-decay rates at zero temperature mainly used the "gross theory" (which is indeed a statistical theory of β-decay) due to Takahashi and Yamada [Ta-69] and the microscopic quasiparticle random phase approximation (QRPA) [Kl-84]; shell model calculations are feasible and available for lighter ($A < 40$) nuclei [Br-85]. Fuller, Fowler and Newman [Fu-80] (hereafter referred as FFN) for the first time dealt with in detail the problem of calculating β-decay rates (and also other steller weak interaction rates which include electron capture rates, neutrino energy loss rates etc.) at non-zero temperatures appropriate for presupernova evolution studies and tabulated the rates for 226 ds and fp-shell nuclei with $21 \leq A \leq 60$. They (FFN) have used experimental data for energy levels and transition matrix elements (comparative half lifes $\ell og(ft)_{ij}$) where available and for the unmeasured matrix elements, zeroth order shell model calculations and also detailed shell model results (for GT strengths) wherever available are employed; recently Oda et al

[Od-94] extended for ds-shell nuclei the FFN tabulations by using the results of complete shell model calculations with Wildenthal's interaction [Wi-84]. Steller evolution calculations including FFN rates showed that the FFN rates affect significantly the evolution of presupernova stars - they led to greater reduction of electron fraction throughout the core [We-85]. However more recently Aufderheide et al [Au-90] pointed out that the calculation of presupernova evolution generates neutron rich cores and therefore emphasized the need for reliable β-decay rates for neutron rich $A > 60$ fp-shell nuclei; they tentatively conclude that β-decay of neutron rich nuclei (particularly ^{63}Co; they in fact studied $^{60,62,63,64}Co$ isotopes) prevents the decrease of overall electron fraction and affects substantially the post-core-silicon-burning behavior. With this observation, the calculation of β-decay rates for $A > 60$ neutron excess nuclei has acquired new impetus. Calculations of the rates involve the construction of the bivariate GT strength densities. So far only [Au-90, Au-94, Ka-91] dealt with the neutron excess $A > 60$ fp-shell nuclei; in Ref. [Au-90, Au-94] Aufderheide et al used methods similar to that of FFN and in Ref. [Ka-91] Kar, Sarkar and Ray (hereafter referred as KSR) introduced a method, combining the ideas of the "gross theory" with a zeroth order SAT result (described ahead in Sect. 6.4.3). In this chapter a method is developed for β-decay rates calculations where GT bivariate strength densities are explicitly constructed, starting with an effective nucleon - nucleon interaction, using the bivariate convolution form (Eq. (6.2) ahead) for $\mathbf{I}^{H}_{\mathcal{O}(GT)}$. The theory for constructing NIP GT strength densities, which enter into the IP theory as one of the convolution factors, is given in the preceding chapter. We will now give a preview.

Sect. 6.2 gives the IP theory for constructing GT strength densities and

Sect. 6.3 gives the formalism for calculating β-decay rates where $\mathbf{I}^{H}_{\mathcal{O}(GT)}$ and the state density $I^{H}(E)$ enter explicitly. In Sect. 6.4 the calculational procedure is described. Sect. 6.5 deals with GT NEWSR strength. Sect. 6.6 gives the results of β-decay rates at densities and temperatures typical of presupernova stars. Finally a summary is given in Sect. 6.7. The results given in this chapter are first reported in [Ko-94b].

6.2 IP strength densities for Gamow - Teller transition operator

Given $H = \mathbf{h} + \mathbf{V}$ the IP strength densities $\mathbf{I}^{H=\mathbf{h}+\mathbf{V}}_{\mathcal{O}}(E_i, E_f)$ produced by a transition operator $\mathcal{O}$, as derived in [Fr-87a, Fr-88b], will take a bivariate convolution form with the two convoluting functions being the NIP strength density $\mathbf{I}^{\mathbf{h}}_{\mathcal{O}}$ and a normalized spreading bivariate Gaussian ($\rho_{BIV-\mathcal{G}}$) due to $\mathbf{V}$ (interactions),

$$\mathbf{I}^{H=\mathbf{h}+\mathbf{V}}_{\mathcal{O}}(E_i, E_f) = \mathbf{I}^{\mathbf{h}}_{\mathcal{O}} \otimes \rho^{\mathbf{V}}_{\mathcal{O};BIV-\mathcal{G}}[E_i, E_f] \tag{6.1}$$

In large spectroscopic spaces, just as in the case of state densities (Chapter 3, Eqs. (3.3, 3.4)), one can use an extended version of (6.1) with some plausible approximations [Fr-87a, Fr-88b, Ko-89] by decomposing the space into S-subspaces and unitary configurations. For the $GT(\beta^{\pm})$ operator, using pn unitary configurations and noting that GT operator does not connect (5.3) two different S-subspaces, the IP strength density with partitioning, following [Fr-87a, Fr-88b, Ko-89] together with an additional approximation described ahead, is,

$$\mathbf{I}^{H=\mathrm{h}+\mathrm{V}}_{\mathcal{O}(GT)}(E_i,E_f)=\sum_{S}\sum_{[\mathbf{m}^i_p,\mathbf{m}^i_n],[\mathbf{m}^f_p,\mathbf{m}^f_n]\in S}$$

$$\mathbf{I}^{\mathrm{h};[\mathbf{m}^i_p,\mathbf{m}^i_n],[\mathbf{m}^f_p,\mathbf{m}^f_n]}_{\mathcal{O}(GT)}\otimes\rho^{\mathrm{V};[\mathbf{m}^i_p,\mathbf{m}^i_n],[\mathbf{m}^f_p,\mathbf{m}^f_n]}_{\mathcal{O}(GT)}[E_i,E_f]\,; \tag{6.2a}$$

$$\rho^{\mathrm{V};[\mathbf{m}^i_p,\mathbf{m}^i_n],[\mathbf{m}^f_p,\mathbf{m}^f_n]}_{\mathcal{O}(GT)}(x,y)=$$

$$\rho^{\mathrm{V}}_{\mathcal{O}(GT);BIV-\mathcal{G}}(x,y;0,0,\sigma_{\mathrm{V}}([\mathbf{m}^i_p,\mathbf{m}^i_n]),\sigma_{\mathrm{V}}([\mathbf{m}^f_p,\mathbf{m}^f_n]),\bar{\zeta}) \tag{6.2b}$$

In (6.2b) one is assuming that for $\rho^{\mathrm{V};[\mathbf{m}^i_p,\mathbf{m}^i_n],[\mathbf{m}^f_p,\mathbf{m}^f_n]}_{\mathcal{O}(GT)}$, the marginal centroids are $M_{10}=\langle\mathcal{O}^\dagger\mathcal{O}\mathbf{V}\rangle^{[\mathbf{m}^i_p,\mathbf{m}^i_n]}/\langle\mathcal{O}^\dagger\mathcal{O}\rangle^{[\mathbf{m}^i_p,\mathbf{m}^i_n]}$, $M_{01}=\langle\mathcal{O}\mathcal{O}^\dagger\mathbf{V}\rangle^{[\mathbf{m}^f_p,\mathbf{m}^f_n]}/\langle\mathcal{O}\mathcal{O}^\dagger\rangle^{[\mathbf{m}^f_p,\mathbf{m}^f_n]}$, and the marginal variances are $\mathcal{M}_{20}=\langle\mathcal{O}^\dagger\mathcal{O}\mathbf{V}^2\rangle^{[\mathbf{m}^i_p,\mathbf{m}^i_n]}/\langle\mathcal{O}^\dagger\mathcal{O}\rangle^{[\mathbf{m}^i_p,\mathbf{m}^i_n]}-\{M_{10}\}^2$, $\mathcal{M}_{02}=\langle\mathcal{O}\mathcal{O}^\dagger\mathbf{V}^2\rangle^{[\mathbf{m}^f_p,\mathbf{m}^f_n]}/\langle\mathcal{O}\mathcal{O}^\dagger\rangle^{[\mathbf{m}^f_p,\mathbf{m}^f_n]}-\{M_{01}\}^2$ and they in turn are assumed to be close to the corresponding state density centroids and variances. This approximation is extremely well satisfied by fp-shell interactions. In $S=0$ spaces, with one unitary orbit each for protons and neutrons and $(m_p,m_n)\longrightarrow(m_p\pm1,m_n\mp1)$ for $\beta^\mp$ transitions, the above approximations are equivalent to assuming that $M_{10}=\langle\mathcal{O}^\dagger\mathcal{O}\mathbf{V}\rangle^{m_p,m_n}/\langle\mathcal{O}^\dagger\mathcal{O}\rangle^{m_p,m_n}\simeq\langle\mathbf{V}\rangle^{m_p,m_n}=0$, $\mathcal{M}_{01}=\langle\mathcal{O}^\dagger\mathbf{V}\mathcal{O}\rangle^{m_p,m_n}/\langle\mathcal{O}^\dagger\mathcal{O}\rangle^{m_p,m_n}=\langle\mathcal{O}\mathcal{O}^\dagger\mathbf{V}\rangle^{m_p\pm1,m_n\mp1}/\langle\mathcal{O}\mathcal{O}^\dagger\rangle^{m_p\pm1,m_n\mp1}\simeq\langle\mathbf{V}\rangle^{m_p\pm1,m_n\mp1}=0$, $\mathcal{M}_{20}=\langle\mathcal{O}^\dagger\mathcal{O}\mathbf{V}^2\rangle^{m_p,m_n}/\langle\mathcal{O}^\dagger\mathcal{O}\rangle^{m_p,m_n}-M^2_{10}\simeq\langle\mathbf{V}^2\rangle^{m_p,m_n}$ and $\mathcal{M}_{02}=\langle\mathcal{O}^\dagger\mathbf{V}^2\mathcal{O}\rangle^{m_p,m_n}/\langle\mathcal{O}^\dagger\mathcal{O}\rangle^{m_p,m_n}-M^2_{01}=\langle\mathcal{O}\mathcal{O}^\dagger\mathbf{V}^2\rangle^{m_p\pm1,m_n\mp1}/\langle\mathcal{O}\mathcal{O}^\dagger\rangle^{m_p\pm1,m_n\mp1}-M^2_{01}\simeq\langle\mathbf{V}^2\rangle^{m_p\pm1,m_n\mp1}$ for $GT(\beta^\mp)$ operators; see also (2.38). Using (2.58, 2.71, 2.73), one can calculate $\langle\mathcal{O}^\dagger\mathcal{O}\mathbf{V}^2\rangle^{[\mathbf{m}]}$ and $\langle\mathcal{O}^\dagger\mathcal{O}\rangle^{[\mathbf{m}]}$ traces and test the above approximations. We have verified explicitly that for the fp-shell interactions MWH2 [Mc-70] and FPM13 [Ri-91], the centroid shifts are $\lesssim 0.1\ MeV$ and variances differ from $\langle\mathbf{V}^2\rangle$ by $\lesssim 3\%$.

Besides the assumptions for the marginal centroids and variances, which

are well justified for fp-shell nuclei, (6.2) also assumes that the bivariate correlation coefficient $\zeta = \bar{\zeta}$ is independent of the configurations involved. At present, because of the complexities in the proper definition of ζ as a function of the initial and final configurations, one has to make this assumption [Fr-88b]. From NIP calculations in ds and fp-shells (carried out using the results of Chapter 5), one sees that $0.6 \leq \zeta \leq 0.9$. For example for $\mathcal{O}(GT(\beta^-))$ in ds-shell with ^{17}O energies, $\zeta = 0.78$ for $(m_p = 4, m_n = 4)$ and $\zeta = 0.8$ for $(m_p = 6, m_n = 6)$. Similarly in fp-shell with ^{41}Ca energies, $\zeta = 0.84$ for $(m_p = 6, m_n = 16)$, and $\zeta = 0.87$ for $(m_p = 6, m_n = 10)$. In addition it is known from [Dr-77b, Fr-88b, Sa-93] that for various other operators, with realistic ds-shell interactions $0.6 \leq \zeta \leq 0.9$. Moreover in the two-body EGOE model [Fr-88b], which extends the $\zeta \simeq 1 - 1/m$ result given in Chapter 5 for random one-body hamiltonians, one has the result $\zeta \simeq 1 - 2/m$ where m is the number of active nucleons. Thus in EGOE, $\zeta \simeq 0.8$ for $m = 10$ with a one-body transition operator and a two-body hamiltonian. Therefore in the present calculations, (6.2) is used with $\bar{\zeta}$ a free parameter whose value will be determined by demanding that certain experimental data is reproduced by the theory but with the constraint $0.6 \leq \bar{\zeta} \leq 0.9$.

In this chapter, as we are dealing with fp-shell nuclei, (6.2) is used for constructing $\rho^{\mathrm{V}}_{\mathcal{O}(GT);BIV-\mathcal{G}}$ *and* $\mathbf{I}^{H}_{\mathcal{O}(GT);BIV}$.

6.3 Formalism for β-decay rates at finite temperature

The β-decay rate $T_\beta(E_i \rightarrow E_f)$ is the number of β-decays per second from a given initial state $|E_i\rangle$ of the parent nucleus to the final nuclear state $|E_f\rangle$ and

$T_\beta(E_i \rightarrow E_f) \propto [g_V^2 B_F(E_i \rightarrow E_f) + g_A^2 B_{GT}(E_i \rightarrow E_f)]$, where g_V and g_A are respectively the vector and axial vector coupling constants and B_F and B_{GT} are the Fermi and Gamow - Teller transition strengths respectively. Including the phase space factor f that incorporates the dependence of the rate on nuclear charge Ze and the available β-decay energy (phase space available for the leptons), T_β takes the form $T_\beta(E_i \rightarrow E_f) = Cf(Z, Q_i - E_f)[g_V^2 B_F(E_i \rightarrow E_f) + g_A^2 B_{GT}(E_i \rightarrow E_f)]$ where C is a constant and with Q the Q-value for β-decay from GS, $Q_i = Q + E_i$. Fixing the value of C [Br-77, Wu-66] by using the $\ell og ft$ values ($ft = (\ell n 2) f/T_\beta$) for pure Fermi transitions, one can write down the expressions for ground state half lifes and β-decay rates at finite temperature. Before going further it is important to note that in practice in β-decay rates calculations for fp-shell nuclei the B_F term is neglected as the Fermi strength is concentrated in a narrow energy domain (width $\sim 0.157 ZA^{-1/3} MeV$) and high up in energy (centroid $\sim 1.44 ZA^{-1/3} MeV$) [Ta-69, Ta-73]. With this, by writing B_{GT} in terms of GT strength density $\mathbf{I}^H_{\mathcal{O}(GT)}$ and the state density $I^H(E)$, the expression for GS half lifes is,

$$t_{1/2}(GS) = \{6250 \ \ (s)\} \times$$
$$\left\{ \int_0^Q \left[\left(\frac{g_A}{g_V} \right)^2 3\mathcal{L} \right] \left[\frac{\mathbf{I}^H_{\mathcal{O}(GT)}(E_{GS}, E_f)}{I^H(E_{GS})} \right] f(Z, Q - E_f) dE_f \right\}^{-1} \qquad (6.3)$$

In (6.3), the factor 3 comes due to our definition of $\mathbf{I}^h$ in Chapter 5 [1] and $\mathcal{L}$ is the so called quenching factor which is required because the calculated (shell model) GT sum rule strength is always found to be larger than the observed strength [Ho-83]. The usual value of $0.6 \overset{for}{\wedge} \mathcal{L}$ [Ho-83] and $\left(\frac{g_A}{g_V} \right)^2 = 1.4$ as given

[1] In discrete version $B_{GT}(J_i E_i \rightarrow J_f E_f) = (2J_i + 1)^{-1} \sum_{M_i, M_f(\mu)} |\langle E_f J_f M_f | (\mathcal{O}_{GT})^k_\mu | E_i J_i M_i \rangle|^2$ which in the continuous version becomes $\{I(E_i)\}^{-1} \sum_{\alpha \in E_i, \beta \in E_f, \mu} |\langle E_f \alpha | (\mathcal{O}_{GT})^k_\mu | E_i \beta \rangle|^2$. Noting that $\sum_\alpha |E_i \alpha\rangle \Longrightarrow |E_i\rangle I(E_i)$ and replacing the sum with $\mathbf{I}^h_{\mathcal{O}(GT)}$ using (2.37), gives rise to factor 3 in (6.3).

in [Br-77] are adopted. Our primary concern in this chapter is to calculate β-decay rates $\lambda(T)$ at finite temperature and they are defined by the thermal average (with weight factor $e^{-E/k_BT}I(E)$) of the rates from all parent nucleus states [Fu-80]. Then the expression for $\lambda(T)$ is,

$$\lambda(T) = \frac{\ell n 2(s^{-1})}{6250}\left[\int e^{-E_i/k_BT} I^H(E_i)dE_i\right]^{-1} \times$$
$$\left[\int dE_i e^{-E_i/k_BT} I^H(E_i)\left[\int_0^{Q_i} dE_f \left\{\left(\frac{g_A}{g_V}\right)^2 3\pounds\right\}\right.\right.$$
$$\left.\left.\left[\frac{\mathbf{I}^H_{\mathcal{O}(GT)}(E_i,E_f)}{I^H(E_i)}\right] f(Z,T,Q_i-E_f)\right]\right]$$

$$= \frac{\ell n 2(s^{-1})}{6250}\left[\int e^{-E_i/k_BT} I^H(E_i)dE_i\right]^{-1} \times$$
$$\left[\int dE_i e^{-E_i/k_BT}\left[\int_0^{Q_i} dE_f \left\{\left(\frac{g_A}{g_V}\right)^2 3\pounds\right\}\mathbf{I}^H_{\mathcal{O}(GT)}(E_i,E_f) f(Z,T,Q_i-E_f)\right]\right] \tag{6.4}$$

The second equality in (6.4) shows that in order to calculate β-decay rates one needs to construct explicitly the bivariate GT strength densities $\mathbf{I}^H_{\mathcal{O}(GT)}$ and the stae densities $I^H(E)$. The phase space factor $f(Z,T,Q_i-E_f)$ appearing in (6.4) is given by the integral [Au-90, Fu-80, Wu-66],

$$f(Z,T,E_0=Q_i-E_f) = \int_1^{\epsilon_0} \frac{F(Z,\epsilon_e)\epsilon_e(\epsilon_e^2-1)^{1/2}(\epsilon_0-\epsilon_e)^2}{\{1+exp[(\mu_e-\epsilon_e)/(k_BT)_e]\}}d\epsilon_e. \tag{6.5}$$

In (6.5) $\epsilon_0 = E_0/m_e$, $\mu_e = \mu/m_e$ and $(k_BT)_e = k_BT/m_e$ where m_e is the rest mass of the electron in MeV. For the Coulomb factor $F(Z,\epsilon)$, the Schenter and Vogel [Sc-83] expression is used,

$$F(Z,\epsilon) = \frac{\epsilon}{\sqrt{\epsilon^2-1}} exp[\alpha(Z)+\beta(Z)\sqrt{\epsilon-1}];$$

$$
\begin{aligned}
\alpha(Z) &= -0.811 + 4.46(-2)Z + 1.08(-4)Z^2 && (\epsilon - 1) < 1.2 \\
&= -8.46(-2) + 2.48(-2)Z + 2.37(-4)Z^2 && (\epsilon - 1) \geq 1.2 \\
\beta(Z) &= 0.673 - 1.82(-2)Z + 6.38(-5)Z^2 && (\epsilon - 1) < 1.2 \\
&= 1.15(-2) + 3.58(-4)Z - 6.17(-5)Z^2 && (\epsilon - 1) \geq 1.2
\end{aligned}
\tag{6.6}
$$

It should be mentioned that f in (6.3) follows from (6.5) by dropping the denominator in the integral in the R.H.S. of (6.5). The only unknown quantity left to be determined is the electron chemical potential μ. In the case of presupernova core where the density $\sim 10^8$ gms/cc, the electrons are close to being relativistic and hence μ is found by inverting the expression for the lepton number density. Given the density ρ_7 (ρ in units of 10^7 gms/cc), temperature $\bar{T}$ (T in MeV is denoted by $\bar{T}$) and the electron fraction Y_e in the presupernova star, there are hierarchy of approximate expressions that can be used for μ (see [Au-90, Ra-92]) and in the present calculations Eq. (14) of [Au-90] is used,

$$
\mu = 1.11(\rho_7 Y_e)^{1/3} \left[1 + \left(\frac{\pi}{1.11} \right)^2 \frac{\bar{T}^2}{(\rho_7 Y_e)^{2/3}} \right]^{-1/3} . \tag{6.7}
$$

Using (6.4 - 6.7) β-decay rates can be calculated by constructing state densities $I^H(E)$ and the strength densities $\mathbf{I}^H_{O(GT)}(E_i, E_f)$. The procedure for calculation of these densities is given in the following section together with comments on some of its variants. As an example, the results for five neutron excess fp-shell nuclei $^{61,62}Fe$, $^{62-64}Co$ ($^{61}Fe \rightarrow {}^{61}Co$, $^{62}Fe \rightarrow {}^{62}Co$, $^{62}Co \rightarrow {}^{62}Ni$, $^{63}Co \rightarrow {}^{63}Ni$, $^{64}Co \rightarrow {}^{64}Ni$) are given in Sect. 6.6.

6.4 Calculational procedure

Our primary concern in this chapter is to demonstrate that the theory for β-decay rates calculation given by (6.3 - 6.7) combined with (6.2) and the

methods of Chapters 3 - 5 (i.e. SAT-LSS) is applicable in practice. Because of this limited aim, we followed simpler methods for constructing state and strength densities unlike the more elaborate procedure used for example in Chapter 4 in the case of level densities, and they are described in Sect. 6.4.1 and 6.4.2 respectively. Some useful comments are given in Sect. 6.4.3.

6.4.1 State Densities

For the calculation of state densities $I^H(E)$ the following procedure is adopted. The s.p. orbits are chosen to be the five orbits $1f_{7/2}$, $2p_{3/2}$, $1f_{5/2}$, $2p_{1/2}$ and $1g_{9/2}$ with $s = 0, 0, 0, 0$ and 1 respectively. Following the calculations in Chapter 4 for fp-shell level density data analysis, the traceless SPE for the four fp-orbits are chosen to be $-2.664\ MeV$, $-0.644\ MeV$, $3.526\ MeV$ and $1.366\ MeV$ respectively and the $(fp) - g_{9/2}$ separation $\Delta_{(fp)-g_{9/2}}$ is chosen to be $6MeV$; for ^{64}Co however it is taken to be $7\ MeV$. The calculations are performed in $S = 0 \oplus 1 \oplus 2$ spaces using pn unitary configurations with (fp) and $g_{9/2}$ orbits as unitary orbits; $I^{\rm h}$ is constructed using the above SPE (i.e. no renormalizations due to the interactions are included - their main effect is assumed to be in fixing the value of $\Delta_{(fp)-g_{9/2}}$) and spherical orbits. The density $\rho_G^{\rm V}$ is constructed by calculating the spreading variances using surface delta interaction (SDI) with strength $G = 20/A\ MeV$ (this value follows from Chapter 4). The GS is fixed by demanding that the total level density $I_\ell(E)$ at $8\ MeV$ excitation is same as the value given by the (a, Δ) values that follow from Dilg et al smoothed expression (C.15). This choice is made because for the nuclei under consideration ($^{61-62}Fe$, $^{61-64}Co$, $^{62-64}Ni$) , the low - energy spectrum is not known with certainty to be complete. For example, with Dilg et al values for (a, Δ) together with the back shifted LLC Fermi gas formula

(C.3, C.4), for ^{62}Fe, ^{61}Co and ^{64}Co, the $I_\ell(E)$ (in MeV^{-1}) values at (4, 8) MeV are (13, 455), (61, 1452) and (180, 3765) respectively. In general it is found that with the calculated GS, the density at 4 MeV is quite close (within 30%) to the value predicted by Dilg et al (a, Δ) values. It is also verified that the calculated spin-cutoff factors $(\sigma_J(E))$ are quite close to the values given by (C.10). For example for ^{62}Fe, ^{61}Co ,^{64}Co and ^{62}Ni nuclei the calculated and Dilg et al values at 8 MeV are (3.9, 3.99), (3.72, 4.15), (4.24, 4.40) and (3.40, 3.99) respectively. Also for even-even and odd-odd nuclei for positive parity states and for odd-A nuclei negative parity states, the $S = 2$ intensities in the GS domain are $\leq 30\%$ of the $S = 0$ intensities (thus the $g_{9/2}$ orbit is seen to be important). In addition to these tests, the GT NEWSR as predicted by the present calculations are compared with shell model results as described in Sect. 6.5 ahead. The level density calculations here are carried out in the same spirit as in [Fr-88b] and it is seen that as long as the densities are constructed well upto 8 MeV (the β^--decay Q-values and Eqs. (6.3, 6.4) show that densities only upto ~ 8 MeV are needed in the present exercise), the details of the SPE and interaction $\mathbf{V}$ do not alter the final results significantly. It should be stressed that, as in the studies of [Fr-89a, Fr-89b, Ko-91, Ko-93a, Fr-94] and Chapter 4, there are many other variants of the above procedure which can be used in practice.

6.4.2 Strength densities

The GT strength densities $\mathbf{I}^H_{\mathcal{O}(GT)}(E_i, E_f)$ are constructed for the $GT(\beta^-)$ operator using (6.2) with $\bar{\zeta}$ as a free parameter. In the present study the coulomb correction to GT centroids and the variances [Ta-69] are ignored and it is assumed that the parametrization of $\bar{\zeta}$ takes care of the same ; they

can be easily put back. $\mathbf{I}^{\mathrm{h}}_{\mathcal{O}(GT)}(E_i, E_f)$ is constructed using the results of Chapter 5. In the first calculation $\bar{\zeta}$ is determined for each nucleus by demanding the observed half lifes are reproduced within the constraint $0.6 \leq \bar{\zeta} \leq 0.9$. The deduced values of $\bar{\zeta}$ are 0.6, 0.7, 0.61, 0.68 and 0.72 and the corresponding half lifes (in seconds) are 244, 69.4, 88.8, 31 and 0.3 for ^{61}Fe, ^{62}Fe, ^{62}Co, ^{63}Co and ^{64}Co respectively. The half lifes are calculated using (6.3). These $\bar{\zeta}$ values change quite substantially (also fluctuates) as we go from ^{61}Fe ($\bar{\zeta} = 0.6$) to ^{64}Co ($\bar{\zeta} = 0.72$) while the (valence) particle number m changes only by 3 units. The EGOE form $\bar{\zeta} \simeq a + b/m$ immediately shows that it is not possible to reproduce the above variation within the framework of SAT. Therefore the above values of $\bar{\zeta}$ are not acceptable in a SAT calculation. The plausible alternative is to seek a best fit solution to the observed half lifes of the nuclei under consideration (in the present exercise they are $^{61-62}Fe$, $^{62-64}Co$ isotopes) by assuming the form of $\bar{\zeta}$ to be $\zeta_0 + \zeta_1/m$ where m is the number of valence nucleons/holes, i.e. by minimizing $\sum_{i=nuclei} (\ell og(\tau^i_{1/2})_{cal} - \ell og(\tau^i_{1/2})_{expt})^2$. The resulting $\bar{\zeta}$ values and the corresponding calculated half lifes are given in Table 6.1. The $\bar{\zeta}$ values are around 0.67 (changing from 0.68 for ^{61}Fe to 0.668 for ^{64}Co). It should be obvious that the calculated half lifes, with these $\bar{\zeta}$ values, are the predictions of SAT-LSS. The differences between the calculated and experimental values are of the same order of magnitude as in other models [Ta-69, Kl-84, Ka-91]. Before going further it should be pointed out that in general for a given nucleus, as $\bar{\zeta}$ decreases the calculated half life increases and sometimes the increase is fast.

Using the $\bar{\zeta}$ values given in Table 6.1, the IP strength densities $\mathbf{I}^{H}_{\mathcal{O}(GT)}$ are constructed using (6.2). Using these $\mathbf{I}^{H}_{\mathcal{O}(GT)}$ densities, state densities $I^H(E)$ and Eqs. (6.4 - 6.7), the β-decay rates are calculated.

Table 6.1. Calculated and experimental β^--decay half lifes. The method of determining the correlation coefficient $\bar{\zeta}$ is given in the text. The calculated half lifes are given in the fourth column. The Q-values and experimental data for half lifes are taken from [Le-78]. The KSR results are from [Ka-91, Ra-92] and the QRPA result, which is available only for ^{64}Co in the set of nuclei considered in the table, is from the first reference of [Kl-84].

Nucleus	Q		half life (s)			
	(MeV)	$\bar{\zeta}$	Calc.	Expt.	KSR	QRPA
^{64}Co	7.307	0.668	1.9	0.3	3.5	10.0
^{63}Co	3.662	0.671	52.7	27.5	52.1	–
^{62}Co	5.315	0.675	16.5	90	15.1	–
^{62}Fe	2.327	0.675	267.2	68	183.4	–
^{61}Fe	3.890	0.680	23.0	360	34.5	–

6.4.3 Comments

Firstly, it is useful to recognize that the formalism, for β-decay rates calculations, given by (6.2 - 6.7) together with the procedure outlined above for calculating state and bivariate GT strength densities, allows one to investigate the effects of nucleon-nucleon interaction on the β-decay rates as $\mathbf{I}^H_{\mathcal{O}(GT)}$ and I^H are constructed explicitly in terms of hamiltonian parameters.

Secondly, it should be pointed out that in going from (2.37) to (6.1) and then to (6.2a, 6.2b), in order to construct IP strength densities, involve some general principles/approximations and some of them are yet to be understood well; for example the correlation coefficient is assumed to be independent of the configurations involved.

Thirdly, with the final interest is in calculating β-decay rates for nuclear astrophysics studies, it is plausible that one may adopt a phenomenological/empirical viewpoint in applying (6.2 - 6.7), i.e. in the construction of $\mathbf{I}^H_{\mathcal{O}(GT)}$ and I^H. This is what was done earlier by KSR: The KSR method of constructing $\mathbf{I}^H_{\mathcal{O}(GT)}$ and I^H is based on a simpler version of (6.2), in parts it is an extended version of the "gross theory" given in [Ta-69] and in addition it uses experimental data also. The basic difference beetween the present method and KSR method is that the KSR method assumes single unitary orbit in applying (6.2) so that the summation in (6.2) disappears. Without several unitary orbits the agreements found for level densities, as given in [Ko-91, Fr-94, Ko-93a, Chapter 4], and Sect. 6.4, could not have been obtained and it is well known that the assumption of single unitary orbit is unsatisfactory [Ha-76, Fr-88b, Fr-89a, Fr-89b, Ko-89, Ko-91, Ko-93a, Fr-94] - however this is ignored. With a single unitary orbit $\mathbf{I}^H_{\mathcal{O}(GT)} = \mathbf{I}^{\mathbf{h}}_{\mathcal{O}(GT)} \otimes \rho^{\mathbf{V}}_{\mathcal{O}(GT);\mathcal{G}}$ will be a bivariate Gaussian with CLT applied to $\mathbf{I}^{\mathbf{h}}$. Then the ratio $\mathbf{I}^H/I^H$ in (6.4) is the conditional density $\rho^H_{21;\mathcal{O}(GT)}(E_f|E_i)$ (see (2.23)) which will be a Gaussian (as $\mathbf{I}^H$ is a bivarite Gaussian) with normalization given by GT NEWSR strength $M_{\mathcal{O}(GT)}(E)$. The NEWSR strength is calculated using an expression similar to (6.8) given ahead. The conditional density $\rho^H_{21;\mathcal{O}(GT)-\mathcal{G}}(E_f|E_i)$ is constructed by parametrizing its centroid and variance and in order to correct for the departures from this single Gaussian approximation in some cases KSR *add* [Ra-92, Ka-94] Edgeworth corrections with (γ_1, γ_2) values chosen such that $|\gamma_1| \leq 0.3$ and $|\gamma_2| \leq 0.3$. As can be seen from (2.42) the conditional centroid ϵ_c changes linearly with energy, $\epsilon_c(E_i) = \epsilon_0 + \bar{\zeta} E_i$ and the conditional width is a constant, $\sigma_c = \sigma_0(1 - \bar{\zeta}^2)^{1/2}$ where $\sigma_0 \simeq \sigma_H = (\sigma^2_{\mathbf{h}} + \sigma^2_{\mathbf{V}})^{1/2}$. The centroid ϵ_c is parametrized (assuming $\bar{\zeta} = 1$) and the value of σ_c is fixed, after adding

Coulomb correction as in [Ta-69], by minimizing square of the difference in the logarithm of the calculated and experimental half lifes exactly as in the "gross theory". In addition, instead of calculating $I^H(E)$ and carrying out integration over all E_i's in applying (6.4), KSR use the experimental energies and spins (wherever observed) so that the calculation of state densities is completely avoided. In the formalism presented in Sects. 6.2 - 6.3 and 6.4.1 - 6.4.2, the densities $\mathbf{I}^H$ and I^H are explicitly constructed and used alongwith (6.4) within a single framework unlike in the KSR method where the explicit construction, with interactions, is avoided as described above. It should be added that the s.p. spectrum and the $\mathbf{V}$ used in Sect. 6.4 give $\sigma_H^2 = \sigma_{\mathbf{h}}^2 + \sigma_{\mathbf{V}}^2 \simeq 8\ MeV$ and the expression $\sigma_c = \sigma_H(1 - \bar{\zeta}^2)^{1/2}$ gives, with $\bar{\zeta} \simeq 0.67$, $\sigma_c \simeq 6\ MeV$ which is compatible with the value of σ_c deduced by KSR. In summary KSR approach is a semiempirical approach taking lightly into account some aspects of SAT, and their approach to the construction of strength densities is in the same spirit as the approach to state densities proposed in [Ha-82b]. In addition, the KSR method is a limiting case of the present method.

Finally a biproduct of (6.2) and the results of Chapter 5 is that they give a formalism for calculating GT NEWSR strengths. This is described in the next section before giving the results for β-decay rates.

6.5 GT NEWSR strength

Using (6.2) and the explicit form for $\mathbf{I}^{\mathbf{h}}_{\mathcal{O}(GT)}$ as given in Chapter 5, a simple expression for NEWSR strength $M_{\mathcal{O}(GT)}(E)$ for $\mathcal{O}(GT)$ can be written down,

$$
\begin{aligned}
M_{\mathcal{O}(GT)}(E) &= \sum_{(\mathbf{m}_p,\mathbf{m}_n)} \frac{I^{H;(\mathbf{m}_p,\mathbf{m}_n)}(E)}{I^{H,(m_p,m_n)}(E)} \left\{ 3 \sum_{\alpha,\beta} [\epsilon^2_{\alpha\beta}(\mathcal{O}(GT))] \frac{m_\beta(\mathbf{m}_p,\mathbf{m}_n)}{N_\beta} \times \right. \\
&\qquad \left. \frac{N_\alpha - m_\alpha(\mathbf{m}_p,\mathbf{m}_n)}{N_\alpha} \right\} ; \\
I^{H,(\mathbf{m}_p,\mathbf{m}_n)}(E) &= d(\mathbf{m}_p,\mathbf{m}_n) \rho_{\mathcal{G}}(E; \epsilon_{\mathbf{h}}(\mathbf{m}_p,\mathbf{m}_n), \sigma_{\mathbf{V}}(\mathbf{m}_p,\mathbf{m}_n)) \\
I^{H,(m_p,m_n)}(E) &= \sum_{(\mathbf{m}_p,\mathbf{m}_n) \in (m_p,m_n)} I^{H,(\mathbf{m}_p,\mathbf{m}_n)}(E) \qquad (6.8)
\end{aligned}
$$

In (6.8) $\epsilon_{\alpha\beta}$ define $\mathcal{O}(GT)$ and α and β are proton and neutron spherical orbits respectively for $GT(\beta^-)$ and vice versa for $GT(\beta^+)$. The formula (6.8) whose origin lies in the NIP expression (5.10) for $\mathbf{I}^{\mathbf{h}}_{\mathcal{O}(GT)}$, is quite similar to the sum rule formulas used in earlier studies (though derived using different methods) [Ma-86, Ka-91; Appendix A of [Au-90]] of fp-shell nuclei; thus (6.8) provides a proper justification and corrections to the formulas given in [Ma-86, Ka-91; Appendix A of [Au-90]]. The corrections to (6.8) come from the centroid shifts and the variance corrections to $\rho_{\mathcal{G}}$ as discussed below (6.2) and they are small for fp-shell nuclei. In order to test the applicability of (6.8) for fp-shell nuclei, the $GT(\beta^-)$ NEWSR strengths are calculated for $^{54,56,60}Fe$ and $^{58,60}Ni$ isotopes by first carrying out level density calculations and determining the ground state, exactly as described in Sect. 6.4. These nuclei are chosen as there are corresponding shell model results available in literature [Bl-85, Ra-83], though calculated using different interactions and including only fp-orbits (i.e. without the $g_{9/2}$ orbit). The results shown in Table 6.2 clearly demonstrate that (6.8) gives results that are in close agreement with shell model values. Thus (6.8), which is easy to apply, can be used in future studies of GT NEWSR and quenching of GT strengths. The calculated sum rule strengths (from GS) with quenching factor $\mathcal{L} = 0.6$ for ^{61}Fe, ^{62}Fe, ^{62}Co, ^{63}Co

and ^{64}Co nuclei are 20, 18.9, 18.8, 19.7 and 20.8 respectively. The $^{61-62}Fe$ sum rule strengths are compatible with the ^{60}Fe results given in Table 6.2. We conclude from these results that the various choices made in Sect. 6.4 are quite reasonable.

Table 6.2. Calculated and shell model (SM) results for $GT(\beta^-)$ NEWSR.

Nucleus	NEWSR	
	Calc.	SM
^{54}Fe	17.8	15.1^a
^{56}Fe	22.6	22.1^a
^{60}Fe	31.6	33.5^b
^{58}Ni	20.2	16.6^a
^{60}Ni	24.2	24.6^a

a) [Ra-83], *b*) combining $GT(\beta^+)$ NEWSR value 9.47 given in [Bl-85] with the sum rule result $S_{\beta-} - S_{\beta+} = 3(N-Z)$.

6.6 Results for β-decay rates at finite temperature

Using the formalism given in Sects. 6.2, 6.3 and the procedure outlined in Sect. 6.4, which is described in the flow chart in Fig. 6.1, β-decay rates for the five nuclei ^{61}Fe, ^{62}Fe, ^{62}Co, ^{63}Co and ^{65}Co are calculated at densities $\rho = 10^9$ gm/cc, 10^8 gm/cc, 10^7 gm/cc, temperatures $T = 3 \times 10^9$, 4×10^9, 5×10^9 ^oK ($T = 4 \times 10^9$ ^oK compared to 0.345 MeV) and electron fractions $Y_e = 0.5$, 0.47 and 0.43. The results are given in Table 6.3. It is observed that the excitation energy (of the parent nucleus) contribution to the decay rate is quite significant upto about $(6-8) \times k_BT$ and beyond that their importance ($\sim 10-15\%$) goes down rapidly; note that with $E_i = 5k_BT$, $e^{-E_i/k_BT} \simeq 1/150$.

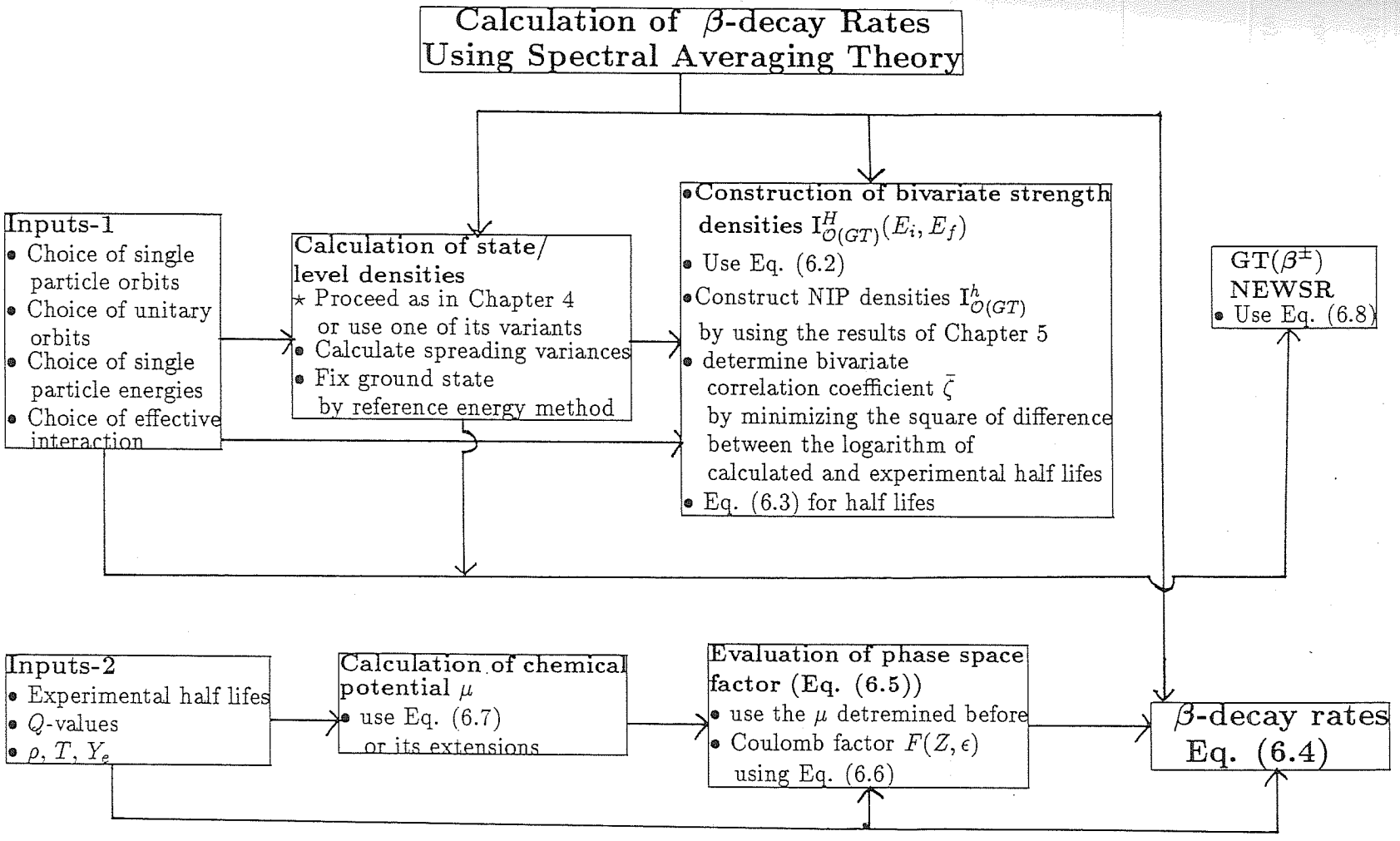


Fig. 6.1 Flow chart describing various steps involved in β - decay rates calculations

It is also observed that for a given nucleus the rates go down as the correlation coefficient $\bar{\zeta}$ decreases. For example for ^{64}Co, with $\bar{\zeta} = 0.668$, $\lambda(T) = 0.345\, s^{-1}$ while with $\bar{\zeta} = 0.72$, $\lambda(T) = 1.33\, s^{-1}$ for $\rho = 10^8$ gm/cc, $T = 4 \times 10^9\ ^oK$ and

Table 6.3. β^--decay rates for ^{64}Co, ^{63}Co, ^{62}Co, ^{62}Fe and ^{61}Fe nuclei

Nucleus	ρ(gms/cc)	Y_e	Temperature (^oK)		
			3×10^9	4×10^9	5×10^9
			Rate (s^{-1})		
^{64}Co	10^9	0.50	0.85×10^{-1}	1.04×10^{-1}	1.30×10^{-1}
		0.47	0.91×10^{-1}	1.11×10^{-1}	1.38×10^{-1}
		0.43	1.00×10^{-1}	1.21×10^{-1}	1.49×10^{-1}
	10^8	0.50	3.10×10^{-1}	3.43×10^{-1}	3.84×10^{-1}
		0.47	3.14×10^{-1}	3.47×10^{-1}	3.87×10^{-1}
		0.43	3.19×10^{-1}	3.52×10^{-1}	3.93×10^{-1}
	10^7	0.50	3.83×10^{-1}	4.14×10^{-1}	4.54×10^{-1}
		0.47	3.83×10^{-1}	4.14×10^{-1}	4.54×10^{-1}
		0.43	3.84×10^{-1}	4.15×10^{-1}	4.55×10^{-1}
^{63}Co	10^9	0.50	0.12×10^{-3}	0.65×10^{-3}	2.26×10^{-3}
		0.47	0.15×10^{-3}	0.76×10^{-3}	2.54×10^{-3}
		0.43	0.21×10^{-3}	0.94×10^{-3}	2.98×10^{-3}
	10^8	0.50	0.85×10^{-2}	1.31×10^{-2}	2.09×10^{-2}
		0.47	0.88×10^{-2}	1.35×10^{-2}	2.14×10^{-2}
		0.43	0.93×10^{-2}	1.41×10^{-2}	2.21×10^{-2}
	10^7	0.50	1.63×10^{-2}	2.17×10^{-2}	3.06×10^{-2}
		0.47	1.64×10^{-2}	2.18×10^{-2}	3.07×10^{-2}
		0.43	1.65×10^{-2}	2.19×10^{-2}	3.08×10^{-2}
^{62}Co	10^9	0.50	0.29×10^{-2}	0.50×10^{-2}	0.84×10^{-2}
		0.47	0.34×10^{-2}	0.56×10^{-2}	0.92×10^{-2}
		0.43	0.41×10^{-2}	0.65×10^{-2}	1.04×10^{-2}
	10^8	0.50	3.06×10^{-2}	3.64×10^{-2}	4.41×10^{-2}
		0.47	3.12×10^{-2}	3.71×10^{-2}	4.48×10^{-2}
		0.43	3.22×10^{-2}	3.80×10^{-2}	4.58×10^{-2}
	10^7	0.50	4.41×10^{-2}	4.97×10^{-2}	5.74×10^{-2}
		0.47	4.42×10^{-2}	4.99×10^{-2}	5.76×10^{-2}
		0.43	4.44×10^{-2}	5.00×10^{-2}	5.77×10^{-2}

Table 6.3 (cont'd)

Nucleus	ρ(gms/cc)	Y_e	Temperature (^oK)		
			3×10^9	4×10^9	5×10^9
			Rate (s^{-1})		
^{62}Fe	10^9	0.50	0.04×10^{-4}	1.16×10^{-4}	9.99×10^{-4}
		0.47	0.06×10^{-4}	1.42×10^{-4}	11.50×10^{-4}
		0.43	0.09×10^{-4}	1.88×10^{-4}	14.00×10^{-4}
	10^8	0.50	2.40×10^{-3}	6.56×10^{-3}	1.62×10^{-2}
		0.47	2.57×10^{-3}	6.86×10^{-3}	1.67×10^{-2}
		0.43	2.83×10^{-3}	7.29×10^{-3}	1.73×10^{-2}
	10^7	0.50	8.11×10^{-3}	1.43×10^{-2}	2.71×10^{-2}
		0.47	8.19×10^{-3}	1.44×10^{-2}	2.72×10^{-2}
		0.43	8.30×10^{-3}	1.46×10^{-2}	2.74×10^{-3}
^{61}Fe	10^9	0.50	0.36×10^{-3}	1.51×10^{-3}	4.52×10^{-3}
		0.47	0.45×10^{-3}	1.76×10^{-3}	5.07×10^{-3}
		0.43	0.62×10^{-3}	2.18×10^{-3}	5.93×10^{-3}
	10^8	0.50	1.89×10^{-2}	2.71×10^{-2}	3.98×10^{-2}
		0.47	1.96×10^{-2}	2.78×10^{-2}	4.07×10^{-2}
		0.43	2.06×10^{-2}	2.89×10^{-2}	4.19×10^{-2}
	10^7	0.50	3.44×10^{-2}	4.33×10^{-2}	5.72×10^{-2}
		0.47	3.46×10^{-2}	4.35×10^{-2}	5.74×10^{-2}
		0.43	3.48×10^{-2}	4.37×10^{-2}	5.76×10^{-2}

$Y_e = 0.5$ and for the same set of (ρ, T, Y_e) values, for ^{62}Co, $\lambda(T) = 3.64 \times 10^{-2}$ s^{-1} for $\bar{\zeta} = 0.675$ and $\lambda(T) = 0.46 \times 10^{-2}$ s^{-1} for $\bar{\zeta} = 0.610$. By comparing the rates in Table 6.3 with the results given by Aufderheide et al [Au-90], one observes that the numbers for ^{63}Co are quite similar (in [Au-90] the rates are tabulated for $\rho = 10^8$ gm/cc, 10^7 gm/cc, $T = 3 \times 10^9$, 4×10^9, 5×10^9 ^oK and $Y_e = 0.5$) while for ^{62}Co the numbers in Table 6.3 are smaller by a factor 5 and that for ^{64}Co by a factor 8. The numbers given in Table 6.3 are much closer to KSR results [Ka-91, Ka-94] and this should not be surprising as the method employed by KSR derives from (6.2). More importantly, the variation in $\lambda(T)$ with T as can be seen from our results in Table 6.3 is not to be found in the first KSR tabulation [Ka-91] but similar variation is found

in their latest compilation of the rates [Ka-94]. For example for ^{63}Co nucleus with $\rho = 10^9$ gm/cc, $Y_e = 0.5$, for $T = 3 \times 10^9\ ^oK$, $4 \times 10^9\ ^oK$, $5 \times 10^9\ ^oK$ the rates $\lambda(T)$ from [Ka-94] and Table 6.3 are (in s^{-1}) (0.37×10^{-3}, 0.94×10^{-3}, 2.07×10^{-3}) and (0.12×10^{-3}, 0.65×10^{-3}, 2.26×10^{-3}). Similarly for ^{63}Co with $\rho = 10^8$ gm/cc, $Y_e = 0.5$ the numbers are (3.6×10^{-2}, 4.11×10^{-2}, 4.66×10^{-2}) and (3.06×10^{-2}, 3.64×10^{-2}, 4.41×10^{-2}) respectively. In the case of ^{62}Fe with $\rho = 10^8$ gm/cc, $Y_e = 0.47$ the numbers are (5.79×10^{-3}, 7.31×10^{-3}, 9.46×10^{-3}) and (2.57×10^{-3}, 6.86×10^{-3}, 16.7×10^{-3}) respectively. Thus it is plausible to conclude that the method proposed in this chapter, where IP state and strength densities are constructed and used for the first time in β-decay rates calculations, is reliable. The goodness of the present method, which is based on the smoothed form for GT densities, derives partly from the fact that the β-decay rates involve an averaging (thermal average to be precise). In the present method, as the densities are constructed by superposing unitary orbit densities, it is easy to go beyond $0\hbar\omega$ spaces.

6.7 Summary

In this chapter a method based on smoothed forms, derived using the principles of SAT-LSS, for GT strength densities is developed for calculating β-decay rates. This method is simple as the earlier methods [Au-90, Ka-91] but at the same time it incorporates much more microscopic informations as the desities $\mathbf{I}^H_{\mathcal{O}(GT)}$ and $I^H(E)$ are explicitly constructed with *interactions* and used. The present exercise represents a first application of the bivariate convolution form for strength densities in nuclear astrophysics problems. A different and new result that is derived from the β-decay rates calculations is that they

determine a value for the bivariate correlation coefficient (between the nuclear hamiltonian and GT operator) $\bar{\zeta}$; $\bar{\zeta} \simeq 0.67$. In addition, an expression for GT NEWSR strength is deduced. Applications are carried out for some $A > 60$ neutron excess fp-shell nuclei.

Chapter 7

Conclusions and Future Outlook

In this thesis the statistical Spectral Averaging Theory in Large Shell Model Spaces (SAT-LSS) for state, expectation value and strength densities is explored , developed further (for strength densities) and applied (for calculating level densities and β-decay rates) to establish that it is a viable interacting particle theory for understanding, analyzing and predicting statistical properties of nuclei. To this end several studies are carried out in the thesis.

In SAT-LSS, (i) using a significant unitary group decomposition under which a one plus two-body nuclear hamiltonian decomposes into orthogonal effective one-body part $\mathbf{h}$ and irreducible two-body part $\mathbf{V}$ ($H \rightarrow \mathbf{h} + \mathbf{V}$); (ii) applying the CLT's locally and (iii) decomposing the shell model space into distant non-interacting S - subspaces (for light nuclei S denotes $\hbar\omega$ excitation), the state densities take a convolution form, $I^H = \sum_S I^{\mathbf{h},S} \otimes \rho_{\mathcal{G}}^{\mathbf{V},S}[E]$ where $I^{\mathbf{h}}$ is renormalized NIP state density and $\rho_{\mathcal{G}}$ is a normalized Gaussian density. Similar convolution forms are derived for spin-cutoff and occupancy densities. Firstly, systematic studies of two important aspects of the level density theory

are carried out in the thesis and they are: (a) a part of the interaction that produces non-NIP like shifts of the single particle energies, that is neglected in the theory, is conclusively demonstrated (using norms of operators and considering large number of effective interactions) to be indeed small all across the periodic table; (b) moment methods for constructing locally smoothed forms for NIP state, spin-cutoff and occupancy densities which are one of the convolution factors in the IP theory, are comprehensively tested for the three densities and also for their S - decompositions in an example of 12 protons and 12 neutrons in a large shell model space consisting of 16 orbits (s, p, ds, fp, sdg and $1h_{11/2}$) with $0-4\ \hbar\omega$ excitations. All the technical details of SAT-LSS are so far worked out in pn formalism and these results are employed in the above studies. In future it will be useful to develop the complete formalism in isospin form.

For a first systematic analysis of experimental data using the convolution forms for state and spin-cutoff densities, in a given region of the periodic table, fp-shell nuclei are chosen as the example. The reason for this choice is that there is significant amount of experimental data (at various energies) for several fp-shell nuclei. In addition, nuclei in this region of the periodic table have acquired new significance recently as some of them play an important role in nuclear astrophysics problems, double β-decay, problem of quenching of GT sum rule strengths etc. The calculations, using surface delta interaction with strength G, are carried out in large spaces by including configurations upto $2\hbar\omega$ excitations and by employing eight spherical orbits (ds, fp, $1g_{9/2}$) for the five nuclei ^{55}Mn, ^{56}Fe, ^{59}Co, ^{60}Co and ^{60}Ni and by extending for obvious reasons, to ten spherical orbits (ds, fp, $1g_{9/2}$, $2d_{5/2}$, $1g_{7/2}$) for the three $A > 60$ nuclei ^{62}Ni, ^{63}Cu and ^{65}Cu. In general the convolution form for the densities is

seen to provide an excellent representation of the observed total level densities and spin-cutoff factors. The calculations determine a magnitude parameter of the interaction - the strength G which is found to be $\sim 20/A\ MeV$ for all the nuclei is compatible with the values deduced from low-energy spectroscopy. It will be interesting to extend the analysis using SAT-LSS to *ds*-shell nuclei and for these nuclei considerable amount of experimental data are available in literature [Ba-77]. In addition it will be useful to carry out calculations with two parameter SDI, P + Q.Q interaction and interactions derived from microscopic theories etc. and also construct fixed parity densities with two reference energies; these studies require new experimental data. All these studies will shed further light on the applicability of SAT-LSS in analyzing level density data.

Using some plausible arguments it was shown by French et al [Fr-88b] that the bivariate strength density $\mathbf{I}^H_{\mathcal{O}}(E_i, E_f)$ for a transition operator $\mathcal{O}$ takes a convolution form, $\mathbf{I}^H_{\mathcal{O}}(E_i, E_f) = \mathbf{I}^{\mathbf{h}}_{\mathcal{O}} \otimes \rho^{\mathbf{V}}_{BIV-\mathcal{G};\mathcal{O}}[E_i, E_f]$. Leaving aside the question of determining the five parameters of the spreading bivariate Gaussian due to $\mathbf{V}$, one needs good methods for constructing the NIP density $\mathbf{I}^{\mathbf{h}}_{\mathcal{O}}$ in large spaces. A complete formalism for constructing the exact NIP strength densities using spherical orbits is worked out for one-body transition operators. For rapid construction of the bivariate NIP densities and also to carry out S-decomposition, trace propagation formulas for bivariate moments M_{rs} with $r + s \leq 2$ are derived for unitary orbit partial densities which determine the bivariate Gaussian representation for the partial densities. In a large space numerical example with $GT(\beta^-)$ transition operator, the superposition of unitary orbit partial bivariate Gaussian densities is seen to give a good representation of the exact NIP strength densities. Trace propagation formulas for

M_{rs} with $r+s \leq 4$ are also derived in m-particle scalar spaces, which are useful for many purposes. The formalism developed for NIP strength densities for one-body transition operator is applied in the thesis to construct GT strength densities. In addition one can apply the formalism directly for a systematic study of electromagnetic (for example $E2$ and $M1$) transition strength sum rules and distributions. Although the present exercise is restricted to one-body transition operators, the methods and results extend to the case of half-body (single nucleon transfer) and two-body transition operators (relevant for TRNI studies). It is important to work out the technical details in these cases and also develop methods that yield approximate values (the methods that yield exact values will obviously be cumbersome to be used in practice) for higher order bivariate cumulants (K_{rs} with $r+s \geq 3$). With these developments and similarly for the bivariate spreading function with angular momentum incorporated, the bivariate convolution form can be employed commonly in analyzing wide variety of strength density data.

A method to calculate β-decay rates at finite temperature is developed by writing the expression for the rates explicitly in terms of bivariate GT strength densities ($\mathbf{I}^{H}_{\mathcal{O}(GT)}$) and state densities of parent nucleus besides having the usual phase space factors. The method developed in this thesis for constructing NIP strength densities is applied together with a plausible procedure for constructing the GT bivariate spreading Gaussian due to interactions. Recently there is considerable interest in evaluating β-decay rates for $A > 60$ fp-shell nuclei as these rates play a very important role in determining the structure of the core of massive supernova stars and hence on their subsequent evolution towards gravitational collapse and supernova explosion phases. Therefore as an example, using our method (which is based on SAT-LSS), β-decay rates for

$^{61,62}Fe$ and $^{62-64}Co$ isotopes are calculated at presupernova matter densities $\rho = 10^7 - 10^8$ gm/cc, temperatures $T = (3-5) \times 10^9\ ^oK$ and for various values of the electron fraction Y_e. The results of the β-decay rates calculations demonstrate that one can use the present method, with interactions, for meaningful calculations of β-decay rates. As a biproduct, the calculations produced a value (via observed β-decay half lifes), for the bivariate correlation coefficient $\bar{\zeta}$ between the hamiltonian and the GT operator to be $\bar{\zeta} \sim 0.67$. In addition an expression for the GT NEWSR strength is also deduced. It should be mentioned that the GT strength densities constructed using interactions in SAT-LSS can be used in electron capture rates calculations and with this it is possible to generate detailed and complete tabulation of β-decay and electron capture rates for various (ρ, T, Y_e) values for all neutron exceess fp-shell nuclei relevant for presupernova evolution calculations. Then they can be used, for example as carried out recently by Aufderheide et al [Au-94] using a tabulation they generated, in steller evolution codes and study the influence of the calculated rates on the evolution of presupernova stars. This study is beyond the scope of the present thesis. In addition, the GT strength densities have important applications in solar neutrino experiments [Od-86]. The present exercise which represents a first application, with interactions, of the bivariate convolution form for strength densities, with the bivariate densities constructed interms of partial bivariate moments, in nuclear astrophysics problems together with earlier applications to the problem of deriving bound on TRNI in nucleon-nucleon force [Fr-88b] and single particle transfer strengths [Po-91] show that the strength density formalism given by SAT-LSS is a viable tool for studying a wide variety of nuclear physics and nuclear astrophysics problems.

The studies carried out in the thesis provide a better understanding of SAT-LSS and establish that this theory provides a powerful formalism for analyzing and applying statistical properties of atomic nuclei. Some of the future studies in SAT-LSS should include:

1) A viable method/model, for incorporating $S = 0 \oplus 2 \oplus 4 \oplus ....$ mixing effects into the convolution forms for state, spin-cutoff, occupancy, GT and other strength densities etc. should be developed.

2) It is plausible to argue that [Fr-94] SAT-LSS is a natural theory in the 'quantum chaotic' domain of complex nuclei — good understanding of this aspect is called for. Although for many observables SAT-LSS extends below the region of onset of chaos (i.e. below the reference energy) it is essential to develop good methods for incorporating effects due to non-chaotic states (collective effects may be incorporated via further convolutions or otherwise).

3) One important result of the level density analysis of fp-shell nuclei is that they determine from the resonance (chaotic) domain data a value for a magnitude parameter of nuclear hamiltonian. Similarly the β-decay half lifes determine a value for the bivariate correlation coefficient between H and GT operators. The information thus deduced is found to be compatible with those deduced from low energy spectroscopy. *Thus it appears that the complex spectroscopy in the chaotic domain gives information about nuclear hamiltonian and opens up the subject of information propagation in complex systems.* This aspect of SAT-LSS requires further study.

4) With SAT-LSS one is in a position to deal, in a realistic approach with

problems in nuclear astrophysics. Much of the future of SAT-LSS in applications side, appear to be in carrying out large scale applications in nuclear astrophysics where one needs level densities, partition functions, orbit occupancies, β-decay rates etc.

5) IP strength density formalism with partitioning should be studied in more detail and this may pave way for avoiding some of the approximations that are used at present.

6) A usable theory for incorporating angular momentum in strength densities, perhaps in terms of trivariate and tetravariate distributions, should be worked out.

7) With SAT-LSS one has a powerful "statistical mechanical" method for dealing with large shell model spaces (the scope of complete shell model matrix diagonalization is extended recently from *ds*-shell [Br-88] to *fp*-shell upto $A = 48$ nuclei [Ca-94; see also Na-94]), there are very few alternative approaches available for the same. Comparisons with the recently introduced Monte Carlo method for the shell model [Ko-94d] may give new insights into SAT-LSS.

8) Various problems in nuclear structure at finite temperature [Al-91, Al-93 and references therein], pre-equilibrium reactions, heavy ion physics etc. can be studied using SAT-LSS and the principles/methods therein. Studies in these areas will enhance the scope of SAT-LSS.

References

Ab-64 M. Abramowtiz and I.A. Stegun, editors, *Handbook of Mathematical Functions*, NBS Applied Mathematics Series, 55 (U.S. Govt. Printing Office, Washington D.C., 1964).

Ab-91 A. Abzouzi, E. Caurier and A.P. Zuker, Phys. Rev. Lett. **66**, 1134 (1991).

Al-91 Y. Alhassid, in *High Spin Physics and Gamma-Soft Nuclei*, edited by J.K. Saladin, R.A. Sorensen, C.M. Vincent (World Scientific, Singapore, 1991), p. 15.

Al-93 Y. Alhassid and B.W. Bush, Nucl. Phys. **A565**, 399 (1993); R. Rossignoli, N. Canosa and P. Ring, Phys. Rev. Lett. **72**, 4070 (1994); B.K. Agrawal and A. Ansari, Nucl. Phys. **A567**, 1 (1994).

Ar-91 A. D'Arrigo, G. Giardina and A. Taccone, Phys. Lett. **B262**, 1 (1991).

Au-90 M.B. Aufderhide, G.E. Brown, T.T.S. Kuo, D.B. Stout and P. Vogel, Ap. J. **362**, 241 (1990).

Au-94 M.B. Aufderheide, I. Fushiki, S.E. Woosley and D.H. Hartmann, Ap. J. Supp. **91**, 389 (1994).

Ay-74a S. Ayik and J.N. Ginocchio, Nucl. Phys. **A221**, 285 (1974).

Ay-74b S. Ayik and J.N. Ginocchio, Nucl. Phys. **A234**, 13 (1974).

Ba-68 M. Baranger and K. Kumar, Nucl. Phys. **A110**, 490 (1968); Nucl. Phys. **A62**, 113 (1965).

Ba-70 H. Baba, Nucl. Phys. **A159**, 625 (1970).

Ba-77 M. Backerman, Nucl. Phys. **A278**, 333 (1977).

Be-36 H.A. Bethe, Phys. Rev. **50**, 332 (1936); H.A. Bethe, Rev. Mod. Phys. **9**, 69 (1937).

Be-69 D.R. Bes and R.M. Sorensen, Adv. Nucl. Phys. **2**, 129 (1969).

Be-73 A.N. Behkami and J.R. Huizenga, Nucl. Phys. **A217**, 78 (1973).

Be-79 H.A. Bethe, G.E. Brown, J. Applegate and J.M. Lattimer, Nucl. Phys. **A324**, 487 (1979).

Bl-54 C. Bloch, Phys. Rev. **9**, 1094 (1954).

Bl-85 S.D. Bloom and G.M. Fuller, Nucl. Phys. **A440**, 511 (1985).

Bo-69 A. Bohr and B.R. Mottelson, *Nuclear Structure* Vol. I (W.A.Benjamin, Reading, Massachusetts, 1969).

Bo-75 A. Bohr and B.R. Mottelson, *Nuclear Structure* Vol. II (W.A.Benjamin, Reading, Massachusetts, 1975).

Bo-84 O. Bohigas and M.J. Giannoni, in *Mathematical and Computational Methods in Nuclear Physics*, edited by J.S. Dehesa, J.M.G. Gomez and A. Polls (Springer-Verlag, Heidelberg, 1984), p. 1.

Bo-85 G. Bonsignori, M. Savoia, K. Allaart, A. Van Egmond and G. Te Velde, Nucl. Phys. **A432**, 389 (1985).

Bo-88 O. Bohigas and H.A. Weidenmuller, Ann. Rev. Nucl. Part. Sci. **38**, 421 (1988).

Br-70 J. Browne, H. W. Newson, E. G. Bilpuch and G. E. Mitchell; Nucl. Phys. **A153**, 481 (1970).

Br-77 P.J. Brussaard and P.W.M. Glaudemans, *Shell Model Application in Nuclear Spectroscopy* (North Holland, New York, 1977).

Br-81 T. A. Broady, J. F. Flores, J. B. French, P. A. Mello, A. Pandey and S. S. M. Wong; Rev. Mod. Phys. **53**, 385 (1981).

Br-85 B.A. Brown and B.H. Wildenthal, At. Data Nucl. Data Tables **33**, 347 (1985).

Br-88 B.A. Brown and B.H. Wildenthal, Ann. Rev. Nucl. Part. Sci. **38**, 29 (1988).

Ca-94 E. Caurier, A.P. Zucker, A. Poves and G. Martinez-Pinedo, Phys. Rev. **C50**, 225 (1994); A. Poves and J. Retamosa, Nucl. Phys. **A571**, 221 (1994); E. Caurier, A. Poves and A.P. Zuker, Phys. Lett. **B256**, 301 (1991).

Ce-93 N. Cerf, Nucl. Phys. **A554**, 85 (1993).

Ce-94 N. Cerf, Phys. Rev. **C49**, 852 (1994).

Ch-71 F.S. Chang, J.B. French, T.H. Thio, Ann. Phys. (N.Y.) **66**, 137 (1971).

Ch-80 M. Chakrabarty, V.K.B. Kota and J.C. Parikh, Ann. Phys. (N.Y.) **127**, 413 (1980).

Da-80 D.J. Dalton, S.M. Grimes, J.P. Vary and S.A. Williams, editors, *Moment Methods in Many Fermion Systems* (Plenum, N.Y., 1980).

Di-73 W. Dilg, W. Schantl, H. Vonach and M. Uhl, Nucl. Phys. **A217**, 269 (1973).

Dr-75 J.P. Draayer, J.B. French, V. Potbhare and S.S.M. Wong, Phys. Lett. **B55**, 349 (1975).

Dr-77a J.P. Draayer, J.B. French and S.S.M. Wong, Ann. Phys. (N.Y.) **106**, 472 (1977).

Dr-77b J.P. Draayer, J.B. French and S.S.M. Wong, Ann. Phys. (N.Y.) **106**, 503 (1977).

Dy-63 F.J. Dyson and M.L. Mehta, J. Math. Phys. **4**, 701 (1963).

Ed-74 A.R. Edmonds, *Angular Momentum in Quantum Mechanics* (Princeton University Press, N.J., 1974).

Er-60 T. Ericson, Adv. Phys. **9**, 425 (1960).

Er-66 T. Ericson and T. Mayer-Kuckuk, Ann Rev. Nucl. Sci. **16**, 183 (1966).

Fr-66 J.B. French, in *Many-Body Description of Nuclei and Reactions, Proc. Int. Sch. Phys., Enrico Fermi, Course 36*, edited by C. Bloch (Academic Press, N.Y., 1966), p. 278.

Fr-67 J. B. French, in *Nuclear Structure*, edited by A. Hossain, Harun-ar-Rashid and M. Islam (North Holland, Amsterdam, 1967), p. 85.

Fr-69a J.B. French, in *Isospin in Nuclear Physics*, edited by D.H. Wilkinson (North Holland, Amsterdam, 1969), p. 154.

Fr-69b J.B. French, E.C. Halbert, J.B. McGrory and S.S.M. Wong, in *Advances in Nuclear Physics*, Vol. 3, edited by M. Baranger and E. Vogt (Plenum, N.Y., 1969), p. 193.

Fr-71a J.B. French and K.F. Ratcliff, Phys. Rev. **C3**, 94 (1971).

Fr-71b J.B. French and J.C. Parikh, Phys. Lett. **B35**, 1 (1971).

Fr-72 J.B. French, in *Dynamic Structure of Nuclear States*, edited by D.J. Rowe, L.E.H. Trainor, S.S.M. Wong and T.W. Donnelly (University of Toronto Press, Toronto, 1972), p. 154.

Fr-79 J.B. French and J.P. Draayer, in *Group Theoretical Methods in Physics*, edited by W. Beiglbock, A. Bohm and E. Takasugi (Springer-Verlag, Berlin, 1979), p. 394.

Fr-82 J.B. French and V.K.B. Kota, Ann. Rev. Nucl. Part. Sci. **32**, 35 (1982).

Fr-83a J.B. French, Nucl. Phys. **A396**, 87c (1983).

Fr-83b J.B. French and V.K.B. Kota, Phys. Rev. Lett. **51**, 2183 (1983).

Fr-84 J.B. French, in *Mathematical and Computational Methods in Nuclear Physics*, edited by J.S. Dehesa, J.M.G. Gomez and A. Polls (Springer-Verlag, Berlin, 1984), p. 394.

Fr-87a J.B. French, V.K.B. Kota, A. Pandey, S. Tomsovic, Phys. Rev. Lett. **58**, 2400 (1987).

Fr-87b J. B. French, A. Pandey and J. Smith, in *Time Reversal Tests in Neutron Physics*, edited by N. R. Roberson, C. R. Gould and J. D. Bowman (World Scientific, Singapore, 1987), p. 80.

Fr-88a J.B. French, V.K.B. Kota, A. Pandey and S. Tomsovic, Ann. Phys. (N.Y.) **181**, 198 (1988).

Fr-88b J.B. French, V.K.B. Kota, A. Pandey and S. Tomsovic, Ann. Phys. (N.Y.) **181**, 235 (1988).

Fr-89a J.B. French and V.K.B. Kota, *Nuclear State Densities and Smoothed Partition Functions I. General theory* (University of Rochester Report **UR-1116**, 1989).

Fr-89b J.B. French, V.K.B. Kota and J.F. Smith, *Nuclear State Densities and Smoothed Partition Functions II. Expectation Values* (University of Rochester Report **UR-1122**, 1989).

Fr-89c J.B. French and V.K.B. Kota, Pramana-J. Phys. **32**, 459 (1989).

Fr-94 J.B. French, R.U. Haq and V.K.B. Kota, to be submitted for publication (1994).

Fu-80 G.M. Fuller, W.A. Fowler and M.J. Newman, Ap. J. Suppl. **42**, 447 (1980); Ap. J. **252**, 715 (1982); Ap. J. Suppl. **48**, 279 (1982); Ap. J. **293**, 1 (1985).

Gi-65 A. Gilbert and A. G. W. Cameron, Can. J. Phys. **43**, 1446 (1965).

Gr-83 S.M. Grimes, S.D. Bloom, H.K. Vonach and R.F. Hausman, Jr., Phys. Rev. **C27**, 2893 (1983); B. Strohmaier, S.M. Grimes and H. Satyanarayana, Phys. Rev. **C36**, 1604 (1987); B. Strohmaier and S.M. Grimes, Z. Phys. **A329**, 431 (1988).

Gr-88 S.M. Grimes, Phys. Rev. **C38**, 2362 (1988).

Ha-71 E.C. Halbert, J.B. McGrory, B.H. Wildenthal and S.P. Pandya, in *Advances in Nuclear Physics*, Vol. 3, edited by M. Baranger and E. Vogt (Plenum, N.Y., 1971), p. 315.

Ha-76 R.U. Haq and J.C. Parikh, Nucl. Phys. **A273**, 410 (1976).

Ha-79 T.R. Halmane, *Statistical Spectroscopic Studies in Nuclear Structure Physics*, Ph.D Thesis (University of Rochester, 1979); T.R. Halmane and J.B. French, Phys. Rev. **C25**, 2019 (1982); T.R. Halmane and J.B. French, Z. Phys. **A304**, 363 (1982).

Ha-80 R.U. Haq and S.S.M. Wong, Phys. Lett. **B93**, 357 (1980).

Ha-82a R.U. Haq, A. Pandey and O. Bohigas, Phys. Rev. Lett. **48**, 1086 (1982); O. Bohigas, R.U. Haq and A. Pandey, Phys. Rev. Lett. **54**, 1645 (1985).

Ha-82b R.U. Haq and S.S.M. Wong, Can. J. Phys. **60**, 1502 (1982).

Ha-92 R.U. Haq and V.K.B. Kota, *Report on the package LVLDN_INT for level density calculations*, (unpublished, 1992).

Ha-83 G. Hansen and A.S. Jensen, Nucl. Phys. **A406**, 236 (1983).

He-75 K.T. Hecht, Comm. Math. Phys. **41**, 135 (1975).

Hi-69 M. Hillman and J.R. Grover, Phys. Rev. **C185**, 1303 (1969).

Ho-83 Proceedings of the international conference on *Electromagnetic Properties of Atomic Nuclei*, edited by H. Honie and H. Ohuma (Tokyo Institute of Technology Press, Japan, 1983).

Hu-51 H. Hurwitz (Jr.) and H. Bethe, Phys. Rev. **81**, 804 (1951).

Hu-69 J. R. Huizenga, H. K. Vonach, A. A. Katsanos, A. J. Gorski and C. J. Stephan, Phys. Rev. **182**, 1149 (1969).

Hu-72 J.R. Huizenga and L.G. Moretto, Ann. Rev. Nucl. Sci. **22**, 427 (1972).

Ig-70 A.V. Ignatyuk, V.S. Stavinski and Yu. N. Shubin, Nucl. Phys. **11**, 563 (1970).

Ig-76 A.V. Ignatyuk, M.G. Itkis, V.N. Okolovich, G.N. Smirenkin and A.S. Tishin, Sov. J. Nucl. Phys. **21**, 612 (1976).

Ig-83 A.V. Ignatyuk, *The Statistical Properties of the Excited Atomic Nuclei*, (Energoatamitzdat, Moscow, 1983).

Il-92 A. S. Iljinov, M. V. Mebel, N. Bianchi, E. De Sanctis, C. Guareldo, V. Lucherini, V. Muccifora, E. Polli, A. R. Reolon and P. Rossi, Nucl. Phys. **A543**, 517 (1992).

Ja-86 C. Jacquemin and S. K. Kataria, Z. Phys. **A324**, 261 (1986).

Ja-92 K. Jain and D. Majumdar, in Proceedings of the DAE symposium on *Nuclear Physics*, Vol. 35B, edited by D. R. Chakrabarty and S. Kumar (Bombay, 1992), p. 26.

Je-52 J.H.D. Jensen and J.M. Luttinger, Phys. Rev. **86**, 907 (1952).

Ji-92 M.F. Jiang, R. Machleidt, D.B. Stout and T.T.S. Kuo, Phys. Rev. **C46**, 910 (1992).

Jo-92 C.W. Johnson, S.E. Koonin, G.H. Lang and W.E. Ormand, Phys. Rev. Lett. **69**, 3157 (1992); Y. Alhaasid, D.J. Dean, S.E. Koonin, G. Lang and W.E. Ormand, Phys. Rev. Lett. **72**, 613 (1994).

Ka-66a I. Kanestrom, Nucl. Phys. **83**, 380 (1966).

Ka-66b A.A. Katsanos, J.R. Huizenga and H.K. Vonach, Phys. Rev. **141**, 1053 (1966).

Ka-69 S. Kahana, H.C. Lee and C.K. Scott, Phys. Rev. **185**, 1378 (1969).

Ka-70 A.A. Katsanos, R.W. Shaw Jr., R. Vandenbosch and D. Chamberlin, Phys. Rev. **C1** 594 (1970).

Ka-80 S.K. Kataria and V.S. Ramamurthy, Nucl. Phys. **A349**, 10 (1980); S.K. Kataria, V.S. Ramamurthy and S.S. Kapoor, Phys. Rev. **C18**, 549 (1978).

Ka-81 K. Kar, Nucl. Phys. **A368**, 285 (1981).

Ka-91 K. Kar, S. Sarkar and A. Ray, Phys. Lett. **B261**, 217 (1991);[Erratum - Phys. Lett. **B277**, 528 (1992)].

Ka-94 K. Kar, Private communication to V.K.B. Kota (1994).

Ke-69 M. Kendall and A. Stuart, *Advanced Theory of Statistics*, Vol. 1, 3rd edn. (Hanfer publishing company, N.Y., 1969); A. Stuart and J. K. Ord, *Kendall's Advanced Theory of Statistics*, Vol. 1, 5th edn. (Charles Griffin and Company, London, 1987).

Kl-84 H.V. Klapdor, J. Metzinger and T. Oda, At. Data Nucl. Data Tables **31**, 81 (1984); A. Standt, E. Bender, K. Muto and H.V. Klapdor-Kleingrothaus, At. Data Nucl. Data Tables **44**, 79 (1990); P. Moller and J. Randrup, Nucl. Phys. **A514** (1990) 1.

Ko-72 D. Kopsch and S. Cierjacks, in *Statistical Properties of Nuclei*, edited by J. Garg (Plenum Press, N.Y., 1972), p. 455.

Ko-79a V.K.B. Kota and V. Potbhare, Nucl. Phys. **A331**, 93 (1979).

Ko-79b V.K.B. Kota, Phys. Rev. **C20**, 347 (1979).

Ko-82 V.K.B. Kota, S.P. Pandya and V. Potbhare, Phys. Rev. **C25**, 1667 (1982).

Ko-84a V.K.B. Kota, Z. Phys. **A315**, 91 (1984).

Ko-84b V.K.B. Kota, *Fortran Programs for Statistical Spectroscopy Calculations* (University of Rochester Report **UR-887**, 1984).

Ko-85 V.K.B. Kota and V. Potbhare, Z. Phys. **A322**, 129 (1985).

Ko-89 V.K.B. Kota and K. Kar, Pramana-J.Phys. **32**, 647 (1989).

Ko-91 V.K.B. Kota, in *Capture Gamma-ray Spectroscopy and Related Topics*, edited by R.W. Hoff (AIP conference proceedings 238, N.Y., 1991), p. 685.

Ko-92a V. K. B. Kota and D. Majumdar, *Tests of Moment Methods for Spin-cutoff and Occupancy Densities for Non-Interacting Particle Systems* (Physical Research Laboratory Report **PRL-TH-/92-12**, 1992); in Proceedings of the DAE symposium on *Nuclear Physics*, Vol. 34B, edited by S. Kailash and P. Singh (Bombay, 1991), p. 23.

Ko-92b V. K. B. Kota and D. Majumdar, *Unitary Decomposition of Spherical Configuration Scalar Part of Nuclear Hamiltonians All Across The Periodic Table* (Physical Research Laboratory Report **PRL-TH-/92-21**, 1992); in Proceedings of the DAE symposium on *Nuclear Physics*, Vol. 34B, edited by S. Kailash and P. Singh (Bombay, 1991), p. 49.

Ko-93a V.K.B. Kota, *Recent Developments in Statistical Nuclear Spectroscopy: Level Densities* (Physical Research Laboratory Report **PRL-TH-/93-7**, 1993); to appear in the Proceedings of the symposium on *Recent Trends in Nuclear Physics* held at M.S. University, Tirunelveli (India), during March 15-18, 1993.

Ko-93b V.K.B. Kota, Europhys. Lett. **23**, 481 (1993); G. Maino, A. Mengoni and A. Ventura, Phys. Rev. **C42**, 988 (1990); A. Mengoni, S. Maino, A. Ventura and Y. Nakajima, to appear in the Proceedings of the international conference on *Perspectives for the Interacting Boson Model* held at Padova (Italy), during June 13-17, 1994.

Ko-94a V.K.B. Kota and D. Majumdar, *Bivariate Distributions in Statistical Spectroscopy Studies: Non-Interacting Particle Strength Densities For One-Body Transition Operators* (Physical Research Laboratory Report **PRL-TH-/94-25**, 1994).

Ko-94b V.K.B. Kota and D. Majumdar, *Interacting Particle Strength Densities: β-Decay Rates For Some $A > 60$ Nuclei Relevant for Presupernova Evolution Calculations* (Physical Research Laboratory Report **PRL-TH-/94-26**, 1994).

Ko-94c V.K.B. Kota, D. Majumdar and R.U. Haq, *Nuclear Level Densities in Spectral Averaging Theory in Large Shell Model Spaces: First Systematic Study of fp-Shell Nuclei* (Physical Research Laboratory Report **PRL-TH-/94-37**, 1994); to appear in the Proceedings of the DAE symposium on *Nuclear Physics*, to be held at Bhubaneswar (India), during December 26-30, 1994.

Ko-94d S.E. Koonin, Nucl. Phys. **A574**, 1c (1994).

Ku-65 T.T.S. Kuo and G.E. Brown, Phys. Lett. **18**, 54 (1965); Nucl. Phys. **85**, 40 (1966).

Ku-67 T.T.S. Kuo, Nucl. Phys. **A103**, 71 (1967).

Ku-69 Private communication from T.T.S. Kuo to K.H. Bhatt; D.P. Ahalpara, K.H. Bhatt and R. Sahu, J. Phys. **G11**, 735 (1985).

Ku-71 Private communication from T.T.S. Kuo to J.B. French; K.F. Ratcliff, Phys. Rev. **C3**, 117 (1971).

La-54 J.M.B. Lang and K.J. LeCouteur, Proc. Phys. Soc. (London) **A67**, 585 (1954).

La-66 D.W. Lang, Nucl. Phys. **77**, 545 (1966).

La-88 B. Lauritzen, P. Arve and G.F. Bertsch, Phys. Rev. Lett. **61**, 2835 (1988); B. Lauritzen and G.F. Bertsch, Phys. Rev. **C39**, 2412 (1989); G. Puddu, P.F. Bortignon and R.A. Broglia, Ann. Phys. **206**, 409 (1991).

La-90 G.J.H. Labarge and R.U. Haq, Can. J. Phys. **68**, 301 (1990).

Le-78 *Table of Isotopes*, VIIth edn., edited by C. M. Lederer and V. S. Shirley (John Wiley & Sons, N.Y., 1978).

Le-94 R.J. Leclair, *Information Content of Quantum Spectra*, M.Sc. Thesis (Laurentian University, Sudbery, Canada, 1994).

Li-71 D. P. Lindstorm, H. W. Newson, E. G. Bilpuch and G. E. Bilpuch, Nucl. Phys. **A168**, 37 (1971).

Li-72 D. P. Lindstorm, H. W. Newson, E. G. Bilpuch and G. E. Bilpuch, Nucl. Phys. **A187**, 481 (1972).

Lu-72a C. C. Lu, L. C. Vaz and J. R. Huizenga, Nucl. Phys. **A190**, 229 (1972).

Lu-72b C. C. Lu, L. C. Vaz and J. R. Huizenga; Nucl. Phys. **A197**, 321 (1972).

Ma-65 M.G. Mayer and J.H.D. Jensen, *Elementary Theory of Nuclear Shell Structure* (John Wiley and Sons, N.Y., 1965).

Ma-69 M. Maruyama, Nucl. Phys. **A131**, 145 1969.

Ma-86 M.H. Macfarlane, Phys. Lett. **182**, 265 (1986).

Mc-70 J.B. McGrory, B.H. Wildenthal, E.C. Halbert, Phys. Rev. **C2**, 186 (1970); S.K. Sharma and K.H. Bhatt, Phys. Rev. Lett. **30**, 623 (1973).

Mi-80 G.E. Mitchell in *Moment Methods in Many-Fermion Systems*, edited by B.J. Dalton, S.M. Grimes, J.P. Vary and S.A. Williams (Plenum, N.Y., 1980) p. 33.

Mo-75 K.K. Mon and J.B. French, Ann. Phys.(N.Y.) **95**, 90 (1975).

Mu-81 S.F. Mughabghab, M. Divadeenam and N. E. Holden, *Neutron Cross Sections*, Vol. 1, Part A ($Z = 1 - 60$) (Academic Press, N.Y., 1981).

Mu-84 S. F. Mughabghab, *Neutron Cross Sections*, Vol. 1, Part B ($Z = 61 - 100$) (Academic Press, N.Y., 1984).

Na-94 H. Nakada, T. Sebe and T. Otsuka, Nucl. Phys. **A571**, 467 (1994).

Nu-77 Nuclear Data Sheets **20**, 286 (1977).

Nu-83 Nuclear Data Sheets **39**, 687 (1983).

Nu-85 Nuclear Data Sheets **44**, 529 (1985).

Nu-86a Nuclear Data Sheets **47**, 178 (1986).

Nu-86b Nuclear Data Sheets **48**, 284 (1986).

Nu-90 Nuclear Data Sheets **60**, 366 (1990).

Nu-91 Nuclear Data Sheets **64**, 834 (1991).

Od-86 T. Oda, *Particles and Nuclei*, edited by H. Terazawa (World Scientific, Singapore, 1986), P. 255.

Od-94 T. Oda, M. Hino, K. Muto, M. Takahara and K. Sato, At. Data Nucl. Data Tables **56**, 231 (1994).

Pa-78 J.C. Parikh, *Group Symmetries in Nuclear Structure* (Plenum, N.Y., 1978).

Pa-93 V. Paar, D.K. Sunko, S. Brant, M.G. Mustafa and R.G. Lanier, Z. Phys. **A345**, 343 (1993).

Pi-94 B. Pichon, Nucl. Phys. **A568**, 553 (1994).

Pl-88 Z. Pluhar and H.A. Weidenmüller, Phys. Rev. **C38**, 1046 (1988).

Po-75 V. Potbhare, *Spectral Averaging Methods in Nuclear Physics*, Ph.D Thesis (University of Rochester, 1975).

Po-76 V. Potbhare and S.P. Pandya, Nucl. Phys. **A256**, 253 (1976).

Po-77 V. Potbhare, Nucl. Phys. **A289**, 373 (1977).

Po-91 V. Potbhare and N. Tresseler, Nucl. Phys. **A530**, 171 (1991).

Pr-72 B.M. Preedom, B.H. Wildenthal, Phys. Rev. **C6**, 1633 (1972).

Qu-74 C. Quesne and S. Spitz, Ann. Phys. (N.Y.) **85**, 115 (1974); Ann. Phys. (N.Y.) **112**, 304 (1978).

Qu-75 C. Quesne J. Math. Phys. **16**, 2427 (1975);

Ra-71 K.F. Ratcliff, Phys. Rev. **C3**, 117 (1971).

Ra-83 J. Rapaport, T. Taddeucci, T.P. Welch, C. Gaarde, J. Larsen, D.J. Horen, E. Sugarbaker, P. Koncz, C.C. Foster, C.D. Goodman, C.A. Goulding and T. Masterson, Nucl. Phys. **A410**, 371 (1983).

Ra-84 A. Ray, S.M. Chitre and K. Kar, Ap. J. **286**, 766 (1984).

Ra-92 A. Ray, K. Kar, S. Sarkar and S. Chakravarti, in *Nuclei in Cosmos*, edited by F. Kappler and K. Wisshak, (IOP publishing, London, 1992).

Ri-91 W.A. Richter, M.G. Vander Merwe, R.E. Julies and B.A. Brown, Nucl. Phys. **A523**, 325 (1991).

Ro-57 N. Rosenzweig, Phys. Rev. **108**, 817 (1957); P.B. Kahn and N. Rosenzweig, Phys. Rev. **187**, 1193 (1969).

Ro-92 G. Rohr, *Level density data based on neutron resonances* (Private communications to V.K.B. Kota, 1992); G. Rohr, L. Maisano and R. Shelly, in *Specialists Meeting on Neutron Cross Sections of Fission Product Nuclei* (Bologna, Italy, 1979), p. 197.

Sa-63 M. Sano and S. Yamasaki, Prog. Theor. Phys. **29**, 397 (1963).

Sa-87a K. Sato and S. Yoshida, Z. Phys. **A327**, 421 (1987); Z. Phys. **A330**, 265 (1988); Z. Phys. **A333**, 141 (1989); K. Sato, Y. Takahashi and S. Yoshida, Z. Phys. **A339**, 129 (1991).

Sa-87b S. Sarkar, K. Kar and V.K.B. Kota, Phys. Rev. **C36**, 2700 (1987).

Sa-88 S. Sarkar and K. Kar, J. Phys. **G14**, L123 (1988); Phys. Rev. **C40**, 1826 (1989).

Sa-93 S. Sarkar, *Spectral Distribution Theory and Strengths of Gamow Teller and M1 Excitations*, Ph.D. Thesis, (University of Calcutta, 1993).

Sc-83 G.K. Schenter and P. Vogel, Nucl. Sci. Eng. **83**, 393 (1983).

Sm-87 J.F. Smith, *Statistical Nuclear Spectroscopy: New Methods and Applications; Level Densities and Related Functions for Interacting-Particle Nuclei*, Ph.D Thesis (University of Rochester, 1987).

Sp-65 B.M. Spicer and J.M. Eisenberg, Nucl. Phys. **63**, 520 (1965).

Ta-69 K. Takahashi and M. Yamada, Prog. Theor. Phys. **41**, 1479 (1969); K. Takahashi, M. Yamada and T. Kondoh, At. Data Nucl. Data Tables **12**, 101 (1973).

Va-37 C. Van Lier and G.E. Uhlenbeck, Physica **4**, 531 (1937).

Va-60 R. Vandenbosch and J. R. Huizenga, Phys. Rev. **120**, 1313 (1960).

Va-77 J.P. Vary and S.N. Yang, Phys. Rev. **C15**, 1545 (1977).

Vo-69 H. Vonach and M. Hille, Nucl. Phys. **A127**, 289 (1969).

Vo-86 T. Von Egidy, A. N. Behkami and H. H. Schimdt; Nucl. Phys. **A454**, 109 (1986); T. Von Egidy, H. H. Schimdt and A. N. Behkami, Nucl. Phys. **A481**, 189 (1988); A.N. Behkami and Z. Kargar, J. Phys. **G18**, 1023 (1992).

We-37 V.F. Weisskopf, Phys. Rev. **52**, 295 (1937).

We-85 T.A. Weaver, S.E. Woosely and G.M. Fuller, *Numerical Astrophysics* editors J. Centrella, J. LeBlanc and R. Bowers (Portola: Science Book International, 1985), p. 374.

Wi-55 E.P. Wigner, Ann. Math. **62**, 548 (1955).

Wi-84 B.H. Wildenthal, Prog. Part. Nucl. Phys. **11**, 5 (1984).

Wo-80a S.E. Woosley, in *Moment Methods in Many Fermion Systems* edited by B.J. Dalton, S.M. Grimmes, J.P. Vary and S.A. Williams (Plenum, N.Y., 1980), p. 61.

Wo-80b S.S.M. Wong, E. Zhao and X. Zhu, Ap. J. (Lett) **242**, L179 (1980).

Wo-86 S.S.M. Wong, *Nuclear Statistical Spectroscopy*, (Oxford University Press, N.Y., 1986).

Wu-66 C.S. Wu and S.A. Moszkowski, *Beta Decay* (Interscience Publishers, N.Y., 1966).

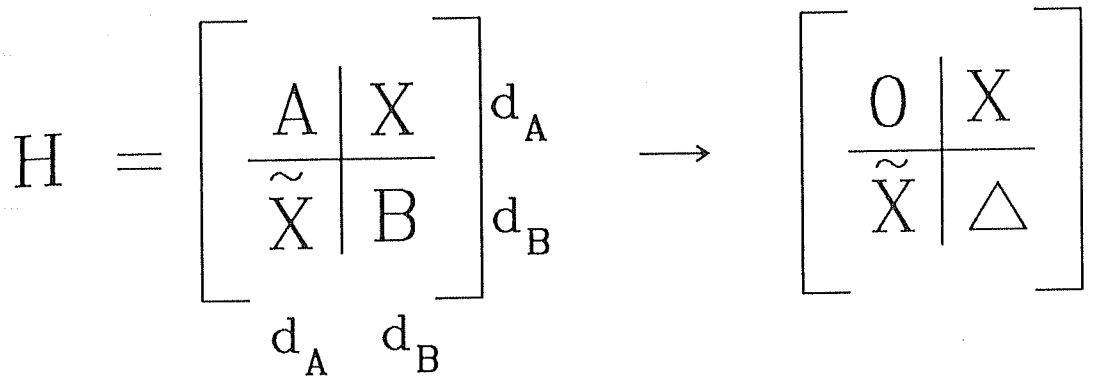
Appendix A

Mixing Between Distant Configurations: $S = 0 \oplus 2$ Shell Model Example

In order to understand the $S = 0 \oplus S = 2$ mixing effects, a simple schematic model is solved in [Fr-83b, Fr-84]. The predictions of this model are tested with a realistic interaction in a shell model $S = 0 \oplus 2$ space and the results are given here.

A.1 Two spike model

In the two spike model considered in [Fr-83a, Fr-84] the hamiltonian (real symmetric) H is a 2×2 block matrix with A and B being the diagonal blocks with dimensions d_A and d_B respectively; $(d_A \leq d_B)$ and X is the off-diagonal block whose transpose is $\widetilde{X}$,



It is further assumed that $A = [0] \longrightarrow A_{ij} = 0$ and $B = [\Delta] \Longrightarrow B_{ij} = (\Delta)\delta_{ij}$; where Δ is a constant. The matrix X is represented by an EGOE. The partial variance σ_{12}^2 and the mixing parameter τ are,

$$\sigma_{12}^2 = \frac{1}{d_A} \sum X_{ij}^2 \tag{A.1}$$

$$\tau = \sigma_{12}^2 / \Delta^2 \tag{A.2}$$

The formal expressions for the state densities $I_\Delta(E)$ and the partial densities $I_\Delta^A(E)$ and $I_\Delta^B(E)$ are given by,

$$I_\Delta(E) = \langle\langle \delta(H - E) \rangle\rangle = I_\Delta^A(E) + I_\Delta^B(E) \tag{A.3}$$

$$\begin{aligned} I_\Delta^A(E) &= \langle\langle \delta(H - E) \rangle\rangle^A \\ &= \sum_{\alpha=1}^{d_A} \left| C_{\alpha(A),E} \right|^2 \; ; \; \alpha = 1, 2, 3, ...d_A \\ I_\Delta^B(E) &= \langle\langle \delta(H - E) \rangle\rangle^B \\ &= \sum_{\beta=1}^{d_B} |C_{\beta(B),E}|^2 \; ; \; \beta = 1, 2, 3, ...d_B \end{aligned} \tag{A.4}$$

In (A.4), $\alpha(A)$ and $\beta(B)$ are the basis states defining the matrices A and B

respectively. Note that $|E\rangle = \sum_{\alpha=1}^{d_A} C_{\alpha(A),E}\,|\alpha\rangle + \sum_{\beta=1}^{d_B} C_{\beta(B),E}\,|\beta\rangle$. The moments of $I_\Delta^A(E)$ are

$$\begin{aligned} M_p(I_\Delta^A) &= \langle H^p \rangle^A \\ &= \frac{1}{d_A} \sum_E \sum_{\alpha=1}^{d_A} |C_{\alpha(A),E}|^2 E^p \\ &= \frac{1}{d_A} \sum_E I_\Delta^A(E) E^p \end{aligned} \tag{A.5}$$

Then it is easily seen that $M_0(I_\Delta^A) = 1$, $M_1(I_\Delta^A) = 0$ and $M_2(I_\Delta^A) = \sigma_{12}^2$. The EGOE representation for X gives [Fr-83b, Fr-84],

$$\begin{aligned} I_0^A(E) &= d_A |E| (\sigma_{12}^2)^{-1} exp(-E^2/\sigma_{12}^2) \;\; ; \; -\infty \le E \le +\infty \\ I_\Delta^A(E) &= \left| \frac{E-\Delta}{E} \right|^{1/2} I_0^A(\sqrt{E(E-\Delta)}); \;\; E \le 0, \; E \ge \Delta \end{aligned} \tag{A.6}$$

Thus $I_\Delta^A(E)$ is bimodal and using (A.6), one can calculate the modal centroid and variance for the lower mode. Discrete version of (A.6), gives for $I_0^A(E)$,

$$I_0^A(E_i) dE_i = 1/2\,, \;\; E_i \neq 0 \tag{A.7}$$

at each non zero eigenvalue E_i of the matrix H. Then with $x_i(x_i + \Delta) = E_i^2$, $I_\Delta^A(E)$ is given by,

$$\begin{aligned} x_i &= -\frac{\Delta}{2} \left\{ 1 - \sqrt{1 + 4E_i^2/\Delta^2} \right\} \\ I_\Delta^A(E = -x_i) &= \sqrt{\frac{x_i + \Delta}{x_i}} \Big/ \left[\sqrt{\frac{x_i}{x_i + \Delta}} + \sqrt{\frac{x_i + \Delta}{x_i}} \right] \\ I_\Delta^A(E = \Delta + x_i) &= \sqrt{\frac{x_i}{x_i + \Delta}} \Big/ \left[\sqrt{\frac{x_i}{x_i + \Delta}} + \sqrt{\frac{x_i + \Delta}{x_i}} \right]. \end{aligned} \tag{A.8}$$

In a shell model example (A.6 - A.8) are tested and the results are given below.

A.2 Numerical test

To test (A.6 - A.8) a shell model calculation is performed in $(ds)^{6\ J=0\ T=0\ ;\ S=0} \oplus [(ds)^4 \times (fp)^2]^{J=0\ T=0\ ;\ S=2}$ space. The dimensions of the $S = 0$ (A block) and $S = 2$ (B block) spaces are $d_A = 71$ and $d_B = 243$. The matrix dimension of H is $d = d_A + d_B = 324$. Employing the Kuo interaction [Ku-71] in the above space, H matrix is constructed using the Rochester - Oak Ridge shell model code [Fr-69b] and then A and B matrices are modified such that $A_{ij} = 0$ and $B_{ij} = (\Delta)\delta_{ij}$. For the above matrix, the partial variance $\sigma_{12}^2 = 5.6044\ MeV^2$. Then the following results are obtained:

[1] Using (A.4) $I^A_{\Delta=0}(E)$ is constructed and verified that $I^A_{\Delta=0}(E) = 1/2$. The histogram for $I^A_{\Delta=0}(E)$ is in good agreement with I^A_0 of (A.6) as shown in Fig. A.1a

[2] For $\tau = 0.1, 0.2, 0.3, 0.5, 1.0, 10.0$ cases $I^A_\Delta(E)$ is constructed and is found to be well represented by (A.6); see for example Figs. A.1b - A.1e.

[3] The ϵ_M/Δ, σ_M^2/σ_{12}^2 for the lower mode are compared with the prediction from (A.6) and the results are given in Table A.1. Thus the shell model calculation confirms that the EGOE results given by (A.6) are good.

[4] The shell model calculations reproduce exactly the results in (A.7, A.8).

[5] Finally it should be mentioned that after completing the calculations, we learnt that the results shown in Figs. A.1 a - e and Table A.1 are also obtained independently by Leclair [Le-94].

Table A.1

τ	ϵ_M/Δ		σ^2_M/σ^2_{12}	
	EGOE[@]	SM[†]	EGOE[@]	SM[†]
0.1	−0.09	−0.8	0.06	0.04
0.2	−0.16	−0.15	0.09	0.07
0.3	−0.22	−0.21	0.11	0.08
0.5	−0.33	−0.31	0.13	0.10
1.0	−0.55	−0.52	0.16	0.12
10.0	−2.37	−2.33	0.20	0.16

[@] The EGOE results follow from Eq. (A.6 - A.8)

[†] Results of the shell model calculations

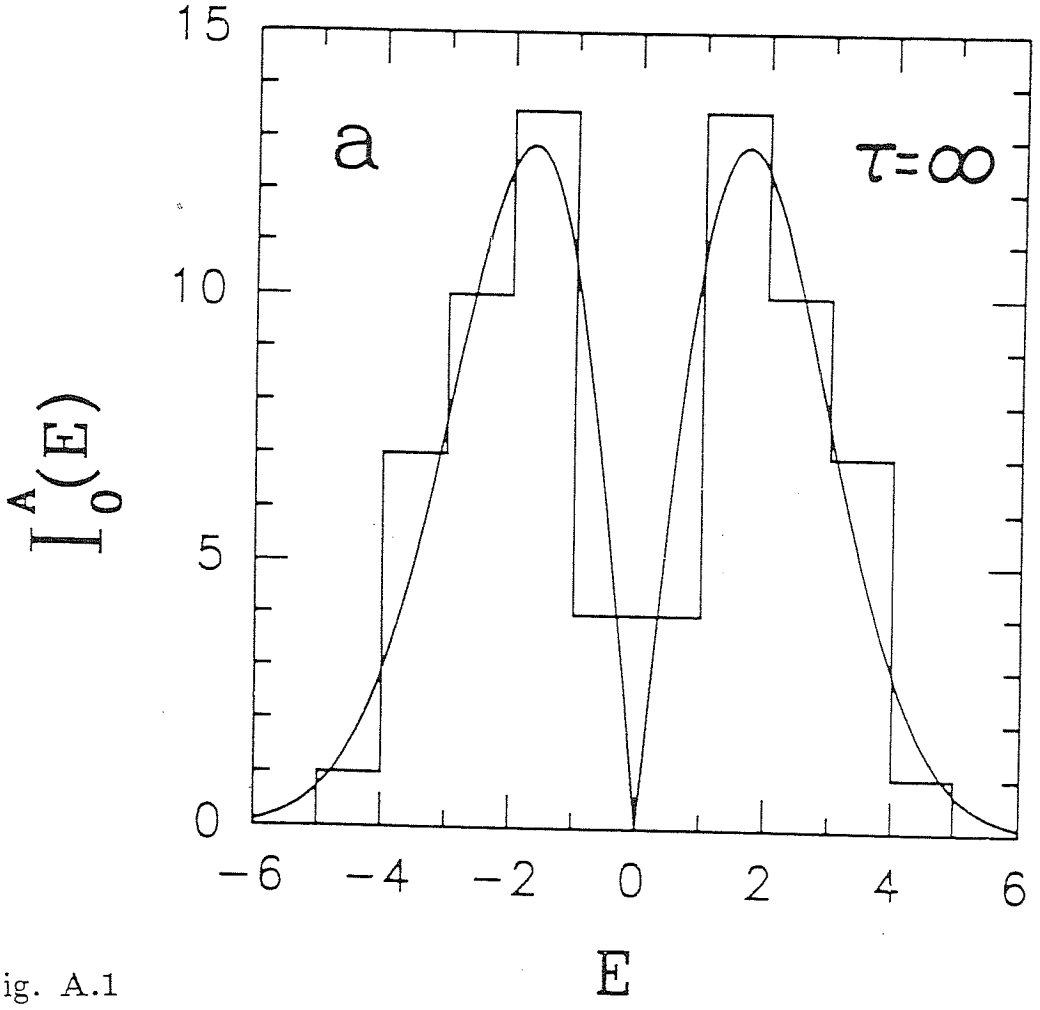


Fig. A.1

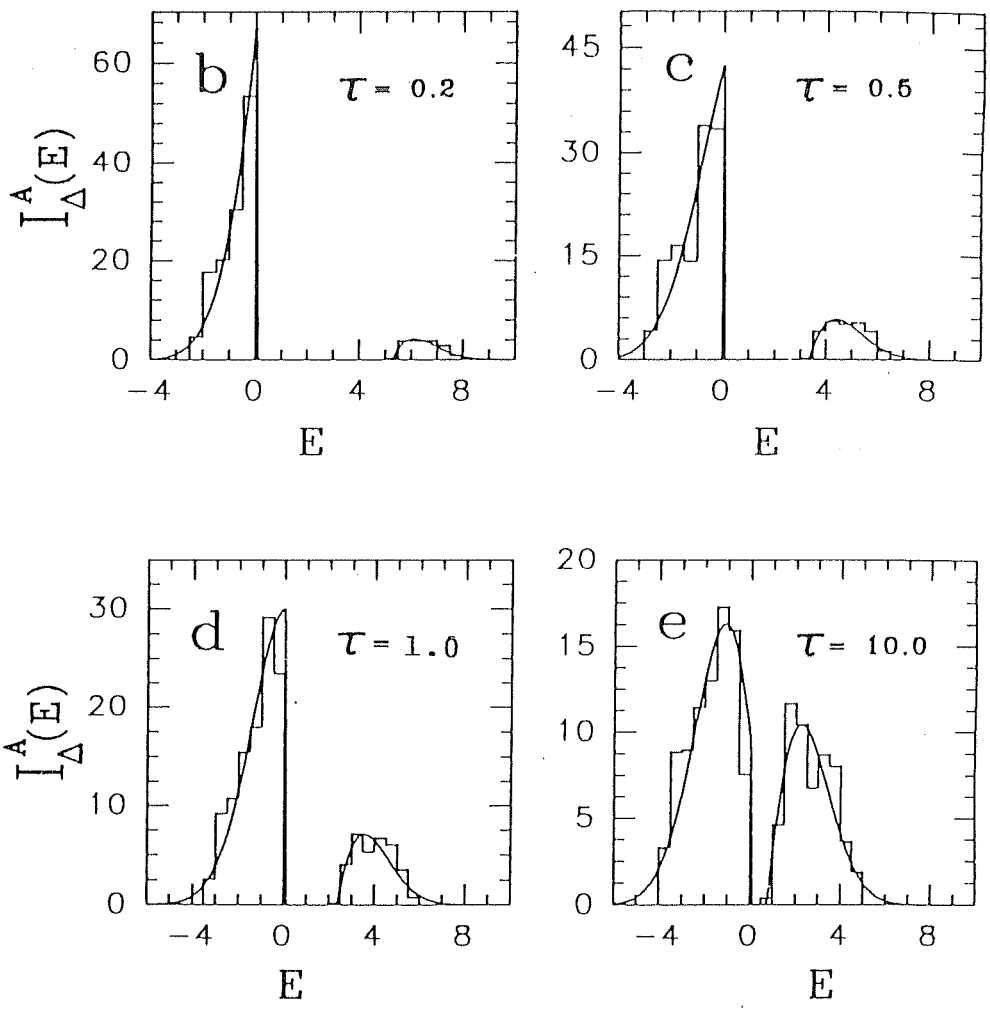


Fig. A.1 (cont'd)

Appendix B

Matrix Elements of Surface Delta Interaction and Pairing Plus Quadrupole-Quadrupole Interaction

B.1 Surface Delta Interaction (SDI)

The mathematical form of the two-body surface delta interaction (SDI) is given by

$$V_{SDI}(1,2) = -4\pi G'_T \delta(\vec{r}(1) - \vec{r}(2))\, \delta(r(1) - R_0) \qquad \text{(B.1)}$$

where G'_T is the strength parameter of the interaction, T denotes isospin, 1,2 denote the particle index, $\vec{r}(1)$ and $\vec{r}(2)$ are the radius vectors of the position of the particles 1 and 2 respectively and R_0 is the nuclear radius. The matrix

elements of the SDI in isospin formalism can be written as [Br-77]

$$\left\langle j_a j_b | V^{SDI} | j_c j_d \right\rangle_{JT} = V^{JT}_{abcd} = (-1)^{n_a+n_b+n_c+n_d} \times$$

$$\frac{G_T}{2(2J+1)} \left[\frac{(2j_a+1)(2j_b+1)(2j_c+1)(2j_d+1)}{(1+\delta_{ab})(1+\delta_{cd})} \right]^{1/2} \times$$

$$\Big\{ (-1)^{j_b+j_d+\ell_b+\ell_d} \langle j_b \ -\tfrac{1}{2} \ j_a \ \tfrac{1}{2} | J \, 0 \rangle \times$$

$$\langle j_d \ -\tfrac{1}{2} \ j_c \ \tfrac{1}{2} | J 0 \rangle \left[1 - (-1)^{l_a+l_b+J+T} \right] -$$

$$\langle j_b \ \tfrac{1}{2} \ j_a \ \tfrac{1}{2} | J \, 1 \rangle \ \langle j_d \ \tfrac{1}{2} \ j_c \ \tfrac{1}{2} | J \, 1 \rangle \left[1 + (-1)^T \right] \Big\} \qquad \text{(B.2)}$$

where $G_T = G'_T C(R_0)$, $C(R_0)$ is a radial integral. In pn formalism the pp(nn) and pn matrix elements follow from $V^{J,pp}_{abcd} = V^{J,\,T=1}_{abcd}$ and $V^{J,pn}_{abcd} = \frac{1}{2}\left[(1+\delta_{ab})(1+\delta_{cd})\right]^{1/2} \left[V^{J,T=0}_{abcd} + V^{J,T=1}_{abcd} \right]$. Taking $G_0 = G_1 = G$ in (B.2), the explicit formula for the pp matrix elements of SDI is,

$$V^{J,pp}_{abcd} = \langle j_a \ j_b \ J | V(pp) | j_c \ j_d \ J \rangle$$

$$= (-1)^{n_a+n_b+n_c+n_d} \times \frac{G}{2(2J+1)} \left[\frac{(2j_a+1)(2j_b+1)(2j_c+1)(2j_d+1)}{(1+\delta_{ab})(1+\delta_{cd})} \right]^{1/2} \times$$

$$\Big\{ (-1)^{j_b+j_d+\ell_b+\ell_d} \langle j_b \ -\tfrac{1}{2} \ j_a \ \tfrac{1}{2} | J \, 0 \rangle \times$$

$$\langle j_d \ -\tfrac{1}{2} \ j_c \ \tfrac{1}{2} | J \, 1 \rangle \left[1 + (-1)^{\ell_a+\ell_b+J} \right] \Big\} \qquad \text{(B.3)}$$

Similarly $V^{J,nn}_{abcd}$ are defined with strength G. The pn matrix elements are,

$$V^{J,pn}_{abcd} = \langle j_a \ j_b \ J | V(pn) | j_c \ j_d \ J \rangle$$

$$= (-1)^{n_a+n_b+n_c+n_d} \times \frac{G}{2(2J+1)} \left[(2j_a+1)(2j_b+1)(2j_c+1)(2j_d+1) \right]^{1/2} \times$$

$$\Big\{ (-1)^{j_b+j_d+\ell_b+\ell_d} \langle j_b \ -\tfrac{1}{2} \ j_a \ -\tfrac{1}{2} | J \, 0 \rangle \langle j_d \ -\tfrac{1}{2} \ j_c \ \tfrac{1}{2} | J \, 0 \rangle -$$

$$\langle j_b \ \tfrac{1}{2} \ j_a \ \tfrac{1}{2} | J \, 1 \rangle \langle j_d \ \tfrac{1}{2} \ j_c \ \tfrac{1}{2} | J \, 1 \rangle \Big\} \qquad \text{(B.4)}$$

It should be pointed out that low energy spectroscopy determines the value of G to be approximately $25/A \ MeV$ [Br-77]. Some useful properties of SDI are:

(i) $V_{\alpha\beta}(SDI-pp) = -\frac{G}{2}(N_\alpha/(N_\alpha-\delta_{\alpha\beta}))$; (ii) $V_{\alpha\beta}(SDI-nn) = -\frac{G}{2}N_\alpha/(N_\alpha-\delta_{\alpha\beta}))$; (iii) $V_{\alpha\beta}(SDI-pn) = -G$; (iv) $\zeta^1_\alpha([\mathrm{m}]) = 0$ for all values of α and [m]'s; (v) $V_{\boldsymbol{\alpha\beta}}(SDI-pp) = \frac{G}{2}(N_{\boldsymbol{\alpha}}/(N_{\boldsymbol{\alpha}}-\delta_{\boldsymbol{\alpha\beta}}))$; (vi) $V_{\boldsymbol{\alpha\beta}}(SDI-nn) = \frac{G}{2}(N_{\boldsymbol{\alpha}}/(N_{\boldsymbol{\alpha}}-\delta_{\boldsymbol{\alpha\beta}}))$; (vii) $V_{\boldsymbol{\alpha\beta}}(SDI-pn) = -G$. Note that SDI-pp stands for pp part of SDI interaction and similarly SDI-nn, SDI-pn are defined. From (iv) it follows that SDI do not produce any SPE renormalizations.

B.2 Pairing plus quadrupole-quadrupole interaction (P + Q.Q)

The P + Q.Q hamiltonian is defined in terms of the pp and nn pairing hamiltonians H^P_p and H^P_n and the pp, nn and pn quadrupole-quadrupole hamiltonians $\bar{Q}_p.\bar{Q}_p$, $\bar{Q}_n.\bar{Q}_n$ and $\bar{Q}_p.\bar{Q}_n$,

$$H_{P+Q.Q} = G_pH^P_p + G_nH^P_n + G^Q_{pp}\bar{Q}_p.\bar{Q}_p + G^Q_{nn}\bar{Q}_n.\bar{Q}_n + G^Q_{pn}\bar{Q}_p.\bar{Q}_n \tag{B.5}$$

$$\left\langle (j_aj_b)J|H^P_\rho|(j_cj_d)J\right\rangle^{\text{a.s.m}} = \delta_{ab}\delta_{cd}\delta_{J=0}\times$$

$$\sqrt{(2j_a+1)(2j_c+1)}(-1)^{\ell_a-\ell_c};\ \rho = p \text{ or } n \tag{B.6}$$

$$\bar{Q}_{\mu;p} = \sqrt{\frac{16\pi}{5}}\frac{r_p^2}{b_p^2}Y^2_\mu(\theta_p,\phi_p),\ \bar{Q}_{\mu;n} = \sqrt{\frac{16\pi}{5}}\frac{r_n^2}{b_n^2}Y^2_\mu(\theta_n,\phi_n) \tag{B.7}$$

As can be seen from (B.6), the pairing hamiltonians are defined in terms of their antisymmetric matrix elements (a.s.m.). The matrix elements of $Q.Q$ hamiltonians are given by,

$$\langle (j_aj_b)J|\bar{Q}.\bar{Q}|(j_cj_d)J\rangle^{\text{n.a.s.m}} = (-1)^{j_a+j_b+J}\left\{\begin{array}{ccc} j_a & j_b & J \\ j_d & j_c & 2\end{array}\right\}\times$$

$$\langle j_a||\bar{Q}||j_c\rangle\langle j_b||\bar{Q}||j_d\rangle; \tag{B.8}$$

$$\langle N_a \ell_a \tfrac{1}{2} j_a || \bar{Q} || N_c \ell_c \tfrac{1}{2} j_c \rangle = \langle N_a \ell_a || r^2/b^2 || N_c \ell_c \rangle \times$$
$$\sqrt{2j_a+1} \langle j_b \tfrac{1}{2} 20 | j_c \tfrac{1}{2} \rangle \left\{ 1 + (-1)^{\ell_a + \ell_c} \right\} \qquad \text{(B.9)}$$

$$\begin{aligned}
\left\langle N, \ell || r^2/b^2 || N, \ell \right\rangle &= N + 3/2 \\
\left\langle N, \ell+2 || r^2/b^2 || N, \ell \right\rangle &= -[(N-\ell)(N+\ell+3)]^{1/2} \\
\left\langle N+2, \ell || r^2/b^2 || N, \ell \right\rangle &= -\frac{1}{2}[(N-\ell+2)(N+\ell+3)]^{1/2} \\
\left\langle N+2, \ell+2 || r^2/b^2 || N, \ell \right\rangle &= \frac{1}{2}[(N+\ell+3)(N+\ell+5)]^{1/2} \\
\left\langle N+2, \ell-2 || r^2/b^2 || N, \ell \right\rangle &= \frac{1}{2}[(N-\ell+2)(N-\ell+4)]^{1/2} \qquad \text{(B.10)}
\end{aligned}$$

$$\langle (j_a j_b) J | \bar{Q}_\rho . \bar{Q}_\rho | (j_c j_d) J \rangle^{\text{a.s.m}} = [(1+\delta_{ab})(1+\delta_{cd})]^{-1/2} \times$$
$$\left\{ \left\langle (j_a j_b) J | \bar{Q}_\rho . \bar{Q}_\rho | (j_c j_d) J \right\rangle^{\text{n.a.s.m}} - \right.$$
$$\left. (-1)^{j_c + j_d + J} \left\langle (j_a j_b) J | \bar{Q}_\rho . \bar{Q}_\rho | (j_c j_d) J \right\rangle^{\text{n.a.s.m}} \right\} \; ; \; \rho = p, n \qquad \text{(B.11)}$$

$$\langle (j_a j_b) J | \bar{Q}_p . \bar{Q}_n | (j_c j_d) J \rangle^{\text{a.s.m}} = \langle (j_a j_b) J | \bar{Q}_p . \bar{Q}_n | (j_c j_d) J \rangle^{\text{n.a.s.m}} \qquad \text{(B.12)}$$

In (B.8) - (B.12) n.a.s.m. stands for non antisymmetric matrix elements. The relationship between the strengths (G_p, G_n) and $(G^Q_{pp}, G^Q_{nn}, G^Q_{pn})$ with the standard parameters [Ba-68, Be-69, Br-77] $(\bar{G}_p, \bar{G}_n, \chi')$ are

$$\begin{aligned}
G_p &= \bar{G}_p/4; \qquad \bar{G}_p = 27/A \\
G_n &= \bar{G}_n/4; \qquad \bar{G}_n = 22/A \qquad \text{(B.13)}
\end{aligned}$$

$$\begin{aligned}
G^Q_{pp} &= -\frac{\chi'}{2} x_0 \left(\frac{5}{16\pi} \right) \alpha_p^2 \\
G^Q_{nn} &= -\frac{\chi'}{2} x_0 \left(\frac{5}{16\pi} \right) \alpha_n^2 \\
G^Q_{pn} &= -\chi' x_0 \left(\frac{5}{16\pi} \right) \alpha_p \alpha_n
\end{aligned}$$

$$\alpha_p = (2Z/A)^{1/3};\ \alpha_n = (2N/A)^{1/3};\ x_0 \simeq 2$$

$$\chi' \simeq 242 A^{-5/3}\ MeV$$

$$\text{or} \simeq \frac{242}{A^{5/3}} \left\{ 1 + \left(\frac{3A}{2} \right)^{-1/3} \right\}\ MeV \simeq 280\, A^{-5/3} MeV \qquad \text{(B.14)}$$

The definition of Q.Q interaction given in (B.5 - B.12) is somewhat different from the form given in [Ba-68, Be-69]. The value of x_0 in (B.14) is verified by calculating variances of Q.Q interaction in *ds* - shell examples and comparing them with the variances produced by CW [Va-77] interaction. Similar checks are made for a heavy nucleus by comparing with variances obtained with SDI. It is useful to mention that for the pairing interaction $V_{\alpha\beta}(pn) = 0$ and $\zeta^1_\alpha([\mathbf{m}]) = 0$ for all α's and $[\mathbf{m}]$'s. Similarly $V_{\alpha\beta}(Q.Q - \text{pn}) = 0$ for all (α, β).

Appendix C

Compilation of Level Density and Spin-Cutoff Factor Data for fp-Shell Nuclei

Experimental data for level densities (also for spin-cutoff factors) is normally available in two forms: (i) values for the level densities at some select energies; (ii) values for the level density parameters assuming a form for the level densities. In the later case, usually the NIP Fermi gas forms (reviews of NIP level density theories are given for example in [Er-60, Er-66, Hu-72, Da-80]) are used and this is always the case with the data available in literature for fp - shell nuclei. Therefore, in Sect. C.1 an overview of the Fermi gas forms for level densities and spin-cutoff factors is given. Sect. C.2 describes briefly the various experimental methods for obtaining level density and spin-cutoff factor data. Finally in Sect. C.3 the data compilation for the eight fp - shell nuclei ^{55}Mn, ^{56}Fe, ^{59}Co, ^{60}Co, ^{60}Ni, ^{62}Ni, ^{63}Mn and ^{65}Cu (their selection follows from Sect. 4.2.1) is given.

C.1 Fermi gas forms for level densities and spin-cutoff factors

Fermi gas forms for state densities

For identical particle systems, the celebrated formula $I(E) = \frac{1}{\sqrt{48E}} exp\ 2\sqrt{aE}$ for state densities is due to Bethe [Be-36] and it is derived by considering the nucleus to be degenerate Fermi gas and assuming that the density depends only on the single particle state density $g(\epsilon_f)$ at the Fermi surface. Replacing the true s.p. spectrum by a uniform spectrum with spacing g^{-1} and then using Hardy Ramanujan partition formula [Ab-64; p. 825, Va-37] immediately gives the above Bethe formula with $a = \frac{\pi^2}{6} g(\epsilon_f)$. For the realistic pn systems, the form for the state densities follows easily by using the fact that the pn NIP density is a simple convolution of the proton and neutron state densities, $I_{pn}(E) = I_p \otimes I_n[E]$. Using the Bethe form for I_p and I_n and evaluating the convoluting integral using saddle point approximation, the formula for the state density (with $g_p(\epsilon_f) = g_n(\epsilon_f) = g/2$ and dropping the pn indices from now onwards) is $I(E) = (\sqrt{\pi}/12a^{1/4}E^{5/4}) exp 2\sqrt{aE}$. However in practice the energies should be back-shifted with $E \rightarrow E - \Delta$ in the above Fermi gas formula for $I(E)$. Hurwitz and Bethe [Hu-51] for the first time pointed out the importance of shifting the energies. The origin of the energy shift lies in (i) shell effects: for example Rosenzweig [Ro-57] demonstrated this by dealing with periodic s.p. spectrum with or without degeneracies; (ii) pairing effects: by solving the so called temperature dependent gap equation, Sano and Yamasaki [Sa-63] showed that pairing interaction produces a shift of energies in the Fermi gas formula. However as Vonach and Hill [Vo-69] pointed out in general it is good to treat Δ as a free parameter (Δ is usually smaller than

the pairing shift). The explicit back shifted Fermi gas form for state density $I(E)$, in terms of the parameters a and Δ, is

$$I(E) = \frac{\sqrt{\pi}}{12a^{1/4}(E-\Delta)^{5/4}} exp\ 2\sqrt{a(E-\Delta)} \qquad \text{(C.1)}$$

Given the density $I(E)$, nuclear temperature T is defined as $T^{-1} = \frac{\partial}{\partial E} ln\ I(E)$ and on the other hand the thermodynamic (statistical) temperature t is defined in terms of the entropy S, $t^{-1} = \frac{\partial S}{\partial E}$. In general one can write E in powers of T as $E = T^n/\bar{a}$ where $\bar{a}$ is a constant. For a degenerate Fermi gas, $n = 2$ and using this gives $E = aT^2 \Longrightarrow I(E) = Cexp2\sqrt{aE}$ where a and C are constants. This Weisskopf formula [We-37] is same as Bethe's formula (C.1) but with no energy denominator. Gilbert and Cameron [Gi-65] argued that in general it is good to use constant temperature formula in analyzing low energy level density data and on the other hand Maruyama [Ma-69, Ig-70] showed that for the nuclei near closed shells, constant temperature formula is relevant. The constant temperature formula (with back shifting denoted by E_0), used recently by Von Egidy et al [Vo-86] in analyzing large amount of low energy data, is

$$I(E) = \frac{1}{T} exp\{(E-E_0)/T\}. \qquad \text{(C.2)}$$

The Lang LeCouteur (LLC) level density formula [La-54], which is commonly used in data analysis, was derived by first considering free energy and it differs from (C.1) in the energy denominator (it involves the temperature 't'),

$$I(E) = \frac{\sqrt{\pi}}{12a^{1/4}(E-\Delta+t)^{5/4}} exp\ 2\sqrt{a(E-\Delta)},$$

$$U = E - \Delta = at^2 - t. \qquad \text{(C.3)}$$

$$t = \frac{1 \pm \sqrt{4a(E-\Delta)+1}}{2a} \simeq \sqrt{\frac{E-\Delta}{a}} \qquad \text{(C.4)}$$

The result in (C.4) that $t \simeq \sqrt{(E-\Delta)/a}$ also follows from (C.1) and the definition of T ($T \sim t$).

Angular momentum decomposition: fixed-J densities

In order to analyze the data on observable level densities, it is necessary to decompose state densities into fixed-J level densities. Starting with fixed (E, M) bivariate densities $\rho(E,M)$ where M is a eigenvalue of the J_Z operator and recognizing that $\rho(E,M)$ can be written as $\rho(E,M) = \rho(E)\rho(M|E)$, then applying CLT for the conditional $\rho(M|E)$ density gives the J - decomposition of $I(E)$. Noting that the centroid $\langle J_Z \rangle^E$ of $\rho(M|E)$ is always zero and denoting the variance $\langle J_Z^2 \rangle^E$ by $\sigma_J^2(E)$ (the spin-cutoff factor), $I(E,M) = \dfrac{I(E)}{\sqrt{2\pi}\sigma_J(E)} exp\ -\dfrac{M^2}{2\sigma_J^2(E)}$. Now the elementary subtraction $I(E, M = J) - I(E, M = J+1)$ gives the fixed-J level densities which are denoted hereafter by $I_\ell(E,J)$. The formulas for $I_\ell(E,J)$, for the level densities $I_\ell(E, J_1 : J_2)$ in the spin window $J_1 - J_2$ ($I_\ell(E, J_1 : J_2)$ gives number of levels per MeV at energy E with spins between J_1 and J_2) and total level density $I_\ell(E)$ (which gives number of levels per MeV at energy E irrespective of the J value) are,

$$\begin{aligned} I_\ell(E,J) &= \frac{1}{\sqrt{2\pi}\sigma_J(E)} \left[exp\left\{ -\frac{J^2}{2\sigma_J^2(E)} \right\} - exp\left\{ -\frac{(J+1)^2}{2\sigma_J^2(E)} \right\} \right] I(E) \\ &\simeq -\frac{\partial}{\partial M} I(E,M)\Big|_{M=J+1/2} \\ &= \frac{2J+1}{\sqrt{8\pi}\sigma_J^3(E)} exp\left\{ -\frac{(J+1/2)^2}{2\sigma_J^2(E)} \right\} I(E) \\ &= C_J(E) I(E) \end{aligned} \qquad \text{(C.5)}$$

$$I_\ell(E,J) = (2J+1) exp\left\{ -\frac{(J+1/2)^2}{2\sigma_J^2} \right\} I_\ell(E,0)\ ;$$

$$I_\ell(E,0) = \frac{1}{\sqrt{8\pi}\sigma_J^3} I(E) \tag{C.6}$$

$$\begin{aligned} I_\ell(E, J_1 : J_2) &= \frac{1}{\sqrt{2\pi}\sigma_J(E)} \left[exp\left\{ -\frac{(J_1)^2}{2\sigma_J^2(E)} \right\} - exp\left\{ -\frac{(J_2+1)^2}{2\sigma_J^2(E)} \right\} \right] I(E) \\ &\simeq \left[\sum_{J=J_1}^{J_2} C_J(E) \right] I(E) \\ &= C_{J_1:J_2}(E) I(E) \; ; \end{aligned} \tag{C.7}$$

$$I_\ell(E) = \sum_J I_\ell(E,J) = I_\ell(E, 0:\infty) = C_{0:\infty} I(E)$$

$$= \frac{1}{\sqrt{2\pi}\sigma_J(E)} I(E) = [\sqrt{2\pi}\sigma_J(E) C_{J_1:J_2}(E)]^{-1} I_\ell(E, J_1 : J_2) = 2\sigma_J^2(E) I_\ell(E,0) \tag{C.8}$$

Formulas for spin-cutoff factors

The spin-cutoff factors can be written in terms of a and Δ and rigid body moment of inertia $\mathcal{I}_{rig}$ for a 'A' nucleon system. Adding the rotational hamiltonian $V_R = J^2\hbar^2/(2\mathcal{I}_{rig})$ to the NIP hamiltonian h gives $H = h + V_R$ and then assuming that h and V_R are independent leads to $E = E_h + E_{V_R}$. Using the Fermi gas form (C.1) for $I_h(E)$ immediately gives $I_H(E) \sim exp 2\sqrt{a(E - E_{V_R})}$, where $E_{V_R} = \hbar^2 J(J+1)/(2\mathcal{I}_{rig})$. Writing $I_\ell(E,J)$ given in (C.5) in the form of $exp\; 2\sqrt{a(E-E')}$ by using (C.1) for $I(E)$, it is easily seen that $E' = \frac{J(J+1)}{2\sigma_J^2}\sqrt{\frac{E}{a}}$. Then by equating the expressions for E_{V_R} and E' yields a formula for $\sigma_J^2(E)$, $\sigma_J^2(E) = \frac{\mathcal{I}_{rig}}{\hbar^2}\sqrt{\frac{E-\Delta}{a}}$. In practice $\mathcal{I}_{rig}$ is replaced by $\chi\mathcal{I}_{rig}$ with χ a free parameter. With this and also noting from (C.4) that $t \simeq \sqrt{(E-\Delta)/a}$, a formula for $\sigma_J^2(E)$ is (with m the nucleon mass) [Wo-80a],

$$\sigma_J^2(E) = \frac{\chi\mathcal{I}_{rig}}{\hbar^2}\sqrt{\frac{E-\Delta}{a}} \simeq \frac{\chi I_{rig}}{\hbar^2} t \tag{C.9}$$

With $\mathcal{I}_{rig} = 2/5mAR^2$ and $R = r_0 A^{1/3}\, fm$ ($r_0 \simeq 1.2$), a simpler formula is

$$\sigma_J^2(E) = 0.0096(\chi)(r_0^2)A^{5/3}t \tag{C.10}$$

Unless otherwise specified, $\chi = 1$ in (C.9, C.10) from now onwards. A simpler expression in terms of mass number A follows by recognizing that (i) $\mathcal{I}_{rig}$ can be written in terms of $\langle J_Z^2 \rangle^1$ and 'a' as given for example in [La-66]; (ii) using Fermi gas model to derive expressions for $\langle J_Z^2 \rangle^1$ in terms of A, $\langle J_Z^2 \rangle^1 \propto A^{2/3}$ as follows for example from [Je-52]. The resulting formula for $\sigma_J^2(E)$, as given by Gilbert and Cameron [Gi-65], is

$$\sigma_J^2(E) = 0.0888\sqrt{a(E-\Delta)}A^{2/3} \tag{C.11}$$

Parity decomposition

The state density is sum of fixed parity (π) densities $I^\pi(E)$ and assuming the equilibration (as commonly used in data analysis [1]) of $I^\pi(E)$ densities gives,

$$\begin{aligned} I(E) &= I^+(E) + I^-(E) \\ I^+(E) &\simeq I^-(E) \simeq \frac{1}{2} I(E) \end{aligned} \tag{C.12}$$

Similar expressions for $I_\ell^\pi(E,J)$, $I_\ell^\pi(E, J_1 : J_2)$ and $I_\ell^\pi(E)$ can be written down in terms of $I_\ell(E,J)$, $I_\ell(E, J_1 : J_2)$ and $I_\ell(E)$ respectively. Given fixed parity spin-cutoff factors $\sigma_J^2(E;\pi)$, following (C.12) it is assumed that,

$$\sigma_J^2(E) = \frac{1}{2}\{\sigma_J^2(E;+) + \sigma_J^2(E;-)\}\,;$$

[1] Using parity equilibration in data analysis demands that this feature should come out in a IP theory but this need not be the case with NIP densities. In fact in the NIP calculations presented in Sect. 3.3 (both in the exact and moment methods) it is found that the parity ratio $w = (I^+ - I^-)/(I^+ + I^-)$ fluctuates around zero and tends to zero only at higher energies. In a recent NIP study, Cerf [Ce-93; also Pi-94] produced a theory for understanding this result. It should be mentioned that in our IP calculations (reported in Chapter 4) we do find parity equilibration. But however, in order to firmly establish this result it is necessary to use two different reference energies one for each parity. Good experimental data for this is not available for the fp - shell nuclei considered in Chapter 4.

$$\sigma_J^2(E;+) \simeq \sigma_J^2(E;-) \tag{C.13}$$

a and Δ parameters

Using the oscillator s.p. spectrum and filling the shells with A nucleons upto shell number N, it is easy to derive that $g(\epsilon_f) \sim 2(N+3/2)^2/(\hbar\omega)$, $A = (2/3)(N+2)^3$ and $\hbar\omega = 41A^{-1/3}\ MeV$. This then gives $a \simeq 0.105A[1 - \left(\frac{2}{3}\right)^{1/3} A^{-1/3}]$. Extending this to pn systems, leads to $I_Z = (N-Z)/2$ dependence for the 'a' parameter, $a = 0.015A[1 - (2/3)^{1/3}A^{-1/3} - (2/9)I_Z^2]$. Thus $a \sim A/10$. By considering more general potentials it is shown that [Ig-76, Ka-80, Il-92] 'a' in general takes the form that $a = \alpha A[1 + \gamma B_s A^{-1/3}]$ where α and γ are constants and B_s is the surface energy. There are several other variants to this formula where 'a' is related to for example neutron and proton separation energies [Ka-80], shell correction energies [Gi-65], excitation energy E dependence [Ba-70] etc.

There are various parametrization for 'Δ' available in literature and the simplest one is where the formula [Bo-69] for odd-even mass difference $\bar{\Delta} \sim 12/A^{1/2}\ MeV$ is used and this gives $\Delta = 2\bar{\Delta}$ for even-even nuclei, $\bar{\Delta}$ for odd-even and even-odd nuclei and zero for odd-odd nuclei. Several other parametrization are given for example in [Gi-65, Di-73, Ig-83, Il-92].

C.2 Brief description of the experimental methods

Direct counting of levels

At low excitation energies, the nuclear energy levels can be measured - in some cases with the spin and the parity and in some cases without spin

and/or parity. In an energy domain $E-\frac{\epsilon}{2}$ to $E+\frac{\epsilon}{2}$ with $\epsilon \sim 1MeV$, assuming that all the levels are identified experimentally, simple counting of the number of levels gives $I_\ell(E)$. This method is severly constrained by the requirement that all the levels in a given energy domain must be identified experimentally. Because of this, direct counting yields level density data only upto 3-4 MeV excitation (in many cases at energies lower than this). It is useful to mention that Von Egidy et al [Vo-86] compiled complete set of low energy data for a number of nuclei but they constrain the spin and parity window. This data is not used in the present compilation as its analysis requires a knowledge of spin-cutoff factors at low energies (spin-cutoff factors are poorly defined and determined at low energies).

Neutron or proton resonance experiments

In the neutron resonance experiments, a nucleus in its ground state is bombarded with a slow neutron (with energy ranging from few eV to a keV) as a result of which an excited compound nucleus is formed with the excitation energy equal to the neutron binding energy (B_n). Near the neutron binding energy (resonance energy), 100-200 resonances can be observed in the compound nucleus and the width of these resonances is very small compared to the mean resonance spacing. Thus in the slow neutron experiments, at the resonance energy, the number of resonances can be counted in a small energy window and this then gives the mean level spacing (D) at B_n. If the angular momentum and parity of the target nucleus is J^π, then the spins and parities of the resonances are $(J+\frac{1}{2})^\pi$ and $(J-\frac{1}{2})^\pi$. For a target with zero spin, the resonance spin and parity is $\frac{1}{2}^+$. Thus from the mean level spacing D, $I_\ell^\pi(E;J_1:J_2)$ can be calculated from which $I_\ell(E)$ is deduced using (C.3 - C.8,

C.10, C.12, C.13) at neutron binding energy (at one energy only). The neutron resonance data is available [Mu-81, Mu-84, Ro-92] for ^{60}Co, ^{60}Ni and ^{62}Ni.

A proton resonance experiment is basically a (p, p') reaction [Mi-80]. For the resonances to be observed, the level (resonance) width Γ has to be much less than the mean spacing (between the resonances) D. In the actual experiment the target (even-even nucleus) is bombarded with protons of energy $\sim$ 2 - 3 MeV and then the energies, spins and parities of about 100-200 compound states are determined. The reaction cross-section is plotted against the proton energy and the resonances are counted. Here the resonance data are restricted to the medium and light nuclei due to the Coulomb barrier. With B_p the proton separation energy and that the resonances are observed with incident protons having energy in the range E_{p_1} to E_{p_2}, the resonance energy is then taken to be $E = B_p + (E_{p_1} + E_{p_2})/2$. Thus the average spacing between the resonances is calculated by direct observation of the resonances and it is converted into level density and interpreted as density at the energy E given above. In practice this will be in error (as $I(E)$ changes like $2\sqrt{aE}$) as $E_{p_1} - E_{p_2} \sim 1MeV$. Some authors take this error into account and in fact produce $I_\ell(E)$ at two energies around E given above. Wherever this analysis is available, those values are taken or otherwise the above procedure is followed to get proton resonance density. The proton resonance data is available for the odd nuclei ^{55}Mn, ^{59}Co and $^{63,65}Cu$.

Charge particle spectra

In these experiments the level densities are not measured directly but the level density parameters are extracted out by analyzing the data from charge particle nuclear reactions of the type $A(a, b)B$ where a and b represent charge

particles (i.e. α particles, proton etc.). The differential cross sections ($\frac{d^2\sigma_{ab}}{d\epsilon_b d\Omega_b}$) data are analyzed using an extended form of Weisskopf formula [We-37] where the angular momentum is incorporated fully [Lu-72a, Hu-72],

$$\frac{d^2\sigma_{ab}(\epsilon_b,\theta)}{d\epsilon_b d\Omega_b} = \sum_{L=0\ (L\,even)}^{\infty} B_L(\epsilon_b) P_L(cos\theta)$$

$$B_L(\epsilon_b) = \tfrac{1}{4}(2K_a+1)^{-1}(2i_a+1)^{-1}k_a^{-2} \sum_{S_a,S_b,K_b,\ell_a,\ell_b,J} (-1)^{S_a-S_b} T_a^{\ell_a}(\epsilon_a) T_b^{\ell_b}(\epsilon_b)$$
$$\times Z(\ell_a J \ell_a J; S_a L) Z(\ell_b J \ell_b J; S_b L) I_{\ell;b}(U_b, K_b) [G(J)]^{-1}$$

$$G(J) = \sum_{b'} \int_0^{(U_{b'})_{max}} dU_{b'} \sum_{\ell_{b'}=0}^{(\ell_{b'})_{max}} T_{b'}^{\ell_{b'}}(\epsilon_{b'}) \sum_{S_{b'}=|J-\ell_{b'}|}^{J+\ell_{b'}} \sum_{K_{b'}=|S_{b'}-i_{b'}|}^{S_{b'}+i_{b'}} I_{\ell;b'}(U_{b'}, K_{b'}). \tag{C.14}$$

In (C.14) K_a, i_a, J, K_b and i_b are the spins of the target, projectile, compound nucleus, residual nucleus and emitted particle respectively. S_a and S_b are the channel spins in the incident and outgoing channels respectively; ℓ_a and ℓ_b are the orbital angular momenta of the incident and outgoing particles respectively; k_a is the wave number of the incident particle; $P_L(cos\theta)$ is the Legendre polynomial of order L. $T_a^{\ell_a}(\epsilon_a)$ and $T_b^{\ell_b}(\epsilon_b)$ are transmission coefficients for the projectile and emitted particles respectively with the channel energies ϵ_a and ϵ_b (the channel energy ϵ is defined as the sum of the kinetic energies with respect to the center of mass of the emitted particle and recoil nucleus). The $Z(\ell_a\, J\, \ell_a J;\, S_a\, L)$ and $Z(\ell_b\, J\, \ell_b J;\, S_b\, L)$ are Z coefficients and are defined as sums of products of Racah W coefficients and Clebsch-Gordon coefficients; $Z(\ell\, J\, \ell\, J;\, S\, L) = (2J+1)(2\ell+1)W(\ell\, J\, \ell\, J;\, S\, L)\langle \ell\, 0\, \ell\, 0 | L\, 0\rangle$. $I_\ell(E,J)$ is level density of the residual nucleus formed by the emission of particle b with channel energy ϵ_b. The sum over b' refers to the sum over all the different types of emitted particles. In the 'exact' analysis using (C.14), spectra from different reactions leading to the same final nucleus are analyzed with one set of

(a, Δ) values and then a complicated search programme produced the values of (a, Δ). In the analysis, the LLC formula (C.3, C.4), angular momentum decomposition formulas (C.5 - C.8) and the spin-cutoff factor formula (C.10) with $r_0 = 1.2$ are used. The charged particle experiments are due to Lu et al [Lu-72a] and they are carried out for the nuclei ^{56}Fe, ^{59}Co, $^{60,62}Ni$ and $^{63,65}Cu$:

Residual Nucleus	Reaction	Residual Nucleus	Reaction
^{56}Fe	$^{56}Fe(\alpha,\alpha')^{56}Fe$ $^{59}Co(p,\alpha)^{56}Fe$	^{63}Cu	$^{63}Cu(p,p')^{63}Cu$ $^{60}Ni(\alpha,p)^{63}Cu$ $^{63}Cu(\alpha,\alpha')^{63}Cu$
^{59}Co	$^{59}Co(p,p')^{59}Co$ $^{56}Fe(\alpha,p)^{59}Co$ $^{59}Co(\alpha,\alpha')^{59}Co$ $^{62}Ni(p,\alpha)^{59}Co$	^{65}Cu	$^{65}Cu(p,p')^{65}Cu$ $^{62}Ni(\alpha,p)^{65}Cu$ $^{65}Cu(\alpha,\alpha')^{65}Cu$
^{60}Ni	$^{60}Ni(\alpha,\alpha')^{60}Ni$ $^{63}Cu(p,\alpha)^{60}Ni$	^{62}Ni	$^{62}Ni(p,p')^{62}Ni$ $^{59}Co(\alpha,p)^{62}Ni$
			$^{62}Ni(\alpha,\alpha')^{62}Ni$ $^{65}Cu(p,\alpha')^{62}Ni$

Lu et al [Lu-72a] deduced one set of (a, Δ) values for the nuclei ^{56}Fe, ^{59}Co, ^{60}Ni, $^{63,65}Cu$ and two sets of (a, Δ) values for ^{62}Ni. The level densities and spin-cutoff factors calculated at different energies using the deduced (a, Δ) parameters and the smoothed NIP forms (C.3 - C.8, C.10) with $r_0 = 1.2$ are treated as experimental data. This data is called Lu et al data in the compilation given in Sect. C.3 (for ^{62}Ni there are Lu at al (a) and Lu at al (b) data corresponding to the two sets of (a, Δ) parameters deduced for this nucleus).

Ericson fluctuations

In the excitation energy domain around 20 MeV of the compound nuclei (in compound nucleus reaction) the cross-sections fluctuate strongly and here the level width Γ is larger than the average spacing D between the resonances. This region is called the Ericson fluctuation region. Using a statistical theory

[Er-66], the average cross-section in Ericson fluctuation domain is related to $\Gamma/D_{J=0}$; $D_{J=0} = [I_\ell(E,0)]^{-1}$. Measurement of average cross-sections and independent knowledge of Γ, then yield a value of $D_{J=0}$ or equivalently (using C.6, C.8) for the total level density $I_\ell(E)$ at various energies in the Ericson fluctuation domain. Using the (p,p') and (p,α) reactions, Ericson fluctuation experiments are carried out and at some energies around 20 MeV excitation in ^{55}Mn, ^{56}Fe, ^{60}Co and ^{60}Ni the total level density $I_\ell(E)$ is deduced. These experiments are due to Katsanos et al [Ka-66b, Ka-70] and Huizenga et al [Hu-69].

Dilg et al data, Katsanos et al and Iljinov et al data

First systematic analysis of the level density data was carried out by Gilbert and Cameron [Gi-65] in 1965. They have used a constant temperature formula (C.2) for level densities at low energy domain and the back-shifted fermi gas form (C.1) for high energy domain and gave a prescription to join them to obtain a smoothed (continuous) curve for level densities. A more recent analysis of this type is due to Dilg et al [Di-73]. By fitting the low energy level density data and the data from neutron/proton resonance experiments, using the LLC formulas (C.3, C.4) and (C.5 - C.8, C.10) with $r_0 = 1.25$, Dilg et al deduced the values for the level density parameters (a, Δ) for about 200 nuclei. The Dilg et al (a, Δ) values are available for the six nuclei ^{55}Mn, $^{59,60}Co$, ^{62}Ni, $^{63,65}Cu$ in the set considered in Sect. C.3. Using (a, Δ) values that are deduced for $\sim$ 200 nuclei, Dilg et al constructed smoothed formulas for (a, Δ) as a function of the mass number A. The smoothed formulas are

$$\begin{aligned} a(MeV^{-1}) &= 2.40 + 0.067A \\ \Delta(MeV) &= P - 130/A \end{aligned}$$

$$
\begin{aligned}
P &= 25.6A^{-1/2} \text{ for even-even nuclei} \\
&= 12.8A^{-1/2} \text{ for odd-mass nuclei} \\
&= 29.4A^{-1} \text{ for odd-odd nuclei} \qquad \text{(C.15)}
\end{aligned}
$$

Using (C.15), the (a, Δ) values for ^{56}Fe and ^{60}Ni in the set of nuclei considered in Sect. C.3 are calculated and they are called Dilg et al (a, Δ) values for these two nuclei. The level densities and spin-cutoff factors calculated at different energies using the Dilg et al (a, Δ) parameters and the smoothed NIP forms (C.3 - C.8, C.10) with $r_0 = 1.2$ are treated as experimental data. This data is called Dilg et al data in the compilation given in Sect. C.3.

Katsanos et al [Ka-70] fitted the Ericson fluctuation data (they measured the same) at certain energies (around 20 MeV excitation) and the data at low energies obtained by direct counting, using (C.3 - C.8, C.10) with $r_0 = 1.2$ and deduced (a, Δ) values. The level densities and spin-cutoff factors calculated at different energies using the deduced (a, Δ) parameters and the smoothed NIP forms (C.3 - C.8, C.10) with $r_0 = 1.2$ are treated as experimental data. This data is called Katsanos et al data in the compilation given in Sect. C.3.

Most recent exercise of selection and compilation of level density data from direct counting, proton/neutron resonances and Ericson fluctuations is due to Iljinov et al [Il-92] and wherever possible, this data is used in the compilation given in Sect. C.3.

Data for spin-cutoff factors

The measurement of spin-cutoff factor $\sigma_J^2(E)$, the quantity which characterizes the spin distribution of nuclear levels, cannot be carried out by a commonly available method. However information about $\sigma_J(E)$ basically come

from three kinds of methods. They are: 1) the experiments to measure the isomer ratio; 2) the measurement of angular distribution of particles from charged particle reactions and 3) using the analytical formulas (C.4, C.9 - C.11, C.13) and the deduced values of a and Δ. These three methods are briefly described below.

Long lived excited states are known as isomers. By measuring cross-sections for two isomeric states with quite different angular momenta and comparing their ratios with a statistical theory of nuclear reaction that involves σ_J, a value for $\sigma_J(E)$ is deduced by best fit to data (in the analysis energy dependence of σ_J is ignored). For example in $^{197}Au(p,n)^{197}Hg$, $^{197}Au(d,2n)^{197}Hg$, $Pt(\alpha,xn)^{197}Hg$, $^{196}Hg(n,\gamma)^{197}Hg$, $^{196}Hg(d,p)^{197}Hg$ etc. reactions, for spin $1/2^-$ ^{197}Hg ground state (life time 65 hours) and the isomeric states with spin $13/2^+$ at 0.297 keV excitation (life time 24 hours), the cross sections are measured and by fitting the cross-section ratio to a statistical theory, $\sigma_J(E)$ value is deduced by Vandenbosch and Huizenga [Va-60]. However for the eight fp-shell nuclei of interest to us, there are no $\sigma_J(E)$ data from isomeric ratio measurements.

In the second method, the spin-cutoff factors are obtained from angular distribution of particles emitted in charged particle experiments. In these experiments, the differential cross-section at various angles (denoted by $W(\theta)$) are measured and then using (C.14) and fitting the data for $W(\theta)/W(0)$ to theory with an assumed form for $\sigma_J(E)$, the values for $\sigma_J(E)$ are deduced. Lu et al [Lu-72b] carried out these experiments for fp-shell nuclei and deduced $\sigma_J(E)$ values. In fact they give the following results: (I) using $E^{1/2}$ energy dependence; (II) with no energy dependence,

Reactions	Bombarding energy (MeV)	Final nucleus	excitation energy of the final nucleus $E(MeV)$	Deduced $\sigma_J(E)$	
				I	II
$^{56}Fe(\alpha,\alpha')^{56}Fe$	17	^{56}Fe	5.5 – 9.5	$(3.5-3.8)\pm 0.1$	3.8 ± 0.2
$^{59}Co(\alpha,\alpha')^{59}Co$	17	^{59}Co	5.5 – 9.5	$(3.9-4.4)\pm 0.1$	4.2 ± 0.2
$^{60}Ni(\alpha,\alpha')^{60}Ni$	17	^{60}Ni	5.5 – 9.5	$(3.4-4.0)\pm 0.1$	3.4 ± 0.2
$^{62}Ni(\alpha,\alpha')^{62}Ni$	17	^{62}Ni	5.5 – 9.5	$(3.6-3.7)\pm 0.1$	3.8 ± 0.2
$^{63}Cu(\alpha,\alpha')^{63}Cu$	17	^{63}Cu	5.5 – 9.5	$(3.9-4.2)\pm 0.1$	4.1 ± 0.2
$^{60}Ni(\alpha,p)^{63}Cu$	16.6	^{63}Cu	4.1 – 8.3	$(3.4-3.9)\pm 0.2$	3.7 ± 0.3
$^{62}Ni(\alpha,p)^{65}Cu$	16.2	^{65}Cu	3.3 – 7.3	$(3.8-4.0)\pm 0.2$	4.0 ± 0.3

In the compilation given ahead in Sect. C.3 only the results of set I given in the above table are used. As the energy changes from E_1 to E_2, the $\sigma_J(E)$ changes from σ_1 to σ_2 and in the compilation given in Sect. C.3 it is assumed that at $E = E_1$, $E_1+\delta$, $E_1+2\delta$ and E_2, $\sigma_J(E) = \sigma_1$, $\sigma_1+\delta'$, $\sigma_1+2\delta'$ and σ_2 where $\delta = (E_2-E_1)/3$ and $\delta' = (\sigma_2-\sigma_1)/3$; this is similar to what was done in [Be-73] for ^{56}Fe nucleus. The spin-cutoff values $\sigma_J(E)$ thus obtained at these four energies are referred to as experimental spin-cutoff data (though experiments give only spin-cutoff datum value as shown in the table above).

There are analytical formulas available for $\sigma_J(E)$ as given by (C.9 - C.11, C.4). Knowing (a, Δ) parameters and $\mathcal{I}_{rig}$ or r_0 value, σ_J at different energies can be calculated. Using (C.10) and the a and Δ values given by Dilg et al [Di-73], Lu et al [Lu-72a] and Katsanos et al [Ka-70], $\sigma_J(E)$ values are calculated and compiled in Sect. C.3.

C.3 Compilation of data

The compilation of data for the eight fp-shell nuclei $^{55}_{25}Mn_{30}$, $^{56}_{26}Fe_{30}$, $^{59}_{27}Co_{32}$, $^{60}_{27}Co_{33}$, $^{60}_{28}Ni_{32}$, $^{62}_{28}Ni_{34}$, $^{63}_{29}Cu_{34}$ and $^{65}_{29}Cu_{36}$ are given in this section. The data are obtained from various sources as described earlier. The exact values of

errors in level densities and spin-cutoff factors are compiled if they are available in literature. If errors are not available, as in the case of proton resonance data for ^{65}Cu and the spin-cutoff data from Lu et al [Lu-72b], we put 30% error for $I_\ell(E)$ and 10% error for $\sigma_J(E)$ (they are consistent with the errors that are generally believed to be in the deduced values of $I_\ell(E)$ and $\sigma_J(E)$ respectively).

Nucleus ^{55}Mn

For ^{55}Mn the most recent compilation of level densities deduced from direct counting, Ericson fluctuations and proton resonance data is due to Iljinov et al [Il-92]. Their compilation of data in Ericson fluctuation domain is same as given in [Ka-70]. In the proton resonance experiments [Di-73], 48 resonances are observed with spin $1/2^+$ using protons in the energy range $2.1 - 2.7\ MeV$ (proton separation energy is $8.07\ MeV$). For the level densities from the above three sources of data, Iljinov et al compilation is adopted and they are given Table C.1. The Dilg et al and Katsanos et al data for energies upto 24 MeV are given in Table C.2; the corresponding (a, Δ) values are shown below the table.

Table C.1 Iljinov et al data

E (MeV)	$I_\ell(E)$ (MeV^{-1})	$\Delta I_\ell(E)$ (MeV^{-1})
3.5^a	40	12
10.0^b	3000	800
15.1^c	110000	30000
18.0^c	490000	150000
23.1^c	7300000	2000000

a) direct counting *b*) proton resonances *c*) Ericson fluctuations

Table C.2 Dilg et al and Katsanos et al data

E (MeV)	Dilg et al			Katsanos et al		
	$I_\ell(E)$ (MeV^{-1})	$I(E)$ (MeV^{-1})	$\sigma_J(E)$	$I_\ell(E)$ (MeV^{-1})	$I(E)$ (MeV^{-1})	$\sigma_J(E)$
2.0	9	71	3.2	9	61	2.8
4.0	46	410	3.6	59	474	3.2
6.0	193	1854	3.8	308	2673	3.5
8.0	703	7153	4.1	1333	12300	3.7
10.0	2306	24578	4.3	5061	49082	3.9
12.0	6973	77241	4.4	17413	175926	4.0
14.0	19733	225971	4.6	55359	579285	4.2
16.0	52843	623095	4.7	164937	1779678	4.3
18.0	135026	1634272	4.8	465266	5158878	4.4
20.0	331318	4105805	4.9	1252308	14230104	4.5
22.0	784618	9934711	5.1	3235796	37596835	4.6
24.0	1800606	23254296	5.2	8065205	95642640	4.7

$a = 5.45\ MeV^{-1}$, $\Delta = -1.20\ MeV$	$a = 6.3\ MeV^{-1}$, $\Delta = -0.5\ MeV$

Nucleus ^{56}Fe

No resonance data are available for ^{56}Fe nucleus. The Katsanos et al and

Table C.3 Katsanos et al and Lu et al data

E (MeV)	Katsanos et al			Lu et al		
	$I_\ell(E)$ (MeV^{-1})	$I(E)$ (MeV^{-1})	$\sigma_J(E)$	$I_\ell(E)$ (MeV^{-1})	$I(E)$ (MeV^{-1})	$\sigma_J(E)$
2.0	1	4	2.0	2	10	2.5
4.0	9	64	2.8	12	94	3.1
6.0	64	515	3.2	65	563	3.4
8.0	337	2951	3.5	283	2631	3.7
10.0	1476	13772	3.7	1064	10457	3.9
12.0	5678	55664	3.9	3592	36940	4.1
14.0	19763	201851	4.1	11150	119150	4.3
16.0	63508	671823	4.2	32343	357252	4.4
18.0	191119	2084760	4.4	88672	1008373	4.5
20.0	544228	6100538	4.5	231711	2704451	4.7
22.0	1477992	16978739	4.6	580896	6941267	4.8
24.0	3851586	45242809	4.7	1404340	17144504	4.9

$a = 6.4\ MeV^{-1}$, $\Delta = 1.5\ MeV$	$a = 5.7\ MeV^{-1}$, $\Delta = 0.7\ MeV$

Lu et al data for energies upto 24 MeV are given in Table C.3 and the Dilg et al data for energies upto 24 MeV are given in Table C.4. The most recent compilation of level density data deduced from direct counting and Ericson fluctuations is due to Iljinov et al [Il-92]; their compilation of data in Ericson fluctuation domain is same as given in [Ka-70]. The Iljinov et al data are given in Table C.5. The experimental spin-cutoff data from Lu et al [Lu-72b] are collected in Table C.6; see Sect. C.2.

Table C.4 Dilg et al data

E (MeV)	$I_\ell(E)$ (MeV^{-1})	$I(E)$ (MeV^{-1})	$\sigma_J(E)$
2.0	1	7	2.4
4.0	11	86	3.1
6.0	69	601	3.5
8.0	337	3152	3.7
10.0	1385	13750	4.0
12.0	5050	52575	4.2
14.0	16786	181823	4.3
16.0	51791	580449	4.5
18.0	150252	1735048	4.6
20.0	413765	4906938	4.7
22.0	1089444	13233948	4.9
24.0	2758314	34247030	5.0

$a = 6.15\ MeV^{-1}, \quad \Delta = 1.1\ MeV$

Table C.5 Iljinov et al data

E (MeV)	$I_\ell(E)$ (MeV^{-1})	$\Delta I_\ell(E)$ (MeV^{-1})	E (MeV)	$I_\ell(E)$ (MeV^{-1})	$\Delta I_\ell(E)$ (MeV^{-1})
5.0^a	24	7	19.0^b	260000	70000
5.5^a	32	9	20.0^b	400000	120000
6.0^a	41	12	21.0^b	600000	220000
17.0^b	130000	30000	22.0^b	800000	300000
18.0^b	160000	50000	23.0^b	1200000	400000

a) direct counting *b*) Ericson fluctuations

Table C.6 Experimental spin-cutoff data

E (MeV)	$\sigma_J(E)$
5.50	3.5 ± 0.35
6.83	3.6 ± 0.36
8.16	3.7 ± 0.37
9.50	3.8 ± 0.38

Nucleus ^{59}Co

For ^{59}Co proton resonance data was measured by Lindstrom et al [Li-71, Li-72]. In [Li-71] 32 resonances with spin $1/2^+$ are observed with protons in the energy range $2.14 - 2.65\,MeV$ and in [Li-72] 71 resonances are observed

Table C.7 Iljinov et al data

E (MeV)	$I_\ell(E)$ (MeV^{-1})	$\Delta I_\ell(E)$ (MeV^{-1})
9.60	1700	400
10.00	3000	900

Table C.8 Lu et al and Dilg et al data

E (MeV)	Lu et al			Dilg et al		
	$I_\ell(E)$ (MeV^{-1})	$I(E)$ (MeV^{-1})	$\sigma_J(E)$	$I_\ell(E)$ (MeV^{-1})	$I(E)$ (MeV^{-1})	$\sigma_J(E)$
2.0	10	80	3.1	8	59	3.1
4.0	67	574	3.4	53	465	3.5
6.0	329	3069	3.7	276	2635	3.8
8.0	1371	13588	4.0	1196	12172	4.1
10.0	5060	52588	4.2	4555	48725	4.3
12.0	16986	183748	4.3	15708	175101	4.5
14.0	52869	591900	4.5	50046	577853	4.6
16.0	154589	1783575	4.6	149391	1778754	4.8
18.0	428765	5081176	4.7	422131	5165236	4.9
20.0	1136405	13796208	4.8	1137973	14270322	5.0
22.0	2894900	35925212	5.0	2944576	37758200	5.1
24.0	7120894	90168296	5.1	7349086	96183216	5.2

$a = 6.2\ MeV^{-1}, \quad \Delta = -0.8\ MeV$	$a = 6.31\ MeV^{-1}, \quad \Delta = -0.47\ MeV$

with spin $1/2^+$ with protons in the energy range $2.66 - 3.10\,MeV$ (the proton separation energy being $7.37\,MeV$). By analyzing this resonance data, Iljinov et al obtained $I_\ell(E)$ at $9.6\,MeV$ and $10\,MeV$ as given in Table C.7. The Lu et al and Dilg et al data for energies upto 24 MeV are given in Table C.8. The experimental spin-cutoff data from Lu et al [Lu-72b] are collected in Table C.9; see Sect. C.2.

Table C.9 Experimental spin-cutoff factor data

E (MeV)	$\sigma_J(E)$
5.50	3.90 ± 0.39
6.83	4.07 ± 0.41
8.16	4.23 ± 0.42
9.50	4.40 ± 0.44

Nucleus ^{60}Co

For ^{60}Co, neutron resonance density was measured by Baba [Ba-70] and this datum is recently compiled by Iljinov et al [Il-92]. The resonance energy E_{res} is 7.491 MeV, the resonance spins are $(3^-, 4^-)$ and the mean spacing at E_{res} is $(1400 \pm 200)\,eV$ (Rohr [Ro-92] gives $E_{res} = 7.492\,MeV$ and $D_{res} = (1600 \pm 160)\,eV$). Using this data, (C.3 - C.8, C.10, C.12, C.13) with $r_0 = 1.2$ and $(a,\ \Delta) = (8.01\,MeV^{-1}, 0\,MeV)$ as given in [Il-92], the following neutron resonance data is deduced,

Table C.10 Neutron resonance data

E_{res}	=	$7.491\ MeV$
J_1^π, J_2^π	=	$3^-, 4^-$
$I_\ell(E_{res})$	=	$(4389 \pm 627)\,MeV^{-1}$

The Dilg et al data for energies upto 24 MeV are given in Table C.11. Iljinov

et al [Il-92] compiled data from Ericson fluctuation measurements (the experiments are due to Kopsch and Cierjacks [Ko-72]) and their values are adopted in Table C.12.

Table C.11 Dilg et al data

E (MeV)	$I_\ell(E)$ (MeV^{-1})	$I(E)$ (MeV^{-1})	$\sigma_J(E)$	E (MeV)	$I_\ell(E)$ (MeV^{-1})	$I(E)$ (MeV^{-1})	$\sigma_J(E)$
2.0	62	531	3.4	14.0	297296	3496139	4.7
4.0	367	3438	3.7	16.0	891450	10779080	4.8
6.0	1764	17657	4.0	18.0	2540453	31495226	4.9
8.0	7337	77307	4.2	20.0	6927024	87846392	5.1
10.0	27342	300558	4.4	22.0	18168622	235238780	5.2
12.0	93418	1064605	4.6	24.0	46038104	607590530	5.3

$a = 6.86\ MeV^{-1}, \quad \Delta = -2.16\ MeV$

Table C.12 Iljinov et al data

E (MeV)	$I_\ell(E)$ (MeV^{-1})	$\Delta I_\ell(E)$ (MeV^{-1})
9.50	29000	12000
11.50	100000	40000
13.50	240000	110000

Nucleus ^{60}Ni

For ^{60}Ni neutron resonance data is compiled by Rohr [Ro-92] and Iljinov et al [Il-92]. The resonance spins and the resonance spacing are $J^\pi_{res} = (1^-, 2^-)$ and $D_{res} = (1400 \pm 300)\, eV$. Note that Iljinov et al give $E_{res} = 11.399\, MeV$ while Rohr [Ro-92] and Mughabghab et al [Mu-81] give $E_{res} = 11.389\, MeV$ and we adopt the later. Using this data, (C.3 - C.8, C.10, C.12, C.13) with $r_0 = 1.2$ and $(a, \Delta) = (7.47\, MeV^{-1}, 3.098\, MeV)$ as given in [Il-92], produce the neutron resonance data given in Table C.13. The Lu et al and Dilg et al data for energies upto 24 MeV are given in Table C.14.

Table C.13 Neutron resonance data

E_{res}	=	$11.389\ MeV$
J^{π}	=	$1^-, 2^-$
$I_\ell(E_{res})$	=	$(6006 \pm 1286)\ MeV^{-1}$

Table C.14 Lu et al and Dilg et al data

E	Lu et al			Dilg et al		
(MeV)	$I_\ell(E)$ (MeV^{-1})	$I(E)$ (MeV^{-1})	$\sigma_J(E)$	$I_\ell(E)$ (MeV^{-1})	$I(E)$ (MeV^{-1})	$\sigma_J(E)$
2.0	1	6	2.3	1	7	2.5
4.0	11	81	3.0	12	98	3.2
6.0	72	621	3.4	81	731	3.6
8.0	371	3470	3.7	411	4025	3.9
10.0	1603	15928	4.0	1761	18291	4.1
12.0	6098	63599	4.2	6658	72524	4.3
14.0	21039	228454	4.3	22865	259184	4.5
16.0	67128	754589	4.5	72701	852774	4.7
18.0	200817	2326832	4.6	216899	2621691	4.8
20.0	568956	6772494	4.8	613209	7612653	5.0
22.0	1538392	18761962	4.9	1655235	21049702	5.1
24.0	3993622	49792876	5.0	4291116	55779876	5.2

$a = 6.4\ MeV^{-1}, \Delta = 1.3\ MeV$	$a = 6.42\ MeV^{-1}, \quad \Delta = 1.14\ MeV$

The most recent compilation of level density data deduced from direct counting and Ericson fluctuations measurements is due to Iljinov et al [Il-92]; their compilation of data in Ericson fluctuation domain is same as given in Huizenga

Table C.15 Iljinov et al data

E (MeV)	$I_\ell(E)$ (MeV^{-1})	$\Delta I_\ell(E)$ (MeV^{-1})	E (MeV)	$I_\ell(E)$ (MeV^{-1})	$\Delta I_\ell(E)$ (MeV^{-1})
4.5^a	27	5	18.5^b	500000	200000
5.0^a	32	6	19.5^b	750000	220000
15.5^b	120000	36000	20.5^b	1100000	330000
16.5^b	190000	57000	21.5^b	1800000	540000
17.5^b	310000	90000	22.5^b	2500000	700000

a) direct counting *b*) Ericson fluctuations

et al [Hu-69]. The Iljinov compilation is given in Table C.15. The experimental spin-cutoff data from Lu et al [Lu-72b] are collected in Table C.16; see Sect. C.2.

Table C.16 Experimental spin-cutoff data

E (MeV)	$\sigma_J(E)$
5.50	3.4 ± 0.34
6.83	3.6 ± 0.36
8.16	3.8 ± 0.38
9.50	4.0 ± 0.40

Nucleus ^{62}Ni

For ^{62}Ni the neutron resonance data compiled by Mughabghab et al [Mu-84] is used. The $E_{res} = 10.597\,MeV$, $J^{\pi}_{res} = (1^-, 2^-)$ and $D_{res} = (1.8 \pm 0.3)\,keV$. (Rohr [Ro-92] gives $D_{res} = (1.6 \pm 0.2)\,keV$ while Iljinov et al [Il-92] gives $D_{res} = (1.4 \pm 0.2)\,keV$). Using Mughabghab data, $(a, \Delta) = (8.05\,MeV^{-1}, 3.1\,MeV)$, as given by Iljinov et al, and (C.4 - C.8, C.10, C.12, C.13) with $r_0 = 1.2$ produce the neutron resonance data given in Table C.17.

Table C.17 Neutron resonance data

E_{res}	=	$10.597\,MeV$
$J^{\pi}_1,\ J^{\pi}_2$	=	$1^-,\ 2^-$
$I_\ell(E_{res})$	=	$(4552 \pm 761)\,MeV^{-1}$

The Lu et al (a), Lu et al (b) data for energies upto 24 MeV are given in Table C.18 and the Dilg et al data for energies upto 24 MeV are given in Table C.19. The experimental spin-cutoff data from Lu et al [Lu-72b] are collected in Table C.20; see Sect. C.2.

Table C.18 Lu et al (a) and Lu et al (b) data

E (MeV)	Lu et al (a)			Lu et al (b)		
	$I_\ell(E)$ (MeV^{-1})	$I(E)$ (MeV^{-1})	$\sigma_J(E)$	$I_\ell(E)$ (MeV^{-1})	$I(E)$ (MeV^{-1})	$\sigma_J(E)$
2.0	3	18	3	1	6	2.4
4.0	23	192	3	10	81	3.1
6.0	138	1272	3.7	70	621	3.5
8.0	660	6510	3.9	361	3470	3.8
10.0	2698	28117	4.2	1560	15928	4.1
12.0	9840	107272	4.4	5934	63599	4.3
14.0	32840	371807	4.5	20472	228454	4.5
16.0	101972	1192931	4.7	65319	754589	4.6
18.0	298176	3590401	4.8	195404	2326832	4.8
20.0	828481	10236756	4.9	553620	6772494	4.9
22.0	2202501	27856996	5.0	1496925	18761962	5.0
24.0	5633102	72781472	5.2	3885974	49792876	5.1

$a = 6.4\ MeV^{-1}, \quad \Delta = 0.5\ MeV$	$a = 6.4\ MeV^{-1}, \quad \Delta = 1.3\ MeV$

Table C.19 Dilg et al data

E (MeV)	$I_\ell(E)$ (MeV^{-1})	$I(E)$ (MeV^{-1})	$\sigma_J(E)$	E (MeV)	$I_\ell(E)$ (MeV^{-1})	$I(E)$ (MeV^{-1})	$\sigma_J(E)$
2.0	2	11	2.5	14.0	75392	851067	4.5
4.0	23	183	3.2	16.0	260725	3045518	4.7
6.0	175	1576	3.6	18.0	841705	10131017	4.8
8.0	1007	9817	3.9	20.0	2563920	31694960	4.9
10.0	4809	49744	4.1	22.0	7429486	94079760	5.1
12.0	20057	217590	4.3	24.0	20610884	266778270	5.2

$a = 7.27\ MeV^{-1}, \quad \Delta = 1.07\ MeV$

Table C.20 Experimetal spin-cutoff data

E (MeV)	$\sigma_J(E)$	E (MeV)	$\sigma_J(E)$
5.50	3.60 ± 0.36	8.16	3.67 ± 0.37
6.83	3.63 ± 0.36	9.50	3.70 ± 0.37

Nucleus ^{63}Cu

The Lu et al and Dilg et al data for energies upto 24 MeV are given in Table C.21.

Table C.21 Lu et al and Dilg et al data

E (MeV)	Lu et al			Dilg et al		
	$I_t(E)$ (MeV^{-1})	$I(E)$ (MeV^{-1})	$\sigma_J(E)$	$I_t(E)$ (MeV^{-1})	$I(E)$ (MeV^{-1})	$\sigma_J(E)$
2.0	11	82	3.1	11	91	3.3
4.0	81	711	3.5	79	730	3.7
6.0	457	4348	3.8	423	4251	4.0
8.0	2120	21468	4.0	1893	20202	4.3
10.0	8572	91224	4.2	7424	83166	4.5
12.0	31224	346224	4.4	26327	307100	4.7
14.0	104649	1201905	4.6	86149	1040404	4.8
16.0	327545	3879295	4.7	263844	3284704	5.0
18.0	967868	11780130	4.9	764200	9774401	5.1
20.0	2722307	33957264	5.0	2109864	27650506	5.2
22.0	7335278	93562424	5.1	5586861	74855888	5.3
24.0	19031592	247765220	5.2	14258997	19496662	5.5

$a = 6.8\ MeV^{-1}, \quad \Delta = -0.5\ MeV$	$a = 6.63\ MeV^{-1}, \quad \Delta = -0.67\ MeV$

For ^{63}Cu proton resonance data is available [Br-70, Di-73]. There are 63 resonances observed with spin $1/2^+$ using protons in the energy range 2.1 – 2.7 MeV (the proton separation energy being 8.07 MeV). The resonance experiment is due to Browne et al [Br-70]. Recently Iljinov et al [Il-92] compiled the $I_t(E)$ values (at two energies) obtained by analyzing the proton resonance data and also data at low energies from direct counting. The Iljinov et al data is given in Table C.22. The experimental spin-cutoff data from Lu et al [Lu-72b] are collected in Table C.23; see Sect. C.2.

Table C.22 Iljinov et al data

E (MeV)	$I_\ell(E)$ (MeV^{-1})	$\Delta I_\ell(E)$ (MeV^{-1})
3.5^a	40	7
4.0^a	50	8
8.6^b	2100	600
9.0^b	4100	1200

a) direct counting *b*) proton resonances

Table C.23 Experimental spin-cutoff data

E (MeV)	$\sigma_J(E)$	E (MeV)	$\sigma_J(E)$
5.50	3.9 ± 0.39	4.1	3.40 ± 0.34
6.83	4.0 ± 0.4	5.5	3.57 ± 0.36
8.16	4.1 ± 0.41	6.9	3.73 ± 0.37
9.50	4.2 ± 0.42	8.3	3.90 ± 0.39

Nucleus ^{65}Cu

For ^{65}Cu proton resonance data is available [Br-70, Di-73]). There are 15 resonances observed with spin $1/2^+$ using protons in the energy range $3.15 - 3.25\ MeV$. With the proton separation energy being $7.45\ MeV$ the resonance density at $E = E_{res} = 7.45 + (3.25 + 3.15)/2 = 10.65\,MeV$ is calculated which gives $I_\ell^+(E_{res}; 1/2) = 15/0.1 = 150\,MeV^{-1}$. The $I_\ell^+(E; \frac{1}{2})$ is converted into $I_\ell(E_{res})$ using (C.3-C.8, C.10, C.12, C.13) with $r_0 = 1.25$ and (a, Δ) values given by Dilg et al [Di-73]. In the level density obtained from proton resonances we put an error of 30% (normally this much error one expects) and the data is shown in Table C.24.

Table C.24 Proton resonanace data

E_{res}	=	$10.65\ MeV$
J^π	=	$\frac{1}{2}^+$
$I_\ell(E_{res})$	=	$(6854 \pm 2056)\,MeV^{-1}$

The Lu et al and Dilg et al data for energies upto 24 MeV are given in Table C.25. Low energy level density data compiled by Iljinov et al is given in Table C.26. The experimental spin-cutoff data from Lu et al [Lu-72b] are collected in Table C.27; see Sect. C.2.

Table C.25 Lu et al and Dilg et al data

E (MeV)	Lu et al			Dilg et al		
	$I_\ell(E)$ (MeV^{-1})	$I(E)$ (MeV^{-1})	$\sigma_J(E)$	$I_\ell(E)$ (MeV^{-1})	$I(E)$ (MeV^{-1})	$\sigma_J(E)$
2.0	9	73	3.2	9	79	3.4
4.0	67	606	3.6	60	578	3.9
6.0	364	3587	3.9	297	3122	4.2
8.0	1644	17224	4.2	1249	13935	4.5
10.0	6485	71391	4.4	4637	54300	4.7
12.0	23093	264893	4.6	15660	190871	4.9
14.0	75798	900549	4.7	49003	618171	5.0
16.0	232662	2850448	4.9	143984	1871943	5.2
18.0	674989	8498223	5.0	401160	5357308	5.3
20.0	1865776	24073836	5.2	1067739	14608063	5.5
22.0	4944672	65238848	5.3	2730816	38192120	5.6
24.0	12627143	170039040	5.4	6742644	96222600	5.7
$a = 6.6\ MeV^{-1}, \quad \Delta = -0.5\ MeV$				$a = 6.24\ MeV^{-1}, \quad \Delta = -0.77\ MeV$		

Table C.26 Iljinov et al data

E (MeV)	$I_\ell(E)$ (MeV^{-1})	$\Delta I_\ell(E)$ (MeV^{-1})
3.5	45	9
4.0	56	16

Table C.27 Experimental spin-cutoff data

E (MeV)	$\sigma_J(E)$	E (MeV)	$\sigma_J(E)$
3.30	3.80 ± 0.38	5.96	3.93 ± 0.39
4.63	3.87 ± 0.39	7.30	4.00 ± 0.40

Appendix D

$\epsilon^{(L)}_{\alpha\beta}$ Matrix Elements for Electric and Magnetic Multipole Operators

The electric multipole operator T^{E_L} with multipolarity 2^L, in pn space is defined in terms of proton and neutron effective charges e_p and e_n and its explicit form is,

$$\begin{aligned} T^{E_L} &= e_p \left(\sum_{i=\text{proton}} r_i^L Y^L(\theta_i, \phi_i) \right) \\ &\quad + e_n \left(\sum_{i=\text{neutron}} r_i^L Y^L(\theta_i, \phi_i) \right) \end{aligned} \tag{D.1}$$

The T^{E_L} belongs to category [B] operator (5.2). Writing T^{E_L} in second quantized form and evaluating the reduced matrix elements of $Y^L(\theta, \phi)$ in oscillator single particle orbits, expression for $\epsilon^{(k=L)}_{\alpha\beta}(T^{E_L})$ matrix element is derived,

$$\begin{aligned} \epsilon^{(L)}_{\alpha\beta}(T^{E_L}) &= e_x \langle n_\alpha \ell_\alpha || r^L || n_\beta \ell_\beta \rangle \\ &\quad \times (-1)^{j_\alpha + \frac{1}{2}} \sqrt{\frac{(2j_\alpha + 1)(2j_\beta + 1)}{16\pi}} \begin{pmatrix} j_\alpha & L & j_\beta \\ \frac{1}{2} & 0 & -\frac{1}{2} \end{pmatrix} \left\{ 1 + (-1)^{\ell_\alpha + \ell_\beta + L} \right\}, \\ &\quad \text{for } x = p \text{ and } (\alpha, \beta) \in p \text{ or for } x = n \text{ and } (\alpha, \beta) \in n \end{aligned}$$

$$= 0, \text{ for } (\alpha \in p \text{ and } \beta \in n) \text{ or } (\alpha \in n \text{ and } \beta \in p) \tag{D.2}$$

The radial matrix elements $\langle n_\alpha \ell_\alpha || r^L || n_\beta \ell_\beta \rangle$ are given by ([Ha-79]),

$$\begin{aligned}
\langle n_f \ell_f | r^k | n_i \ell_i \rangle &= \int R_{n_f \ell_f}(r) r^k R_{n_i \ell_i}(r) r^2 dr \\
&= \sum_{\mu_f=0}^{n_f} \sum_{\mu_i=0}^{n_i} (-1)^{\mu_f + \mu_i} \left(\frac{1}{2\nu}\right)^{k/2} \begin{pmatrix} n_f \\ \mu_f \end{pmatrix} \begin{pmatrix} n_i \\ \mu_i \end{pmatrix} \\
&\times \sqrt{\frac{(2\ell_f + 2n_f + 1)!!\ (2\ell_i + 2n_i + 1)!!}{n_f!\ n_i!\ 2^{n_i + n_f}}} \\
&\times \frac{(\ell_f + \ell_i + 2\mu_f + 2\mu_i + k + 1)!!}{(2\ell_f + 2\mu_f + 1)!!\ (2\ell_i + 2\mu_i + 1)!!} \\
&\times \begin{cases} 1 & \text{if } \ell_1 + \ell_2 + k \text{ is even} \\ \sqrt{\frac{2}{\pi}} & \text{if } \ell_1 + \ell_2 + k \text{ is odd} \end{cases}
\end{aligned} \tag{D.3}$$

In Eq. (D.3), $\nu = \frac{1}{b^2} = \frac{m\omega}{\hbar}$; $\nu \simeq 0.96 A^{-1/3}\ fm^{-2}$.

The Magnetic multipole operator T^{M_L} with multipolarity 2^L in pn space is defined in terms of magnetic g-factors g_ℓ^p, g_s^p, g_ℓ^n and g_s^n

$$\begin{aligned}
T^{M_L} &= \sum_{i=\text{proton}} \left[\vec{\nabla}_i r_i^L Y_m^L(\theta_i\, \phi_i)\right] \cdot \left[g_l^p \frac{2\vec{\ell_i}}{L+1} + g_s^p \vec{s}_i\right] \\
&+ \sum_{i=\text{neutron}} \left[\vec{\nabla}_i r_i^L Y_m^L(\theta_i\, \phi_i)\right] \cdot \left[g_l^n \frac{2\vec{\ell_i}}{L+1} + g_s^n \vec{s}_i\right]
\end{aligned} \tag{D.4}$$

Writing $\tilde{g}$ as

$$\tilde{g}^x = \frac{2}{L+1} g_\ell^x \tag{D.5}$$

where $x = p$ or n and evaluating the gradient $\nabla'_\mu r^L Y_m^L$ using Eqs. 5.7.1 - 5.7.2 of [Ed-74] and Eqs. (A.2.19, A.2.20, A.2.21) of [Br-77] one gets

$$T^{M_L} = \sum_{i=\text{proton}} \sqrt{L(2L+1)} r_i^{L-1} \left\{ Y^{L-1}(\theta_i,\phi_i) \left[\tilde{g}^p \vec{j}_i + (g_{s_i}^p - \tilde{g}^p)\vec{s}_i \right]^1 \right\}_M^L + \sum_{i=\text{neutron}} \sqrt{L(2L+1)} r_i^{L-1} \left\{ Y^{L-1}(\theta_i,\phi_i) \left[\tilde{g}^n \vec{j}_i + (g_{s_i}^n - \tilde{g}^n)\vec{s}_i \right]^1 \right\}_M^L . \tag{D.6}$$

The $\epsilon_{\alpha\beta}^{(L)}(T^{M_L})$ matrix elements of T^{M_L} operator can be derived by evaluating the reduced matrix elements of $\left\{ Y^{L-1}(\theta,\phi) \left[\tilde{g}\vec{j} + (g_s - \tilde{g})\vec{s} \right] \right\}^L$ and the result is,

$$\begin{aligned}
\epsilon_{\alpha\beta}^{(L)}(T^{M_L}) &= \langle n_\alpha \ell_\alpha || r^{L-1} || n_\beta \ell_\beta \rangle \sqrt{L(2L+1)} \\
&\quad \times \left\{ \left[\frac{2g_\ell^x}{L+1} (-1)^{L+j_\alpha+j_\beta} \sqrt{j_\beta(j_\beta+1)(2j_\beta+1)} \right. \right. \\
&\quad \left. \times \begin{Bmatrix} L-1 & 1 & L \\ j_\beta & j_\alpha & j_\beta \end{Bmatrix} \langle j_\alpha || Y^{L-1}(\theta,\phi) || j_\beta \rangle \right] \\
&\quad + \left[\left(g_s^x - \frac{2g_\ell^x}{L+1} \right) \sqrt{\frac{3}{2}(2j_\alpha+1)(2j_\beta+1)} \right. \\
&\quad \left. \left. \times \begin{Bmatrix} \ell_\alpha & \ell_\beta & L-1 \\ \frac{1}{2} & \frac{1}{2} & 1 \\ j_\alpha & j_\beta & L \end{Bmatrix} \langle \ell_\alpha || Y^{L-1}(\theta,\phi) || \ell_\beta \rangle \right] \right\} , \\
&\quad \text{for } x = p \text{ and } (\alpha,\beta) \in p \text{ or for } x = n \text{ and } (\alpha,\beta) \in n \\
&= 0, \text{ for } (\alpha \in p \text{ and } \beta \in n) \text{ or } (\alpha \in n \text{ and } \beta \in p) .
\end{aligned} \tag{D.7}$$

In order to use the above equation, one should have the expressions for the double barred matrix elements $\langle \ell_\alpha || Y^L(\theta,\phi) || \ell_\beta \rangle$ and $\langle j_\alpha || Y^L(\theta,\phi) || j_\beta \rangle$ and they are,

$$\langle \ell_\alpha || Y^L(\theta,\phi) || \ell_\beta \rangle = (-1)^{\ell_\alpha} \sqrt{\frac{(2\ell_\alpha+1)(2\ell_\beta+1)(2L+1)}{4\pi}} \begin{pmatrix} \ell_\alpha & L & \ell_\beta \\ 0 & 0 & 0 \end{pmatrix}$$

$$\langle \ell_\alpha \frac{1}{2} j_\alpha || Y^L(\theta,\phi) || \ell_\beta \frac{1}{2} j_\beta \rangle = (-1)^{j_\alpha + 1/2} \sqrt{\frac{(2j_\alpha+1)(2j_\beta+1)(2L+1)}{16\pi}} \times \begin{pmatrix} j_\alpha & L & j_\beta \\ \frac{1}{2} & 0 & -\frac{1}{2} \end{pmatrix} \left\{ 1 + (-1)^{\ell_\alpha + \ell_\beta + L} \right\} . \quad \text{(D.8)}$$

The expression for the radial matrix element $\langle n_\alpha \ell_\alpha || r^{L-1} || n_\beta \ell_\beta \rangle$ appearing in (D.7) is given by (D.3).